# NAVAL POSTGRADUATE SCHOOL
## MONTEREY, CALIFORNIA


# DISSERTATION

**THE ASSIMILATION OF SATELLITE ALTIMETER DATA INTO A GLOBAL EDDY RESOLVING OCEAN MODEL**

by

Robin Telrud Tokmakian

June 1997

Dissertation Advisor: Albert J. Semtner

**Approved for public release; distribution is unlimited.**

# REPORT DOCUMENTATION PAGE

Form Approved OMB No. 0704-0188



| 1. AGENCY USE ONLY *(Leave blank)* | 2. REPORT DATE | 3. REPORT TYPE AND DATES COVERED |
|---|---|---|
| | June 1997 | Doctoral Dissertation |

| 4. TITLE AND SUBTITLE | 5. FUNDING NUMBERS |
|---|---|
| The Assimilation of Satellite Altimeter Data into a Global Eddy Resolving Ocean Model | NSF OCE-9401910 |
| 6. AUTHOR(S) Robin Telrud Tokmakian | |
| 7. PERFORMING ORGANIZATION NAME(S) AND ADDRESS(ES)<br>Naval Postgraduate School<br>Monterey CA 93943-5000 | 8. PERFORMING ORGANIZATION REPORT NUMBER |
| 9. SPONSORING/MONITORING AGENCY NAME(S) AND ADDRESS(ES)<br>National Science Foundation Physical Oceanography Program, Washington DC20550 | 10.SPONSORING/MONITORING AGENCY REPORT NUMBER |

11. SUPPLEMENTARY NOTES The views expressed in this thesis are those of the author and do not reflect the official policy or position of the Department of Defense or the U.S. Government.

| 12a. DISTRIBUTION/AVAILABILITY STATEMENT | 12b. DISTRIBUTION CODE |
|---|---|
| Approved for public release; distribution is unlimited. | |

13. ABSTRACT

Two assimilation experiments have been conducted using the Semtner/Chervin Parallel Ocean Climate Model at 1/4° resolution to investigate the dynamical changes which occur with the application of the nudging method to incorporate sea surface height observations (with associated vertical corrections to temperature and salinity) into a global eddy resolving ocean model. The first experiment used a previous model run as the observational field to determine if the assimilation technique, nudging, produced significant changes in the simulated fields to adjust the model to the observed fields when starting at a statistically different initial condition. The twin experiment has shown that the model does respond to the inclusion of the observed fields. Both the surface fields and subsurface fields have been adjusted towards these synthetic observations. The second experiment involved the use of a combined altimetric sea surface height anomaly field from the ERS-1 and the T/P satellites. The surface height fields are extended vertically by using the Levitus 94 monthly climatological fields. This dissertation has shown that assimilation of surface height data and an associated vertical adjustment to temperature and salinity, modifies both the surface and subsurface fields. Changes can be seen in both prognostic and diagnostic quantities (such as heat content and meridional overturning) while remaining dynamically consistent with the numerics of the model itself. Comparison of the simulated fields with in situ observations of temperature and salinity show that the model has adjusted towards observations not included in the assimilation process.

| 14. SUBJECT TERMS | 15. NUMBER OF PAGES |
|---|---|
| Oceanography, modeling, assimilation, global, satellite altimetry | 187 |
| | 16. PRICE CODE |

| 17. SECURITY CLASSIFICATION OF REPORT | 18. SECURITY CLASSIFICATION OF THIS PAGE | 19. SECURITY CLASSIFICATION OF ABSTRACT | 20. LIMITATION OF ABSTRACT |
|---|---|---|---|
| Unclassified | Unclassified | Unclassified | UL |

NSN 7540-01-280-5500

Standard Form 298 (Rev. 2-89)
Prescribed by ANSI Std. 239-18 298-102

**Approved for public release; distribution is unlimited.**

# THE ASSIMILATION OF SATELLITE ALTIMETER DATA INTO A GLOBAL EDDY RESOLVING OCEAN MODEL

Robin Telrud Tokmakian
B.A., University of California, Santa Barbara, 1978
M.S., Oregon State University, 1990

Submitted in partial fulfillment
of the requirements for the degree of

**DOCTOR OF PHILOSOPHY IN PHYSICAL OCEANOGRAPHY**

from the

**NAVAL POSTGRADUATE SCHOOL**
**June, 1997**

Author: Robin Tokmakian
Robin Tokmakian

Approved by:

Albert J. Semtner
Professor of Oceanography
Dissertation Supervisor

Ching-Sang Chiu
Associate Professor of
Oceanography

Roger T. Williams
Professor of Meteorology

Newell Garfield
Research Assistant Professor
of Oceanography

Michael J. Zyda
Professor of Computer Science

Robert H. Bourke, Chairman, Department of Oceanography

Maurice D. Weir, Associate Provost for Instruction

## ABSTRACT

Two assimilation experiments have been conducted using the Semtner/Chervin Parallel Ocean Climate Model at 1/4° resolution to investigate the dynamical changes which occur with the application of the nudging method to incorporate sea surface height observations (with associated vertical corrections to temperature and salinity) into a global eddy resolving ocean model. The first experiment used a previous model run as the observational field to determine if the assimilation technique, nudging, produced significant changes in the simulated fields to adjust the model to the observed fields when starting at a statistically different initial condition. The twin experiment has shown that the model does respond to the inclusion of the observed fields. Both the surface fields and subsurface fields have been adjusted towards these synthetic observations. The second experiment involved the use of a combined altimetric sea surface height anomaly field from the ERS-1 and the T/P satellites. The surface height fields are extended vertically by using the Levitus 94 monthly climatological fields. This dissertation has shown that assimilation of surface height data and an associated vertical adjustment to temperature and salinity, modifies both the surface and subsurface fields. Changes can be seen in both prognostic and diagnostic quantities (such as heat content and meridional overturning) while remaining dynamically consistent with the numerics of the model itself. Comparison of the simulated fields with in situ observations of temperature and salinity show that the model has adjusted towards observations not included in the assimilation process.

# TABLE OF CONTENTS

# ACKNOWLEDGMENT

*Happy is she who has knowledge from research and does not turn to injury of her fellows or to unjust deeds, but looks upon ageless order of eternal nature (to learn) in what way and where and how it came to be.*
*Euripides (with modifications by RT)*

This research was funded by a National Science Foundation, Physical Oceanography grant NSF OCE-9401910. Computing resources were provided by the National Center for Atmospheric Research and the Naval Postgraduate School. The satellite data (CLS "CORSSH" product) were provided by Pierre Le Traon and Frédérique Blanc at AVISO of the CLS Space Oceanography Division in France. These data are from the European Space Agency ERS-1satellite and the NASA/CNES Topex/Poseidon satellite. The Levitus 1994 temperature and salinity climatology was kindly provided by Sydney Levitus and his group at the NESDIS of the National Oceanic and Atmospheric Administration. The World Ocean Circulation Experiment observations were provided for by the data centers: Sea Level Fast Delivery Center at the University of Hawaii (then under Gary Mitchum) and the WOCE Hydrographic Office. Additional observational data was extracted through the TOGA/TOA World Wide Web site at "www.pmel.noaa.gov/toga-tao.html". The data providers are all thanked for generously sharing their data sets.

I would like to thank my committee members, Bert Semtner, Ching-Sang Chiu, R. T. Williams, Toby Garfield, and Michael Zyda for their time and constructive criticism of my research. In addition, I thank Bert Semtner for providing me with the opportunity to pursue my PhD. My questions on the use of complicated statistics were expertly answered by Peter Challenor of SOC, UK. Also, Mike Cook provided answers to my obscure MATLAB questions. Barbara Tokmakian is thanked for excellent editing of the draft copy of the thesis. Finally, I would like to thank my family for their support. I especially thank my parents, who listened patiently to my frustrations and successes over many years and have constantly encouraged me. They gave me, not only, guidance towards my educational goals and the desire for life long learning but also an inquisitive nature. I can never thank them enough.

# I. INTRODUCTION

## A. PURPOSE

High resolution global ocean models now produce very realistic simulations in which currents are adequately represented in strength and width, eddies are generated in the correct ocean regions where they are seen in hydrographic data, and seasonal to interannual changes of the near surface flow compare favorably with altimetric measurements of sea surface height fields. These models simulate the narrow widths and strength of the global currents which transport the majority of heat and salt within and between basins. It is important that the currents be accurately represented if any reasonable estimate of the global climate changes are to be made. However, these models are deficient in several ways: timing of turbulent (eddy) activity does not always coincide with reality, the surface heat flux does not get transferred to subsurface layers in a realistic manner, and initial conditions determined from climatological data sets are not fully correct and most likely, need to be adjusted. Without resorting to modifying the numerics of the basic model, some of these deficiencies can be identified and overcome by assimilating surface and subsurface observational data into the model. Excellent global altimetric data sets from both ERS-1/2 and TOPEX/POSEIDON (T/P) provide a necessary global observational data to complete the task.

This thesis describes such an assimilation process and the physical and numerical results. For the first time, the assimilation process has been applied to a global, high resolution primitive equation model ocean model with a free surface. In addition, the assimilation technique of nudging has been extended to consider the variance of the observational data, along with adjusting both the temperature and salinity in the subsurface layers of the model. The analysis of the simulations discusses how assimilation of observational data can be used to identify weaknesses in the numerical model formulation

and suggests how the models can be improved. The analysis is both qualitatitve and quantitative, evaluating both point measurements and integrated quantities.

## B. OCEAN GENERAL CIRCULATION MODEL

The model used in this research is the Semtner/Chervin global ocean model, referred to also as the Parallel Ocean Climate Model (POCM). It is a primitive equation (PE) model based on the early formulation of *Bryan* (1969), updated by *Semtner* (1974) and modified by *Semtner and Chervin* (1988, 1992) to run on a parallel vector computer with multiple processors. The model has 20 layers, uses a B-grid (*Mesinger and Arakawa*, 1976), and a Mercator grid of a 1/4° average cell size. The model is forced by 3-day average wind stresses, computed and interpolated from twice daily European Centre for Medium Weather Forecasting (ECMWF) 10-meter winds. Climatological monthly heat fluxes (*Barnier et al.* 1994), interpolated to 3-day fields, are used and the salt fluxes are handled by relaxing to the Levitus 1994 surface salinity values (*Levitus and Boyer*, 1994). Subsurface restoring to observations occurs only in the vicinity of Gibraltar and in the high-latitude belts 58-65°N and 68-75°S. The model has a prognostic free surface (*Killworth et al.* 1991) to facilitate the nudging of the sea surface height (SSH) field towards the altimeter data and allow for realistic coastlines and bottom topography. Initial conditions are based on a 32-year 1/2° spinup from gridded data, equilibrated at 1/4° using 1985-89 monthly 1000-mb winds. Detailed analysis of the accuracy of the large scale circulation simulated by POCM_4B (the name comes from it being the second run of the Semtner/Chervin POCM model at 1/4° average resolution) can be found in *Stammer et al.* (1996) and of the mesoscale in *McClean et al.* (1997). From the analysis of the nine-year run (1987-1995), it was found that the model is producing realistic circulation patterns on the large scale, but is somewhat deficient in eddy kinetic energy and the uptake of heat in the top layers. *Tokmakian* (1996) conducted a study to examine how well POCM

represented the time series of SSH rather than the statistical variability of SSH. Correlation values computed between the models and tide gauge data for the period of 1988 through 1994 using the POCM have an average correlation over all 94 stations of 0.46 with a median value 0.50. Figure 1 shows several time series of model SSH and measurements made by tide gauges. In all three cases the model is reproducing the observed signal fairly well. The mismatch between model SSH and in situ data is partly the result of not having all the correct forcing included. In other words, if SSH includes the incorporation of an event forced at a time outside of the model run, then these events are not reflected in the model's estimate of SSH. A frequency analysis shows that the model is clearly representing the seasonal cycle in phase and amplitude accurately. The models' SSH anomalies represent, fairly well, the ocean's response to both local and remote wind driven events in a large part of the model. The model has active thermodynamics, allowing for temporal changes in surface heat and freshwater fluxes.

The advantages of using a free-surface primitive equation model over one which has a rigid lid formulation can be seen by examining the basic formulation of the model and the corresponding prognostic variables of the model. In the formulation of a free surface model, the free surface, $\eta$, is a prognostic variable. To determine the influence this prognostic variable has over the related diagnostic stream function of a rigid lid model in the assimilation of data, it needs to be determined where and to what extent the ageostrophic portion of the sea surface height contributes to the flow, both in the barotropic component of velocity and in the vertical velocity.

The total u component of velocity can be written as $u = u_g + u_a + u_e$, where *g* is the geostrophic component, *a* is the ageostrophic component and *e*, the Ekman, or wind-driven, component. The free surface can be used to determine the geostrophic velocity, $u_g = \frac{g\partial\eta}{f\partial x}$. This diagnostic variable is used to assimilate data into in a rigid lid model. With a free surface model, the field that is adjusted is the true SSH ($\eta$), which is then coupled to the layers below by three equations: the continuity equation:

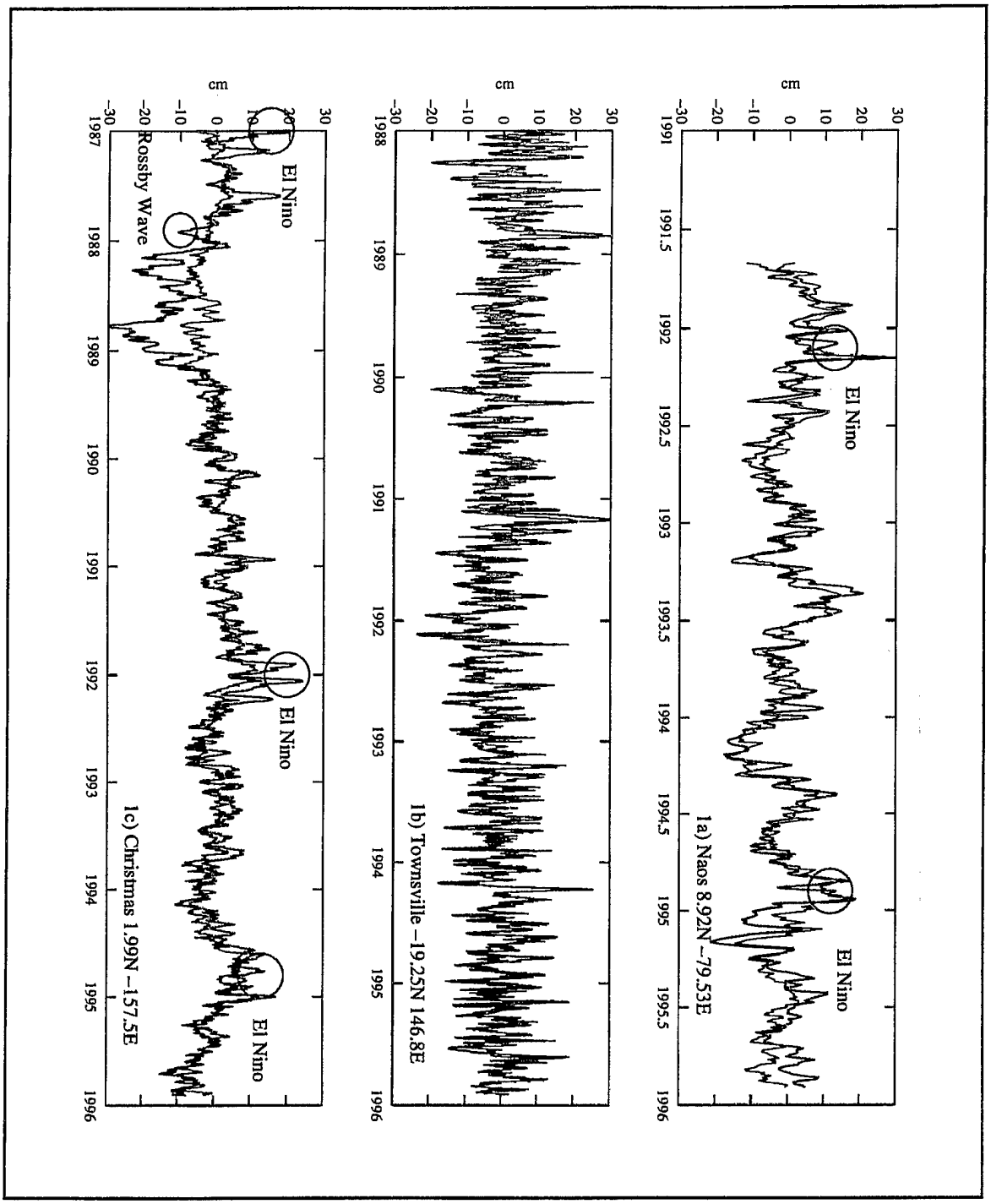


Figure 1. Tide gauge measurement of sea level as compared to the POCM-4B simulated SSH at a) Naos Island in the Gulf of Panama, b) at Townsville on the northeast coast of Australia, and c) at Christmas Island in the tropical Pacific. An annual harmonic has been removed from both signals. Noted on the plots are the El Niño and Rossby wave events. The red line are the model estimates and the black line are the tide gauge measurements.

$$\frac{\partial u}{\partial x} + \frac{\partial v}{\partial y} + \frac{\partial w}{\partial z} = 0 \tag{1.1}$$

and the two momentum equations:

$$\frac{\partial u}{\partial t} + u\frac{\partial u}{\partial x} + v\frac{\partial u}{\partial y} - fv = -g\frac{\partial \eta}{\partial x} \tag{1.2}$$

and

$$\frac{\partial v}{\partial t} + u\frac{\partial v}{\partial x} + v\frac{\partial v}{\partial y} + fu = -g\frac{\partial \eta}{\partial y}. \tag{1.3}$$

By using a rigid lid formulation in a steady state, the first three terms of equations 1.2 and 1.3 are assumed to be zero and the geostrophic definition of velocity results. If a steady state is assumed, then the relative importance of the 2nd and 3rd terms with respect to the fourth term needs to be evaluated using the model fields. These terms, $u\frac{\partial u}{\partial x} + v\frac{\partial u}{\partial y}$ and $u\frac{\partial v}{\partial x} + v\frac{\partial v}{\partial y}$, can be computed using the model's top layer velocity field, with the Ekman component[1] removed and then compared to the right hand side of the equation. The contribution of each of these terms to the total velocity can be estimated by looking at the ratio of the terms to the geostrophic term, fv or fu, respectively. In the tropics ($\pm$ 10°), the ratio is -2.68 $\pm$646.51 for the u equation and 0.11$\pm$20.45 for the v equation, suggesting that in both the u and v equations the non-linear terms dominate the geostrophic term. Outside of tropics, the terms have means of about zero, but with standard deviations of 0.15 and 0.20, respectively, for the u and v equations. While over the whole area, the non-linear effects do not dominate the flow, there are some areas where they do affect the dynamics up to 20% outside the tropics. The global ratio for the u component is shown in Figure 2a, for values greater than 0.1 (or 10%) and for the v component in Figure 2b.

In areas outside the tropics, such as in the region of the Gulf Stream and the Agulhas Current, the non-linear terms contribute to the total flow, especially at small

---

[1]The non-Ekman flow in the top layer of the model can be determined by subtracting the Ekman flow, calculated from the wind stress: $u_e = \frac{1}{g*f}\frac{\partial \tau_y}{\partial z}$ ($\tau_y$ is the y component of wind stress) from the total velocity in the top layer.

scales. This calls into question the general notion (*Oschlies and Willebrand*, 1996) that there is not much difference between assimilating SSH into a free surface model and into a rigid lid model. Thus it is physically better to use a free surface model to assimilate changes in SSH ($\eta$) , rather than using a rigid lid model, so that the non-linear adjustments to $\eta$ are not ignored.

## C. ASSIMILATION METHODS

This thesis concerns the assimilation of data into the above global model; therefore, some background to ocean assimilation is given. Large amounts of time and effort have been expended to investigate techniques for inserting altimeter data into ocean models. *Ghil and Malanotte-Rizzoli* (1991) and *Malanotte-Rizzoli* (1996) provide a general review of the current state of the assimilation using ocean models. Assimilation of data into models has been performed on a variety of models, quasi-geostrophic (QG), PE (layer and with active thermodynamics) and isopycnal models. Basically, there are two types of assimilation methods, sequential and variational. Sequential methods range from the very simple method of nudging to the much more complex and computationally intensive Kalman filter. Variational methods minimize the distance between the model and data over a time interval, subject to a dynamical or smoothness constraint and are also computationally intensive. This research directly benefits from the many studies done on earlier models which used a variety of techniques and evaluated the effectiveness of the assimilation.

### 1. Sequential

Nudging and Kalman filters are methods which attempt to move the model estimates of the flow fields towards observations. They differ, in that the Kalman filter can

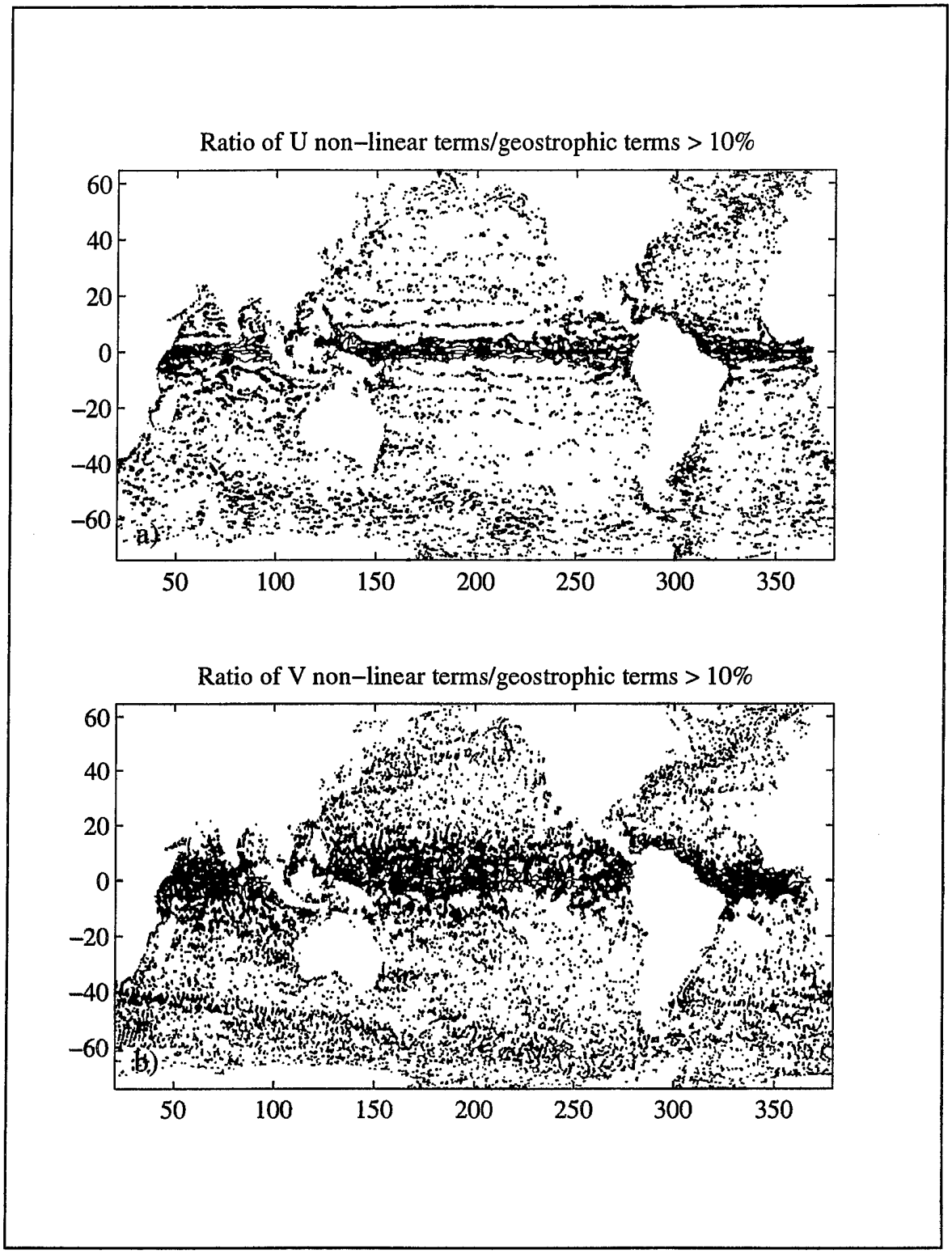


Figure 2. Ratio of the non-linear terms to the geostrophic terms greater than 10%.Blue is positive and red is negative. a) U components and b) V components.

estimate errors in the adjustment that is being made. Simply put, given x(t) as the model estimate of a model prognostic variable at time t and y as the observation at that point, then the model corrected estimate is:

$$x(t)_{corrected} = x(t) + \alpha\,(y(t)-x(t)) \qquad (1.4),$$

where $\alpha$ is a weight assigned to the observation. How $\alpha$ is defined and used is where the nudging method and the Kalman filter differ. Nudging, introduced into the meteorological field by *Anthes* (1974), expands (1.4) into an equation written as:

$$\frac{\partial x}{\partial t} = G + R(y - x) \qquad (1.5),$$

where R is the nudging factor, x is the model estimate and y is the observation. G is the physics in the equation representing all the linear and non-linear terms for estimating the variable x. R can be written as a relaxation value, constant for all of space and time, such as is done for allowing for heat flux changes in a model, that is; R is equal to the inverse of several days. Complicating the equation slightly, R can be modified to include changes in space, accounting for known errors in the observation field. Additionally, a multiplicative term can be incorporated to account for the age of the observation. An observation that is old should not carry the same weight as a more recent observation of a neighboring point. As an example, *Holland and Malanotte-Rizzoli* (1989) use

$$\alpha = \alpha_0 e^{-(x^2+y^2)/L^2_R}\,(e^{-\gamma t}) \qquad (1.6)$$

showing both a gaussian, $(x^2+y^2)/L^2_R$, based on the first Rossby radius of deformation ($L_R$), for spatial weighting, and an exponetial time decay, $-\gamma t$, for temporal weighting.

Different modifications of the basic equation (1.4) produces the Kalman filter equation:

$$\frac{\partial x}{\partial t} = G + \mathbf{K}(y - \mathbf{H}x) \qquad (1.7),$$

where **H** is the matrix that denotes where there are observations and how the data has been interpolated onto a model grid and G, the model physics equal to **A**x(t-1) +**F**, with **A** the transition matrix and **F**, the external forcing. Also,

$$\mathbf{K} = \mathbf{P}\mathbf{H}^T[\mathbf{H}\mathbf{P}\mathbf{H}^T+\mathbf{R}]^{-1} \qquad (1.8),$$

where **P** is the error covariance matrix for the model estimate equal to $\mathbf{A}\mathbf{P}(t-1)\mathbf{A}^T + \mathbf{Q}$ (the process noise) and **R** is the error covariance matrix for the observations. **H** and **R** can be determined prior to a model run, but the matrix **P** can only be determined during the model run at specified time increments. Thus, the inversion of a portion of **K** is computational intensive to find the new estimate for x and makes the use of the Kalman filter impractical for a high resolution simulation. The filter does provide a way to continuously monitor the error in the solutions: $\mathbf{P}_{\mathbf{analysis}}$, for time t, can be defined as equal to [ **I** - **KH**]**P**, where **I** is the identity matrix.

There are two concerns when the filter is applied to non-linear problems. Although the filter is robust for linear problems, it is only approximate for non-linear ones. The second problem is the computationally intensive nature of the Kalman filter. Researchers have developed methods to overcome these problems, somewhat. One approach is the Extended Kalman filter (EKF) (*Budgell,* 1986), which approximates the error evaluation by piece-wise linearization. The second simplification that has been done is to assume that **P** asymptotically approaches a steady state (*Fukumori et al.* 1993) and is calculated only once for equation 1.8. *Fukumori and Malanotte-Rizzoli* (1995) make another approximation by only assimilating the large-scale structure into the model. Thus, the Kalman gain (**K**) matrix is reduced in size and easier to handle.

## 2. Variational

The adjoint method is the variational method most commonly used in oceanographic assimilation efforts. As an inverse problem formulated as an optimization problem, the method consists of minimizing a cost function (the model's numerical equations are the constraints) to find the minimum efficiently (*Tziperman and Thacker*, 1989). A gradient based algorithm is used in which the gradient is computed using the adjoint equations of a model. Unknown model parameters are calculated by fitting model data to observations, with the addition of an optimal estimate of the observational data. Unlike the Kalman filter, this method is not directly related to the assimilation technique used in the present research and therefore, the mathematics of the method will be omitted. The method works as follows. Using some guess for the initial values, estimates of the prognostic variables at t+1 are computed and used in the formation a cost function, **J**, measuring how well the estimates fit the observed values. In an inverse and interactive fashion, the cost function, **J**, is then used to adjust the initial values such that **J** is minimized. Obviously, running the model forward, then backward through the use of its adjoint, at least doubles the cost of the computation, if not more. Thus, the procedure is undesirable for a high resolution global ocean model with over 30 million values to be calculated. *Sirkes et al.* (1996) used an adjoint technique applied to a coarse grid global ocean model in an attempt to improve estimates of eddy parameterizations and to produce a better initial ocean model for coupled ocean-atmosphere climate simulations. Although the results are encouraging, there are still difficulties in the formulation relating to conditioning of the dynamic constraints.

# D. OVERVIEW OF ALTIMETRY: OBSERVATIONAL DATA FOR ASSIMILATION

The ERS-1/2 (*Le Traon et al.* 1995) and T/P (*Fu et al.* 1994) satellites are now providing researchers with high quality and long altimetric time series for use as the observational field to adjust OCGM prognostic fields. In this research, data from both these instruments has been combined to form a joint sea surface height field which is to be assimilated.

An altimeter measures the distance ($h_a$) between the surface of the earth and the location of the satellite. This is done by having the satellite emit a pulse of radiation and then computing $h_a$ by using the time it takes the pulse reflected from the earth's surface to return to the satellite. The height of the sea level (SSH) is determined by subtracting $h_a$ from the total height the satellite is above an orbital reference ellipsoid (H) minus the height of the earth's geoid ($h_g$) (also referred to as a level of no motion). Additionally, corrections ($h_{atm}$) are included in the SSH estimate to account for atmospheric conditions (both dry and wet tropospheric); it takes longer for radiation to travel during wet conditions than dry, in addition to the effect the atmospheric pressure ($h_{inv}$) has on the sea surface (known as the inverse barometer effect). If the researcher is interested in the general circulation of the ocean, then any contribution the tides ($h_{tides}$) make on SSH needs to be removed also. Thus, the total equation for determining SSH from what the satellite measures is:

$$SSH\ (i,t) = H(i,t)\ - h_a\ (i,t) - h_g(i) -\ h_{atm}(i,t) - h_{inv}(i,t)\ - h_{tides}(i,t) \qquad (1.9),$$

where *i* is a spatial location and *t* is the time of the measurement.

Unfortunately, for wavelengths shorter than about 2500 km (*Rapp et al.* 1996), $h_g$ is not known accurately and complicates how the data may be used. Equation 1.9 can be rewritten as follows with SSH separated into a mean ( $\overline{SSH}$ ) and a residual SSH' and the

two static terms, $\overline{SSH}$ and $h_g$ combined:

$$SSH'(i,t) + [h_g(i) + \overline{SSH}(i)] = H(i,t) - h_a(i,t) - h_{atm}(i,t) - h_{inv}(i,t) - h_{tides}(i,t) \qquad (1.10).$$

As the equation is shown in 1.10, the terms on the right are all known at the time the satellite makes its measurement. H is determined from orbital mechanics using a set of either lasers or other tracking devices located on a satellite to track its position (for Topex/Poseidon, it is the DORIS, Dual-Doppler Tracking System Receiver, which receives signals from ground stations for satellite tracking, for ERS-1/2 it is PRARE, Precise Range and Range-rate Equipment[2]). The atmospheric corrections ($h_{atm}$) are determined either from a model and/or the use of the dual frequency altimeter on T/P, and the microwave radiometer on T/P and ERS-1/2. The tidal correction ($h_{tides}$) for both altimeters is determined from an empirical model (CSR 3.0, *Eanes and Bettadpur*, 1995). And last, $h_a$ is the measurement made by the satellite (averaged to 1 Hz from 50 Hz). Thus all the terms are accounted for except for the two static terms. The fact that these satellites fly in orbits which repeatedly sample the same ground track, can be used to determine the value of the combined static terms by finding the mean over time of $[H - h_a - h_{atm} - h_{inv} - h_{tides}]$ at specific spatial locations. Because there are two static terms in the equation 1.10 and neither are known to the accuracy needed for use in studying the ocean, only the mean of the two terms together can be found and removed, leaving only the sea level residual or anomaly, SSH'. Specifics on the data processing required to use altimetric data can be found throughout the literature on satellite altimetry and ocean circulation (e.g. *Tokmakian and Challenor*, 1993).

One additional wrinkle must be taken care of before the altimeter data can be used for assimilation. The assimilation procedure needs to use SSH and not the residual. Thus

[2] The PRARE failed on ERS-1 and the orbit was mostly determined from the use of Laser tracking of the satellite from the ground.

a mean sea level field must be added to the anomaly measurement prior to being incorporated into the model. For the purposes of this research, a mean sea level field was used from a prior run of the model. Analysis by *Rapp et al.* (1996) shows that the 1/4° POCM model mean field closely proximates the mean sea level as estimated empirically from observational data (mainly T/P data) at long wave lengths.

# II. ASSIMILATION TECHNIQUE

The emphasis of this dissertation is to assimilate altimeter SSH data into a high resolution PE model and due to the computation costs of the other methods, the assimilation options are restricted to that of nudging. Two experiments have been conducted. The first one is referred to as a twin experiment. For this experiment, two model runs are made. The first is the control run and the second is the twin, a simulation which uses simulated SSH data from the control run in an attempt to reproduce the conditions seen in the control run. The second experiment uses real altimeter data to force the model more towards what observations show. Unfortunately, the nudging technique does not include a way to assess the error in the estimated field produced by the assimilation as it is compared to the observational field of data; thus some simple statistical tests are also described that are used to evaluate the success of the experiments by comparing the results to the control runs or to the observational data.

## A. NUDGING SPECIFICS

The specific equations for the assimilation follow. The height field is assimilated in a straight forward manner, namely

$$\frac{\partial \eta}{\partial t} = G + R * ( \eta^0 - \eta^m ) \qquad (2.1),$$

where m denotes model data and o denotes observational data, which in this case is the altimeter anomaly height plus a mean height of a previous model run. G is the model physics for this particular equation and R is the relaxation coefficient. R is a function of the error in the observation field times a temporal factor times a spatial factor (*Anthes*, 1974). For example, R at grid point ij is

$$R_{ij} = \varepsilon \; e^{-\delta t/T} \; e^{-(x^2+y^2)/L_R^2} \qquad (2.2),$$

where $\varepsilon$ is an error estimate of the model data point. In this case, $\varepsilon$ is related to $\frac{<\delta h(i,j)>^2}{\max_{ij}<\delta h>^2}$, the normalized variance of SSH at a point. Thus, when the value is small (little variance), the point will be nudged weakly. When it is large, the model SSH will be pushed harder towards the observed value. This term includes observational statistics when nudging the model fields and is somewhat like a Kalman filter which continually updates its error covariance matrix (unlike this one, which is static). The observational SSH provides the two-dimensional set of predetermined $\varepsilon$ values, calculated prior to the assimilation run. The last two terms weight the observation with respect to time and space, an exponential decay in time and a gaussian distribution in space on the order of the size of the Rossby radius of deformation ($L_R$). Daily, the SSH altimetry (either synthetic or observed) data set is gridded to the model grid and a decay factor, $\delta t$, is aged. For example, a new observation has a decay weight of 1 ($\delta t = 0$) and an observation 5 days old has a weight of 0.37, if T is equal also to 5 days. Therefore, as an observation ages over time, it is given less weight.

There are several ways to relate to surface height signature to subsurface quantities. *Hurlburt* (1986) and *Carnes, et al.* (1990) use empirical orthogonal functions (EOFs) of historic temperature profiles to relate the surface height and temperature to subsurface fields. In the EOF method, the vertical profile of temperature is decomposed into orthogonal modes allowing for temperature estimates to be made based on its variance, giving as the EOF equation:

$$\Theta(z) = <T> + \sum_n \lambda_n f_n(z) \qquad (2.3),$$

where $\Theta$ is the new estimate of temperature at z, <T> is the mean temperature for that point, $\lambda_n$ are the eigenvalues, and $f_n(z)$ is the value of the eigenvector at z. To relate SSH to these EOFs, *Carnes, et al.* fit values of measured SSH to the eigenvalues over all space, such that $\lambda_n = b_0 + b_1\eta + b_2\eta^2$. With this new estimate of the eigenvalues, the variance matrix is more like the covariance of <T*η> rather than <T*T>. The vertical structure f(z) is assumed to be constant over the whole region for monthly periods. SSH is a measure of the change in the barotropic component of the flow and thus, the corrections made during assimilation runs are just scaling factors relating to the change in SSH, and are barotropic in nature. But in reality, especially on a global scale, adjustments need to be made also to salinity.

Another approach has been taken by *Haines* (1991) and applied to a PE model by *Cooper and Haines* (1996). This is a dynamic method which adjusts the density field up or down while conserving potential vorticity. This method requires iteration at each grid point, making adjustments, in theory, to both the temperature and salinity fields, until the correct surface pressure is achieved and potential vorticity is conserved. A side note, *Cooper and Haines* use a simplified equation of state: $\rho = 1029. + 0.25T$, which makes it necessary only to make changes in temperature, rather than both temperature and salinity. The method can be computationally intensive and thus not appropriate for a high resolution global model.

*Mellor and Ezer* (1991) found, using a primitive equation model, that predetermined correlations between sea surface height anomalies and subsurface temperatures and salinities were required to translate surface information to the subsurface layers. This is the method chosen for this research. Here, correlations are found between SSH and T for each layer at each grid point and between SSH and S for each layer at each grid point. This type of correlation is more of a baroclinic correction, although, if all the layers have the same correlation between SSH and T and S, then it becomes a barotropic correction. These

relationships are used to create an estimate of the observed subsurface temperatures (or salinities) which correct the simulated fields towards observations. The basic equation for including the correction term in the temperature equation is

$$\frac{\partial T}{\partial t} = G + R * F^T ( \eta^o - \eta^m ) \qquad (2.4),$$

where $F^T$ is an additional term correlating SSH to the subsurface temperature. By replacing T with S a corresponding equation for salinity is defined. The correlation functionals for each model grid point are written as:

$$F^T = \frac{<\delta T \delta \eta>}{<\delta \eta^2>} \qquad \text{and} \qquad F^S = \frac{<\delta S \delta \eta>}{<\delta \eta^2>} \qquad (2.5,2.6).$$

Few global temperature and salinity data sets exist that include a temporal component. Therefore, the twin experiment (see Chapter III) uses statistics from the control run to determine these functionals and the Levitus 1994 (*Levitus and Boyer*, 1994) monthly climatology of T and S has been used in the experiment using observational altimetry (see Chapter IV). The covariance matrix for the experiment using real altimeter observations is computed using the Levitus monthly temperature at a grid point with a monthly SSH field computed from the altimeter data set. This produces a three dimensional set of functionals that is used in the nudging of subsurface fields. It might also be possible to create these global functionals using data from different climatology sets for different oceans, although it would be necessary to examine the compatibility of one data set to another. For example, the Optimum Thermal Interpolation System (OTIS) temperature data set, produced by the US Navy in the North Pacific and North Atlantic oceans, might be used instead of the Levitus 1994 monthly climatology. The method can also be modified to assimilate actual temperature or salinity values.

## B. DESCRIPTION OF STATISTICAL TESTS USED FOR EVALUATION

Basic statistical methods can provide useful ways to evaluate large data sets. Three tests are employed to describe the major differences or simularities between model runs, the Student-t, chi-square, and F tests. With a set of paired runs (control and assimilation), statistical tests such as these are very appropriate in determining the effectiveness of the propagation of altimeter data into the deeper levels of the model.

### 1. Student-T Test

The Student-t test is used to determine if there is a significant difference in the mean of the distribution of one prognostic variable in a given region for the two model runs as shown in the following explanation. Let $a_i$ be a data value at a location from the control run and $b_i$ be a data value for the same variable and location from the assimilation run. $D_i$ represents the difference in the two values ($D_i = a_i - b_i$ ). It is assumed that the differences ($D_i$) are distributed about a mean $\mu$ and that the deviations are normally and independently distributed about this mean. The Student-t distribution tests the null hypothesis that $\mu$=0. The quantity,

$$t = \frac{(<D> - \mu)}{s_D} \qquad (2.7),$$

follows the Student-t distribution with (n-1) degrees of freedom, where <D> is the mean over all pairs of the $D_i$ , $s_D$ is the estimate of the standard deviation of the differences:

$$s_D = \sum \frac{(D_i - <D>)^2}{\sqrt{n(n-1)}} \qquad (2.8),$$

and n = number of pairs (*Snedecor and Cochran*, 1989). For this paper, n is always greater than 120 and the probability value from the table for (n-1) = ∞ can be used. That is, if t > 3.29, there is less than a 0.1% chance that the null hypothesis ($\mu$=0 ) is true. In other words, the two populations have different means.

### 2.Chi-Square Test , $\chi^2$

The $\chi^2$ goodness of fit test is used to examine the similarity of the distribution of the data from the two sets of data. Let $o_i$ = the number of observed values (or values from the assimilation model run) that fall into bin $i$ and $e_i$ is the number of expected values (or values from the control run) that fall into bin $i$. Then,

$$\chi^2 = \sum \frac{(o_i - e_i)^2}{e_i} \qquad (2.9),$$

where the sum is over all bins. The null hypothesis is: the observations are from the same population as the expected population. For the tests applied to the data presented in this paper, the number of bins are in the neighborhood of 25, some required more and some less. In general, a conservative approach is to determine if the distributions are similar or not. For example, if the number of bins (n) equal 25 (degrees of freedom: df = n-1) and the calculated $\chi^2$ is greater than 47 (determined from $\chi^2$ tables, see *Snedecor and Cochran*, 1989), then there is a less than 0.5 % chance that the two distributions are the same. The advantage of the $\chi^2$ test over the Student-t test, is that the the $\chi^2$ does not expect the data to be distributed normally and to be independent.

### 3. The F Test

Related to the $\chi^2$ test is the F test. The F test, when used to compare two populations, determines if the null hypothesis is true: $s_1^2$ and $s_2^2$, sample variances from independent samples, have true variance $\sigma^2$. Given that $F = s_1^2/s_2^2$, then the null hypothesis will be satisfied if the observed $F < F_{0.025}$. $F_{0.025}$ is determined from tables such as is found in *Snedecor and Cochran*, 1989. For large degrees of freedom, F approaches 1 when the null hypothesis is true.

Theoretically, these statistical tests should show that fields from a twin experiment should be similar and that when real altimeter data is assimilated, the fields of the control run and the assimilation run should be statistically different.

# III. TWIN EXPERIMENT

A twin experiment was conducted to determine if the assimilation process could reproduce a known mode state (*i.e.* the control state) when initialized from a different starting location. The twin experiment, thus, is a test that has known initial and final states which can be used to evaluate the effectiveness of an assimilation process. To simplify the text when describing the results, the control run will be referred to as run "C", the assimilation run (produced using synthetic altimeter data from the control run) as run "T" and the run which starts at the same point as "T" but without assimilation is run "I" for initial run (or field). The rest of the chapter gives the details of the test and the results. A success for the twin experiment is if, at the end of the T run, the prognostic and diagnostic (such as potential vorticity) fields resemble the control run, C. Analysis will not be done in this section which shows if the model, itself, is simulating a realistic ocean.

## A. SETUP

The control model run is from the simulation referred to as the Semtner/Chervin or POCM_4B. The year 1992 from this simulation will be the control for the twin experiment. An evaluation of this model run is described in detail in *Stammer et al.* (1996). The model was forced with wind stress fields created from nine years (1987-1995) of 10 meter ECMWF wind velocity fields and the *Barnier et al.* (1994) monthly climatological heat flux. The twin experiment model run (T) is in the exact same configuration as the control run (C), with the same forcing, with the exception of the inclusion of numerical code to handle the assimilation of simulated altimeter data and an associated vertical structure. The T (or assimilation) run is initialized with a three dimensional field for day 362 of 1987, a statistically different field than that which is used to initialize the C run (day 365.9 of 1991). The twin experiment is to determine if, by starting at a different initial field, the

model can be nudged towards simulating the ocean's circulation as seen in the control run. The twin experiment was conducted for a period of one year.

Figure 3a shows the initial SSH field for run T and while 3b shows a similar SSH field for run C. The difference between the two fields is shown in Figure 3c. Large differences are clear in the North Pacific, where the SSH field from the initial day (Figure 3a) is much higher than from the initial field from the C run. In the Antarctic Circumpolar Current (ACC) and in the North Atlantic, the differences appear more on the mesoscale, rather than on a basin wide scale.

## 1. Synthetic Altimeter Observations and Associated Vertical Functionals

A simulated sampling pattern associated with the 35 day repeat period of ERS-1 in both time and space was created and then used to sample the SSH ($\eta$) of run C for the year 1992, every three days, creating a synthetic SSH assimilation field for every day of 1992. The ERS-1 sampling is replicated in both time and space for this experiment. Figure 4 shows an area from the North Atlantic which shows the grid points that are sampled in a ten day period. At 60°N, the track separation is at 39km, nearly the same as the grid spacing of the OCGM. Near the equator, the altimeter sampling is about 50-60km, about the sampling of every other model grid point. These fields are the observations to be incorporated into the model. Figure 5 shows the corresponding synthetic observations for early in December of 1992. It shows the dense coverage of the satellite track coverage of the model grid.

Next, equations 2.5 and 2.6 are used to form the vertical functionals which associated SSH with subsurface temperature and salinity. The covariance quantities: $<\delta T \delta\eta>$, $<\delta S \delta\eta>$, and $<\delta\eta^2>$ are formed (for this experiment) using three years of previous model output covering the years 1987 through 1989. Because all the observations

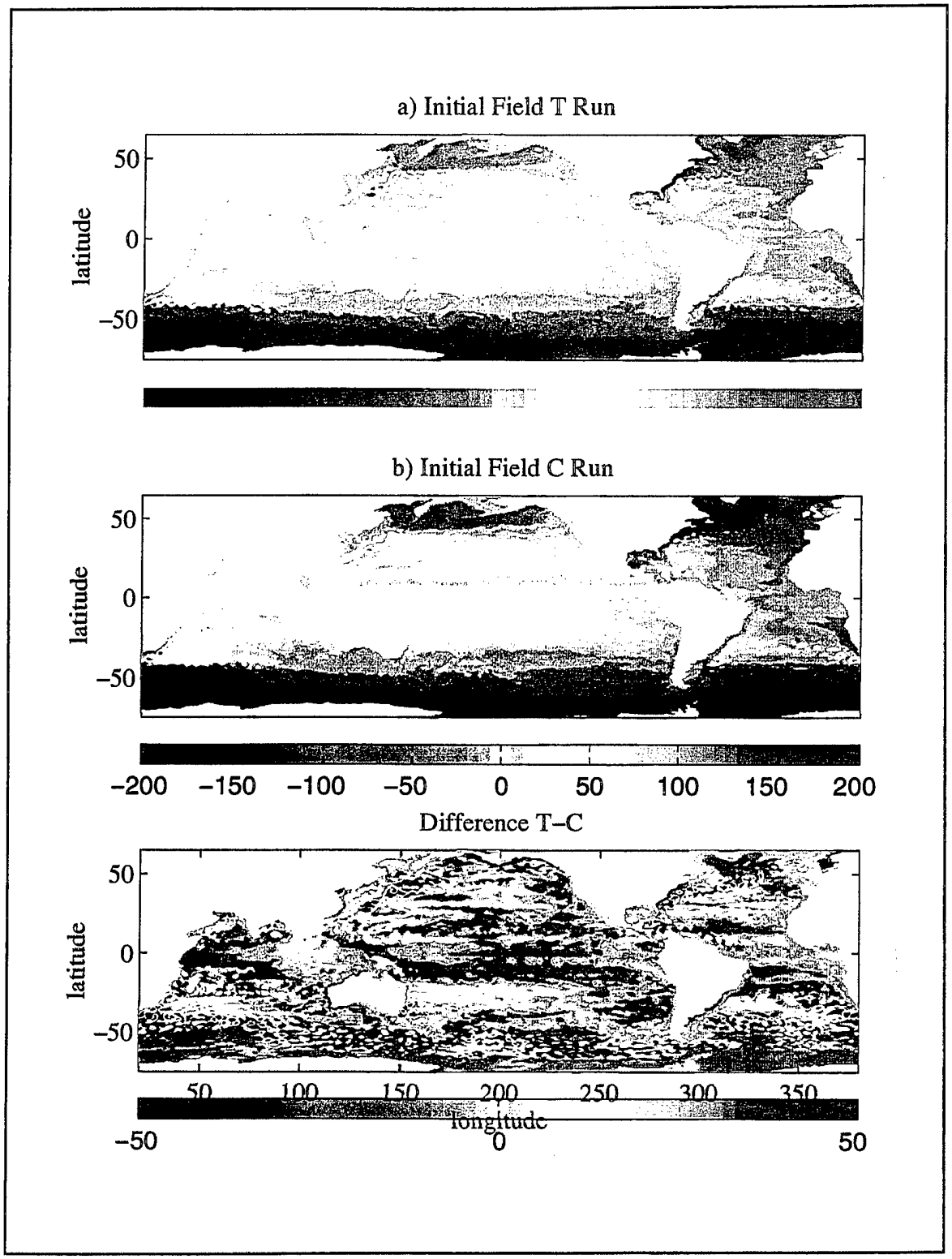


Figure 3. a) Initial SSH field for T run (December 28, 1987). Units in centimeters. b) Initial SSH field for C run (December 28, 1992). c) Difference between T field and C field. Scale in units of centimeters.

and associated vertical structures are from runs of the same model, their dynamical properties are the same and the fields are dynamically consistent. Averages of the vertical functionals over 20° squares have been formed and normalized in each layer by $\frac{F\_temp_k}{\text{maximum value in k}} * \frac{\text{standard deviation of layer 1}}{\text{standard deviation of k}}$, where k is the layer, to give a relative picture of how the vertical structure in either temperature (Figure 6a) or salinity (Figure 6b) are nudged. For example, in Figure 6a, in the 20° box centered at 370°E, 5°S, temperature is nudged strongly at the surface and very little at depth, while at 250°E, 45°S, there is little relationship between the vertical temperature variations and the height variations.

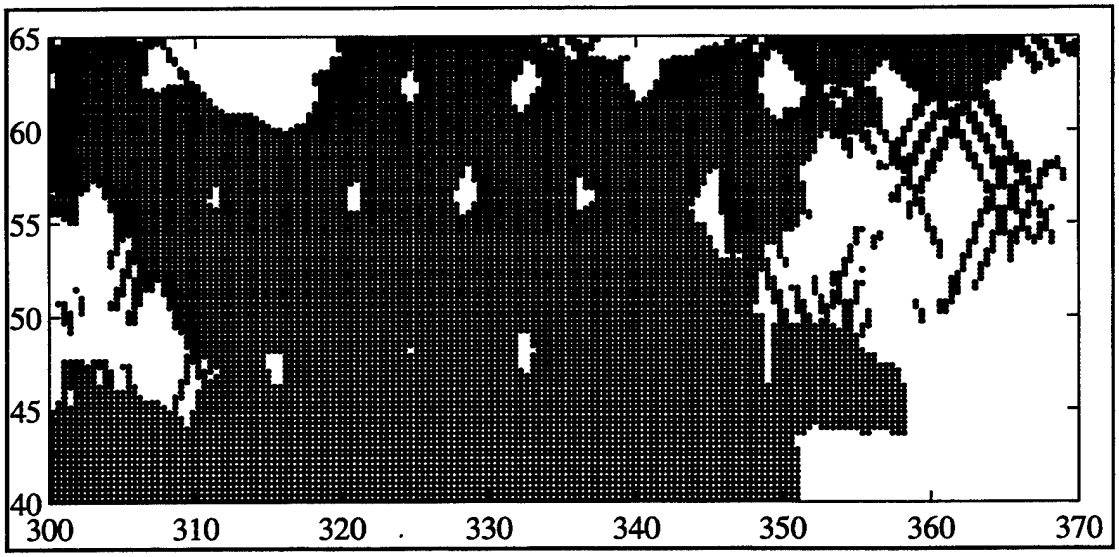


Figure 4. Example of the sampling grid over ten days of the model grid for creating synthetic altimetric SSH fields for assimilation during the T run.

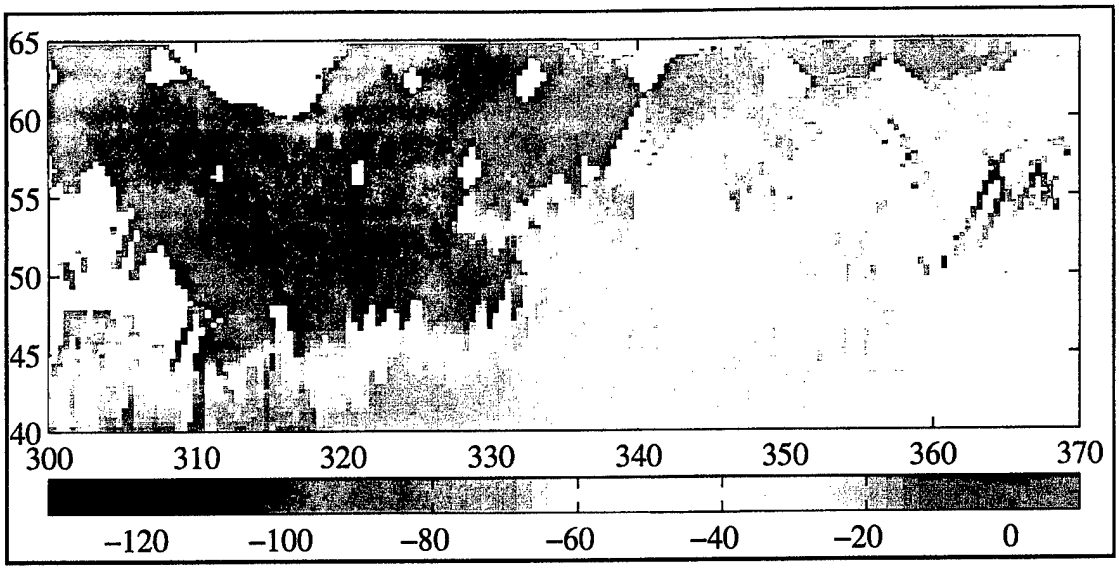

Figure 5. SSH field corresponding to the sampling field in Figure 4. Units in centimeters.

## 2. Additional Coefficients in Nudging Expression

Included in the nudging equation (Equations 2.1 and 2.2) are two additional terms which need to be calculated to contribute the weighting term associated with the nudging scheme. The first term is a weight, $\varepsilon$, associated with the normalized variance of SSH at a grid point with the underlying relaxation coefficient at three days. This term is created by using the variance of SSH over three years (1987-1989). Also included in the weight is an exponential which extends the data, sampled at a grid point, over a wider area. This term is a gaussian term with the Rossby radius of deformation ($L_R$) as the controlling term. $L_R$ is determined also from the model data using a 3 year mean.

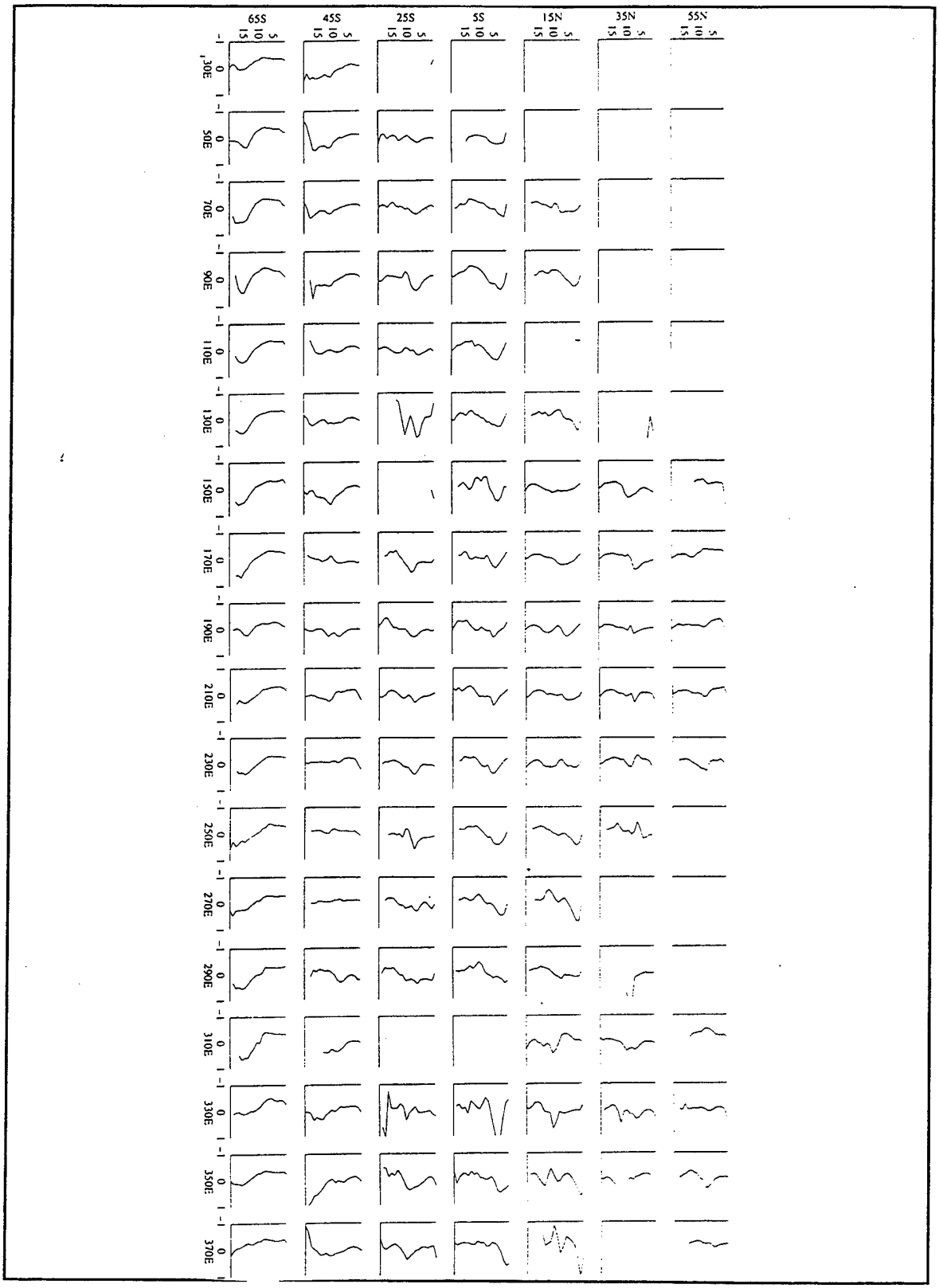


Figure 6. a) 20°x20° mean, normalized functional for temperature produced from equation 2.5 in Chapter II. Y axis of each square refers to the model layer, with 1 being at the surface. Blank squares are over land.

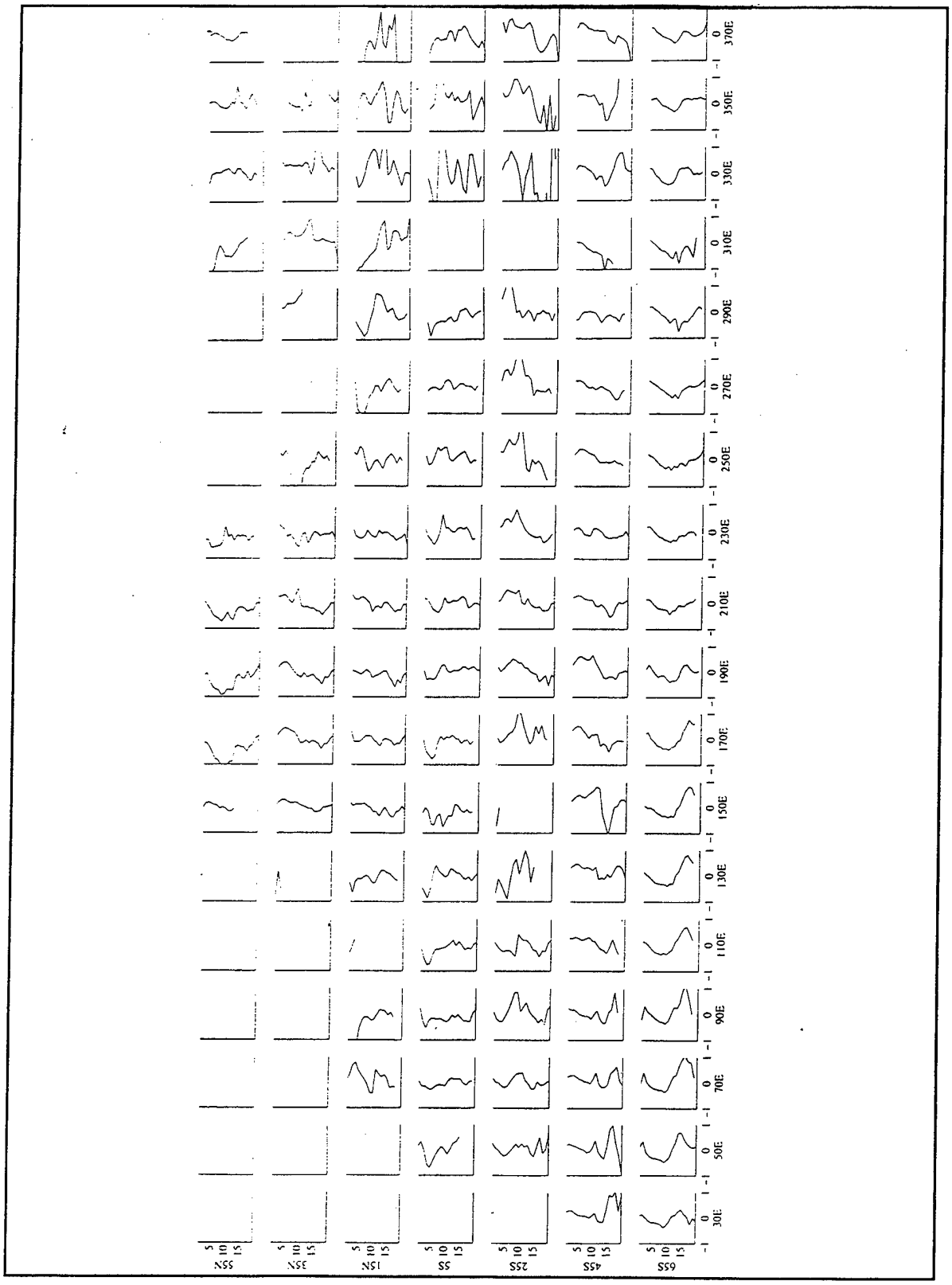

Figure 6b) Similar 20°x20° mean normalized functional for salinity.

## B. STATISTICAL COMPARISONS

### 1. RMS Differences

Root mean square (RMS) differences of SSH, temperature, and salinity over the global oceans and individual basins over time is one measure of how a model is adjusting the assimilation process. Figure 7 shows the time series of RMS differences between the SSH of the T and C runs over the first 250 days of 1992. The differences are normalized by the maximum difference of each time series. This allows for the comparison of how each region is adjusting, in addition to the global adjustment. The global difference has dropped to about 50% of the initial value between the two runs, with the South Atlantic basin dropping the quickest. Much more significant adjustments are occurring where the largest differences are seen in Figure 3c, in the Indian and the North Pacific, which have reduced the error to the order of 25% and 30%. These values are similar to both *Oschilles and Willibrand* (1996) and *Cooper and Haines* (1996) which use only regional high resolution PE models, with different assimilation schemes and somewhat idealized forcing (climatology instead of daily varying wind stress and monthly varying heat flux). These curves show that the present method is having some success, especially considering that the model is not being adjusted over large areas of the world's ocean where the variability is changing little or not at all (related to the $\varepsilon$ term of the nudging coefficient).

Similarly, the time series of the RMS difference in temperature and salinity is shown in Figure 8a and b. The plots show the global RMS differences in temperature and salinity over time for the top twelve layers of the model, down to approximately 1200 meters normalized by the maximum difference seen in each layer. As expected, the largest change is seen in the near surface layers. But even in layer 12, the temperature difference has been reduced by 30% by day 250. The decrease and then the increase (around day 100) in the temperature difference in layer one is due to the adjustment the model is making

to the heat flux term, rather than to the assimilation process. This can be compared to the salinity RMS differences (Figure 8b) where the difference drops and then stays low.

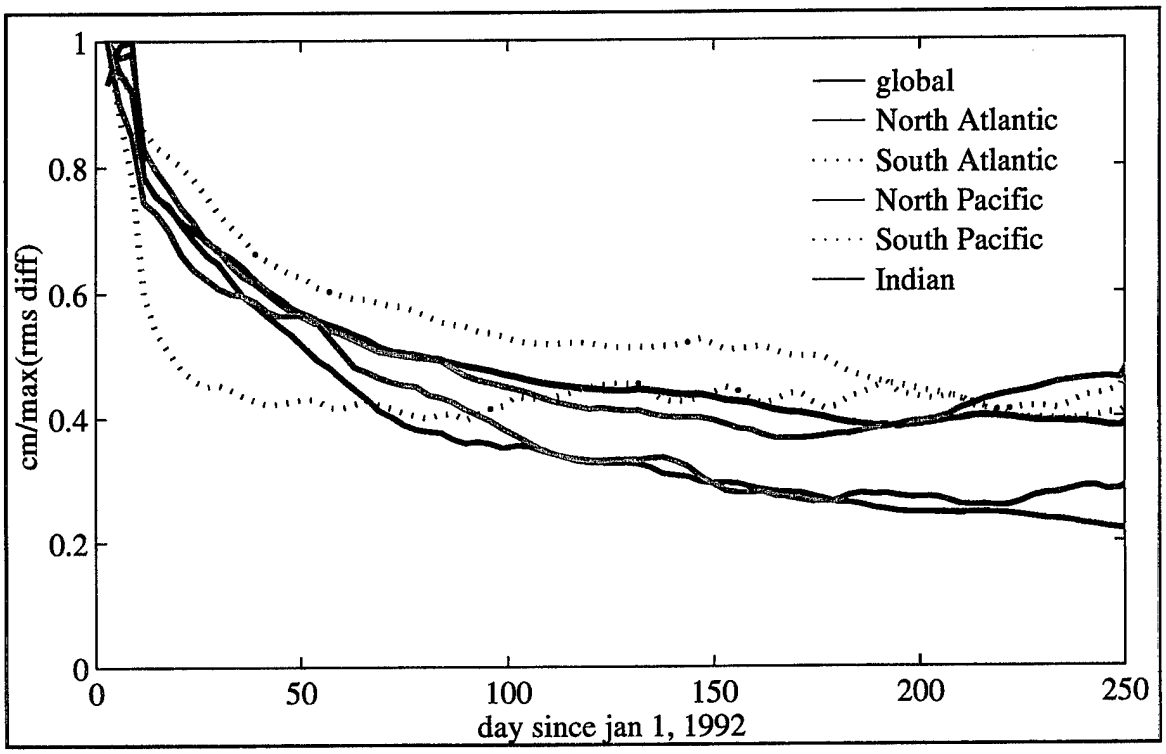


Figure 7. Plots of time series of RMS differences between T run fields and C run fields of SSH. Solid black line represents the global RMS differences over time, solid red correspond to the North Atlantic, dotted red line: South Atlantic, solid blue line: North Pacific, dotted blue line: South Pacific, and green line to the Indian. Values have been normalized by the maximum RMS difference calculated for the specific basin or globe.

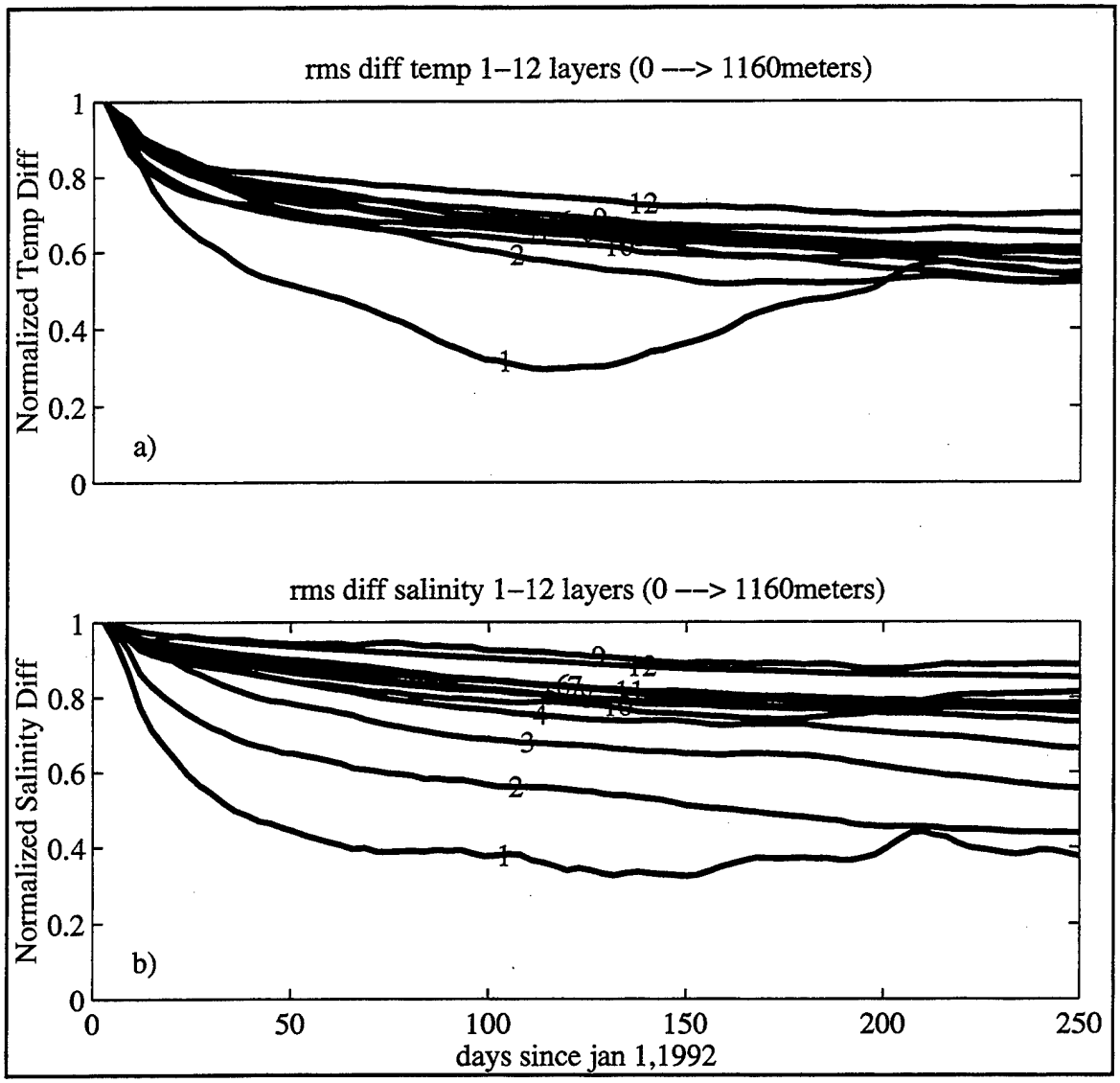


Figure 8. Same as for figure 7, but showing the RMS difference in a) temperature and b) salinity for each layer. Values have been normalized by maximum RMS value seen in each layer. The numbers on plot identify the layer.

## 2. Statistical Tests

The two statistical tests, the student-T test and the F-test, are used for a quick evaluation of the distributions of various model prognostic variables for different regions. It is important to note the assimilation of data using the nudging method will not immediately adjust the values of the model's variables to the observational values. Rather, the model is gently pushed towards what is observed. Changes in the deeper layers will also be difficult to see immediately, mainly because over large parts of the ocean, the deep ocean is decoupled from the surface. Thus, these simple tests are useful to determine if, in time, the monthly averages are approaching the values of the control field.

Figure 9a-h show two sets of student-t values for temperature from the twin experiment. Using equation 2.7, the t-test value is calculated between the various mean fields for the globe and for various regions: North and South Atlantic, North and South Pacific, Indian, tropical oceans and the Southern Ocean. Some of these regions overlap. The vertical scale is the t-test value with any value above 1.64, statistically different. Along the horizontal axis, the t-test value for SSH is at x=1 and for the 20 layers of temperature, the values are at x = 2-21. On the left side (Figures 9a-1,9b-1,9c-1, etc.), the plots show t-values computed between different months of the control run, December 1987 and January 1992 (thin dash-dot line), and between December 1987 and December 1992 (bold dash-dot line) to establish a baseline of how the model differs between years without any assimilation. Note the values are very similar between the two lines, especially below layer three. Statistically, these plots suggest there is no difference in the means of temperature between the initial field when it is compared to January of 1992 and when compared to December of 1992. These plots also suggest what differences to expect between two years of the model when no assimilation is performed.

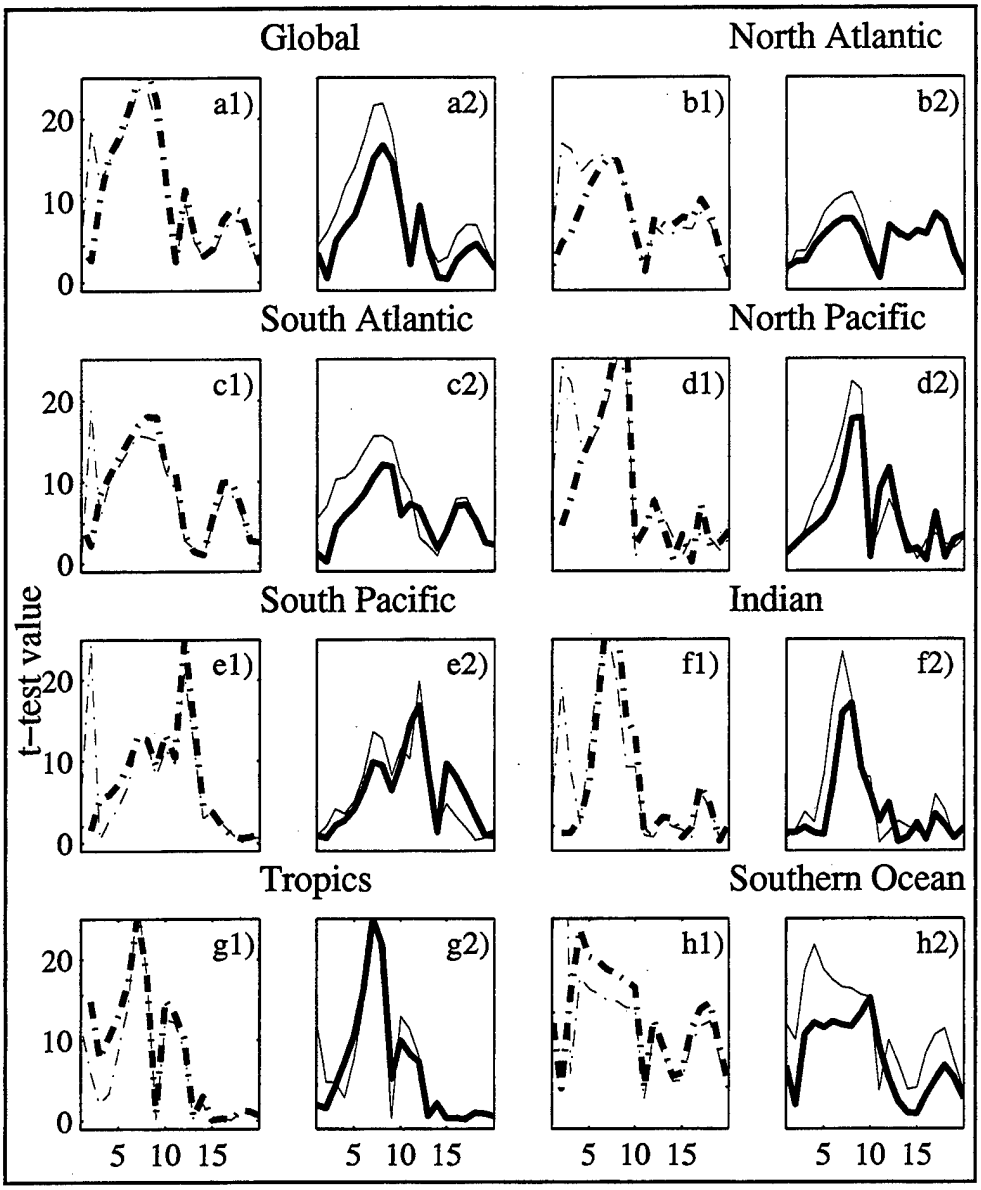


Figure 9. Plots showing the t-test values calculated between different model fields for the globe and for different basins. A pair of panels comprise each figure. Y-axis is the t-test value, 1.64 is the significance level for a null hypothesis. X-axis is read as follows: x = 1, t-test value for SSH, x=2-21, t-test value for temperature, levels 1-20. There are six areas: a) global values b) North Atlantic, c) South Atlantic, d) North Pacific, e) South Pacific, f) Indian, g) Tropics, h) Southern Ocean. There are two panels per figure letter. The left panel represents the t-test values between a field from December 1987 (I field, initial field of T run) and January 1992-C run (thin dashed line) and December 1987 and December 1992 (bold dashed line). On the right, the t-test values have been computed between the Januarys of the T and C runs (thin line) and the Decembers of the T and C runs (bold line).

The right set of panels show corresponding plots of t-values between the T and C runs (Figures 9a-2,9b-2,9c-2, etc.) for January 1992 (thin line, early in the simulation) and for December 1992 (bold line; at the end of run). Since the T run has been initialized with the December 87 field, it is expected that the thin lines on Figure 9a2, b2, etc. are close to the thin lines on Figure 9a1, b1, etc. If the two plots are overlayed, one on top of the other, they are quite similar. This means that in the early part of the assimilation process, the mean of the temperature field has changed very little. When comparing the two lines in the right panels (Figure 9a2, b2, etc.), it is seen that in all regions, except the tropics (Figure 9g1 and 2), there is a reduction in the t-test values from the beginning of the year (thin line) to the end of the year (bold solid line), much greater than seen in the t-test value between the years in the control run (Figures 9a1, b1, etc.). These sets of plots also suggest the differences in the means near the surface are mostly due to differences in the wind stress fields forcing the model, exhibited by the differences in the t-values shown in the panels on the left side because only the wind stress is significantly different in the two runs.

The results shown in Figure 9 are consistent with the RMS differences that shown in Figure 8, that is, the assimilation is affecting the temperatures down to about 1000 meters, with very little change below. What these plots show is that there has been greater change in the model's temperature and SSH fields when assimilation is performed, then when it is not; and that change is towards the control field, rather than away because the values are getting smaller, consistently.

Figure 10a-h show a similar set of t-test values for the salinity field. Similarly to the patterns for temperature, the pattern of reduced t-test values (Figure 10a2, b2, etc. ) is seen for layers 1 through 10 for the t-test over those values computed between two years of the control simulation (Figure 10a1, b1,etc.). There seems to be little change in the pattern

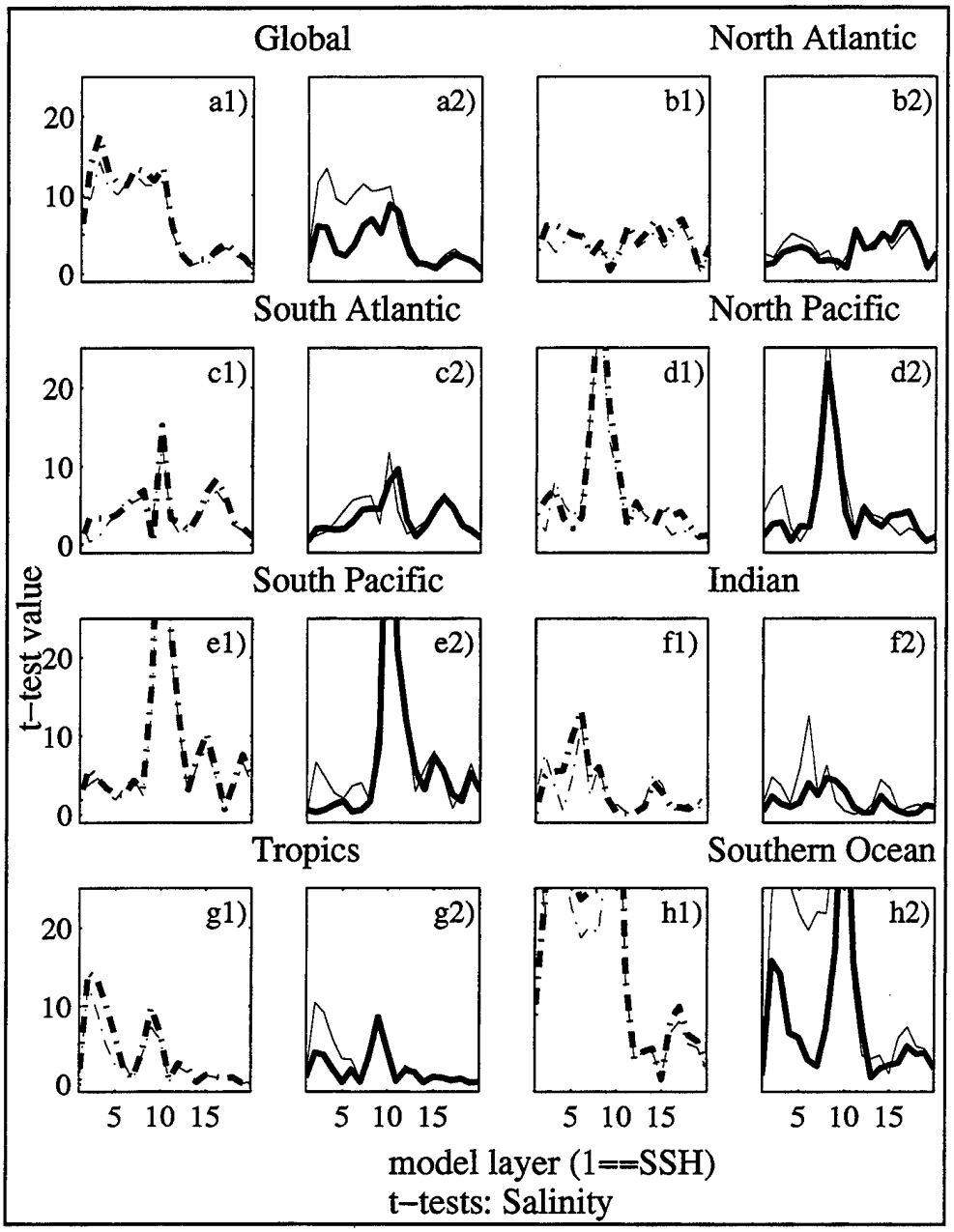


Figure 10. Same as 9, but representing t-test values computed from salinity fields. X=1->20 corresponds to model levels 1->20.

in the North Atlantic (Figure 10b) because all the calculations show that difference between the December 1992 T and C runs (bold line in Figure 10b2) is very similar to the t-test values calculated for the comparison between the December 1987 fields and December 1992 fields of the C run (dashed bold line in Figure 10b1) when the two years are very

different. The Southern Ocean (Figure 10h) exhibits a much different picture. Here it appears that the model is making significant modifications to the salinity field to adjust it towards the control field.

As stated in Chapter II B3, the F-test is a technique to examine the differences in variance between two sets of data. Figures 11a-h show the computed F values for the total globe and various regions for SSH and temperature in a similar fashion to that done for the t-test. The vertical scale is the F-test value with the significance level at 1.0. The left panels of the figures are the values computed between different years and months of the control field (C Dec. 1987 - C Jan 1992 and C Dec 1987 - C Dec. 1992, dash-dot lines); and the right panels are the C-T comparisons (T Jan 1992 - C Jan 1992 and T Dec 1992 and C Dec 1992). Again, as in the Student-t calculations, the comparison of control fields do not change much between the different months, while between runs T and C (solid lines), the F-test computed values have changed and in most cases, are adjusting towards 1. Figure 12a-h show the same thing, but for salinity. It is much harder to detect any differences in the variability in the temperature and salinity patterns from these figures, probably only in the top layers of the model. But, this should not be that surprising, given that the observations are from the control run and one would expect similar variability for both simulations.

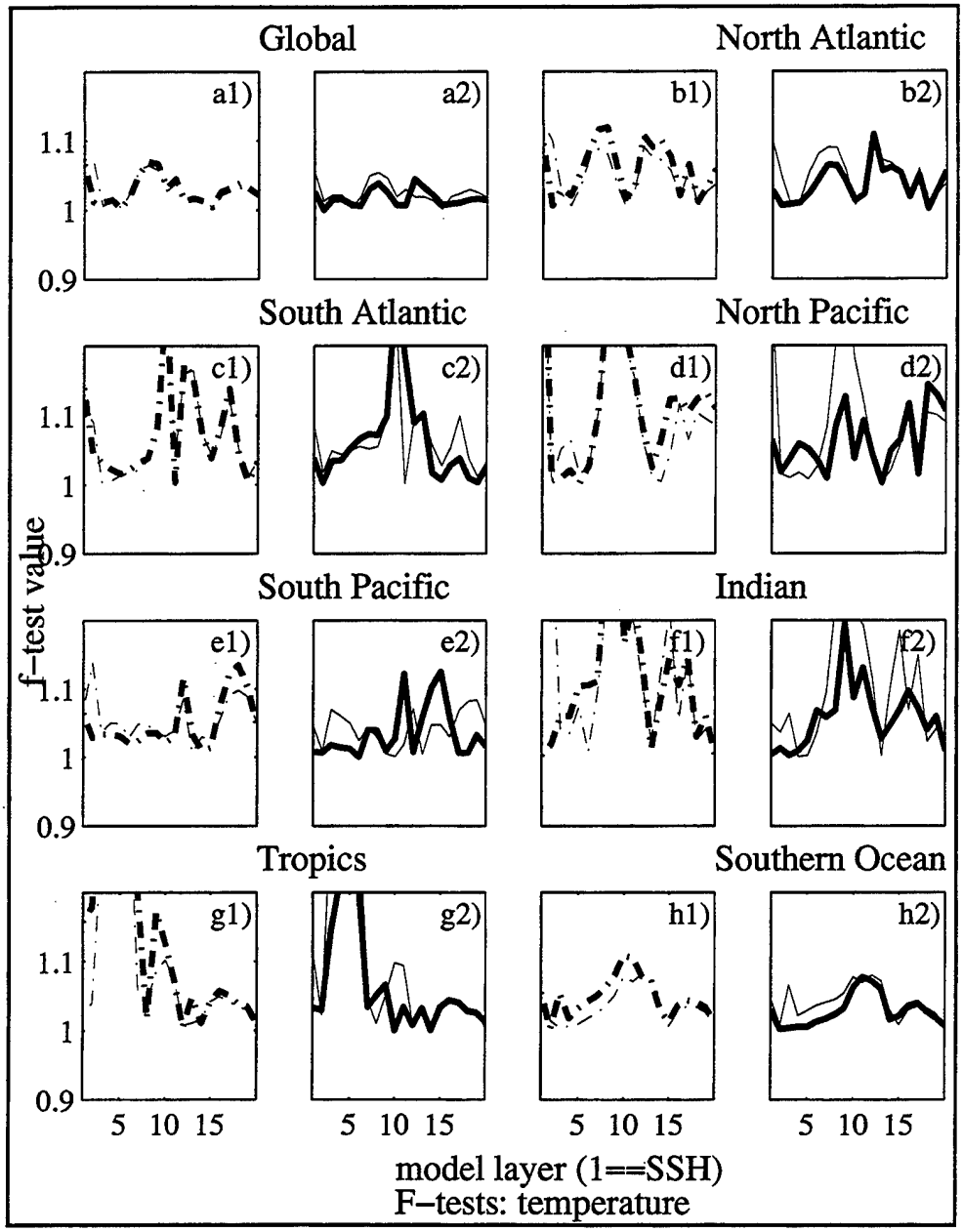


Figure 11. Same as 9, except the Y-axis represents the results of F-test computations, with the significance level at 1.0.

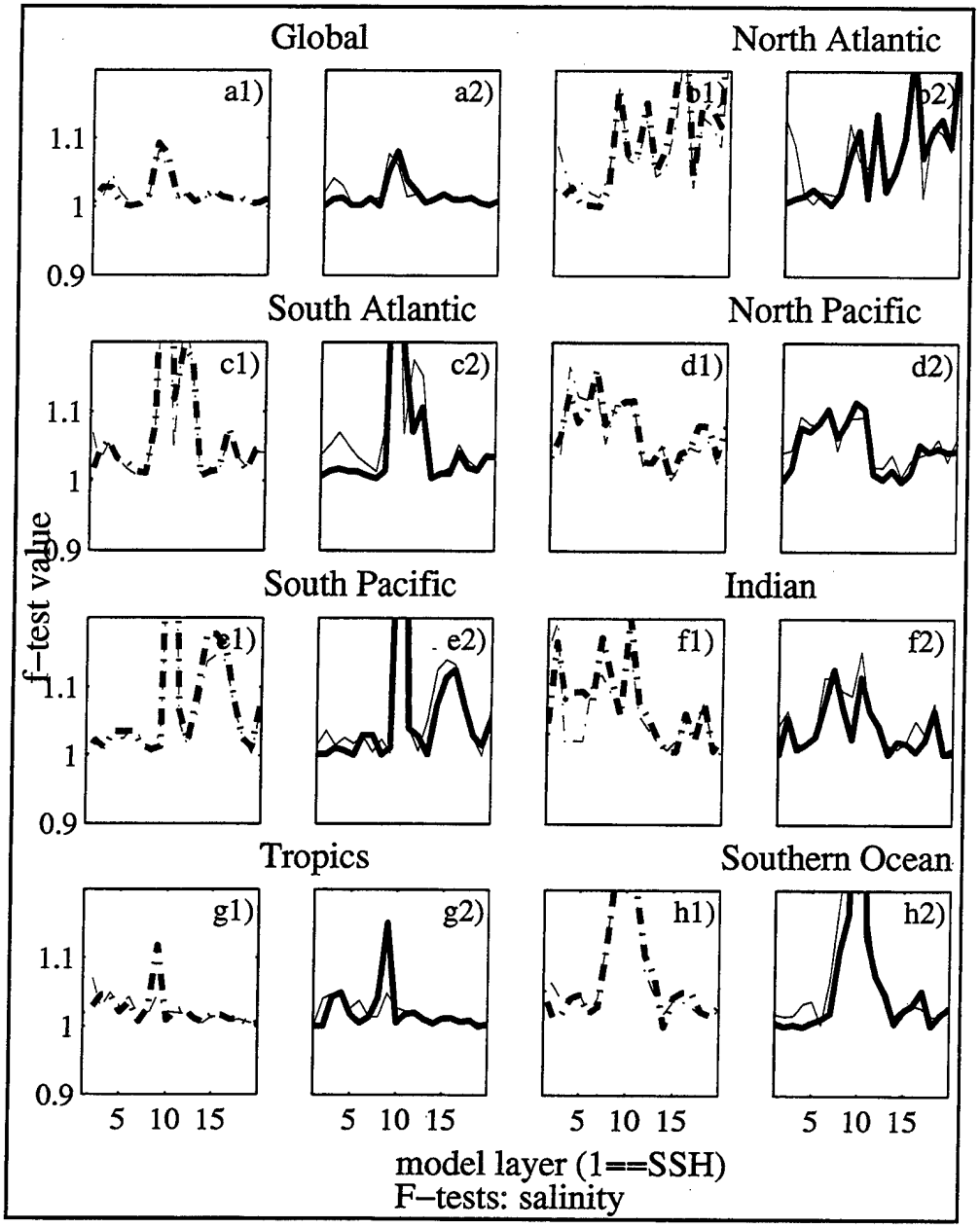


Figure 12. Same as 11, except representing F-test values computed from salinity fields. X =1->20 corresponds to model levels 1->20.

## C. POTENTIAL VORTICITY

A simple, linear definition of potential vorticity (PV), $Q = \frac{f}{\rho_o}\frac{\partial \rho}{\partial z}$, where $\rho_o$ is the average density, f is the Coriolis parameter and z is the depth, can be used to examine if changes have occurred in the density structure of the T run so it is simulating the control run rather than the I run. Q has been calculated along several density surfaces, $\sigma_0$ = 26.85, 27.0, and 27.3 with a thickness of 0.15 $kgm^{-3}$ (corresponding to how model layers are defined in an isopycnal model, *New et al.* (1995) for September 5, 1992 for both the C and T runs and for December 28, 1987 for run C, the initial field for run T. Table 1 summarizes the results by listing the RMS differences between the two September fields and between each of the September fields and the initial field for the assimilation run in the left three columns. The right three columns are comparing similar RMS differences but using fields from the early part of the experiment (January 2, 1992). RMS differences for both potential vorticity and thickness of the $\sigma$ layer are listed in the table. The table consistently shows, using the RMS differences, that late in the experiment (September 1992), the assimilation run (T) is reproducing the potential vorticity fields calculated from the control (C) run at all three $\sigma$ levels (lines 1,4, and 7, column 4) much better than early in the run (lines 1,4, and 7, column 6). The first 3 columns also show that the RMS difference values produced when comparing run T and run C to the initial field are approximately the same for both potential vorticity and layer thickness. In the right most three columns, it is the RMS differences between the field from a early point in the assimilation compared to the initial field which correspond the best. This is as expected; the early period of run T resembles the initial field, then slowly is nudged more closely to the control run.

| | FIELDS End of twin expr. | RMS diff Qe10 | RMS Δz (m) | FIELDS Begin. of twin expr. | RMS diff Qe10 | RMS Δz (m) |
|---|---|---|---|---|---|---|
| | $\sigma_0$ = **26.85** | | | $\sigma_0$ = **26.85** | | |
| 1 | Sep 5 92 (C) - Sep 5 (T) 92 | 2.41 | 35.51 | Jan 2 92(C) - Jan 02 (T) 92 | 3.92 | 55.08 |
| 2 | Dec 29 87 (I) - Sep 5 (T) 92 | 165.22 | 25.97 | Dec 29 87 (I) - Jan 2 (T) 92 | 1.76 | 22.21 |
| 3 | Dec 29 87 (I) - Sep 5 (C) 92 | 165.24 | 35.22 | Dec 29 87 (I) - Jan 2 (C) 92 | 4.07 | 55.62 |
| | $\sigma_0$ = **27.00** | | | $\sigma_0$ = **27.00** | | |
| 4 | Sep 5 92 (C) - Sep 5 (T) 92 | 1.75 | 37.99 | Jan 2 92(C) - Jan 2 (T) 92 | 3.35 | 52.94 |
| 5 | Dec 29 87 (I) - Sep 5 (T) 92 | 113.15 | 29.73 | Dec 29 87 (I) - Jan 2 (T) 92 | 1.85 | 22.00 |
| 6 | Dec 29 87 (I) - Sep 5 (C) 92 | 113.16 | 40.76 | Dec 29 87 (I) - Jan 2 (C) 92 | 3.57 | 53.84 |
| | $\sigma_0$ = **27.30** | | | $\sigma_0$ = **27.30** | | |
| 7 | Sep 5 (C) - Sep 5 (T) 92 | 1.69 | 33.63 | Jan 2 (C) - Jan 2 (T) 92 | 3.11 | 43.26 |
| 8 | Dec 29 87 (I) - Sep 5 (T) 92 | 2.89 | 30.00 | Dec 29 87 (I) - Jan 2 (T) 92 | 2.22 | 19.87 |
| 9 | Dec 29 87 (I) - Sep 5 (C) 92 | 3.16 | 37.35 | Dec 29 87 (I) - Jan 2 (C) 92 | 3.00 | 43.42 |

Table 1. RMS differences in Q and layer depth (Δz) for various pairs of days of the model runs. September 5, 1992 is near the end of the twin experiment. January 2, 1992 is near the beginning of the experiment. December 29, 1987 is the field used to initialize the assimilation run of the twin experiment.

Figures 13, 14, and 15 a-c give plan views of the potential vorticity on the $\sigma_0$=27.0 isopycnal while d and e show the differences between the September 5, 1992 C and T fields and the September fields from the T run and the initial field near Dec. 29, 1995. The changes in PV for the different runs (C and T) over the North Atlantic (Figure 13) are most obvious in the very north of the model domain. The 27.0 isopycnal surface in the T run (Figure 13a) no longer outcrops along a diagonal from 45°N, 300°E to 55°N, 350°E as seen in the initial field (Figure 13c), but now is shown to have a similar PV value as for the C run (Figure 13b). Similarly, the lowest PV values along this isopycnal are similar to the C run, rather than the initial run. Figure 14 shows a similar view of the North Pacific. The band of high PV starting at about 40°N,160°E and continuing to about 190°E and spreading southwards is more representative of the C run (Figure 14b) than of the initial field (Figure

14c). In the tropical Pacific (Figure 15), the PV remains similar between the three runs, except in the eastern Pacific, where blobs of higher PV water are found in the T run similar to those seen in the C run.

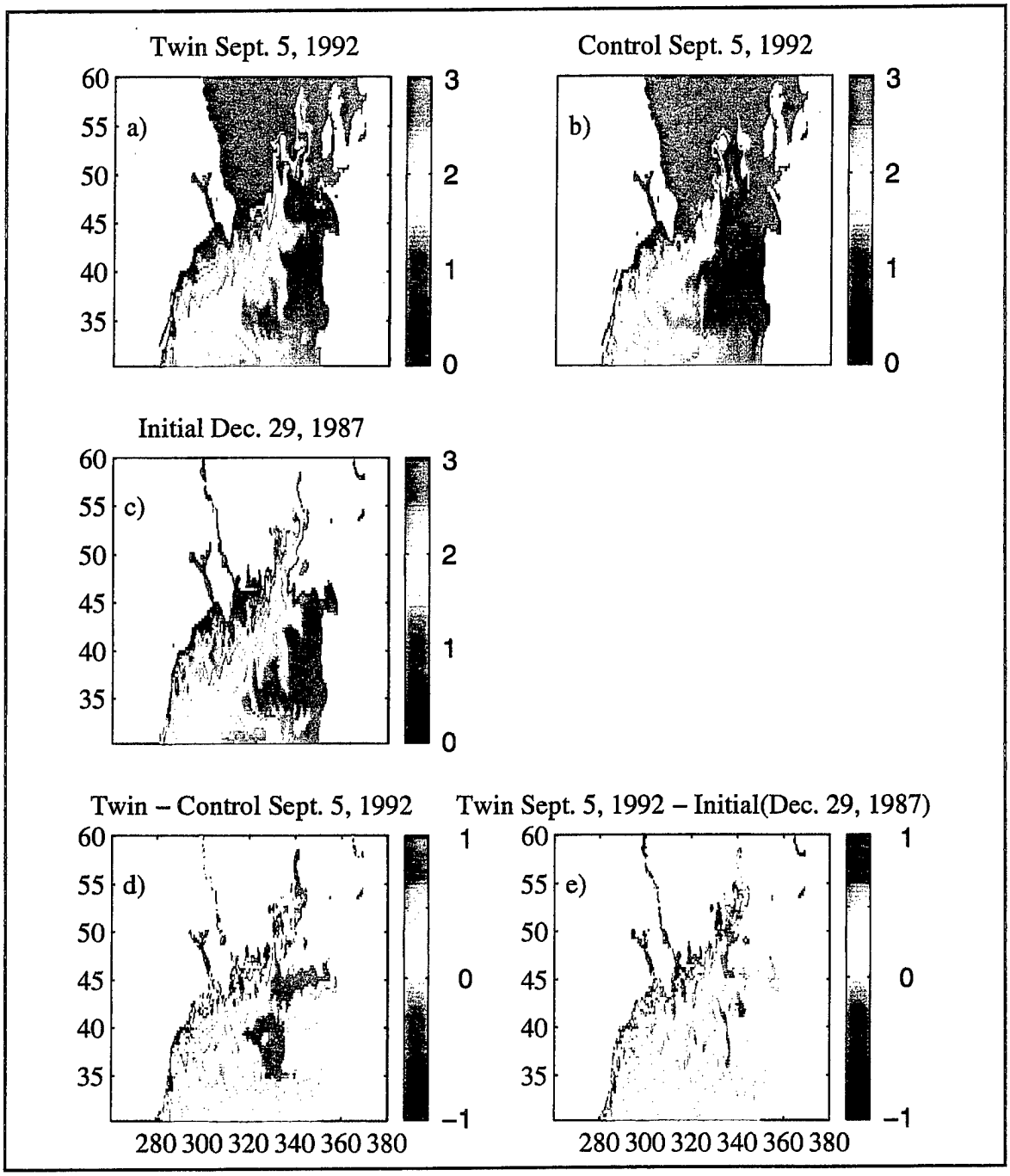


Figure 13. PV on isopycnal surface = 27.0 in the North Atlantic. a) PV calculated from T run, day Sept.5, 1992. b) same but for C run, c) Initial field from T run. d) difference between T and C PV fields. e) difference between T and I PV fields. Units are <Qe10>.

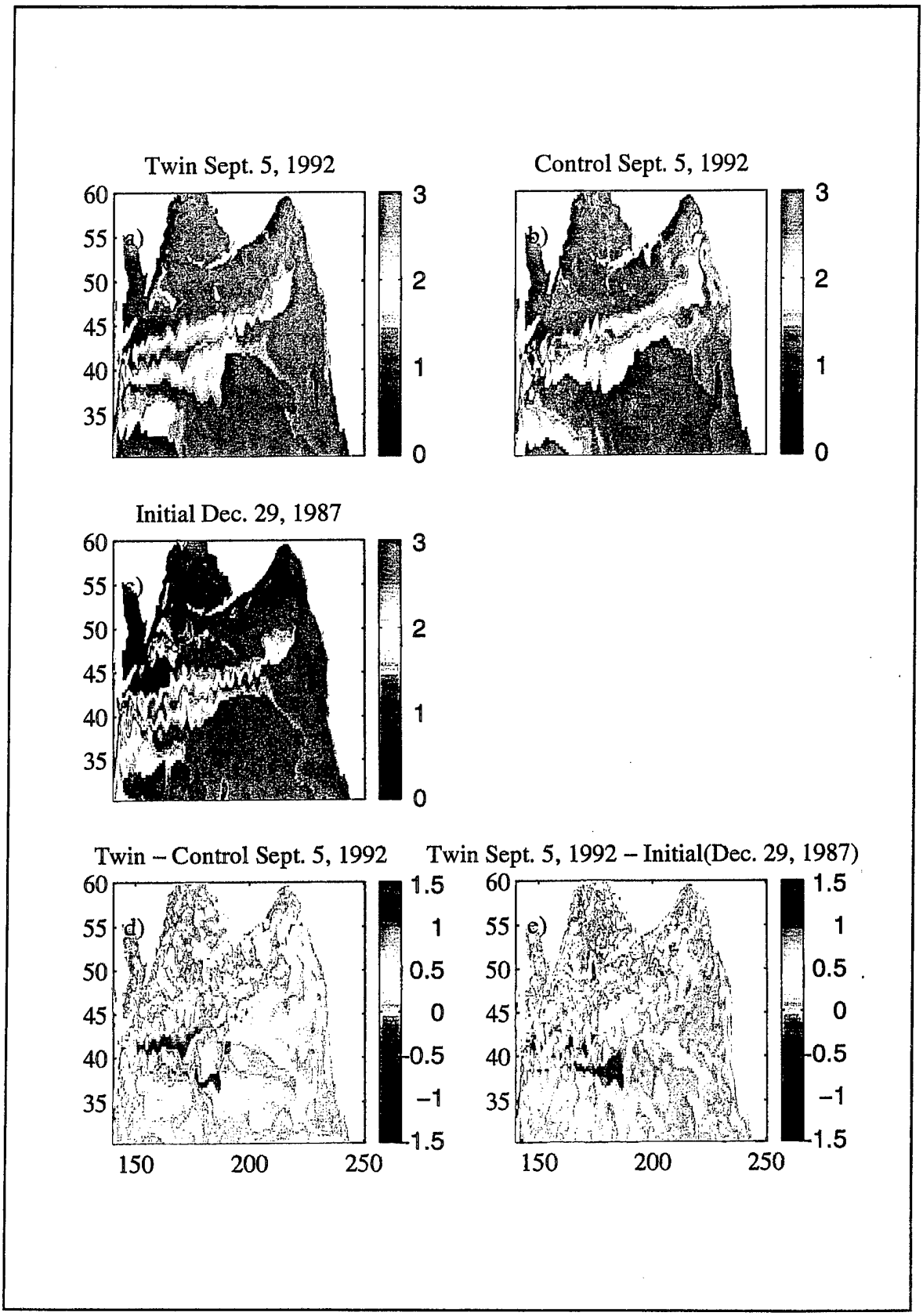


Figure 14. Same as Figure 13, except for North Pacific.

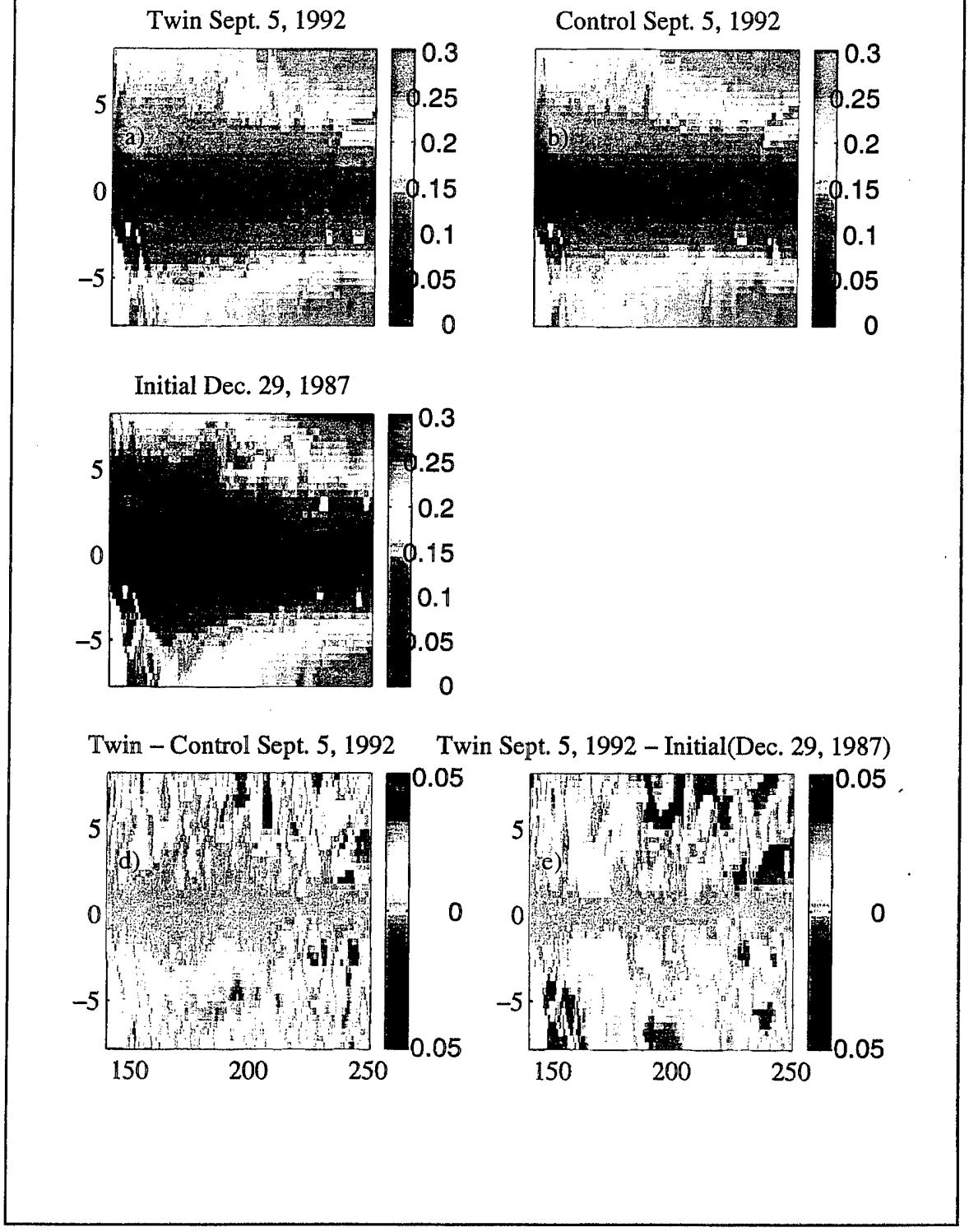


Figure 15. Same as Figure 13, expect for tropical Pacific.

# D. REGIONAL ANALYSIS

## 1. Southern Ocean

Three meridional sections across the Southern Ocean have been examined. From east to west, the sections taken are across the full width of the Southern Ocean at 20°E (South Africa), 150°E (Australia), and at 290°E (Drake Passage). The meridional sections extend from the model's southern point at 75°S to 35°S. Volume transports across the three sections are listed in Table 2, calculated from instaneous fields from Sept. 1992 and the initial field from 1988.

| Section | Initial | Control | Twin |
|---|---|---|---|
| S. Africa 20°E | 162 SV | 160 SV | 167 SV |
| Australia 150°E | 164 SV | 166 SV | 172 SV |
| Drake 290°E | 166 SV | 161 SV | 167 SV |

Table 2. Volume transports across three zonal sections of the Southern Ocean at 20°, 150°, and 290°E from 75°S to 35°S. Units are in Sverdrups, 1SV = 10e6 $m^3s^{-1}$.

The mean of all the transports is 165 +/- 3.5 SV, with the highest transport values found in the twin experiment across the Australia section (172 SV). After the assimilation, the run T has produced transports higher than run C by around 6 to 7 SV for all three sections. Both have consistent values between the South Africa section and the Drake Passage. Figure 16 shows the SSH from snapshots of the model on Sept. 5, 1992 for the runs T and C and the initial run I (Dec. 29, 1987). For the Drake Passage (Figure 16c) and for the meridian south of Australia (Figure 16b) the adjustment of SSH in run T (dashed line) towards the control run (solid line) can be seen. The red line represents the relative strength of the nudging coefficient at the surface. All the differences between the initial

field (dotted lines) are not due to the assimilation of SSH. Some of the differences are due to the application of a different wind stress field. However, when changes appear consistently over a group of latitudes such as in Figure 16b between 65°S and 55°S and around 43°S, the change is mostly due to a large change in the underlying vertical structure.

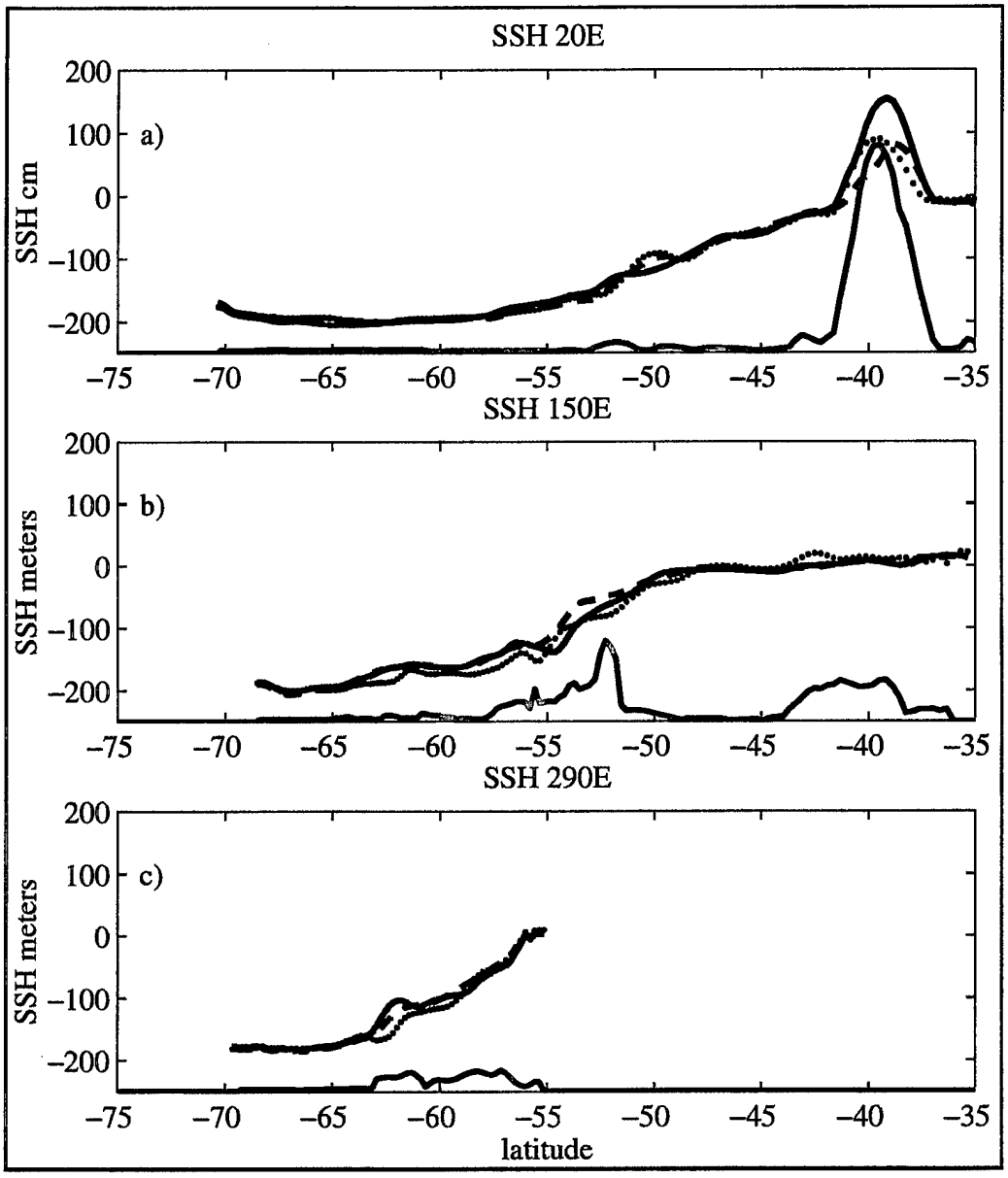


Figure 16. Meridional plots (black lines) of SSH in centimeters at 20°E, 150°E, and 290°E between 75°S and 35°S. Solid line is from C run, dashed line is from T run, and dotted line is the initial state from I. Red line is the relative weight associated with the nudging term.

Figure 17, representing the differences in density between the snapshots of run T and the initial field (I) of the three meridional sections, shows that at 150°E (Figure 17b) the water has become less dense between about layers 3 and 12 (60 meters to 1000 meters, approximately) between 65° and 55°S, leading to an increase in the height field in the assimilation run (dashed line in Figure 16b), similar to the SSH of the control run (solid line, in Figure 16b). In contrast, between 43°S and 35°S, the density has increased with the assimilation process and thus, the SSH signal is reduced.

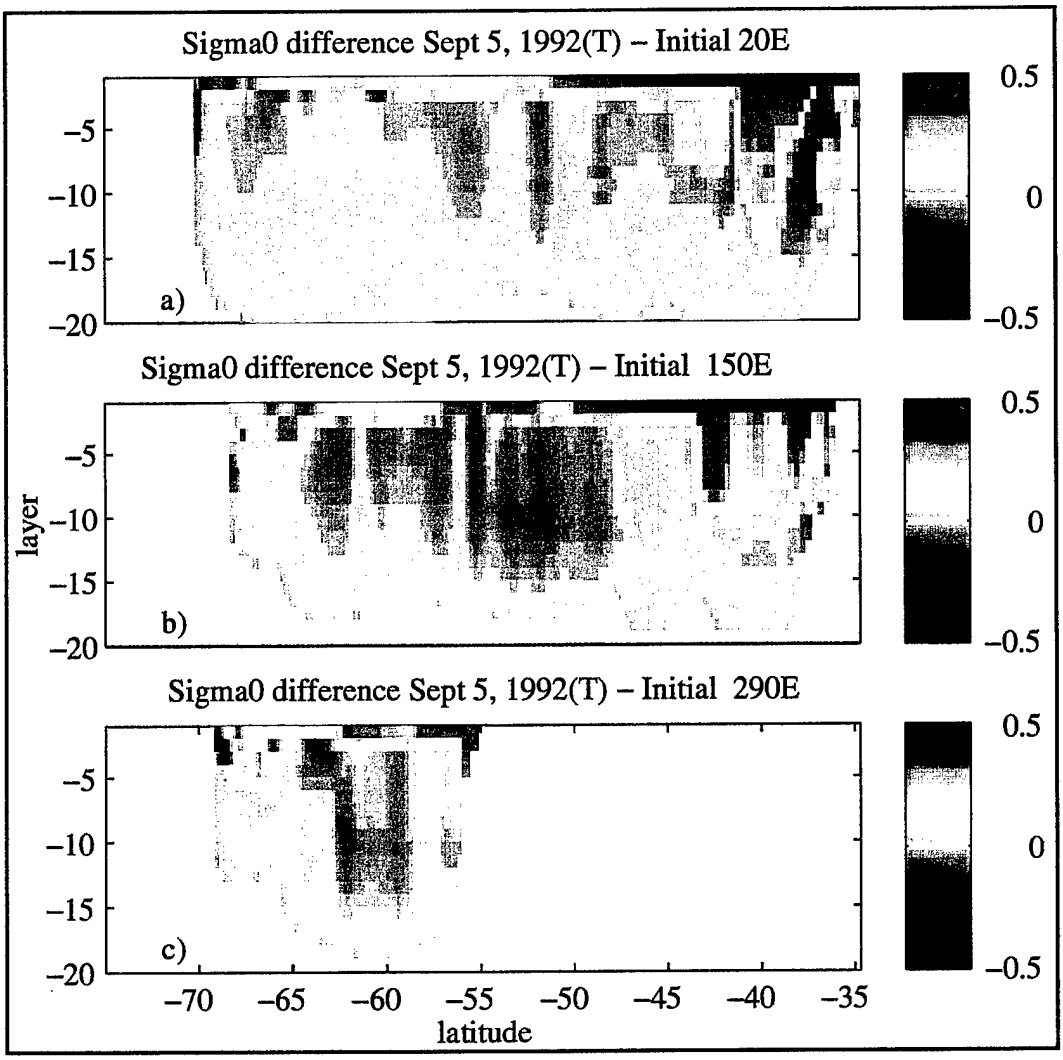


Figure 17. Plots of differences in $\sigma_0$between Sept. 5, 1992 T field and Initial field along the meridians at a) 20°E, b) 150°E, and c) 290°E between 75°S and 35°S. Scale in units of $kgm^{-3}$. X axis is model layer.

At 20°E (Figure 16a) , the large SSH signal produced in the Aguhlas retroflection region at -40°S, is not being adjusted as expected by the assimilation. Figure 18 shows the density differences between the T and C fields for Sept. 5, 1992. For the meridional section in density at 20°S (Figure 18a), the T run is substantially denser than run C (and thus, the SSH signal will be lower). Why the assimilation is not adjusting its deeper layers to the correct density can be found by examining the functionals (see Eq.2.5 and 2.6) which relate the surface heights to subsurface values. Figure 19 (temperature) and Figure 20 (salinity) show the functionals for the three meridians across the Southern Ocean. At

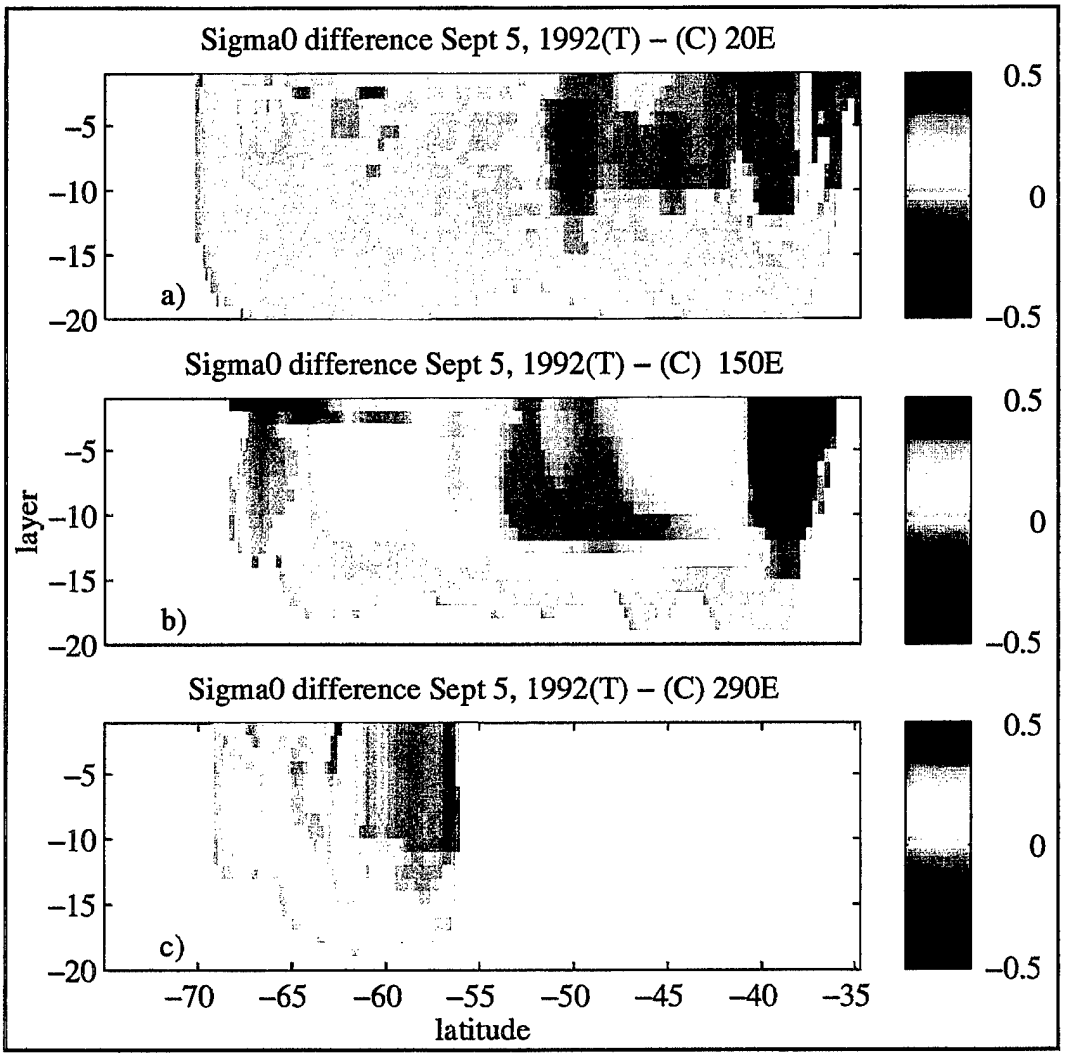


Figure 18. Same as Figure 17, except for differences in $\sigma_0$ between Sept. 5, 1992 T and C fields.

approximately 40°S in Figure 19a, the functional for both temperature and salinity is much smaller than the values for the function at the same location in Figure 19b (for 150°W, south of Australia). This would suggest that it is the adjustment of the deep layers that is making the most change in the sea surface signal at these locations.

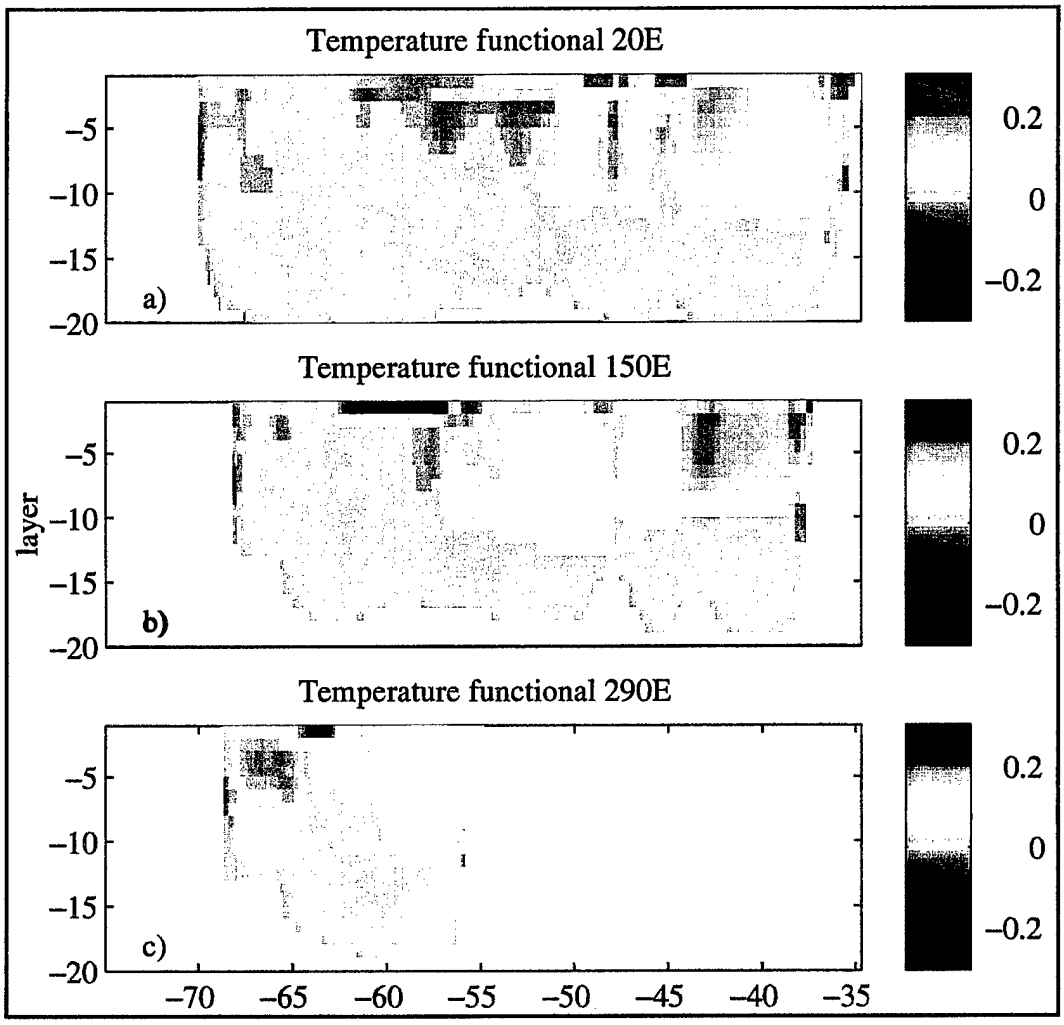


Figure 19. Meridional plots of temperature functional at 20°E, 150°E, and 290°E between 75°S and 35°S. Y axis is model layer. Scale is in units of $C°m^{-1}$.

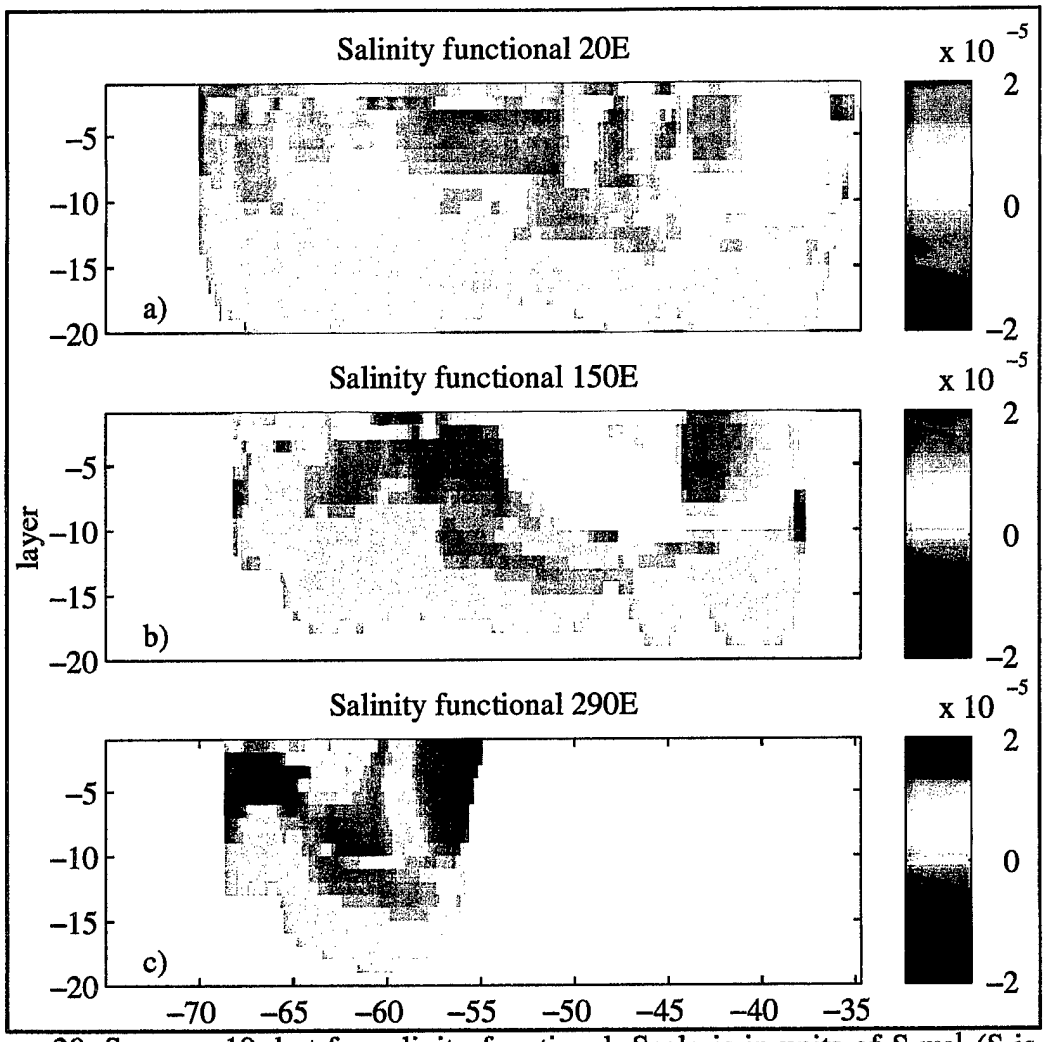

Figure 20. Same as 19, but for salinity functional. Scale is in units of S $m^{-1}$ (S is also defined as a practical salinity scale, PSS).

## 2. Tropical Ocean

A meridional section along 156°E from 5°S to 5°N (Figure 21a-j) shows the U velocity component for three fields, Sept. 1992 T run (21a) and C (21b) run and the initial field (21c). Figures 21d-f , g-i are the corresponding temperature and salinity fields. The assimilation has adjusted the temperature field only slightly, while the salinity field is much fresher in both the T and C simulations at a depth of about 80 to 200 meters (layers 4-7). This freshening is reflected at the sea surface, near -4°S and 2°N, (Figure 21j) with an increase in the SSH value in the T and C fields (dashed and solid lines) over the value

from the initial field, I (dotted line). The red line on Figure 21j shows the relative strength of the nudging coefficient in this region. The assimilation has removed the eastward flow at 4°S, adjusting the flow in the T run (Figure 21a) towards the C run (Figure 21b).

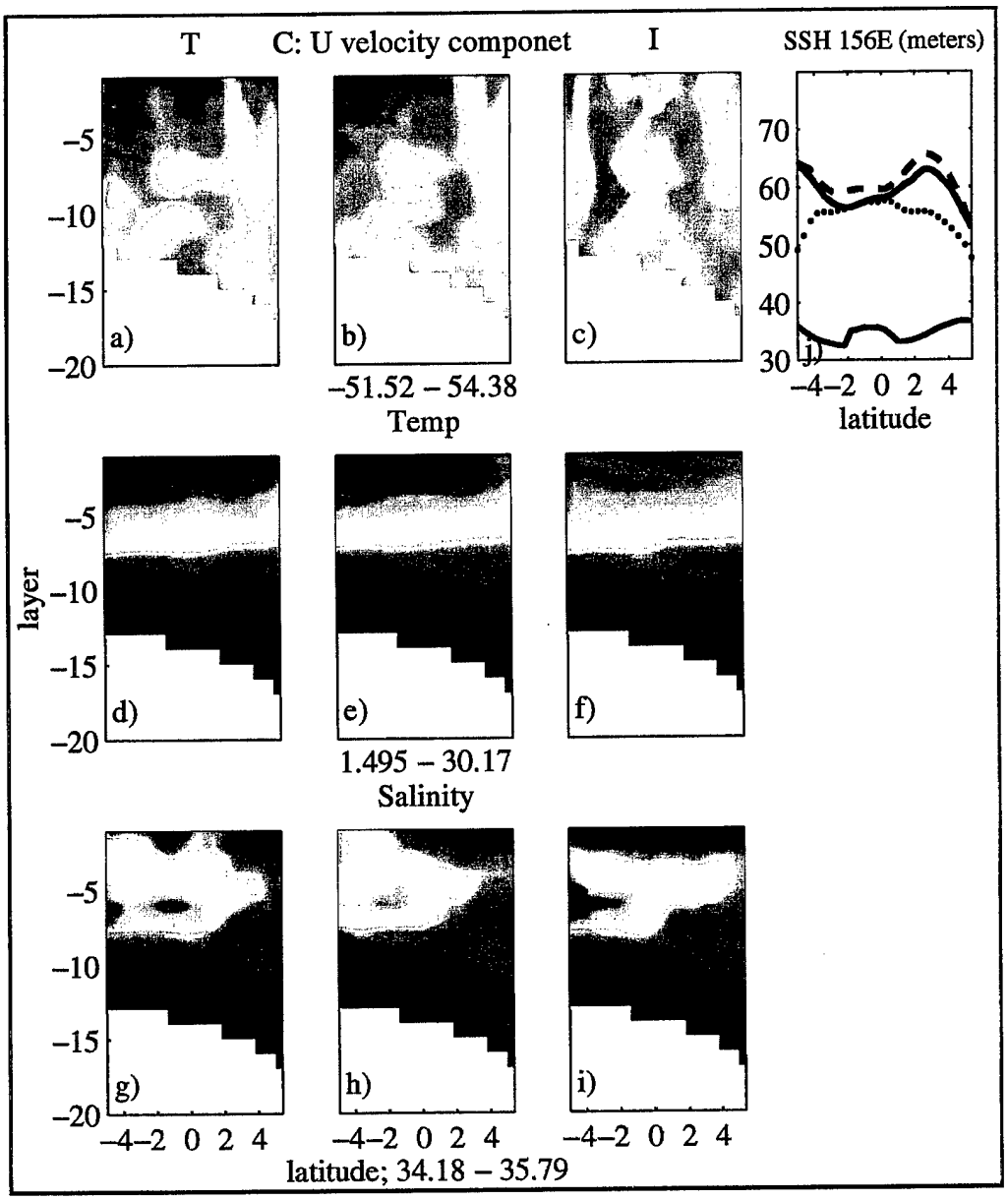


Figure 21. Meridional section for 5°S to 5°N at 156°E of three model prognostic variables from the fields representing Sept. 5, 1992 T and C runs and the I field from December 28, 1987. The top row (a-c) are the zonal velocities, the middle row( d-f) are the temperatures, and the bottom row (g-i) are the salinities. SSH is plot in (j), with the solid blank line from Sept. 5, 1992 of the C run, the dashed line from Sept. 5, 1992 of the T run, and the dotted line from the I field. The red line is the representative nudging term.

### 3. North Atlantic Ocean

The statistical tests calculated for this region (Figures 9b-2, 10b-2, 11b-2, and 12b-2) showed that the fields (T and S) are very similar. Plan views of the means of the variables T, S, U, V, and SSH also show little change (Figures 22 and 23, layers 1 and 6). The December 92 map of standard deviations for run C (Figure 24 (layer 1) and 25 (layer 6), row A) shows a much reduced variability of that over the initial fields (Figure 24, row C). With the assimilation, the variance is reduced (Figure 24, row B), unfortunately, the assimilation has over compensated for the reduction of SSH from the T run to the C run. It can only be speculated that in the adjustment process, the model needs a higher temporal sampling rate to include these smaller scale features. This is much more apparent in the surface layer (Figure 24) than at a depth of around 160m (Figure 25).

### 4. Indian Ocean

An interesting adjustment occurred in the assimilation run in the tropical region of the Indian Ocean. Plan views have been created of the various fields from the December 1992 C and T runs and from December of 1988 of the C run, depicting dramatic differences (Figure 26). This figure shows the small area (20° x 20°) centered at 5°S, 90°E in the Indian ocean, with the top row, A, from the assimilation run, T; the middle row, B, from the control run C; and the last row, D, showing the fields from Dec. of 1988. This last row is provided to show the state of the simulated ocean, if starting from the same field which initialized the T run, but using winds from 1988, instead of 1992. This area corresponds to one of the boxes on Figure 6a and b, displaying the vertical nudging functionals. Because the wind forcing (Figure 26j and 26o) is not the same between 1988 and 1992, a direct comparison can not be made as to how much of the change seen in

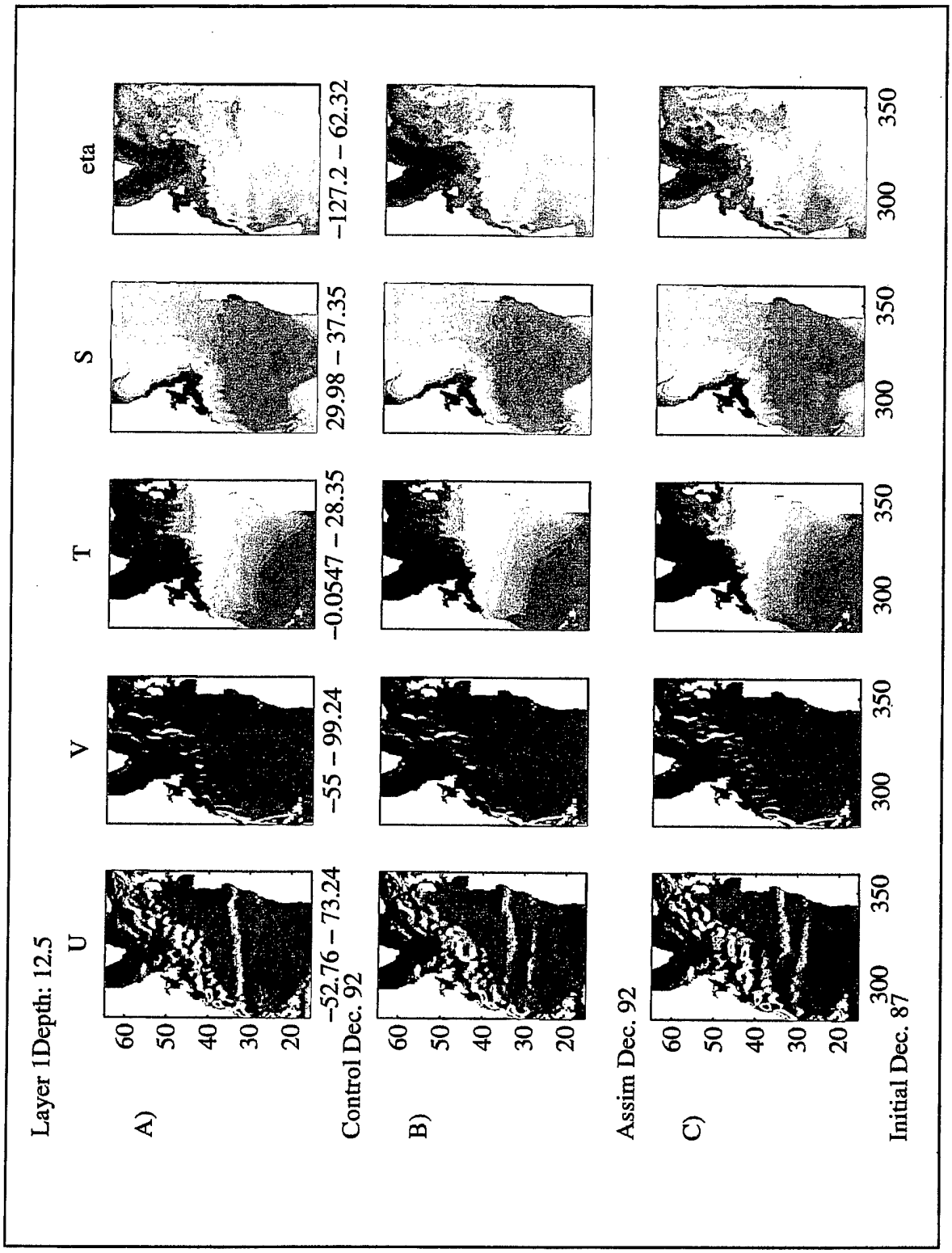


Figure 22. Plan views of monthly averaged u,v,T and S at 12.5 meters and SSH for the North Atlantic. The A row is from the Dec. 1992 C field, the B row is from the Dec. 1992 T field, and row C is the initial or I field (Dec. 28, 1987). The range of the scale for each variable, u,v,T,S, SSH is listed below the image of row A.

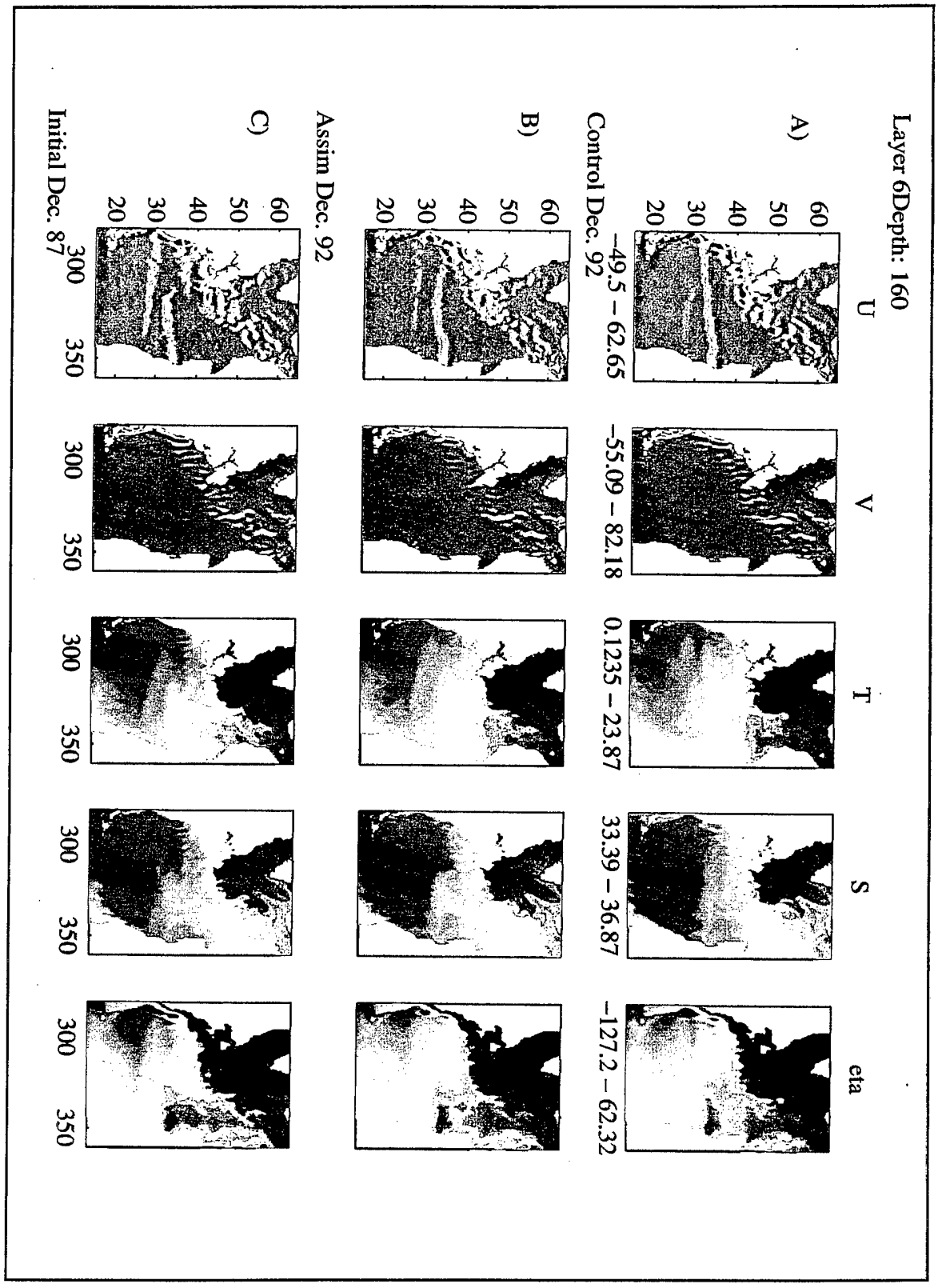


Figure 23. Same as 22, except for layer 6 at 160 meters.

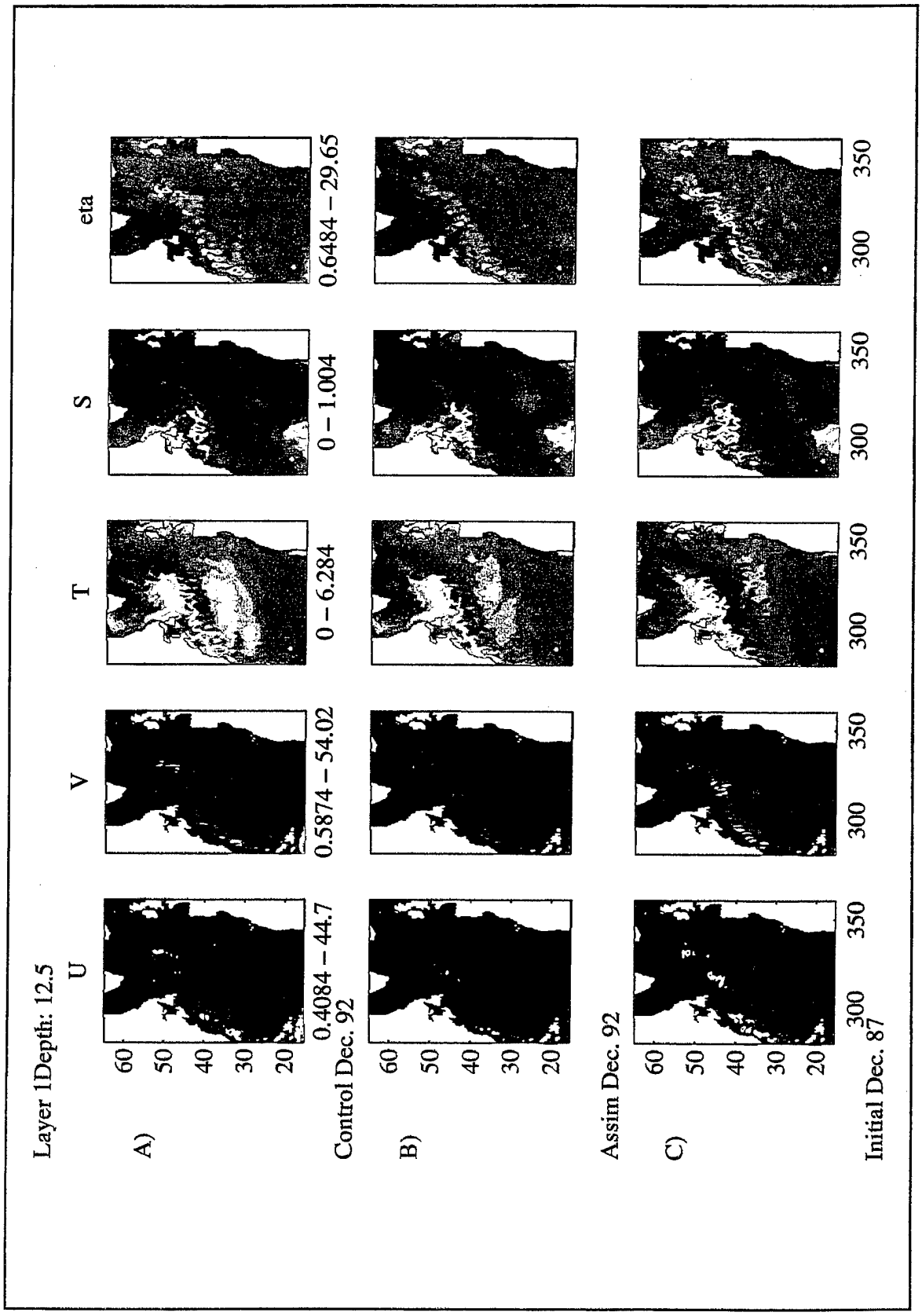


Figure 24. Same as 22, except for standard deviations.

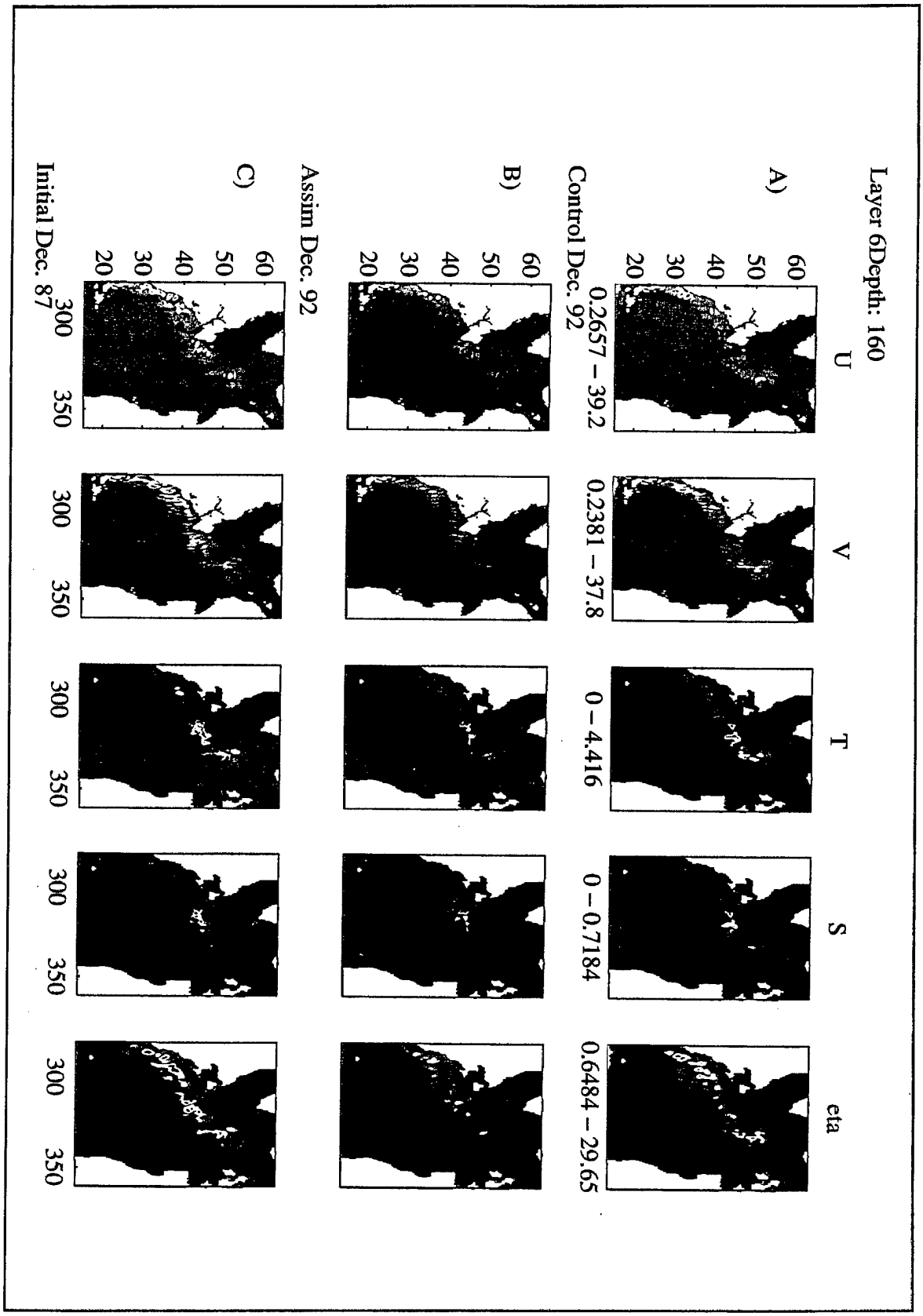


Figure 25. Same as 23, except for standard deviations.

Figure 26- row A, is due to assimilation and how much is due to the difference in wind forcing. It is thought that a large portion of the change at the surface is due to the wind forcing because the nudging value for the top layer temperature in this region is relatively small. But changes are also seen at depth in this area (Figure 27, similar in layout as in Figure 26, but at a depth of about 600m), and the comparison of the fields of the control run for the same month (Figure 26, row B) are quite good in this region. In the temperature field, note the intrusion of a large amount of cold water centered at -5°S, 85°E in Figure 26, row A, corresponding directly to a similar field in the control run (Figure 26, row B). Associated with this change in the temperature field are distinct changes in both the u and v velocity fields. At 600m (Figure 27), similar adjustments have been made in the T run (row A) to adjust the fields towards the control, run C (row B).

## D. CONCLUSIONS

The twin experiment has shown that the assimilation process is adjusting fields both at the surface (SSH) and subsurface (temperature and salinity) towards the control simulation. Comparisons calculated from indirect estimates, such as those shown for potential vorticity, also lead to the conclusion that the model, if somewhat slowly, is adjusting itself towards the control. Four things have been brought to light in the twin experiment: 1) the T run has moved the model simulated fields towards what is observed in the control run and the next step is to run an experiment with real data; 2) most likely, there is a need for a stronger nudging term in the vertical in some regions; 3) higher temporal sampling may allow for better inclusion of mesoscale features; and 4) a longer period is needed to see the effect of the assimilation process when the nudging coefficient is as defined in this experiment.

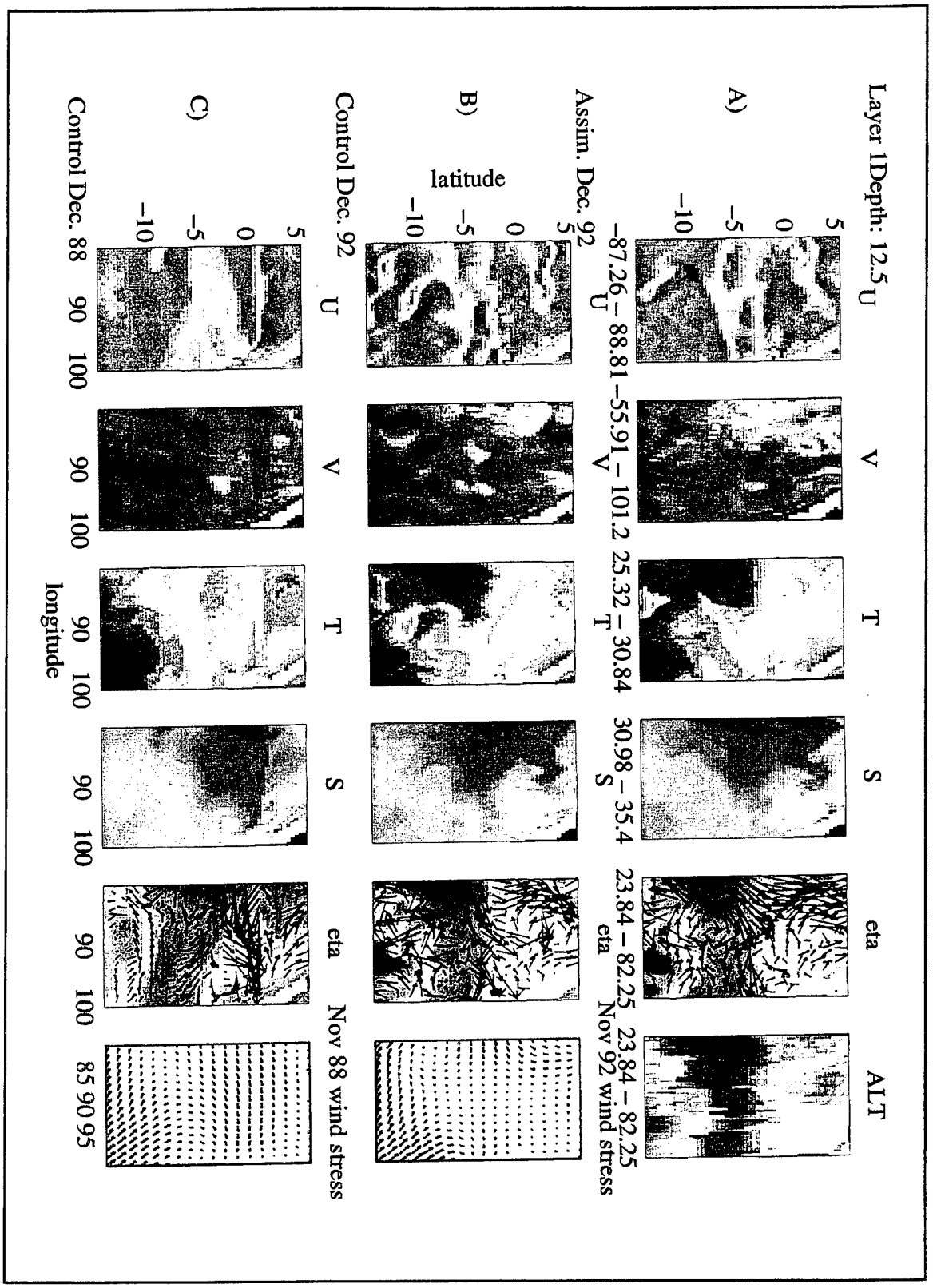


Figure 26. Same as 22, except represent a 20°x20° box centered at 5°S, 90°E in the Indian Ocean. Additional column on right represents in row A, assimilation data; row B, wind field from Nov 92; and row C, wind field for I field, Nov. 88.

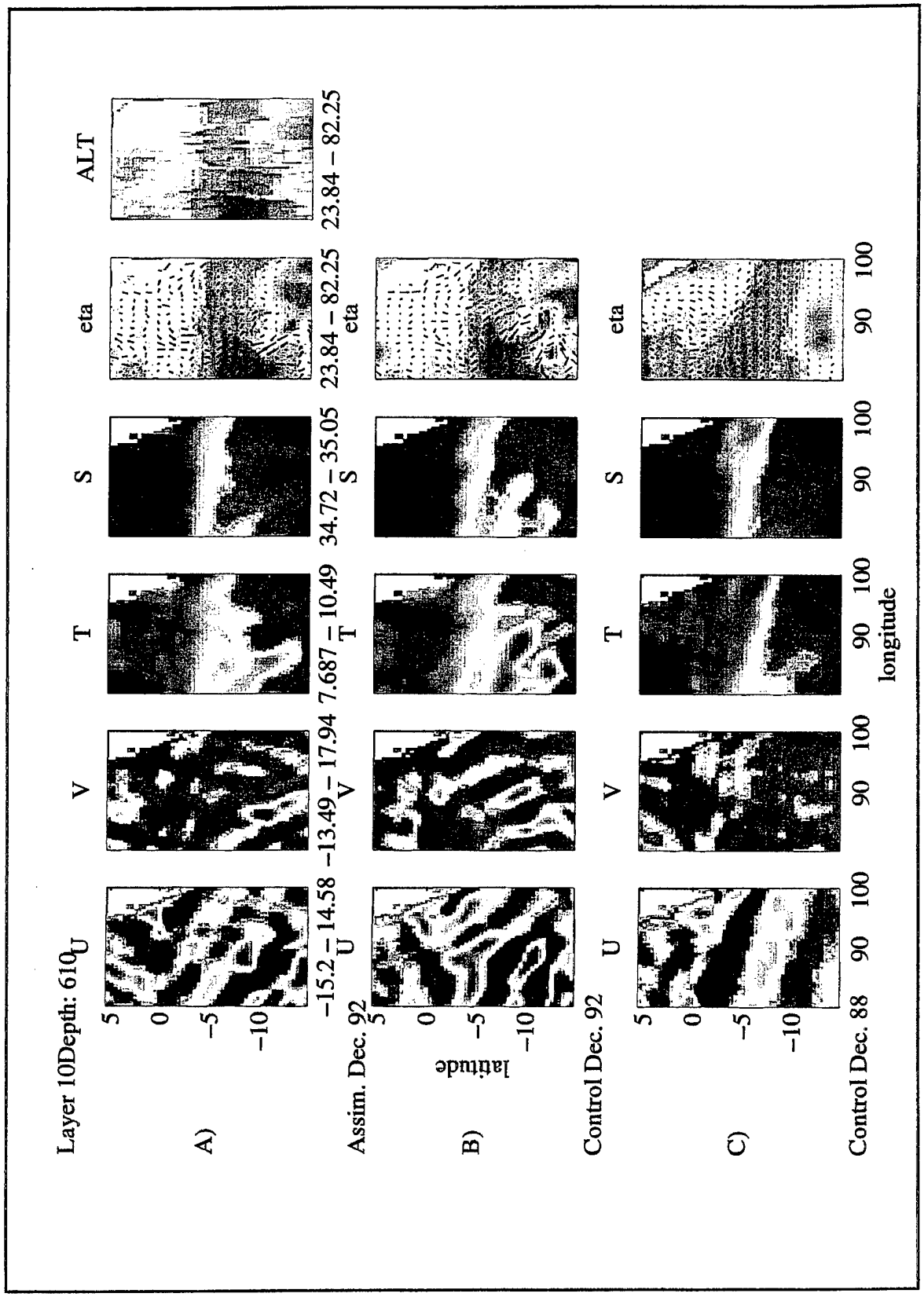


Figure 27. Same 26, except for layer 10 at 610 meters.

# IV. ASSIMILATION OF ERS-1 AND T/P ALTIMETER DATA

One goal in assimilating any observational data into a model is to correct the model towards what has actually occured. Then, once the model is correctly simulating the past and present, it can be analyzed as a 4-D dataset or be used to predict, with some accuracy, what the future state of a system may be. This has been the basic mode of operation for many years with weather forecasting. Although research in the area of assimilating observational data into ocean models has been active for twenty years or so, it is only recently that global data sets for the ocean with adequate temporal and spatial resolution for assimilation have been available. These data sets, for the most part, are created from measurements made from space, either of sea surface height (SSH) using altimeters or sea surface temperature (SST) using infrared instruments. For much smaller regions, instruments have been placed in the ocean for making long term measurements of the state of the ocean which are then used to adjust a model's fields towards reality. A good example of this type of experiment is the Tropical Atmosphere-Ocean (TAO) array set up in the tropical Pacific as part of the Tropical Ocean Global Atmosphere (TOGA) program (*Hayes, et al.* 1991). Extensive time series of current velocity, temperature and salinity have been collected for this data set and various researchers (e.g. *Carton et al.* 1996) have used the data to adjust tropical ocean models towards reality.

On the global scale, the only complete data sets are those gathered from satellites. And, of the satellite data that can be used to adjust models, the best and most complete are those gathered by the altimeters, Topex/Poseidon (T/P) and ERS-1 and 2. SST measurements can not often be made because of cloud cover, thereby producing a somewhat patchy data set. There exists no global data set of temporally varying subsurface measurements on the scale of the POCM model, only climatological sets which are created by averaging observations and interpolating observations over many years. Thus, this

initial experiment of attempting to assimilate observational data into a high resolution global model is limited to the use of satellite altimeter data gathered from both ERS-1 and T/P satellites and subsurface information from climatological (*Levitus 94*) data sets.

The rest of this thesis explains the assimilation process used with observational data and discusses the results of the experiment in light of three things. The first is whether the model's ocean circulation pattern is closer to the observations. The evaluation includes the use of previously described statistical tests to identify regions which have changed the most. In addition, dynamical balances are examined to determine if the assimilation process has changed the basic model dynamical properties. Finally, a comparison is made between the model fields from the control run (run C), with no assimilation, and from the model run with assimilation (run A) to determine if the simulated fields have adjusted to observed fields in time and space.

Second, the question: whether assimilating both ERS-1 and T/P data or T/P data, alone, are equally effective in pushing the model towards observations; is examined in Chapter V. The two satellites have different sampling patterns both in time and space. ERS-1 repeats its ground track every 35 days while T/P samples the same bit of ocean every 10 days. The implications of these two sampling patterns will be examined by looking at differences in the statistics of the model's variables of SSH, temperature, and salinity.

Third and last, in Chapter VI, the adjustments to the model through the use of an assimilation process are examined in an attempt to understand the underlying deficiencies in the model simulation without any assimilation. For example, can the model reproduce the observed ocean with just a change in its initial conditions or are there some regions which will always be unpredictable? Is it important to simulate these turbulent features (such as Gulf Stream eddies) correctly or are statistically consistent fields over some temporal and spatial period accurate enough? This understanding will give a focus to why assimilation should be performed or not in attempting to answer the question: "what additional

information is gained about the global ocean's circulation that was not known before ?".

The basic assimilation experiment is described next. Discussions of the quantitative and qualitative results of the assimilation of ERS-1 and T/P data into a high resolution primitive equation global ocean model complete this chapter. The chapter is then followed by two chapters which discuss items two and three above.

# A. SETUP FOR THE ASSIMILATION OF ERS-1 AND T/P DATA

## 1. Description of the Assimilation Experiment

The second experiment conducted for this thesis consisted of assimilating actual observed SSH anomalies as measured by two altimeters, the European ERS-1 satellite and the US/French T/P satellite. The experiment consisted of running the POCM, Semtner/Chervin model, with the inclusion of assimilation code, for the period from mid-1992 through the end of 1994. ERS-1 and T/P data were used jointly as observational data up to the end of 1993. After this time, ERS-1 was placed in an orbit with a temporal sampling period (168 day repeat), not conducive for use as an effective assimilation data set and only T/P is used for the observational field. A control run exists for the same period in which no assimilation has been performed, known as the POCM_4B model run and described in *Stammer et al.* (1996). The surface forcing used by both the POCM_4B run (C) and for the assimilation run (A) is the same: realistic 10m ECMWF wind stresses for the period 1992-1994 and monthly heat flux climatology described in *Barnier et al.* (1994). Both model runs, with and without assimilation, were performed at the National Center for Atmospheric Research (NCAR) on a Cray Y-MP, 8 processor computer. Although the assimilation period lasted from 1992 through 1994, the evaluation of the model output uses only the two year period spanning 1993 through 1994, thus eliminating some of the

adjustments the model is making initially to the model fields.

## 2. Handling of Altimeter Data

The altimeter data for the assimilation experiment is from the French AVISO data set (*Le Traon et al.* 1995) which was corrected for errors in the estimate of the ERS-1 satellite orbit through the use of minimizing the distance between points (in time and space) sampled both by T/P and ERS-1 (*i.e.* cross-over analysis). These data cover the period from Oct. 6, 1992 through December 23, 1993 (T/P cycles 6-18). At that time, ERS-1 was in a 35 day repeat orbit and T/P has an established orbit of a 10 day repeat cycle. Atmospheric conditions have been corrected for in both data sets as described in Chapter I; and the tidal signal has been removed through the use of the empirical model, CSR 3.0 (*Eanes and Bettadpur*, 1995).

After the corrections where made to the along track altimeter data and a mean over the time period for the instrument was removed, the data were separated into files containing SSH anomalies for each day. These daily files, containing both ERS-1 and T/P data were then interpolated to the model's 1/4° mercator grid. If two satellite samplings occurred at the same point for the same day, the average of the two points was used.

The earth's geoid is not known to the spatial resolution of the model, thus the altimeter SSH measurements are only the deviations of SSH from the 2 year temporal mean of SSH at a point (known as the SSH anomaly). But in the assimilation process, the total SSH signal is needed for the adjustment of the model to an observation. Thus, a SSH mean field needs to be added to the altimeter SSH anomaly values. Several different means can be used. One is a mean that is determined for *in situ* hydrographic data and another one would be an estimate of mean sea level from altimetry itself (e.g. *Rapp et al.* 1996). A hydrographic mean is not easily understood because of the assumptions that have been used for determining a level of no motion. The use of an estimate made from altimetry is

good only to scales on the order of 2000 km, much larger than the model's grid size. *Rapp et al.* showed that the altimetric mean at these long wave lengths compared well to the POCM_4B model, therefore the SSH mean from a previous run of the model (POCM_4A, an average of three years, 1987 through 1989) will be used as an estimate of the mean SSH. The use of a mean which is not the mean of the control run was done to examine how a somewhat different mean SSH field is handled by the assimilation process. A test model run which used the mean SSH field from the control run was also conducted for 1993. The analysis is contained in the appendix. The two mean fields have a global difference in their mean of 1.9 cm +/- 7.8 cm. The mean SSH (<SSH>) field added to the altimetric values is shown in Figure 28a with the mean SSH from the C run for years 1992 through 1994 (corresponding to the assimilation period) shown in Figure 28b.

The assimilation process updates the altimeter observation field each day. If a new observation appears at a grid point, it is given an associated temporal weight of one. For all the observations which are not updated from the newly read daily observations file, the weighting factor associated with an observation is increased by one day, up to a maximum of 30 days.

### 3. Associated Vertical Relationships and Nudging Coefficients

Next, SSH observations need to be associated with the vertical structure of temperature and salinity. The temperature and salinity functions which relate SSH to subsurface values (Equations 2.5 and 2.6) are created as described below for this second experiment. Monthly maps of joint ERS-1 and T/P SSH fields (including the SSH model mean) are created from the joint AVISO data set. A 5x5 point smoother is then applied to each monthly SSH field to remove very high wave number features which do not appear in the temperature and salinity data set used for forming the functionals. The subsurface fields of temperature and salinity used are from the monthly climatological fields of

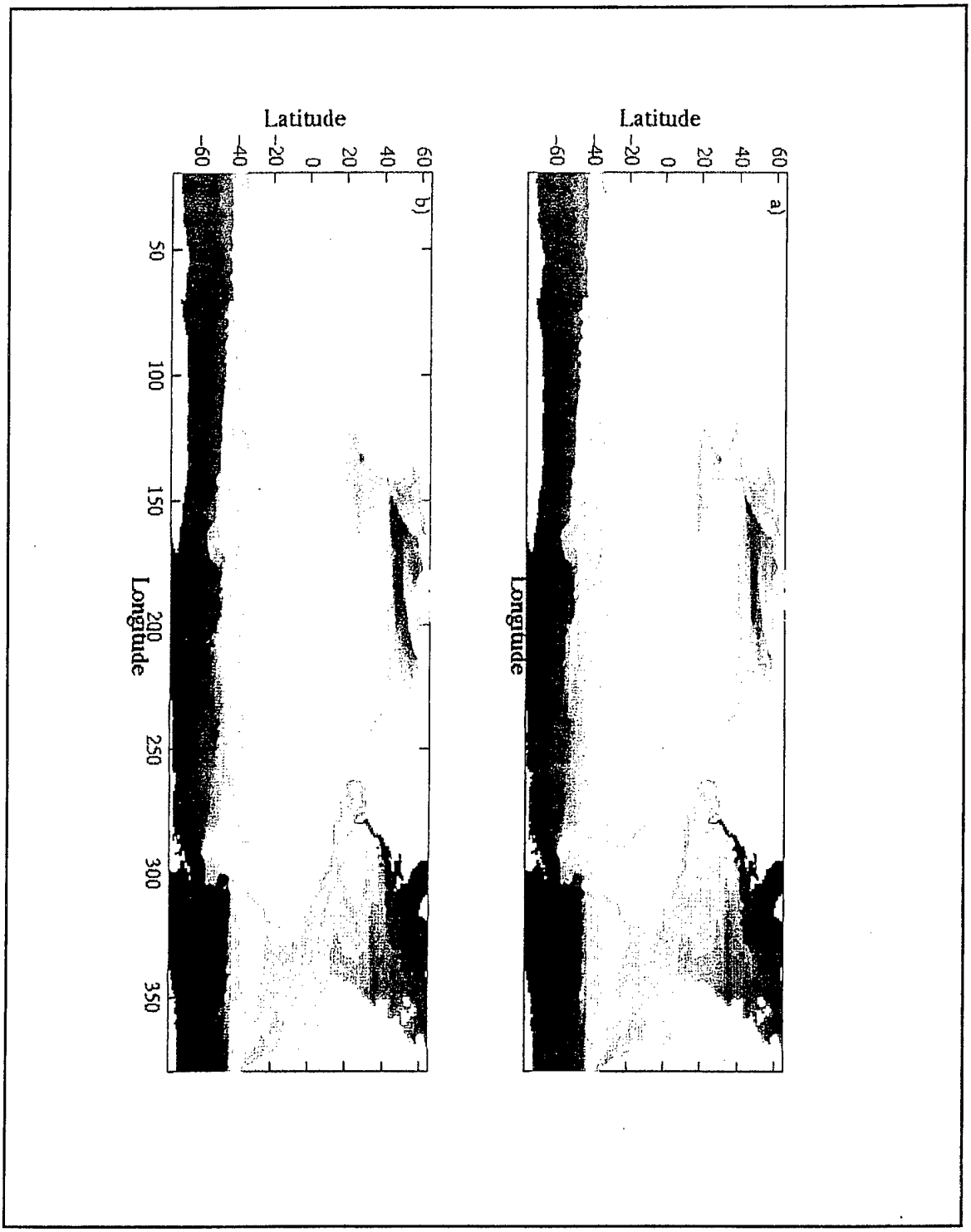


Figure 28. Mean SSH fields for a) 2-year (93/94) C run and b) 3-year (87-89) POCM_4A used for SSH mean to add to altimetric SSH anomaly observations.

temperature and salinity as produced by *Levitus and Boyer* (1994) and *Levitus et al.* (1994). The Levitus fields are improved from the 1982 data (*Levitus*, 1982) and should be somewhat dynamically consistent with the observational altimetric data set, since both result purely from measurements of the real ocean. The *Levitus* 94 data set is not the data set which initialized the ancestor of the current POCM_4B model (a one-half degree model, see *Semtner and Chervin*, 1992), nor is it used to keep the model close to the observed values in the boundary regions. Thus, it provides a set of observed temperatures and salinities (albeit averaged over different time and space periods ) which have not been incorporated into the model previously. The other option available would have been to use fields of temperature and salinity from a previous model run or the control period (1992-1994 of POCM_4B). It is thought that if a set of temperature and salinity data from a previous model run were used to form these functionals, the assimilation process could not be fully tested because the vertical structure would be too similar to the model run without assimilation.

Covariances computed between the monthly SSH fields and the monthly temperature and salinity fields as defined by Equations 2.5 and 2.6, respectively, are then normalized by the variance of the SSH at each grid point. Figures 29a and b are plots of the functionals for the second experiment similar to the Figure 6 for the first experiment, the twin experiment. As is seen, the functions are a somewhat smoother than the functions created for the twin experiment which used 3-day fields over a year to create the covariances.

The last field to be constructed for use in the nudging process is the field that is related to the $\varepsilon$ term in Equation 2.2. This term is the normalized variance of SSH computed from observational satellite values gridded into two degree boxes and with a 5x5 grid smoother applied. The variances are normalized by 40 $cm^2$ (chosen empirically), with any value over 1, set to 1. 40 $cm^2$ is close to the maximum variance, but allows for the elimination of the extremely high variances that occur in the Irish Sea and English Channel.

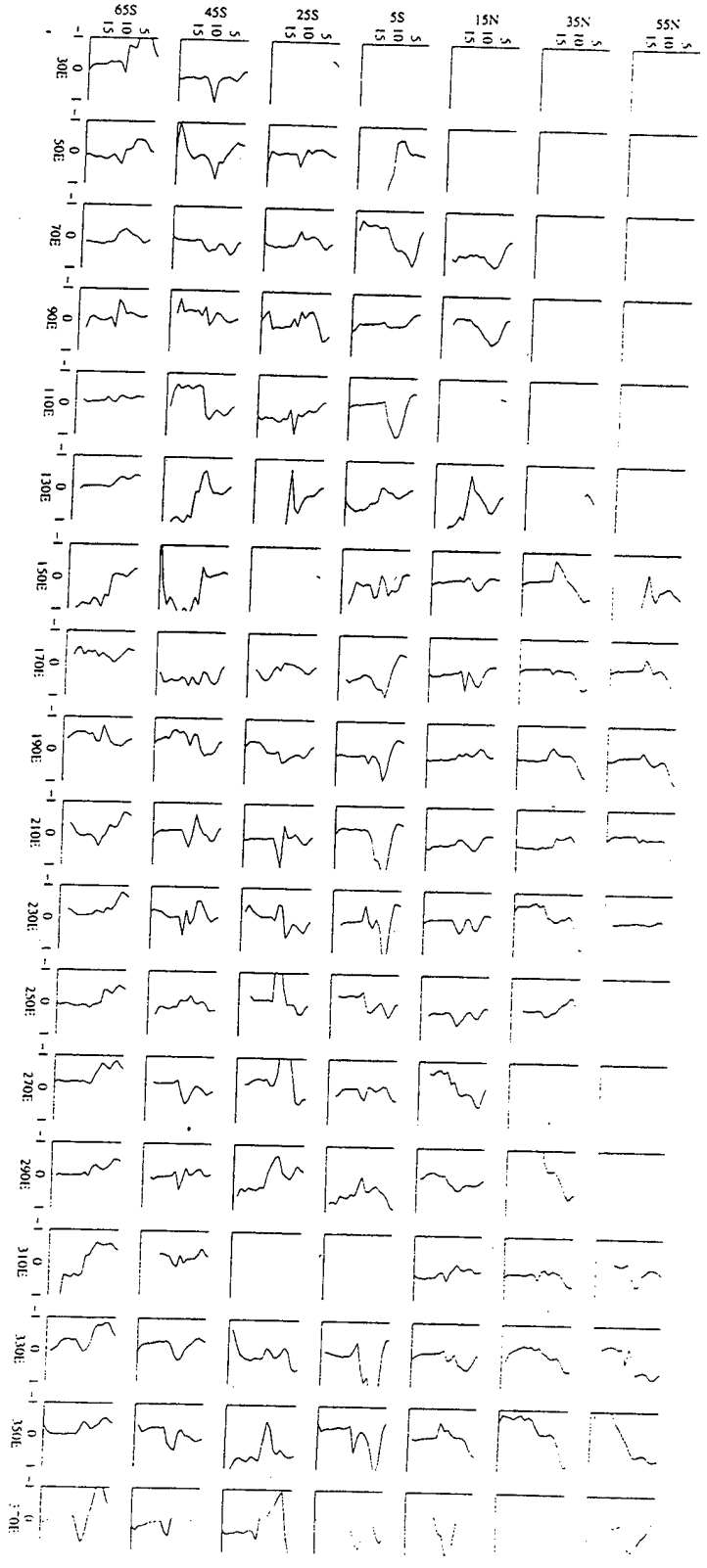


Figure 29a. Functionals as defined for run A averaged over 2°x2° boxes for temperature.

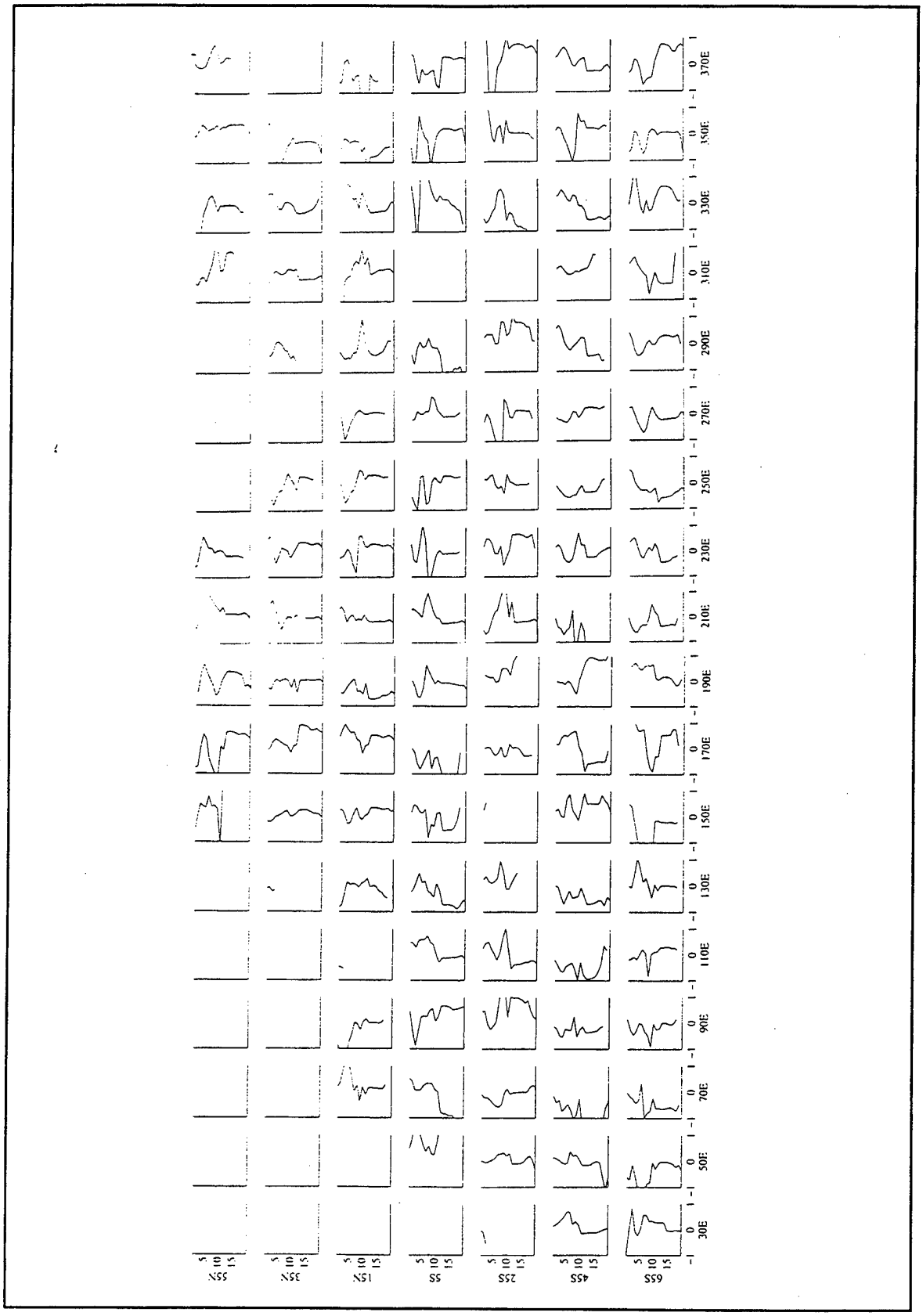

Figure 29b. Same as 29a but for salinity.

Figure 30 shows the spatial structure of the weighting field. The model is pushed very aggressively towards observed values in the region of the Kuroshio, Gulf Stream, and in parts of the Antarctic Circumpolar Current. This map could be made to reflect a much different weighting. For example, it could be all one value or created from simulated fields instead of observed fields. Keeping in mind that the assimilation with observed SSH fields over the globe at high resolution is the first to be attempted, an initial guess to define this relaxation weight field is all that is warranted at this time. Part of the evaluation process is to determine if this field should be modified.

Several model runs of the assimilation process were performed initially to produce a realistic simulation for evaluation. The underlying nudging coefficient (see Equation 2.2) basic relaxation coefficient, R0, was given several values. (In reality, $\varepsilon$ = R0 times the normalized variance of SSH, where R0 is some time reciprocal.) Determined, empirically, the R0 nudging coefficient of the temperature and salinity fields is equal to 30 days. This is directly related to having used monthly fields for the creation of the vertical fields. For the surface fields, R0 is set at a quarter of a day.

Three lines are shown on Figure 31a representing the total model energy A run (black line), the C run (blue line) and an earlier run with R0 equal to half a day (red line), while Figure 31b and c show the total rate of change in the temperature and salinity fields. Only when R0 is increased to 0.25 days (at time = 1993.75 on the red line), does the energy in the model increase. Because of the changes shown between the blue and red line near the end of 1993, the final assimilation run, run A, used R0 equal to one quarter of a day for height. It should be remembered that this value is only for very high variable regions. Regions which show much smaller variances in Figure 30 are not nudged nearly as strong.

Two final checks had to be included in the assimilation process to limit the maximum allowable change in temperature and salinity. The problems exhibited themselves when the model became unstable at depth. The change in the observed and

modeled temperature at a grid point is, therefore, not allowed to change by more than 5°C.

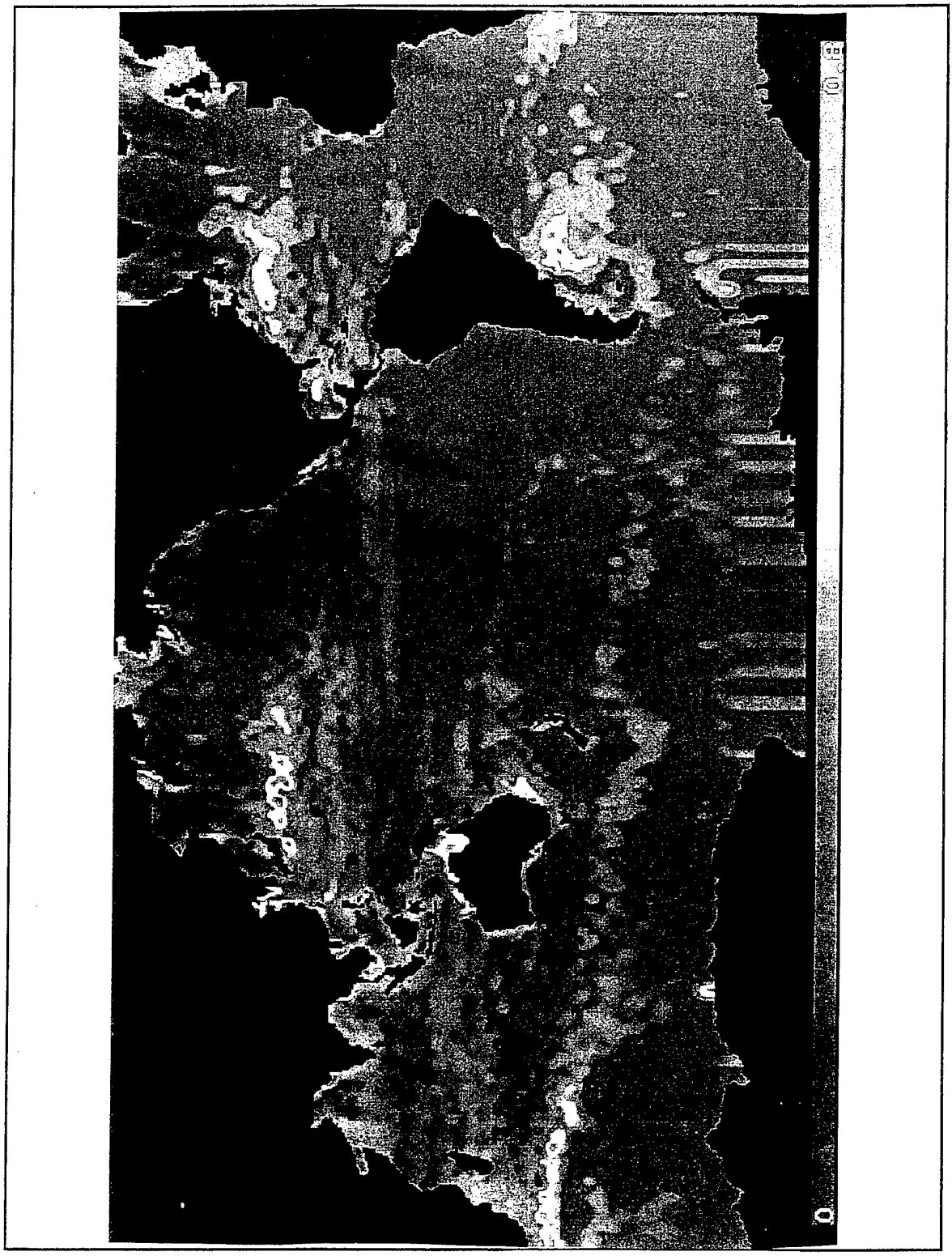

Figure 30. Spatial structure of weighting field for nudging coefficient. Scale is from 0 to 1.

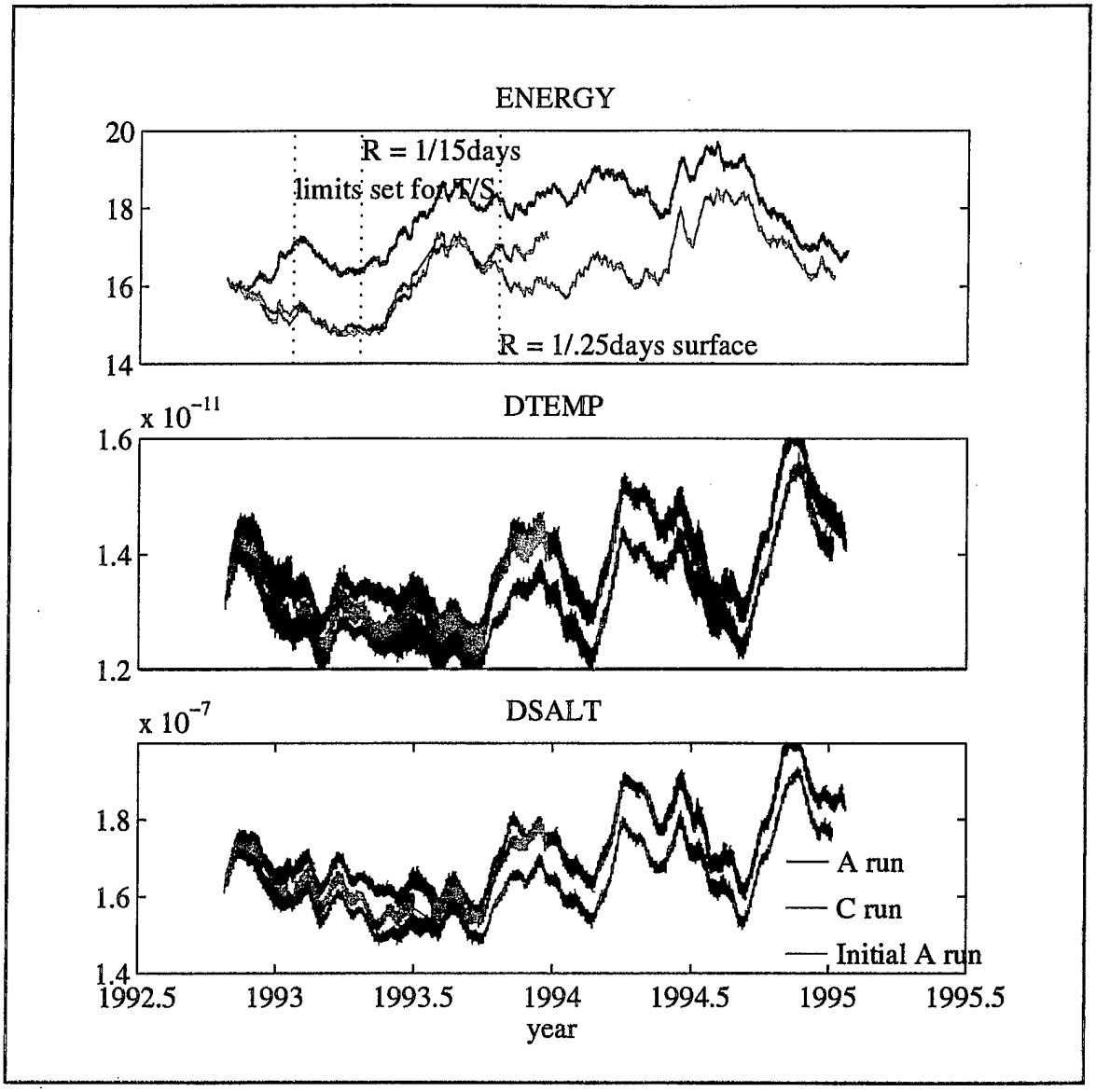


Figure 31. Time series of diagnostic quantities during model run for a) total energy, b) change in temperature, and c) change in salinity. Black line is the A run; blue defines the control run, and red line are the values from an early run with differing nudging parameters.

## B. STATISTICAL EVALUATION

### 1. Comparison of Means and Variances

The statistical tests used for evaluation in the twin experiment are used to examine the magnitude of the changes in the second experiment, involving the assimilation of real altimeter data into an ocean model. Simple comparisons of the differences in the two year (1993/1994) means between the A and C runs of SSH, temperature, and salinity quickly elucidate where the model has changed the greatest. At this point, nothing is being indicated about whether the changes produce a more realistic model. The discussion comparing the model runs to observations is in section D of this chapter. The differences greater than 10 cm between the means of SSH for the two runs are shown in Figure 32a. Changes are clearly seen in regions where they are expected to be seen. In the Kuroshio Extension of the North Pacific, the assimilation of the altimeter data has increased the mean sea level, while in other areas, such as the south subtropical Indian Ocean, the mean has decreased. Throughout the rest of the domain, the significant changes alternate between regions where the C run is higher than the A run and vice versa. Figure 32b shows differences between the C and A runs for the standard deviation of SSH with only differences greater than 5 cm outlined. This figure clearly shows that with the assimilation of altimeter data, the SSH field has become more variable in the Southern Ocean, the Kuroshio Extension, and in the Gulf Stream region. The one region which is showing a decrease, is the path which the Aghulas eddies take in the C run of the model centered near 35°S 10°E. The model C run shows a more northerly path of high variability over which eddies can be tracked. In the A run, the path of the eddies (as defined by the altimeter data being assimilated) as not so distinct. The variability pattern (here represented by the red contours centered at 30°S 10°E) is much as is seen in the variability maps calculated from altimetry data alone. The differences in the eddy kinetic energy (EKE), defined as:

$[(u-\bar{u})^2+(v-\bar{v})^2]$, with the overbar denoting the mean value, for the top layer between the A run and C run is shown in Figure 32c. The EKE field, computed from the velocity components, is a measure of the how the assimilation of SSH is affecting the variables of the model which are only indirectly, through the model's physical equations, related to the variables which are being modified through the assimilation process. Similar to the changes seen in the SSH fields, the EKE has been modified in the regions which are associated with high variability, the Southern Ocean, the Gulf Stream, the Kuroshio Extension, and the tropics. This can be traced to equation 2.2, in which part of the relaxation coefficient, $\varepsilon$, is a function of the variability.

Further down in the water column, at 160 m or level 6, changes in the temperature field can also be seen in both the mean field and the standard deviation field (Figure 33a,b). And again, the changes are the greatest where it is expected, in the regions of high SSH variability.

## 2. Further Statistical Tests

As calculated for the first experiment (twin), statistical tests are used to quantify the changes seen between the C and A run of the model. Figure 34 shows the student-t and F test values calculated between various pairs of monthly fields, globally and for the same regions as shown in Chapter IIIB-2. The thin lines give the values computed between the January 1993 (year 1) temperature and salinity fields for the C and A runs. The bold lines are for January 1994 fields (mid-way point) and the dashed lines are at the end of the experiment December 1994. These comparisons have been calculated using monthly mean fields, rather than the snapshot fields shown for the twin experiment. The horizontal axis for Figure 34a and b is defined to have the SSH t and F test values at x = 1, with the temperature layers 1-19 shown at x=2-20. It be should expected that the greatest difference should be in December 1994. The t-test for temperature and SSH, reflecting how similar

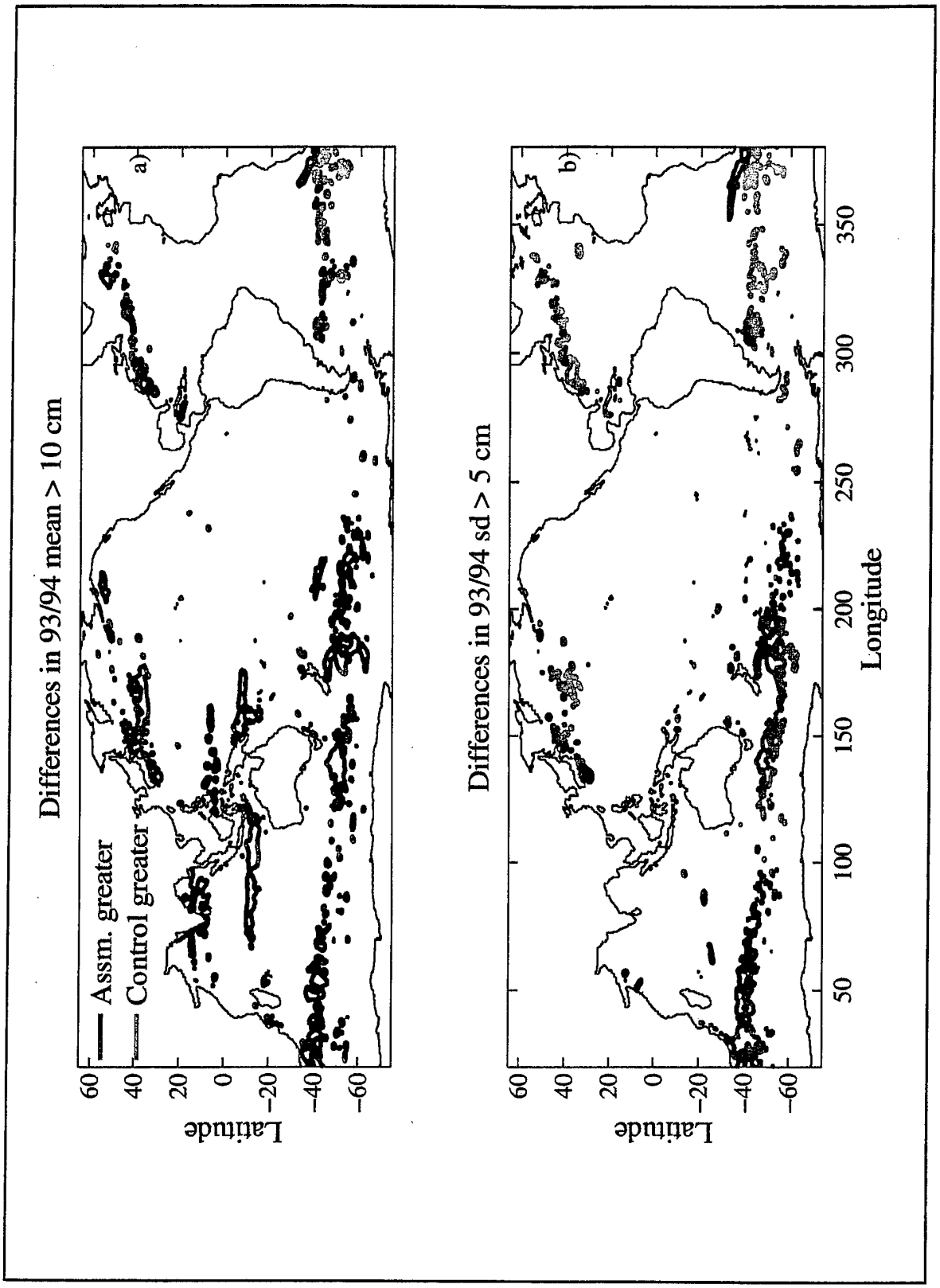


Figure 32. Differences in the SSH fields between the A and C run for a) the 2 year mean (93/94) and b) the 2 year standard deviation. Red defines areas where the A run is greater and B defines areas where the C run is greater.

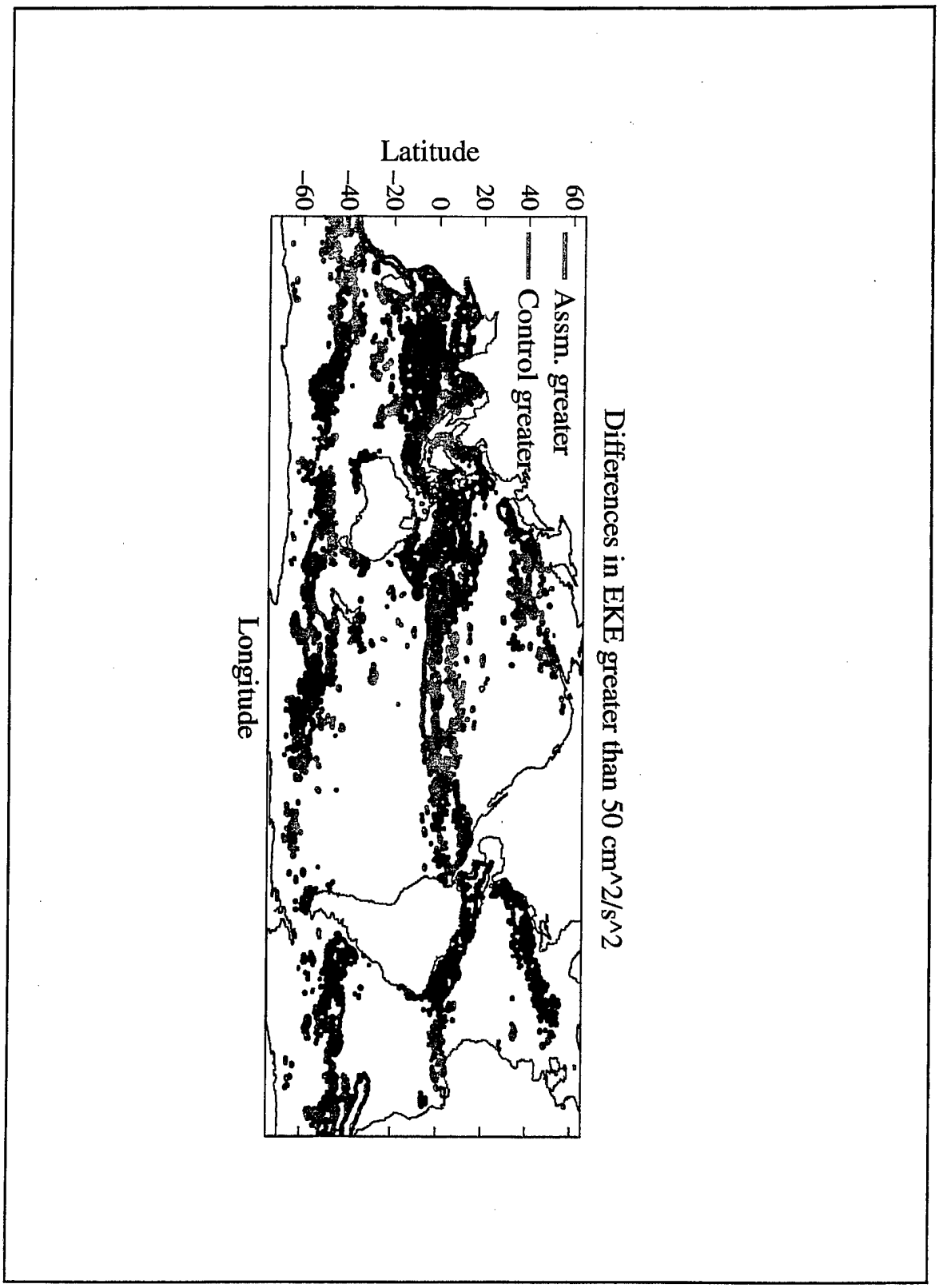


Figure 32c. Differences in the 2 year EKE field determined from a geostrophic calculation using SSH. Red defines areas where the A run is greater and B defines areas where the C run is greater.

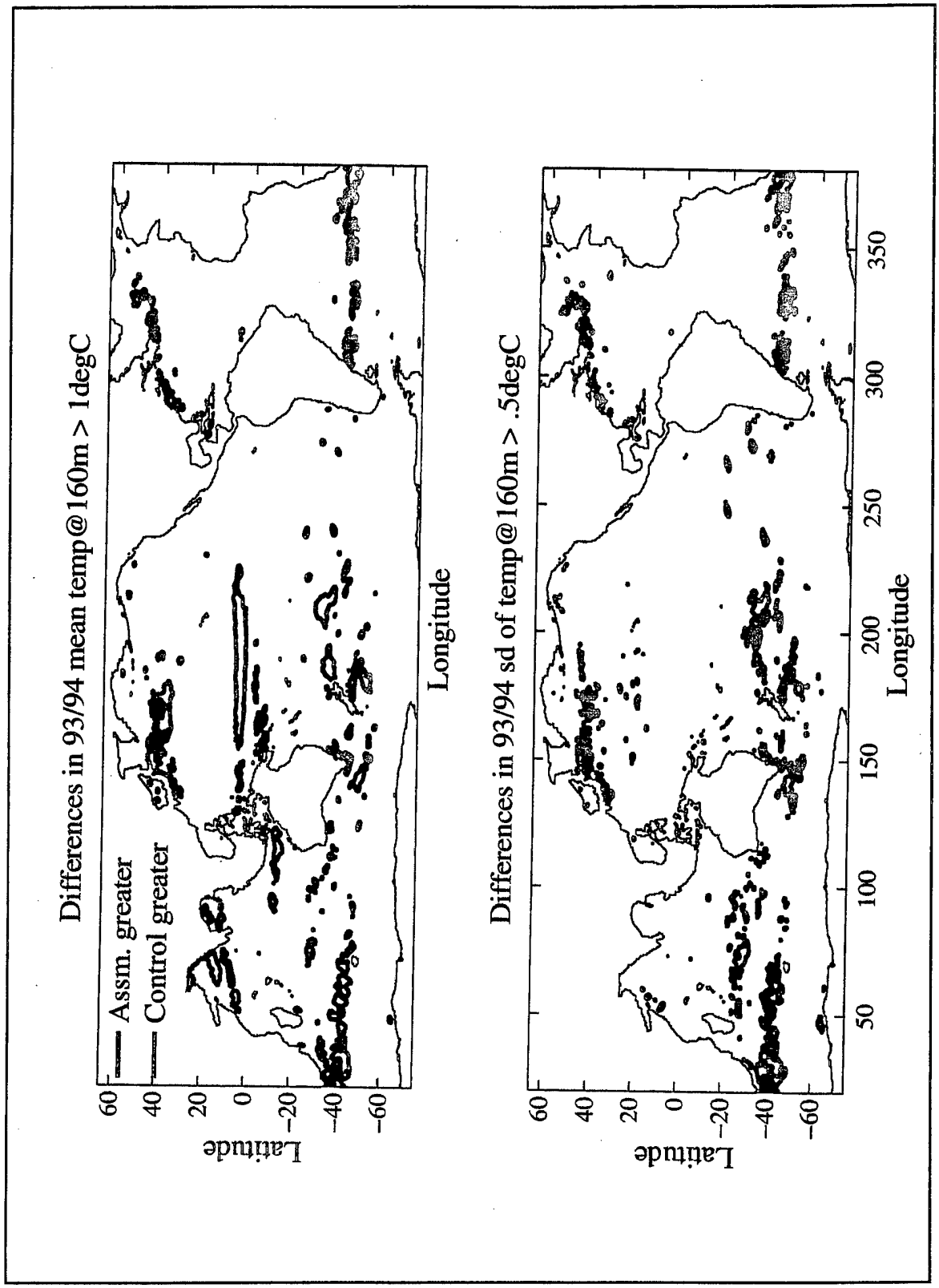


Figure 33. Differences in the temperature field at 160 meters (layer 6) for a) the 2 year mean field and b) the 2 year standard deviation field. Red defines areas where the A run is greater and B defines areas where the C run is greater.

or different the fields are in the mean, shows the global mean (Figure 34a-1) is statistically different only near the surface. Some of the regions, though, have more significant changes in the mean, for example in the Indian Ocean (Figure 34a-6) and the tropics

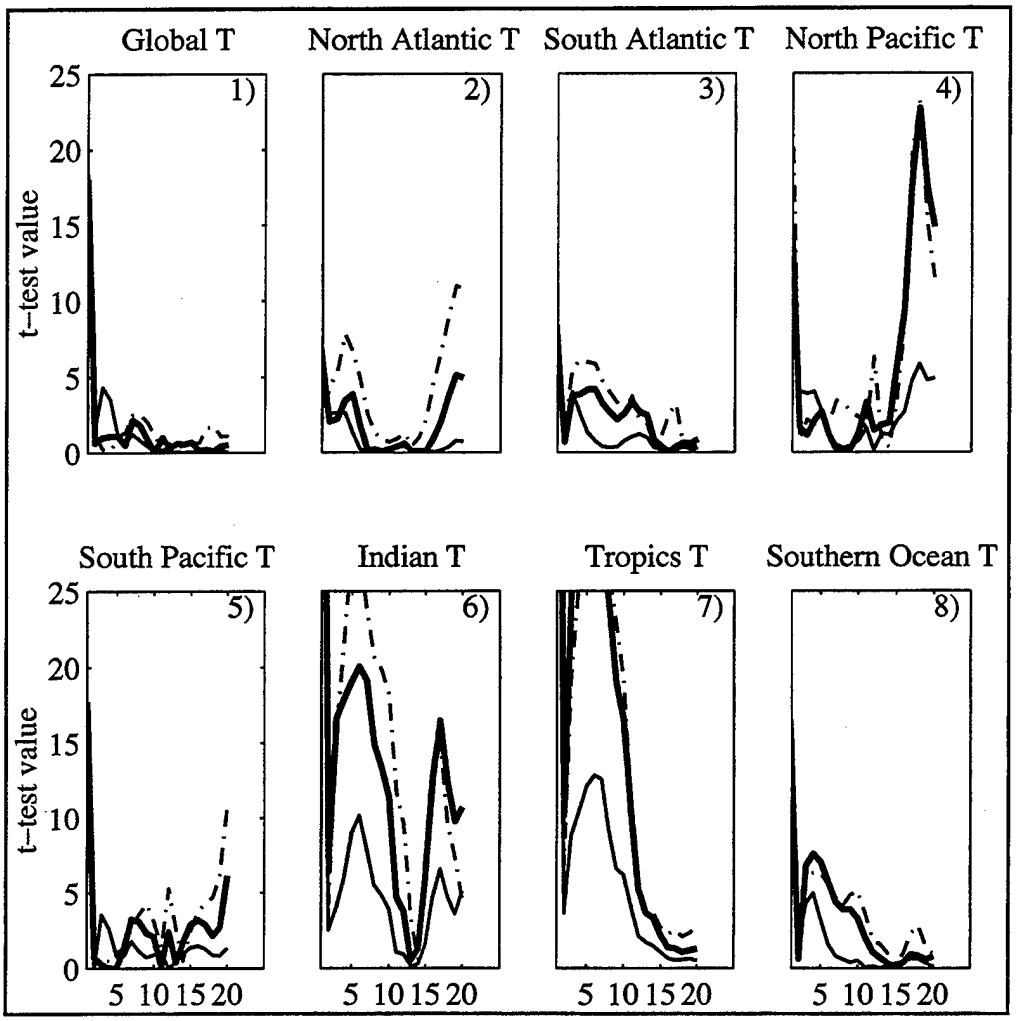


Figure 34a. Plots showing the Student-t test values calculated between different model fields for the globe and for different basins for temperature. A pair of panels comprise each figure. Y-axis is the t-test value, 1.64 is the significance level for a null hypothesis. X-axis is read as follows: x = 1, t-test value for SSH, x=2-21, t-test value for temperature, levels 1-20. There are six areas: 1) global values 2) North Atlantic, 3) South Atlantic, 4) North Pacific, 5) South Pacific, g) Indian, 7) Tropics, 8) Southern Ocean. The t-test values are computed between a pair of model fields, one from the A run and one from the C run. The bold line represents the month of August 1993 (midway in the assimilation run); the dash-dot line represents the month of December 1994 (end of the assimilation run); and thin line represents January 1993 (early in the assimilation run).

(Figure 34a-7). This corresponds directly to the changes seen in the plan view of the differences shown in Figures 32a (surface) and 33a (160 m, level 6). Even in the North Pacific, the t-test value for level 6 (x=7) in Figure 34a-4, shows an increase in the t-test value for the final month (dashed line) of the experiment. The F-test calculations, Figure 34b, shows that the variability is significantly different between the two model runs, with a larger change occurring during the first year than in the second (Figure 34b-1). The North Atlantic is the only region that doesn't show the December 1994 change (dashed line)

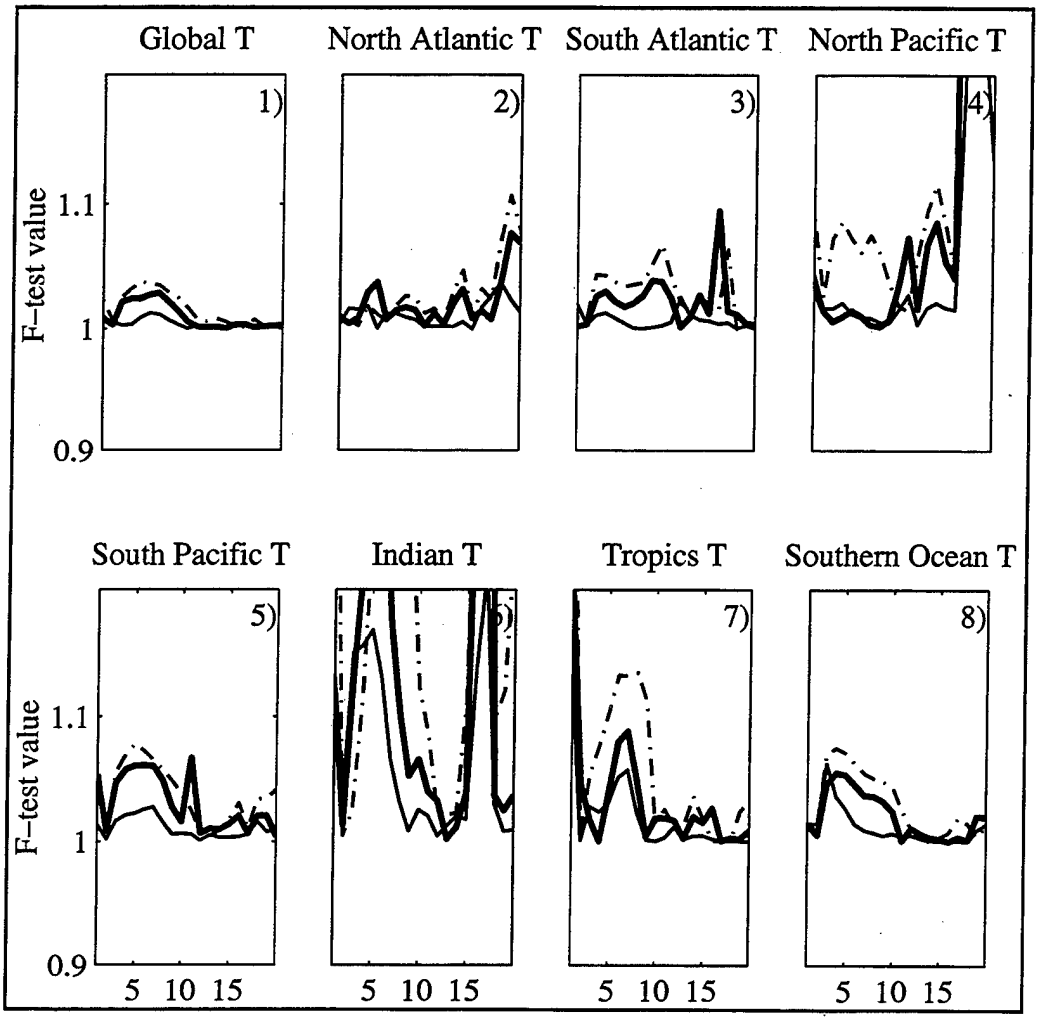


Figure 34b. Same as 34a, but are the F-test values for temperature.

greater than the December 1993 changes (bold line) for top 1500 m (level 12). below this level, it is difficult to understand the significance of the t and F test values because the changes, when they do occur, are very small.

Similar computations have also been done for the salinity fields for the same monthly pairs (Figure 35a,b). The changes do not seem to be as significant for salinity as they were for the temperature fields, although over some regions, such as the Southern Ocean (Figure 35a-8) and the Indian Ocean (Figure 35a-6), there does seem to be significant change in the mean of the salinity field. The F-test calculations (Figure 35b) show that the variability in salinity has been altered, but it is difficult to interpret the results.

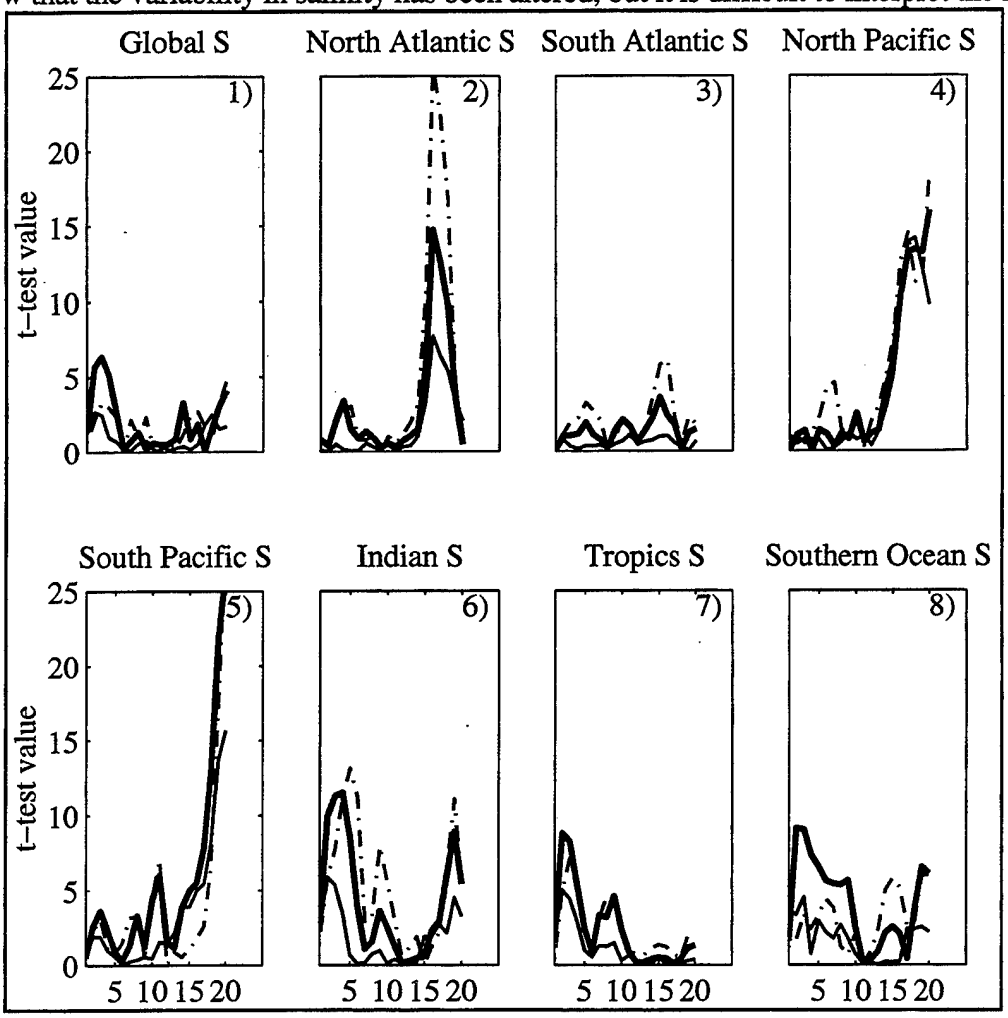


Figure 35a. Same as 34a, but are the t-test values for salinity.

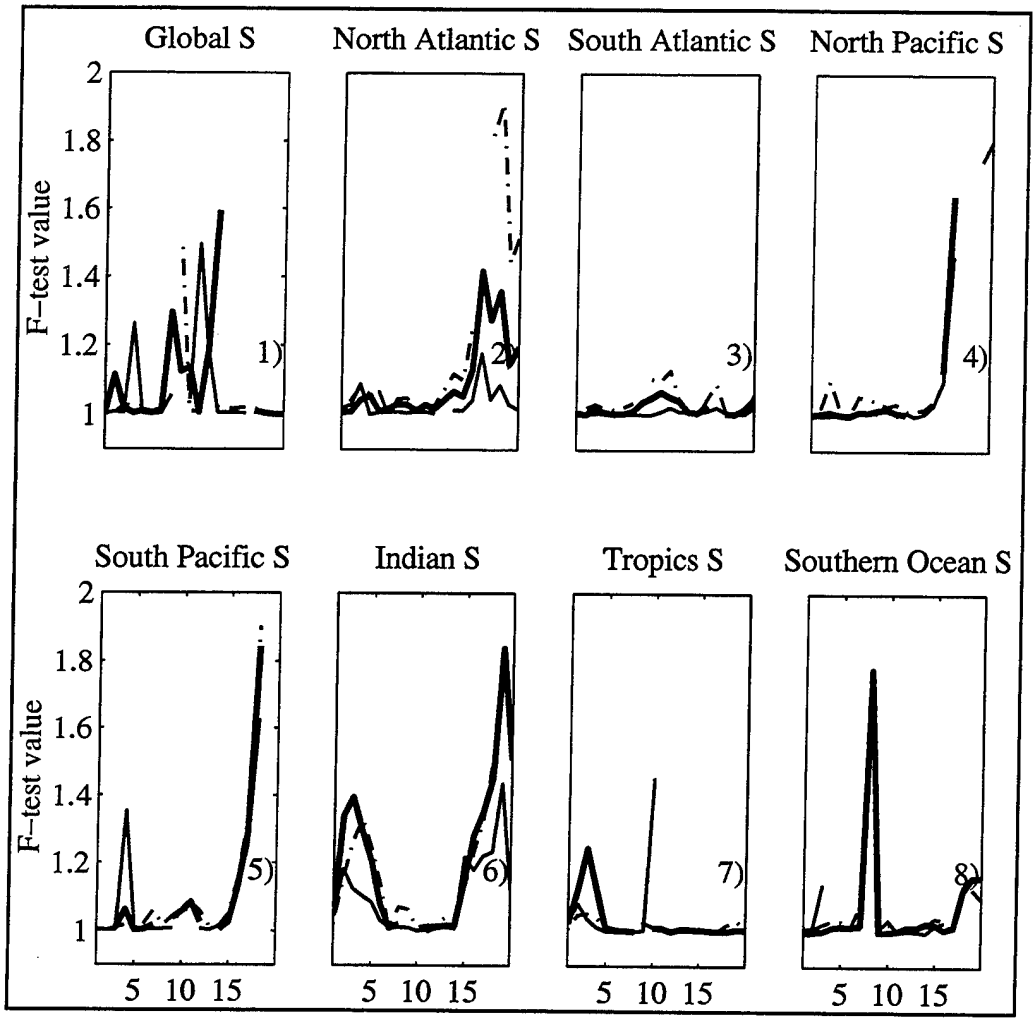


Figure 35b. Same as 34b, but for salinity.

In summary, this section has shown, through the use of statistics, that the model has changed significantly both at the surface and at depth, with the inclusion of observational data via an assimilation process. Further, regional analysis has shown that these modifications to the model's prognostic variables are not the same for all regions and the change is most directly related to the variance in the observed SSH field.

# C. DYNAMICAL CONSIDERATIONS

For an assimilation process to be successful, it should not change the basic dynamics as defined by the model's physical equations. Two things are examined to ascertain whether the inclusion of the assimilated SSH fields and associated vertical structures, has changed the dynamical properties of the model. The balances between the various forces are looked at first, followed by a section which determines if potential vorticity along several Montgomery streamlines (*i.e.* streamlines defined on an isopycnal surface) is consistent between the two runs of the model.

## 1. Balance Between Forces

The u-component of the momentum equation is written as

$$\frac{\partial u}{\partial t} + (u\frac{\partial u}{\partial x} + v\frac{\partial u}{\partial y} + w\frac{\partial u}{\partial z}) - fv = -\frac{1}{\rho_0}\frac{\partial P}{\partial x} + \kappa\frac{\partial^2 u}{\partial z^2} + A(\frac{\partial^2 u}{\partial x^2} + \frac{\partial^2 u}{\partial y^2}) \qquad 4.1,$$

where $\kappa$ and A are specified friction coefficients. The two year mean fields of the A and C runs are used to determine the order of magnitude of the above terms to determine if the assimilation process has modified any of the physical balances defined by the model's numerical equations. The advection term, $u\frac{\partial u}{\partial x} + v\frac{\partial u}{\partial y}$, the Coriolis term, fv, the pressure gradient term written as a function of SSH (via the hydrostatic approximation), $g\frac{\partial \eta}{\partial x}$, and the horizontal friction term, $\frac{\partial^2 u}{\partial x^2} + \frac{\partial^2 u}{\partial y^2}$ are computed separately and then compared. The calculations were performed for the whole globe and can be represented using two meridional bands averaged over 10°, one in the Pacific at 157°E and one in the Atlantic at 32.5°W. Figure 36b shows the magnitude of the each of the four terms centered at 157.5°E, with the dashed line representing the A run and the solid line, the C run. From the plots, it is difficult to see any diversions of the dashed line from the solid line. Thus, the

model output from the two runs give approximately the same values for all the terms (as expected from scale analysis) except for the pressure gradient and Coriolis terms near

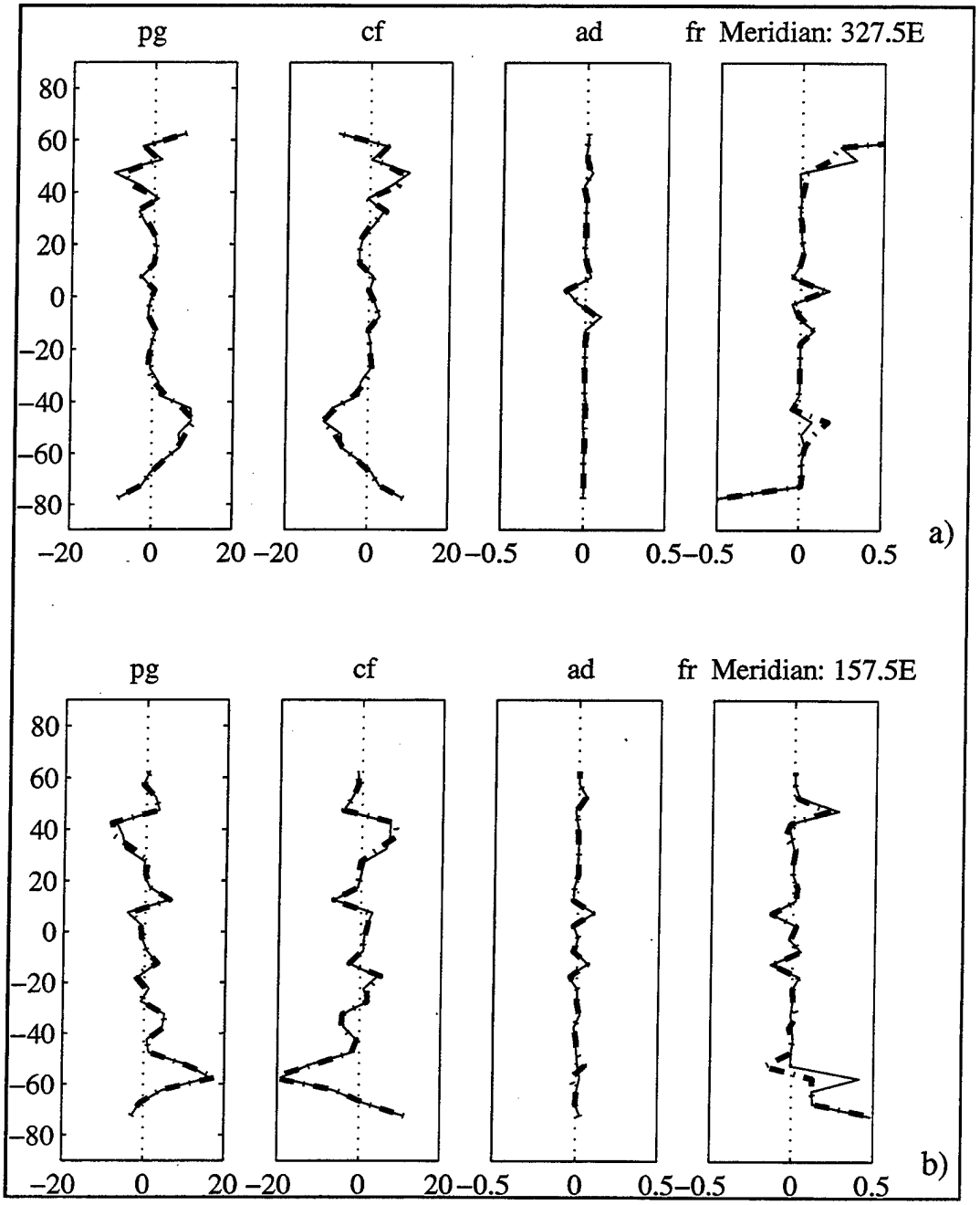


Figure 36. Zonal average over a 10°x10° box of the pressure gradient, Coriolis, advection, and friction terms of the momentum equation, centered at a) 327.5°E in the Atlantic and b) 157.5°E in the Pacific. The solid line is the C run; the dashed line is the A run.

45°N and 45°S and in the Southern Ocean for the friction term. Most important, though, the order of the terms do not differ between the two runs of the model. The meridian in the Atlantic at 327.5°E shows a similar comparison (Figure 36a).

## 2. Potential Vorticity

Potential vorticity (PV) can be used as a diagnostic quantity to evaluate the changes to the dynamics of the model when SSH and a related temperature and salinity structure are assimilated. *Gille* (1997), determined, using model output from the Semtner/Chervin POCM model, that PV is not conserved along Montgomery streamlines in the Southern Ocean. Even with this knowledge of PV behavior along a streamline, potential vorticity can be used to determine if the two runs of the model are dynamically similar by looking for differences in the order of variation in PV between the runs.

An isopycnal surface is a surface which is more dynamically suited for looking at flow properties because the flow is maximized along a surface and minimized across surfaces. The Montgomery streamfunction (*Montgomery*, 1937), the geostrophic flow along an isopycnal and defined as a pressure anomaly term by *Zhang and Hogg* (1992), can be used to represent the geostrophic relation for the horizontal geostrophic velocity. The constraint of a non-divergent flow does not hold as it does in the traditional definition of a streamline. The geostrophic relationship is defined as $\hat{k} \times f\mathbf{u} = \frac{1}{\rho} \nabla_z p$. This equation can be transformed into an equation describing geostrophic flow on an isopycnal by substituting in the hydrostatic equation ($\frac{dP}{dz} = -\rho g$) and using the equation, $\nabla_z A = \nabla_\sigma A - \frac{\partial A}{\partial z} \nabla_\sigma A$, to transform the geostrophic equation to isopycnal coordinates, resulting in:

$$\hat{k} \times f\mathbf{u} = \frac{1}{\rho} \nabla_\sigma p - \nabla_\sigma \int^{P1} \frac{1}{\rho} dp \qquad 4.2.$$

*Zhang and Hogg* analyzed the equation and determined that the non-gradient component can introduce significant error in calculating geostrophic velocities along an isopycnal, when the total pressure is used. If the mean pressure is removed from the pressure term,

the resulting equation substantially reduces the error and gives a more reasonable estimate of the velocity field on an isopycnal. Therefore, in this paper, the Montgomery streamfunction is defined using the pressure anomaly instead of the total pressure with the equation written as:

$$M = \delta(z)\,(p(z) - \bar{p}) - \int^{P} \delta(z)\, dp \qquad 4.3,$$

where z represents the depth of the isopycnal surface and $\delta(z)$ is the volume anomaly defined as

$$\delta(z) = \frac{1}{\rho(z)} - \frac{1}{\rho_0(z)} \qquad 4.4.$$

$\rho(z)$ and $\rho_0(z)$ are the in situ density and the reference density with salinity equal to 34.6 and temperature equal to 2.33°C. For these calculations, the mean pressure removed is equivalent to around 300 meters. The free surface is included by modifying 4.3 to

$$M = \delta\rho_s\eta g + \delta(z)\,(p(z) - \bar{p}) - \int^{P} \delta(z)\, dp \qquad 4.5,$$

with $\rho_s$ equal to the surface density and $\eta$ is the surface height.

PV is calculated as $Q = f\frac{\partial\sigma}{\partial z}$ from the model's prognostic temperature and salinity values and is calculated at the points defined by the Montgomery streamline. Relative vorticity has been eliminated from the computation because *Gille* (1997) has shown that it contributes little to total PV, most of which is determined by the vertical structure.

To examine if the assimilation run is dynamically consistent with the control run, Q, plotted along Montgomery streamlines, is examined for several areas. The flow is examined only to determine if the assimilation values of potential vorticity are consistent with the control run. At a depth of around 1300 meters, Figure 37a shows the 0.09 Montgomery streamline in the Southern Ocean as calculated from equation 4.5 from the

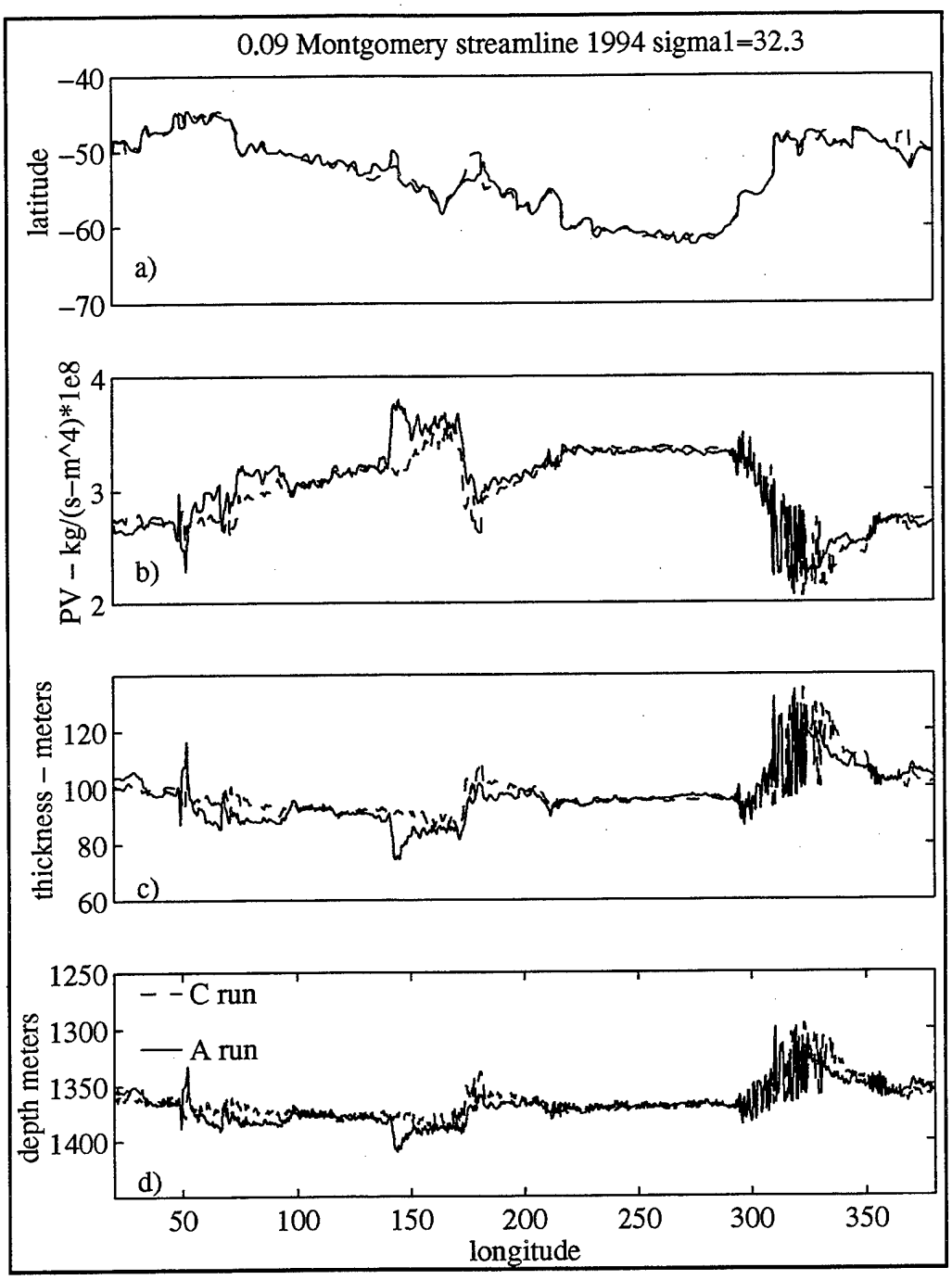


Figure 37.Various quantities along a Montgomery streamline on a density surface of $\sigma_1$ = 32.3 in the Southern Ocean. a) shows the streamline path for the A run (solid line) and the C run (dashed line); b) is the potential vorticity along the path; c) the thickness of the density layer; and d) the depth of the layer.

mean of 1994 along the 32.1 $\sigma_1$ surface. The heavy line represents the quantity as calculated from the C run and the thin lines are those computed from the A run. Panels b-d show the PV, the thickness and the depth of the layer, respectively. Changes have occurred in the model run at this depth directly corresponding, in most cases, to the thickness of the layer, especially between 140° and 150°E, near Tasmania. The minimas and maximas of both runs are of the same order. Around 10°E, the streamline has changed dramatically, but there is little change in the PV along the line. This is the path of the eddies shed by the Agulhas Current into the South Atlantic. This evidence suggests the two runs are producing different, but dynamically similar flow at depth. In other words, the assimilation is not modifying the underlying dynamics of the model.

As we look further up in the water column in the Southern Ocean, a specific streamline shows more differences in location between each of the model runs. For example, Figure 38a-d shows the changes occurring along the -0.05 contour on the $\sigma_1$ surface in the Southern Ocean. The magnitude of the PV along the line remains essentially the same between the two runs of the model. At a depth between 600 and 800 meters, the -0.13 streamline has also been modified between the two model runs, with much larger changes as seen in Figure 39a-d. Above this depth, it becomes increasing more difficult to computationally follow a streamline. This is also true for other regions, such as the North Atlantic and the Kuroshio area of the North Pacific.

In summary, these dynamical comparisons of the balances in the terms of the momentum equation and of the consistency in the flow along streamlines in the Southern Ocean show that the assimilation process is not modifying the basic physics of the model's numerical equations.

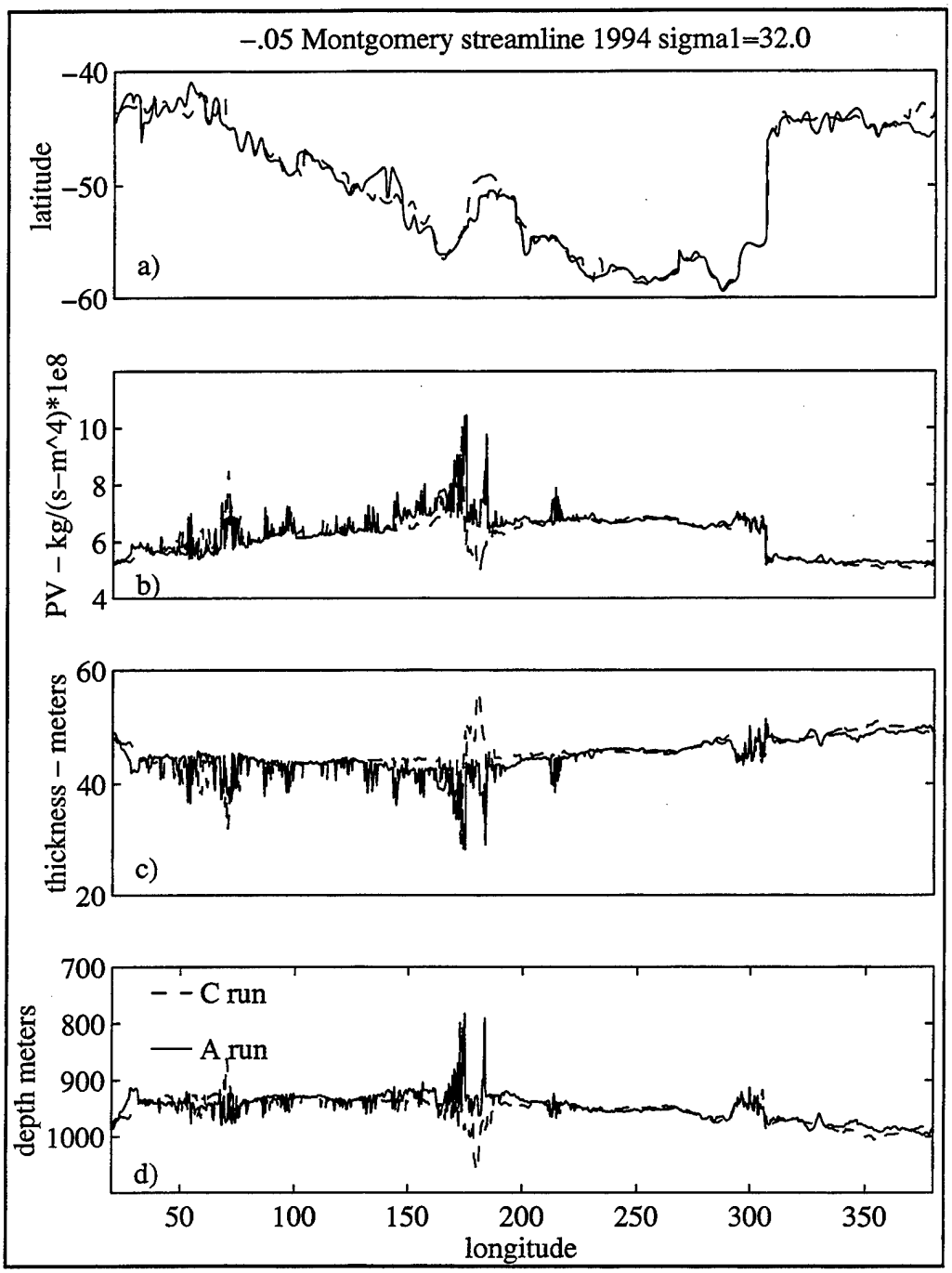


Figure 38. Same as 37, but for $\sigma_1 = 32.0$ in the Southern Ocean.

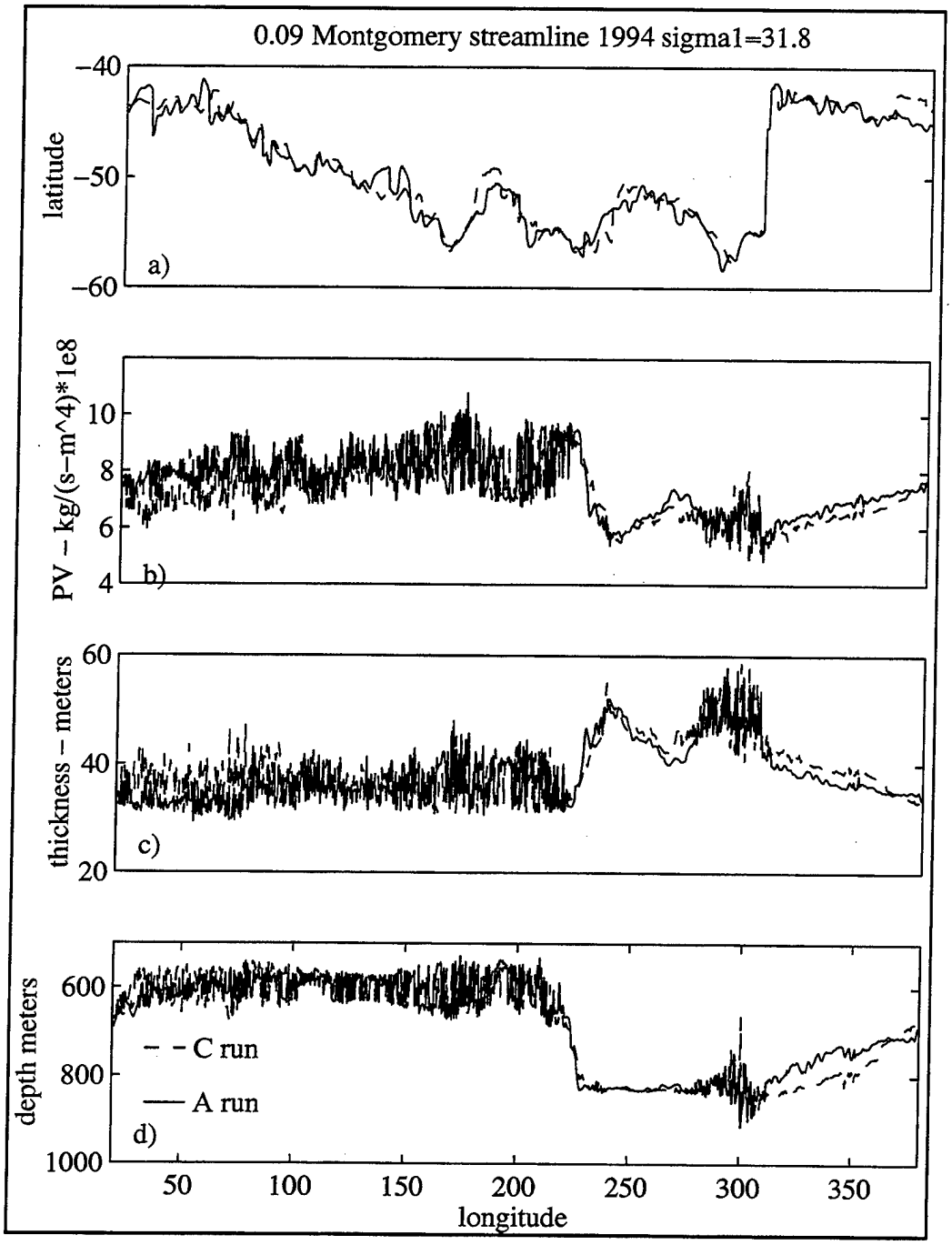


Figure 39. Same as 37, but for $\sigma_1 = 31.8$ in the Southern Ocean.

## D. COMPARISONS TO OBSERVATIONS

As stated above, one of the goals of assimilating observations into a model is to adjust it towards actual observations. This section looks at several things to determine if this goal is being met. The sea surface is examined first by comparing several quantities with observations. This includes examining the differences in the variability and spectra of the surface fields as compared to altimetric data. Also included, is the comparison of time series of model SSH at specific locations to observational tide gauge measurements. Subsurface, the changes in the heat content of the model are examined, along with looking for changes in the thermohaline circulation pattern when observational data is assimilated. This is in addition to comparing the model's diagnostic fields (velocity, temperature, and salinity) with observations sampled at the same time in the ocean, using observations mainly retrieved from the World Ocean Circulation Experiment (WOCE) database. Because the domain of the model is global, this thesis will concentrate on examining the changes in the regions where the assimilation is expected (using the spatial structure of the weighting function, Figure 30 as a guide) to have modified the dynamics the most. These areas are 1) the North Atlantic in the region of the Gulf Stream, 2) the Kuroshio Region in the North Pacific, 3) the tropical ocean, and 4) the Southern Ocean. Results from the evaluation are shown from other areas when they are pertinent to the discussion.

### 1. Sea Surface Height

Figure 32a shows the gross differences in SSH between the two year means of the two model runs, C and A. The SSH field can be examined in closer detail by focusing on a region. The four regions mentioned above are examined to determine if the estimate of SSH has improved in the A run (the assimilation run) over that of the C run (the control). A time series of the RMS difference between the SSH in run A and the observational SSH

(Figure 40), shows that over the first 150 days of the model run, the RMS difference in the observed field drops from over 16 cm to about 13 cm, where it remains for the remainder of the two year run. (If the mean SSH from the C run is used as the mean SSH to add to the SSH anomaly field, the RMS difference drops only slightly, to 12 cm.) A large part of the difference remaining after day 150 is related to the regions of the model which have high variability that is not seen in the observations, but appears in the model fields.

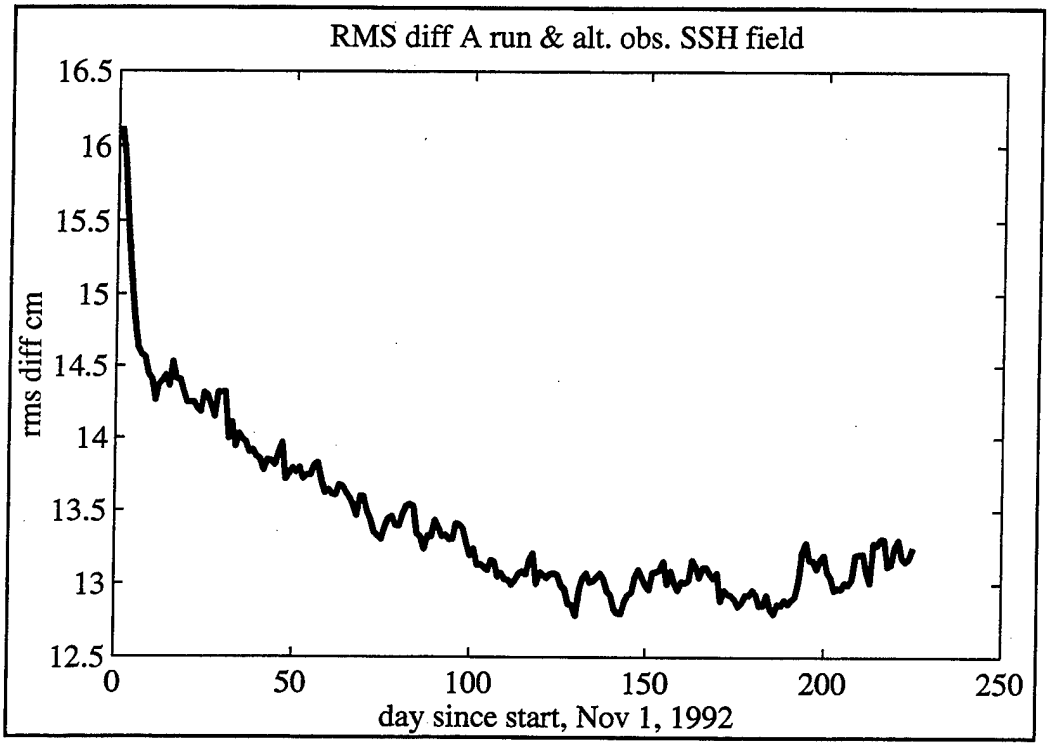


Figure 40. RMS difference between model SSH and the observations from day 0 of A run.

Because the assimilation process is only adjusting those areas where there is high variability in the observations, these other high variable areas largely remain unchanged. This is, perhaps, where a correction should be made to the assimilation process. If the nudging coefficient R, as used in Equation 2.1, were a constant equal to the maximum of the current R, instead of a value dependent on the variance of the SSH at the location, the assimilation process should adjust the model towards the model mean faster in these areas

that have changed relatively little with the present assimilation scheme, this is because the nudging weight is related to the variance of the SSH, not the mean field. The current R value allows for changes with higher variance to be nudging more strongly or in other words, with a shorter relaxation time scale. At this point in time, it is difficult to say which is preferable, partly because the mean used for the observational mean is a model mean. The next paragraph looks at the adjustments to the mean and standard deviations for the regions mentioned above.

Figures 41 through 43 show the standard deviation of SSH for the control field (a), for the observation field (b), and for the assimilation field (c) for 3 of the 4 regions. (The tropical region shows little variance change and is not shown.) The Kuroshio region, Figure 41c, shows clear enhancement of the SSH anomaly field in the latitude band between 30°N and 40°N matching the variability seen in the observations (Figure 41b) with the highest variance. There is still a diagonal band of high variance, not seen in the observations, from about 145°E, 40°N to 160°E, 45°N. In the Gulf Stream region, the band of high variability is flattening out somewhat in the A run (Figure 42c), but not as dramatically as it should, as seen in the observed field (Figure 42b). The Southern Ocean (Figure 43a-c) shows similar variance structure in those regions where the model has been nudged the strongest (40°S, 0° and 70°E, 60°S, 180°E). The assimilation fails to duplicate the variance structure in the Brazil-Malvinas Confluence (45°S, 310°E).

The means of these regions are shown in Figures 44 through 46. The mean of the Southern Ocean has changed little and therefore, is not shown. The Gulf Stream region's mean field from run A shows the permanent eddy-like feature located in Figure 44a at 35°N 289°E as either much reduced or removed completely. SSH plotted along the 290°E meridian shows this change as a change in the location of the Gulf Stream wall (Figure 44d). In the Kuroshio region, the mean contour of -50 cm centered at 50°N, 165°E is enlarged in area in the assimilation (Figure 45c) over the contour in the control run (Figure 45a). This suggests that the assimilation run is closer to the observed mean field (Figure

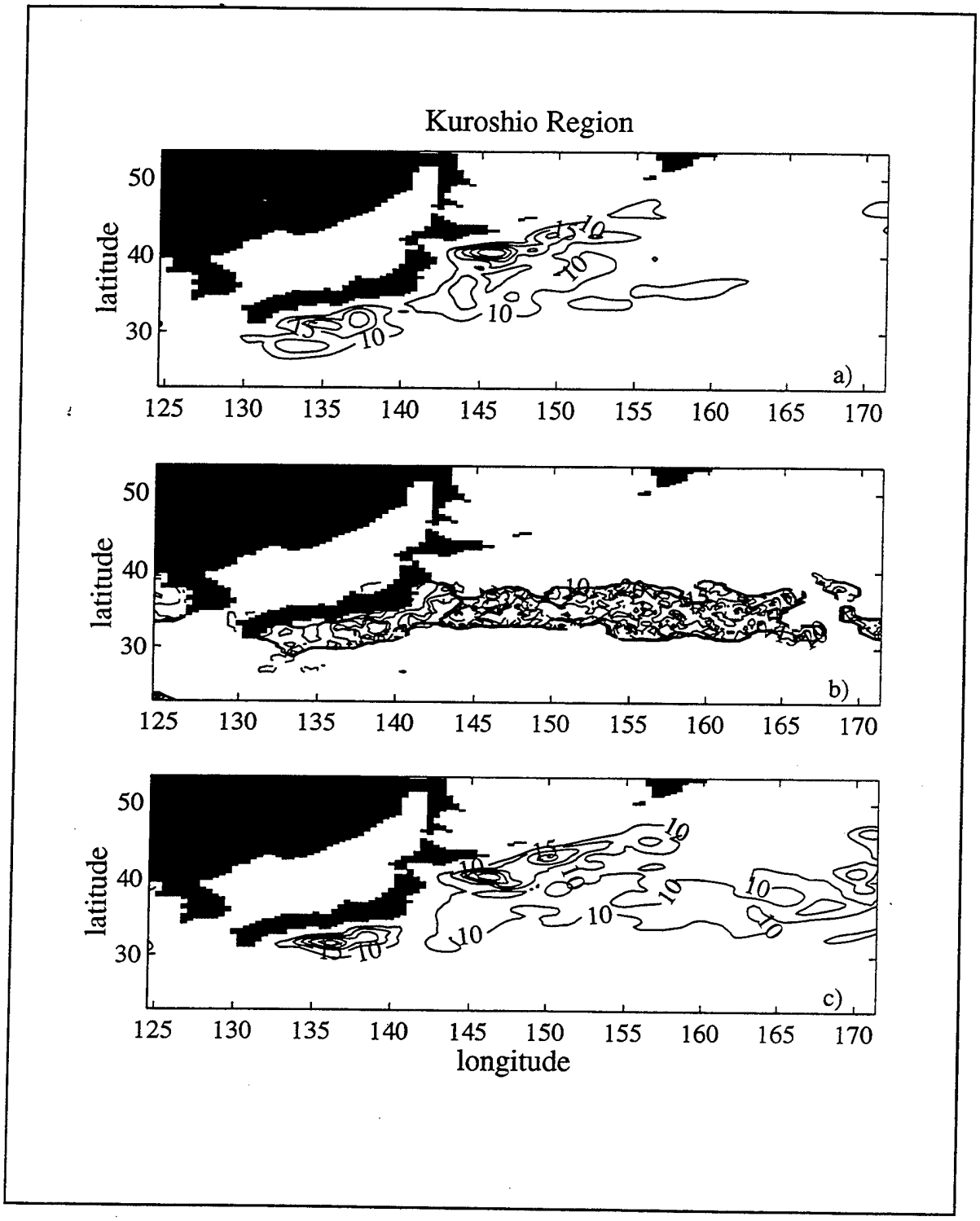


Figure 41. Contours of the 2 year standard deviation of the SSH field for the Kuroshio Region; a) run C, b) observations, and c) run A. . Contours are every 5 cm.

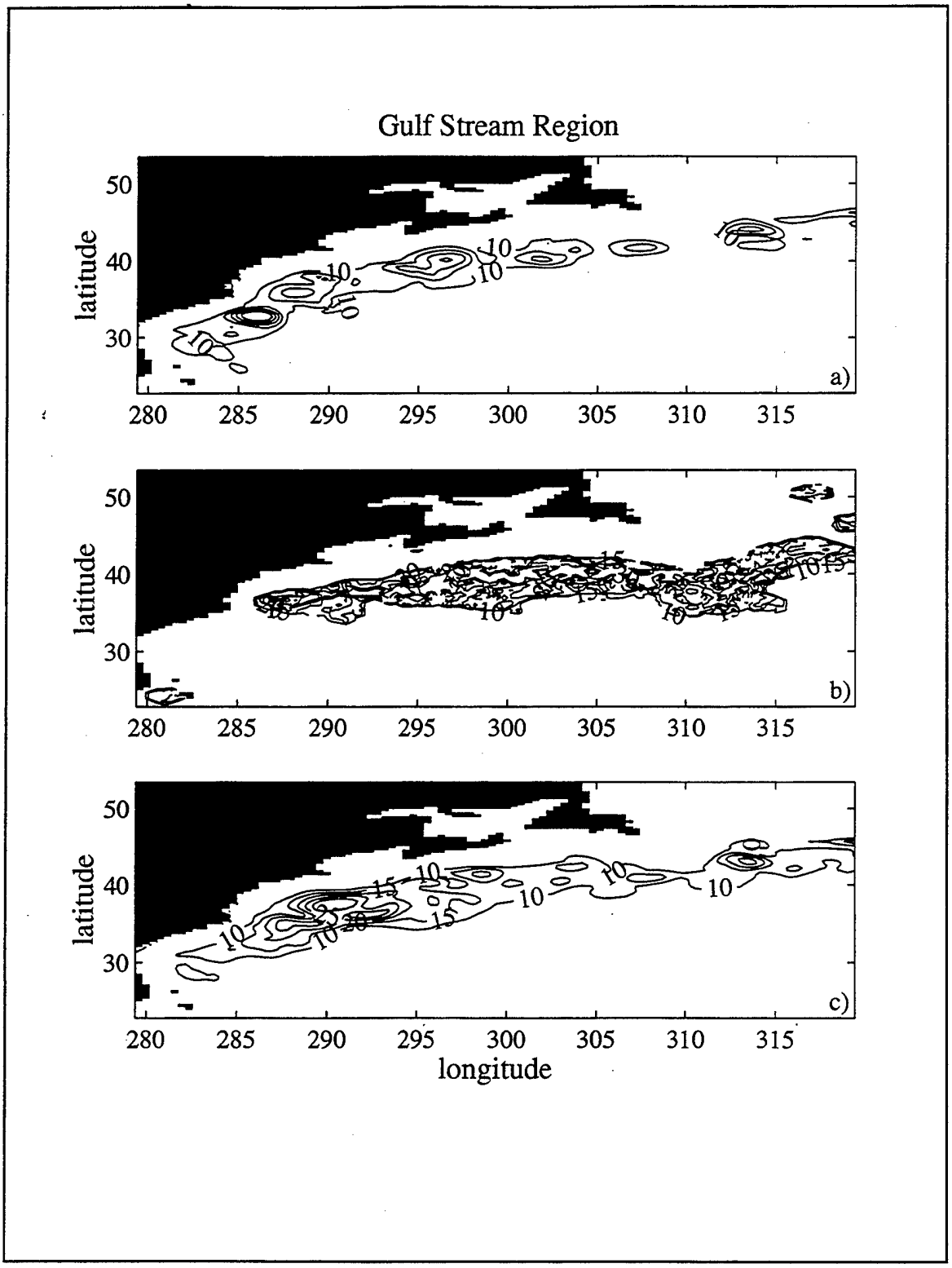


Figure 42. Same as 41, except for the Gulf stream region.

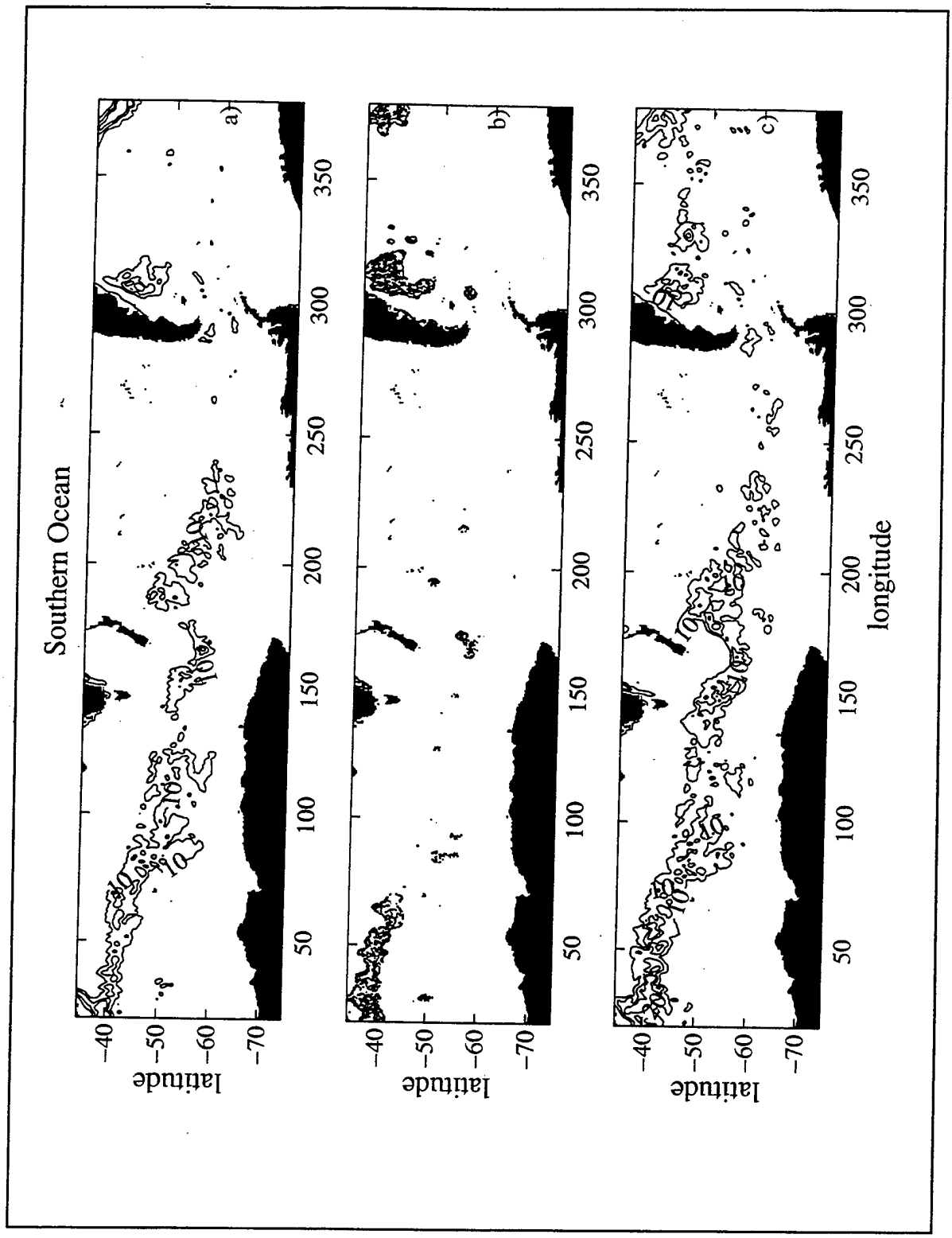


Figure 43. Same as 41, except for the Southern Ocean

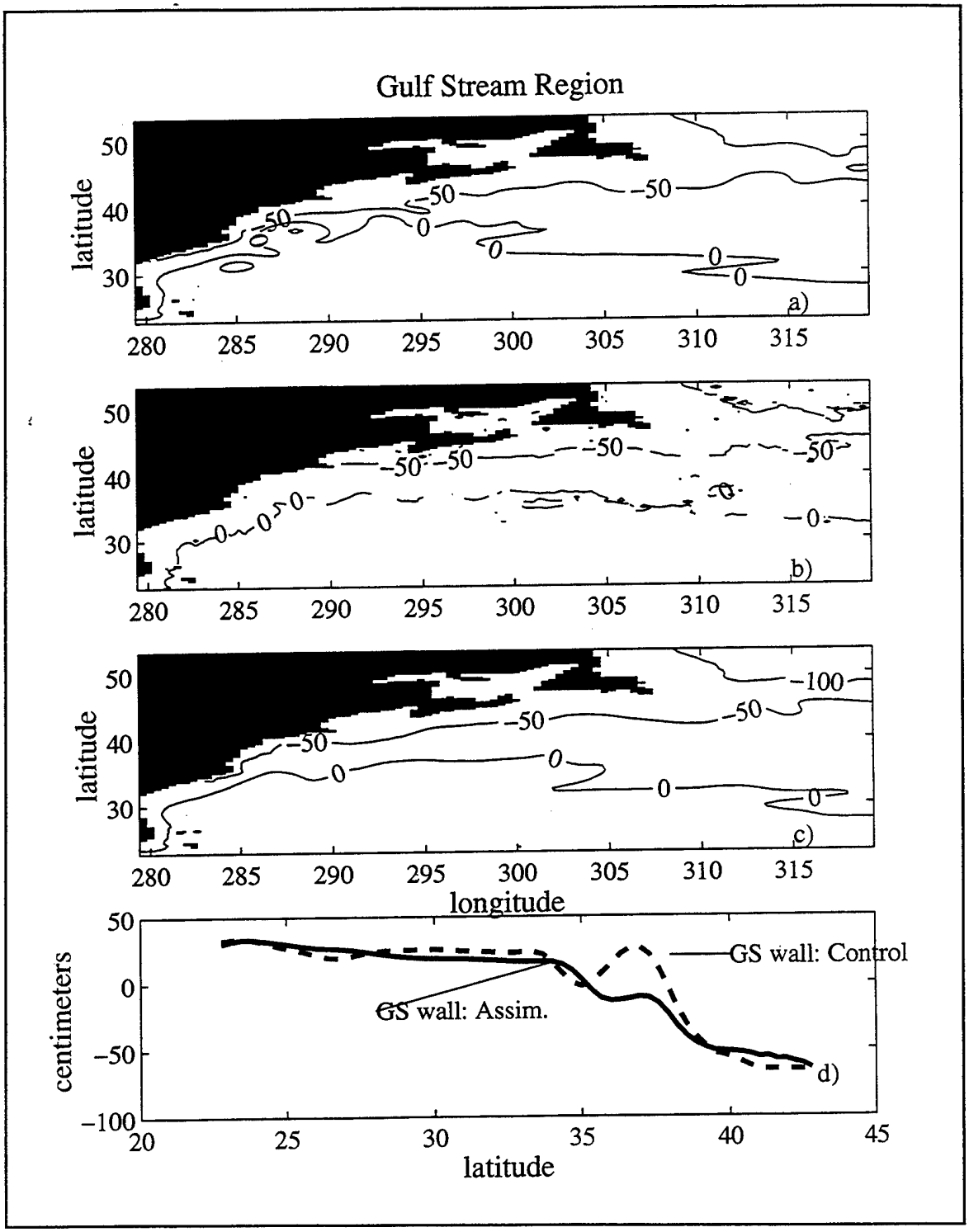


Figure 44. Mean field from the Gulf Stream region. Contours are 50cm. a) the C run, b) the observations, and c) the A run d) shows the mean SSH along 290°E for the C run (dashed line) and the A run (bold line).

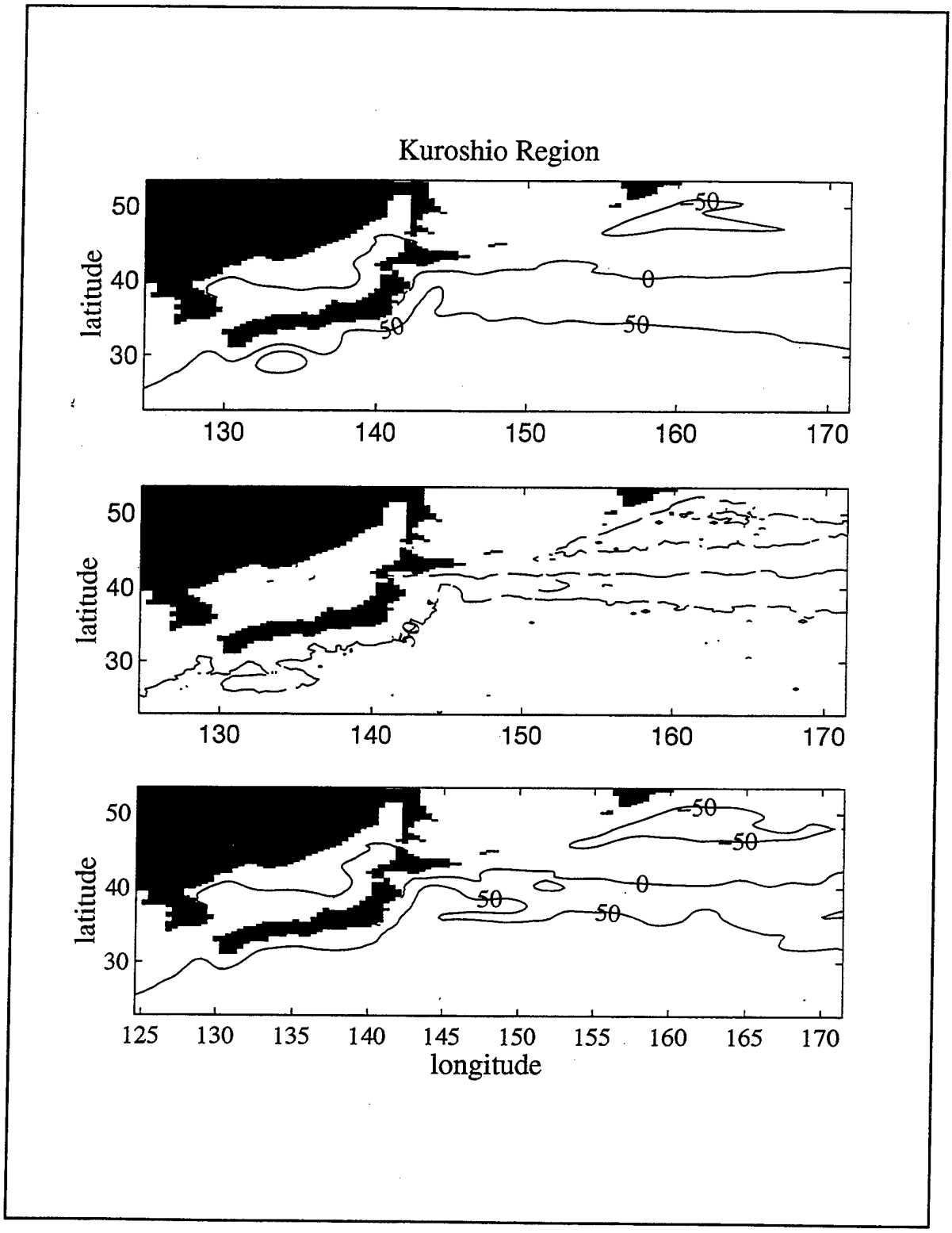


Figure 45. Same as Figure 44a-c, but for the Kuroshio region.

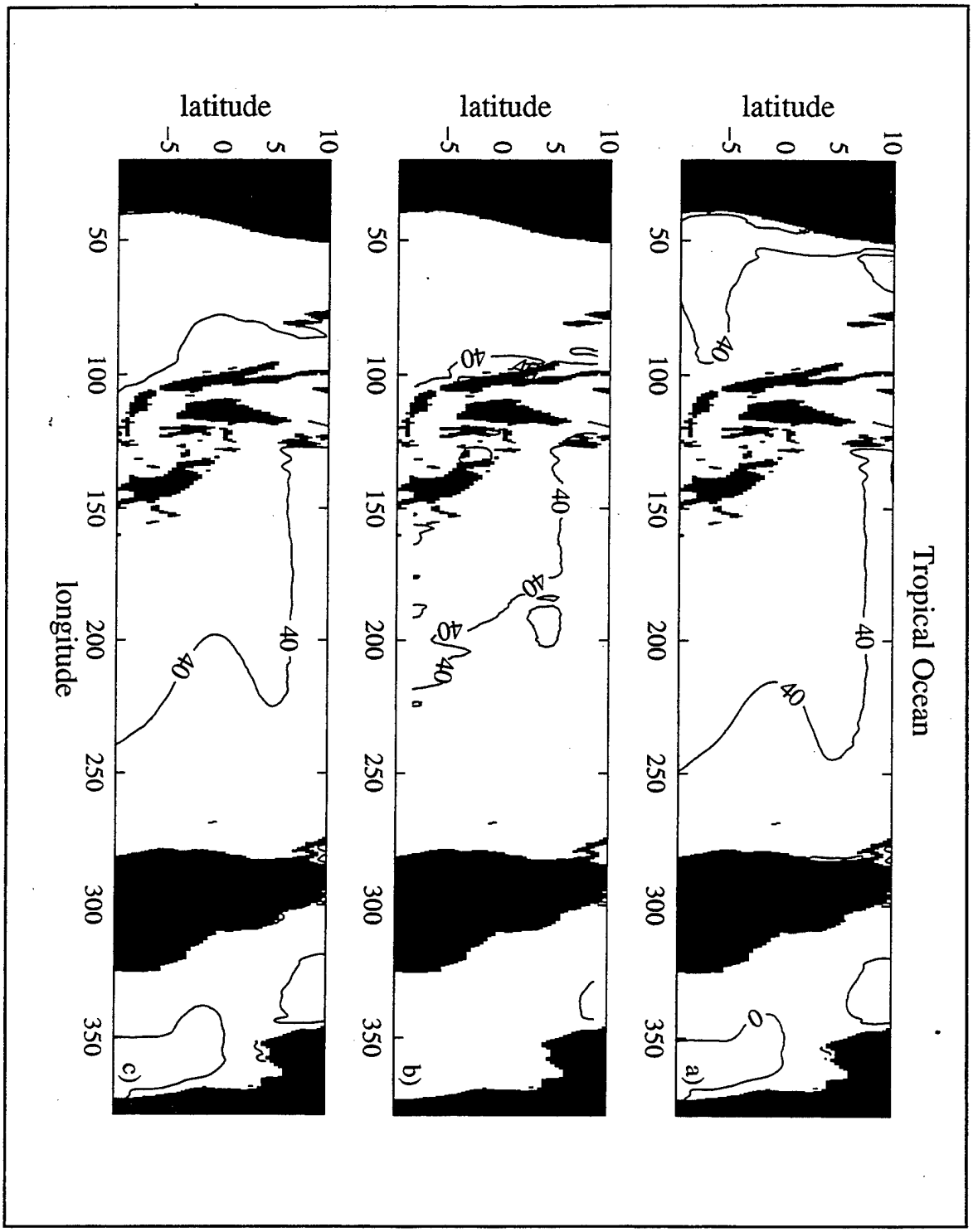


Figure 46. Same as Figure 44a-c, but for the global tropical regions. Contours are 40cm.

45b) than is the SSH from run C. The contours of 0 and 50 (between 35° and 40°N) appear to be closer in the A run to the observed contours than is seen in the C run. In the tropical region (Figure 46), the 50 cm contour has moved westward in the Pacific ocean in the A run from where it is located in the C run. The A run contour (Figure 46c) is closer to the observed field (Figure 46b) than is the C run (Figure 46a). These plots show that the mean of the model has changed along with the variance of it, adjusting it towards the observed mean.

Sea level heights, as measured by tide-gauges, have not been assimilated into the model, and thus, can provide an independent measure of the improvement in the model with the assimilation of altimetric SSH anomalies. Before showing the results of the comparisons of the assimilation run to the tide-gauge measurements, the performance of the control run against these independent measurements (when no observations have been used to adjust the model's prognostic variables) is examined to show that even without assimilating observations, the sea level of the model is simulated adequately.

*Tokmakian* (1996) gives an in-depth comparison of POCM_4B SSH values to sea level measurements of 94 stations over a period of 9 years. Time series of the model SSH, averaged over 60 km and sampled every three days, were created at the locations of the tide gauges. Similarly, the sea level data from the tide-gauges were sub-sampled from the daily values (with a seven day low pass filter applied) to a 3-day time series to correspond to the same sampling of the model. An inverse barometer effect was removed also from the observational data. Finally, the two year mean of each data set was removed before the correlations were computed. The overall mean correlation is 0.48 +/- 0.28 for 1993-1994. At some of the stations, the analysis of the C run shows that the model is reproducing the observed signal quite well. For example, the plots of the time series at Naos Island (Gulf of Panama, 8.9°N 79.5°E) and at Christmas Island (2°N 157.5°E) (Figure 1) shows the El Niño events of November 1991 and 1994 at Christmas Island which are then seen about a month later at Naos Island. This fits the estimated wave speed

of (2.8 m/s) given be *Delcroix et al.* (1994).

To evaluate the improvement to the model with the assimilation of the altimetric data, the same comparison is done with run A. The resulting correlations (with an annual cycle removed from both observations and modeled SSH) to the tide-gauges have been divided into three sets 1) where there is little change in between the C and A runs of the model (to within 0.1 ), 2) where the A run performs better, and 3) where the C run performs better. There are 59 stations where there is little change between model runs. Of these stations, 50 have a correlation better than 0.3 and 41 are over 0.5. In the second group (Table 3), locations at which correlations were less than 0.15 were removed, leaving 19 locations with an improved correlation in the A run. The third group is shown in Table 4. Here 17 locations have worsened with the inclusion of the assimilation

| Tide Gauge | R: A Run | R: C run | Latitude | Longitude |
|---|---|---|---|---|
| POHNPEI | 0.62 | 0.44 | 7.0°N | 158.2°E |
| MAJURO | 0.70 | 0.54 | 7.1°N | 177.4 |
| MALAKAL | 0.19 | 0.03 | 7.3°N | 134.5 |
| FRENCH FrSh | 0.36 | 0.05 | 28.9°N | 166.3°W |
| RIKITEA | 0.51 | 0.34 | 23.1°S | 134.9°W |
| SUVA | 0.71 | 0.54 | 18.1°S | 178.4°E |
| ADAK ISLAND | 0.29 | -0.02 | 51.9°N | 176.6°W |
| CHICHIJIMA | 0.46 | 0.32 | 27.1°N | 142.2°E |
| MIDWAY ISLAND | 0.60 | 0.11 | 28.2°N | 177.4°W |
| JOHNSTON | 0.33 | -0.01 | 16.8°N | 169.5°W |
| HILO | 0.66 | 0.12 | 19.7°N | 155.1°W |
| CHATHAM | 0.52 | 0.18 | 44.0°S | 176.6°W |
| ST.PAUL | 0.73 | 0.58 | 38.7°S | 77.5°E |
| KERGUELEN | 0.56 | 0.31 | 49.4°S | 70.2°E |
| KEY WEST | 0.31 | 0.10 | 24.6°N | 81.8°W |
| SETTLEMENT PT | 0.31 | 0.14 | 26.7°N | 79.0°W |
| PORT STANLEY | 0.48 | 0.27 | 51.7°S | 57.8°W |
| ABURATSU | 0.24 | 0.03 | 31.6°N | 131.4°E |
| NAHA | 0.70 | -0.15 | 26.2°N | 127.7°E |

Table 3. Tide-gauge stations where the correlation, R, is higher for A run than C run. The correlations listed cover the 2 year period 1993-1994. An annual harmonic has been removed.

| Tide Gauge | R: A Run | R: C run | Latitude | Longitude |
|---|---|---|---|---|
| JUAN FERNANDEZ | 0.45 | 0.61 | 33.6°S | 78.8°W |
| PENHRYN | 0.30 | 0.48 | 9.0°S | 158.1°W |
| HONOLULU | 0.17 | 0.53 | 21.3°N | 157.9°W |
| VALPARAISO | 0.45 | 0.61 | 33.0°S | 71.6°W |
| PORT LOUIS | 0.06 | 0.38 | 20.2°S | 57.5°E |
| RODRIGUES | 0.14 | 0.58 | 19.7°S | 63.4°E |
| CALDERA | 0.27 | 0.47 | 27.1°S | 70.8°W |
| DARWIN | 0.28 | 0.45 | 12.5°S | 130.8°E |
| ESPERANCE | 0.27 | 0.68 | 33.9°S | 121.9°E |
| DUCK PIER | 0.40 | 0.70 | 36.2°N | 75.7°W |
| OFUNATO | 0.07 | 0.42 | 39.1°N | 141.7°W |
| CRESCENT CITY | 0.57 | 0.67 | 41.7°N | 124.2°W |
| NEAH BAY | 0.56 | 0.71 | 48.4°N | 124.6°W |
| SAN DIEGO | 0.53 | 0.64 | 32.7°N | 117.2°W |
| YAKUTAT BAY | 0.55 | 0.71 | 59.6°N | 139.7°W |
| KETCHIKAN | 0.44 | 0.62 | 55.3°N | 131.6°W |
| DIEGO RAMIREZ | 0.25 | 0.44 | 56.5°S | 68.7°W |

Table 4. Tide-gauge stations where R is lower for A run than C run. The correlations listed cover the 2 year period 1993-1994. An annual harmonic has been removed.

process. When the annual harmonic is included in the computation of the correlations between time series, eight of the stations in list 3 move to either list 1 or 2 (Darwin, Esperance, Duck Pier, Ofunato, Crescent City, Neah Bay, Yakutat Bay, and Ketchikan), indicating that the high frequency variability along coasts is being degraded by the assimilation process. None of the stations in list 2 move to list 3 if the annual harmonic is included, meaning the annual cycle is not degrading the correlation at the locations improved in run A. The annual harmonic does degrade the correlation values for the A run at three stations, Easter Island, Kushimoto, and Saipan which showed had shown no change in the correlation values for higher than annual frequency variation.

By looking at individual locations, a qualitative evaluation can be made in how the models simulate the sea level. At Naha (26.2°N, 127.7°E), in the Kuroshio region, the correlation between the time series of tide-gauge data (with an annual harmonic removed) and the model increases from -0.15 to 0.70 (Figure 47a). At Naha, it is mostly the long

temporal scale (seasonal or greater) of sea level variation that has increased the correlation value, clearly seen qualitatively in the plot with run A (heavy line) appearing to follow the tide-gauge data (thin line) better than run C (the dotted line). In the tropical region at Pohnpei (7°N, 158.2°E, Figure 47b), the correlation between the C run and the tide-gauge measurements is 0.44 and with the assimilation of the altimetric data (run A), the correlation increases to 0.62. The increase at this location is mostly an improvement in the higher frequency (less than a season) events which occur in 1994, especially around the October/November time frame. In the middle of the North Pacific at Midway Island (Figure 47c), the assimilation improves the model from 0.11 to 0.60, with most of the improvement occurring at high frequency. Note here, the magnitude of the model SSH anomaly still underestimates the observed sea level anomaly.

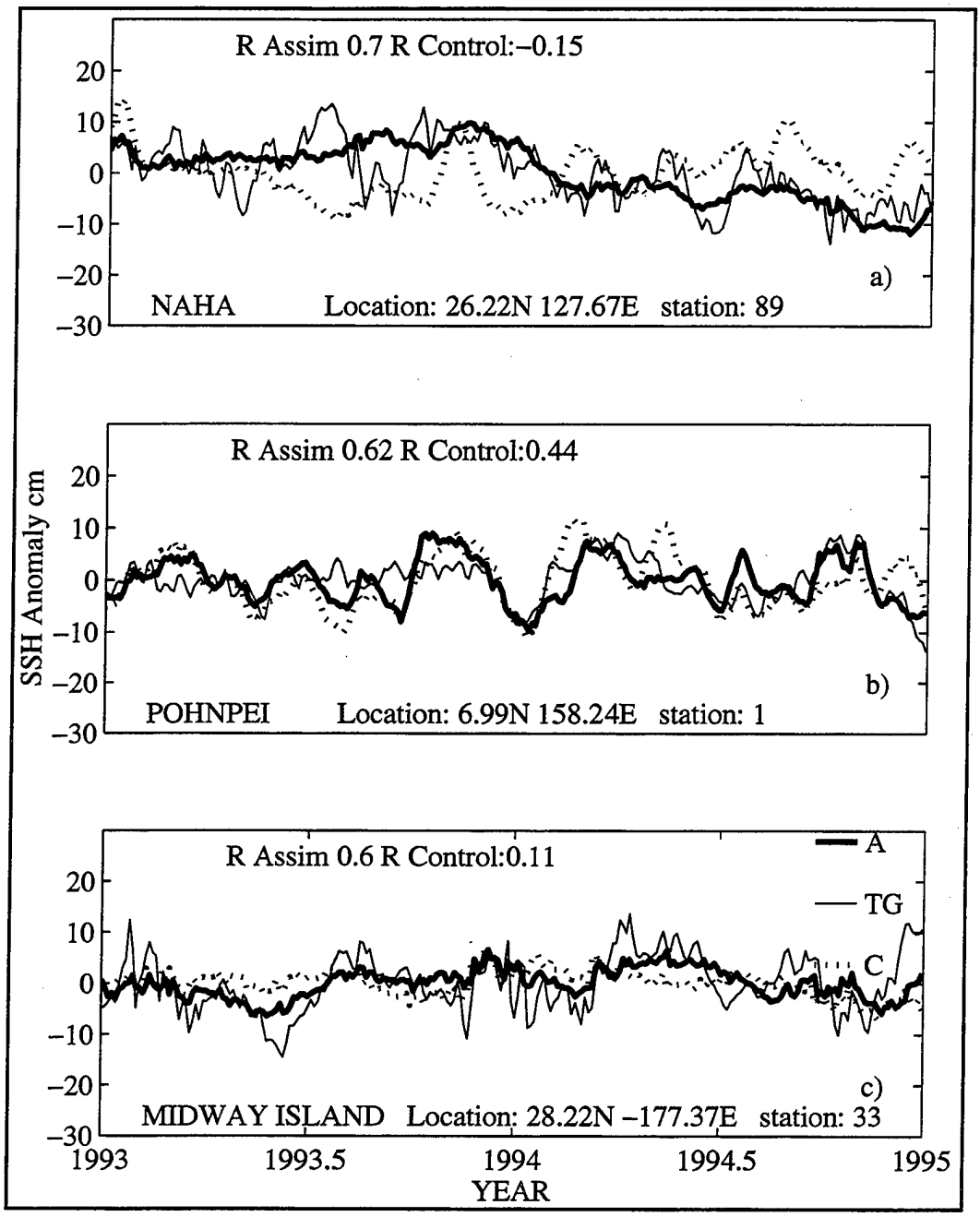


Figure 47. Times series of SSH for 3 stations: a) Naha in the North Pacific, b) Pohnpei in the tropical Pacific, and c) Midway Island in the North Pacific. The bold line represents the A run; the thin line is the data measured with a tide gauge; and c) the dotted line is the SSH from the C run. An annual harmonic has been removed from all the time series.

## 2. Spectra of SSH, Surface Velocity Fields

The differences between the SSH and velocity fields can be further quantified by examining the spectra of these fields. Average 10°x10° spatial SSH meridional spectra are computed as in *Stammer and Böning* (1992), and then averaged over a year from 10 day maps of SSH. A map of every other average spectra is shown in Figure 48 for the whole globe. From the global viewpoint, when averaged over these 20°x 20° areas, the spectra between the two model runs has changed little. If we look at several locations in particular, at the region centered around 45°N, 75°W in the Gulf Stream area and the Kuroshio region (45°N,185°E), the observational spectrum (dotted line) (Figure 49a,b) is different from either of the two model runs, but the still within the error of the observed spectra. At 35°S, 5°E (Figure 49d), the assimilation has reduced the variance of the model at low wave numbers, more representative of the altimetric observations. In the western tropical Pacific (Figure 49c), it appears that the assimilation has not changed the spectrum.

The zonal velocity temporal spectra are calculated from 3 day fields and along two meridians, 30°W in the Atlantic and 200°E in the Pacific at approximately every 10 degrees of latitude. No averaging over latitude bands has been done for these spectra. Figures 50 and 51 show the spectra as it is computed from the C run (thin line) and from the A run (bold line). The figures confirm what has been seen in the change of EKE of the model (Figure 32c). The A run shows a significant increase in the velocity variance over the whole spectra in the Southern Ocean (50°S and 30°S) in the Pacific. In the tropics at 10°S, the A run spectra is slightly higher, but not significantly. While in the North Pacific, there is little change in the spectra along this meridian. This is also consistent with Figure 30, showing the locations where the model is nudged the strongest. There is weak nudging along this line in the 200°E meridian in the Pacific.

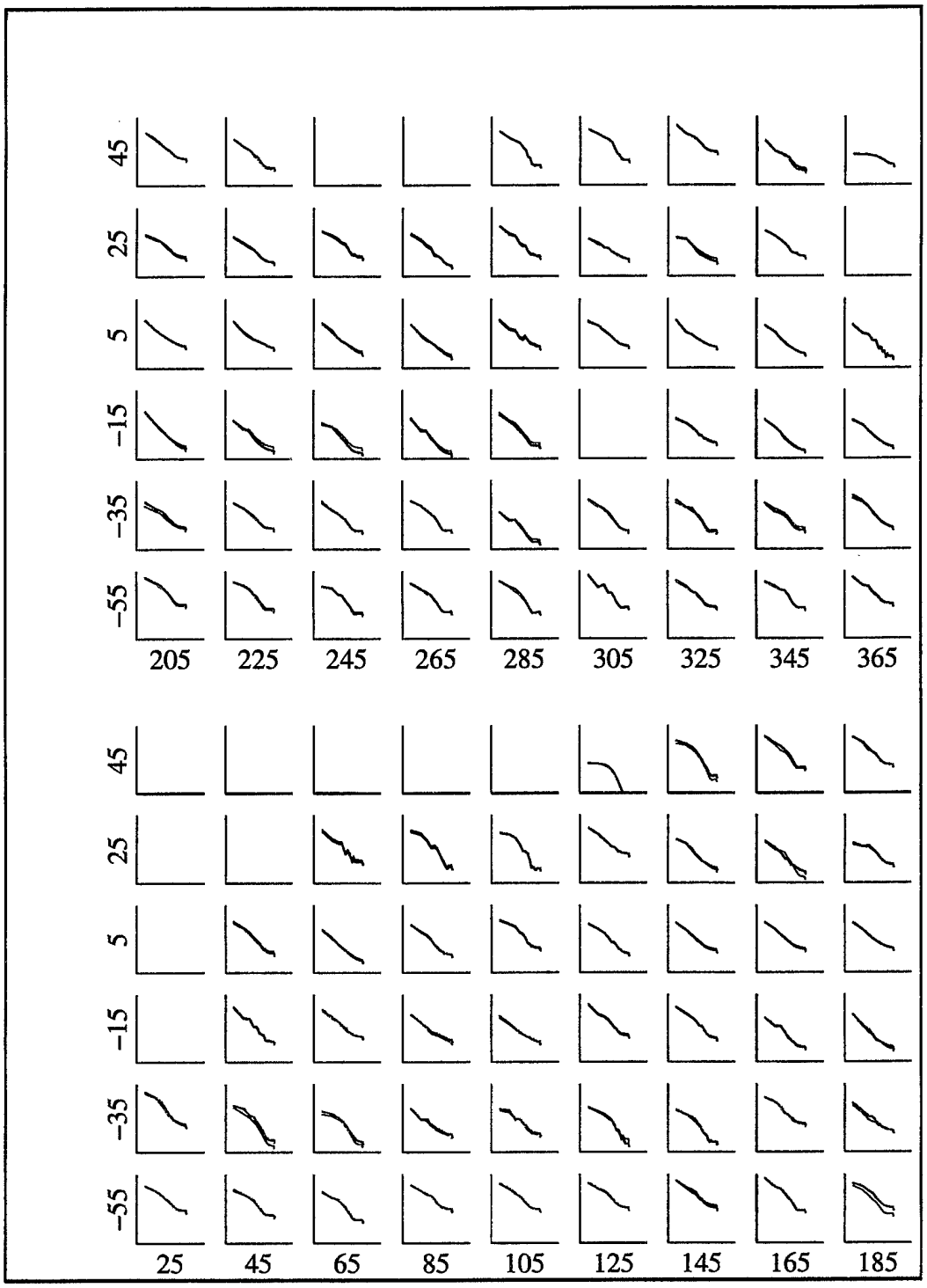


Figure 48. Global spectra of SSH of the A run (black line) and C (red line) averaged over 20°x 20° areas. The left side labels indicate the latitudes and the labels across the bottom indicate longitude. The y axis of each small plot ranges from 5e-4 to 5e-2 and the x axes range from 1e-1 to 1e6.

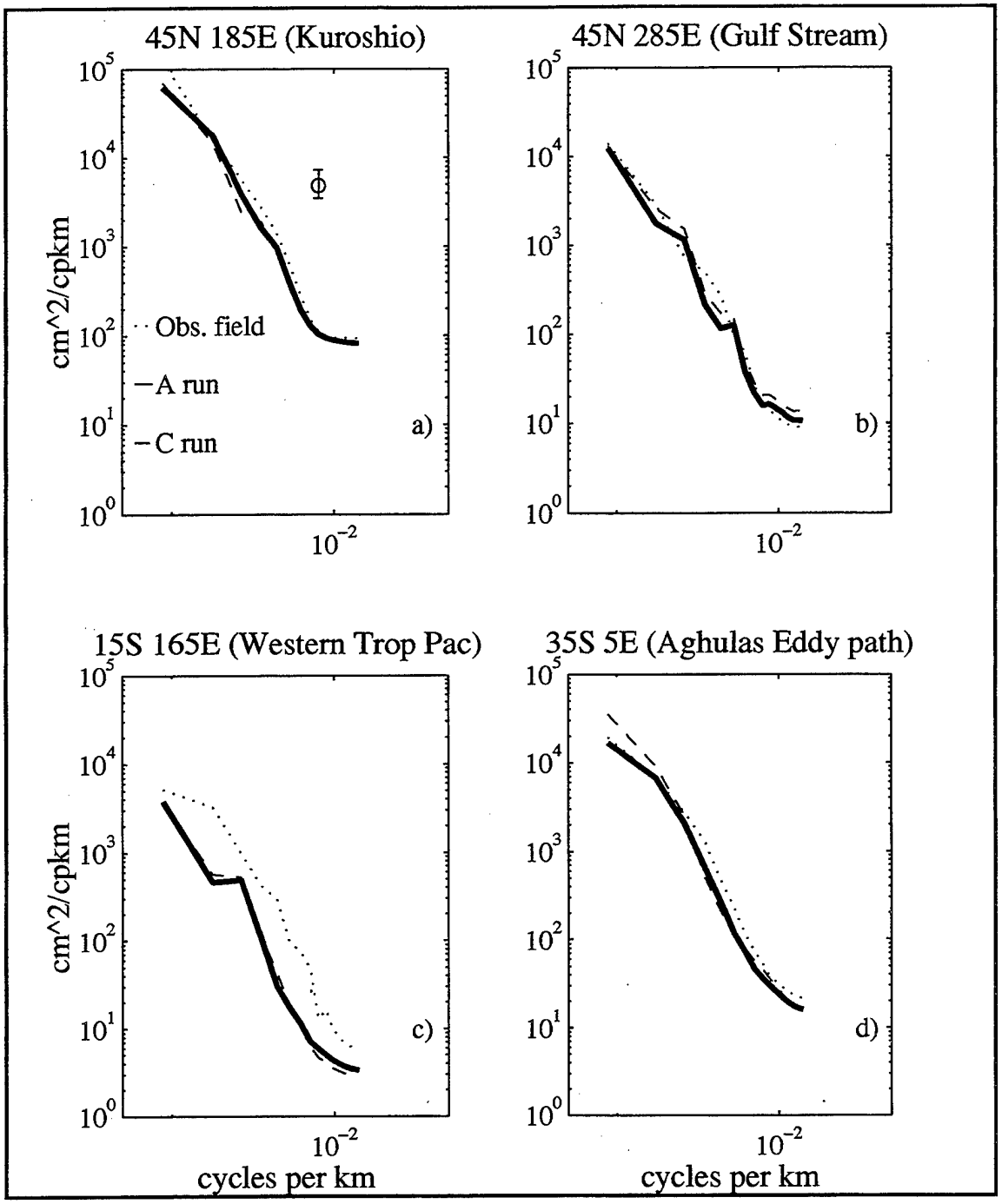


Figure 49. SSH spectra for the a) Kuroshio region, centered at 45°N 185°E; b) for the Gulf Stream region, centered at 45°N 285°E; c) for the western tropical Pacific, 15°S 165°E; and d) for the Aghulas eddy path in the South Atlantic, centered at 35°S 5°E. The dashed line are the C run values, the dotted line is from the A run, and the solid line is the observed spectra.

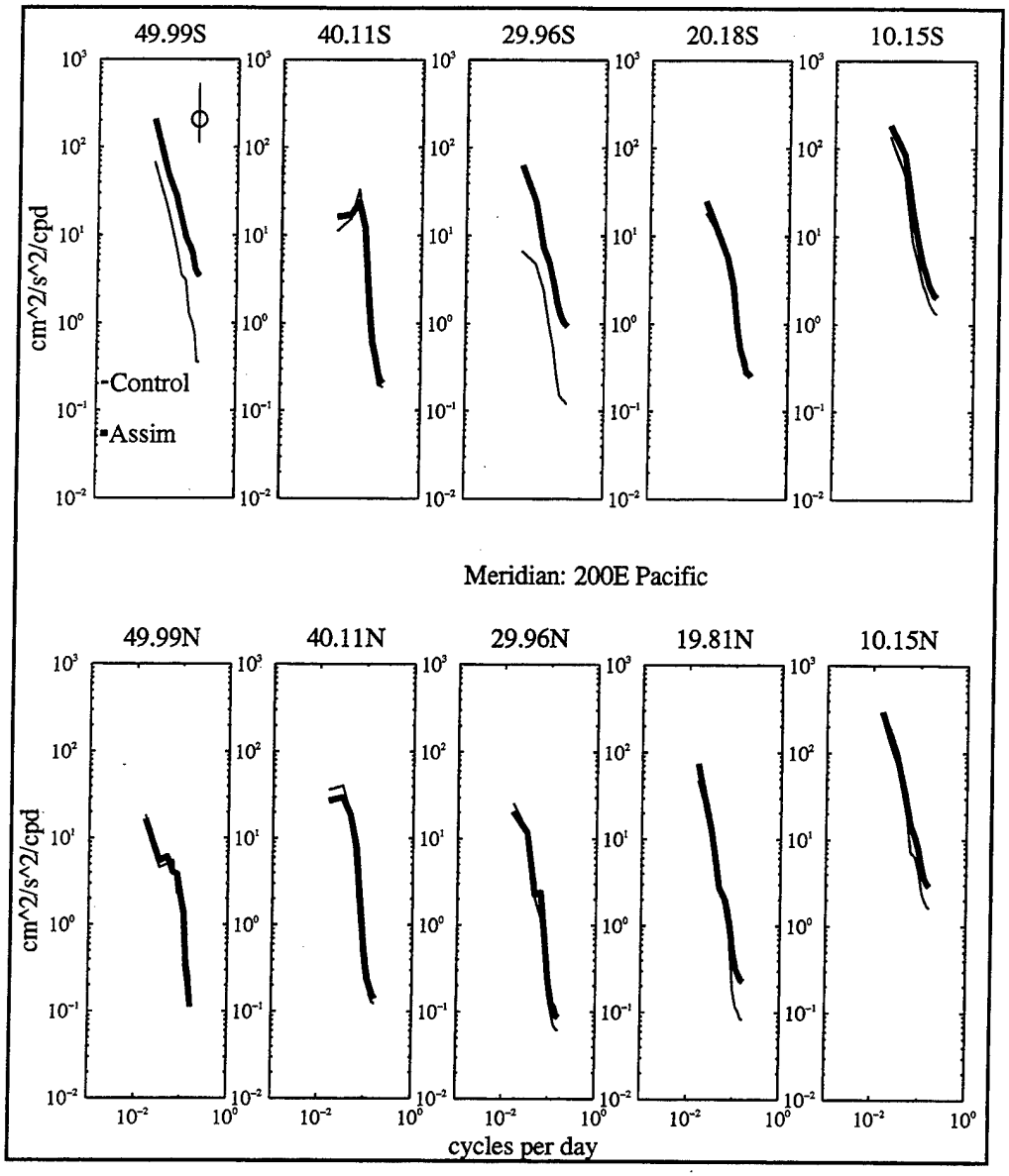


Figure 50. Spectra of the zonal velocity along 200°E in the Pacific, at every 10° of latitude. The bold line are the A run values and the thin line are from the C run.

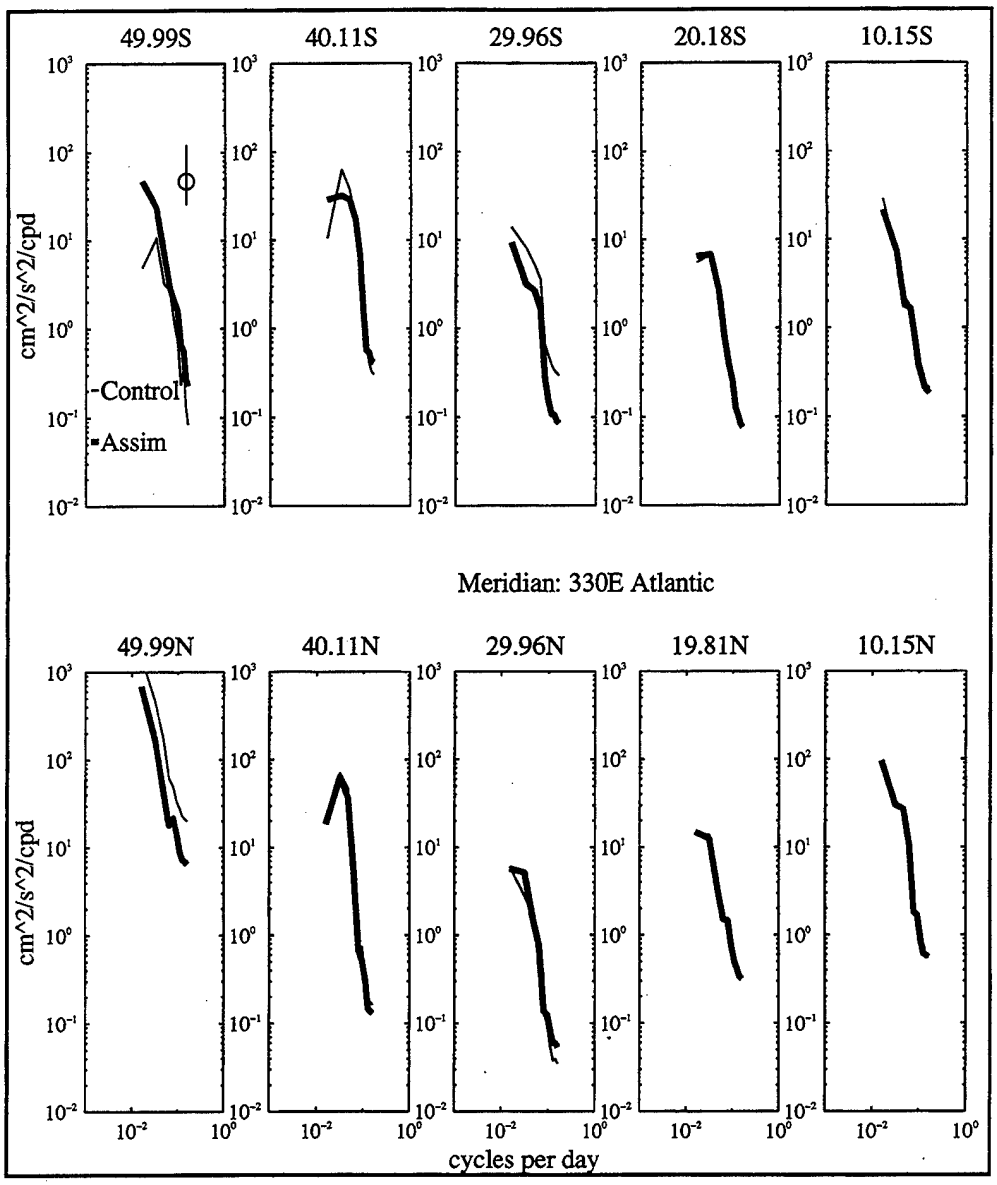


Figure 51. Same as 50, except for the 330°E meridian in the Atlantic.

### 3. Comparisons of Subsurface Prognostic Variables to Observations

The four regions described above are examined again in this section, but now looking at the changes that have occurred in the vertical. The subsurface fields are compared to observational hydrographic data to determine if the vertical relationship

between SSH and temperature or salinity improves the simulation of the subsurface fields. Each area is examined in two ways, first by qualitatively and quantitatively describing the changes in the vertical structure and second by comparing the model sections to an in situ hydrographic section.

*a. Kuroshio Region*

Figures 52 and 53 show plan views of five prognostic model variables, U,V,T,S, and SSH ($\eta$), along with the observation field for the month of December 1993 (approximately half way through the assimilation run). SSH is included for completeness to show how well the observation SSH has been included into to run A's SSH field. Figure 52 shows the fields at a depth of 37.5m (level 2 of the model) while Figure 53 shows the fields at a depth of 160m (level 6) and the surface height field ($\eta$). The bottom panels are for the C run and the top panels are for the A run. Below the first set of panels is the color range for the values for a particular variable. The color scale maps are identical for the C and A run. The velocity vectors for the level are plotted on top of the SSH field. It is evident from these maps that the zonal velocity structure has changed between the C run and the A run, with three zonal frontal like structures appearing in the A run both at the surface and at depth. The temperature structure has also been changed at 160 m showing a tongue of higher temperature water at 37°N, corresponding to the higher height field at the surface at the same location. The 37.5m layer shows changes also in the temperature structure, but the tongue is not as distinct in this layer, although there is a temperature increase in the A run as compared to the C run. At both levels, the salinity does not appear to have changed as much as the temperature. This is due, in part, to the differences in the vertical correlation functions (see Figures 29a,b). It is evident, then, from these maps, that not only has SSH changed in this region, but also temperature and salinity, and therefore, indirectly, the velocity field.

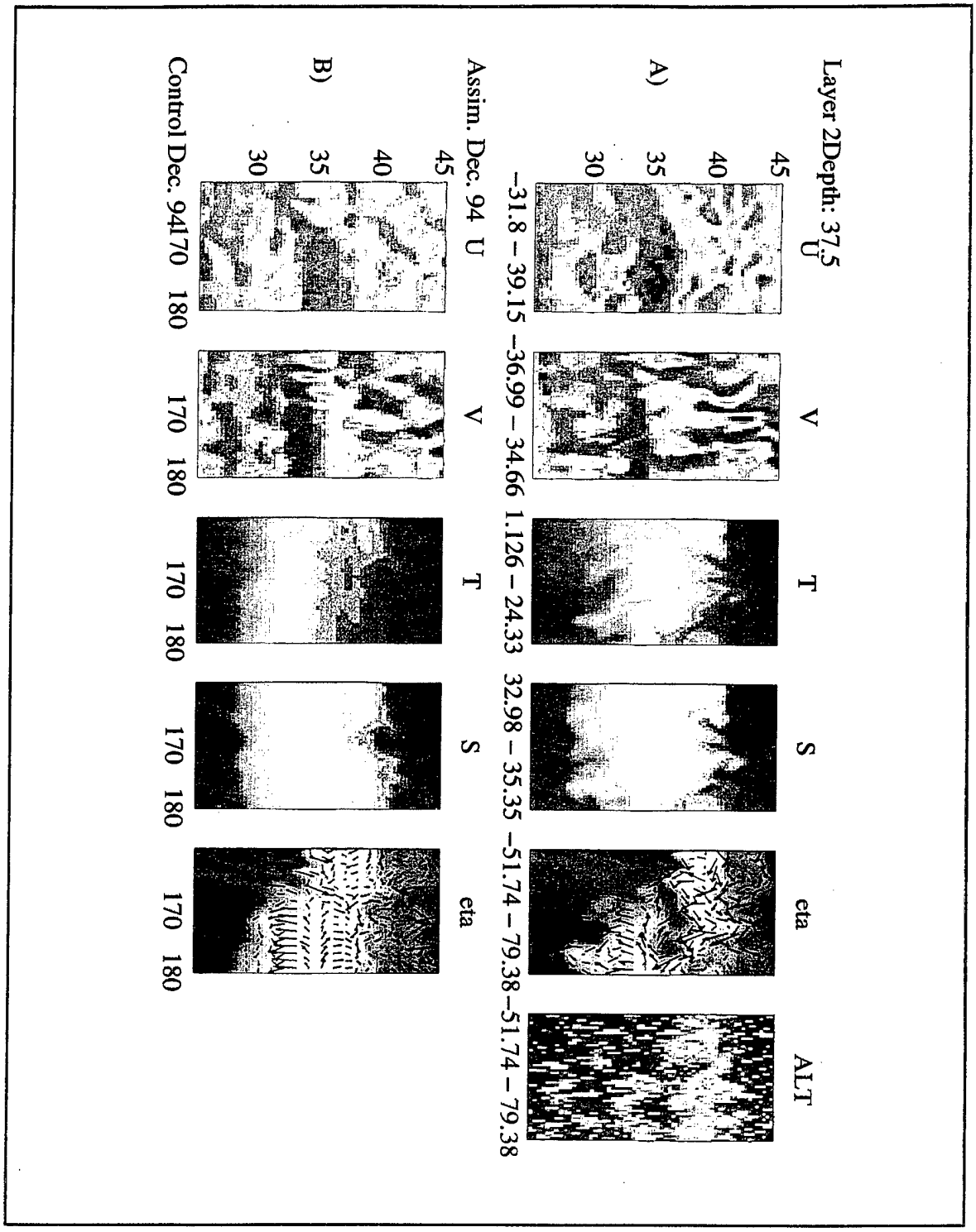


Figure 52. Plan view of model prognostic quantities at level 2 (37.5 meters) in the Kuroshio region for the month of December of 1993. The top row (A) are from the assimilation run and the bottom row are from the C run. The color scale range for each pair of quantities is indicated below the panel in the top row.

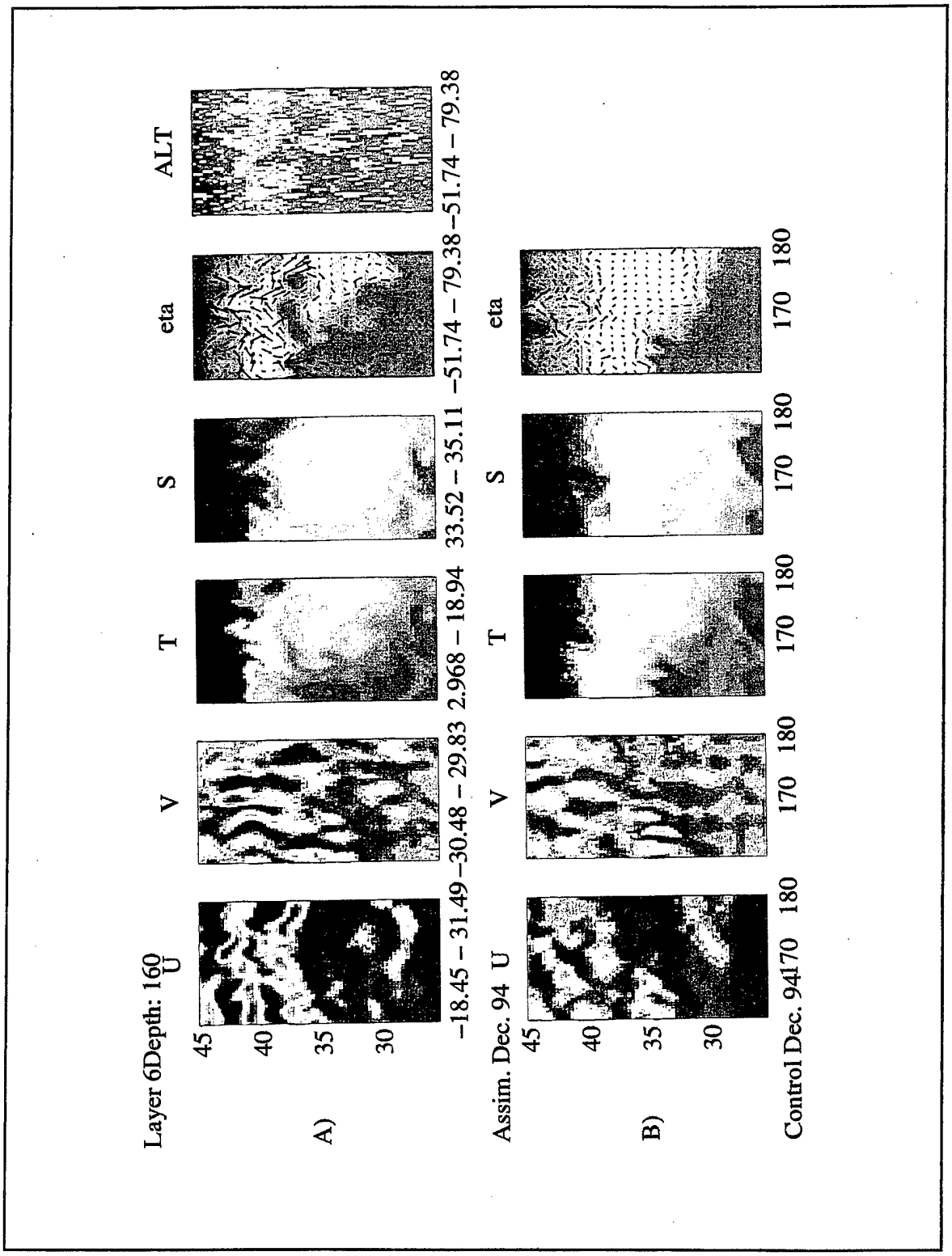


Figure 53. Same as Figure 52, but for level 6 (160 meters).

In August of 1992, WOCE investigators (*Taft*, 1995) collected full depth hydrographic data along the 165°E meridian between about 35° and 50°N (P13). The A run was not begun until after this date, so a comparison is made with the model data from August of 1993, with the possibility that the changes between the consecutive Augusts may not be that different. Figure 54 (taken from *Taft*, 1995) shows the vertical structure of potential temperature for the WOCE line. Included on the figure are annotations of the major frontal structures which were crossed during the sampling of this meridian in the Pacific. At around 47°N is the Subarctic Current, between 40° and 42°N is the Subarctic Front, and at 35°N is the location of the Kuroshio Extension.

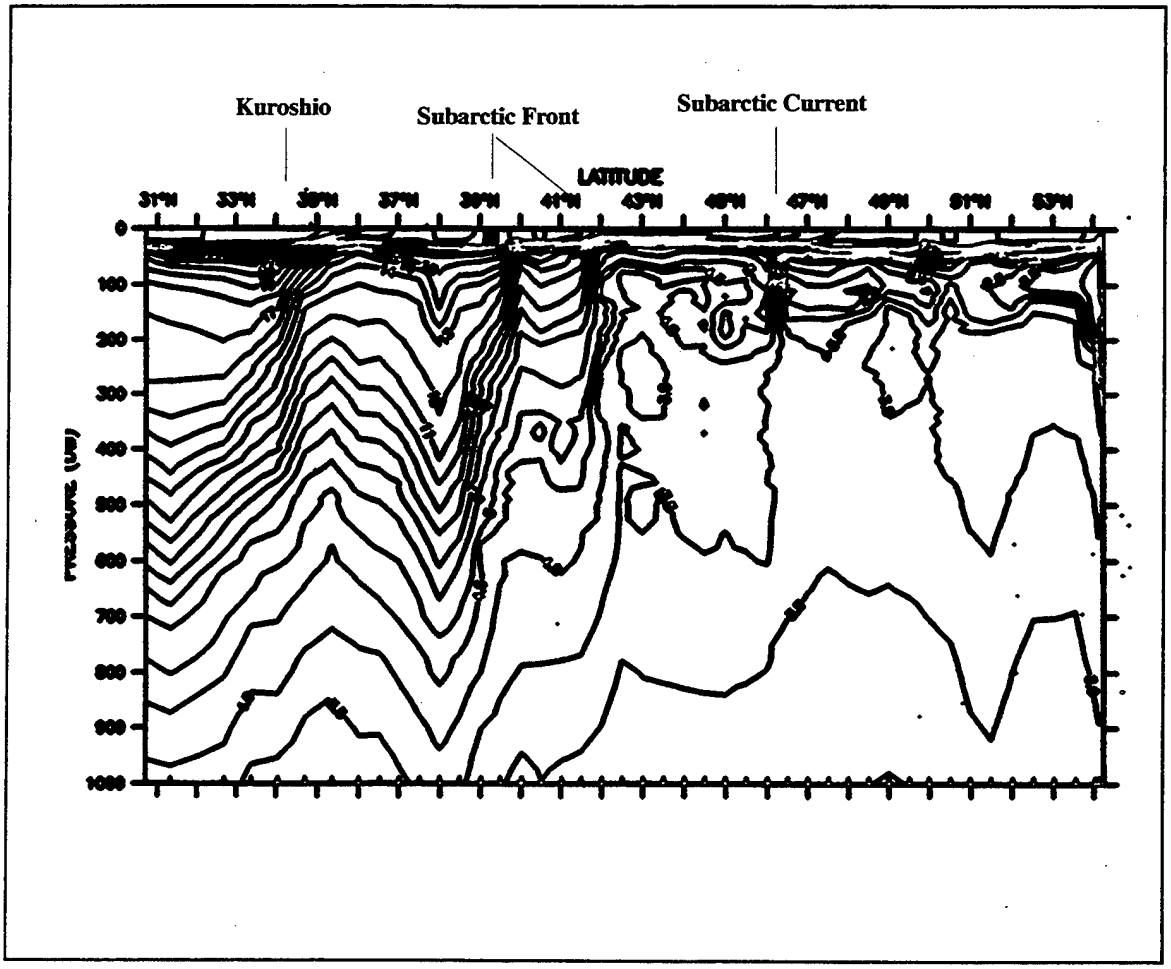


Figure 54. From *Taft* (1995), showing the meridional P13 temperatures (165°E in the North Pacfic).

Figure 55 shows the vertical temperature structure along this same meridian for the C run (Figure 55a) and for the A run (Figure 55b) and for the August *Levitus* 94 climatology (Figure 55c). The heavy lines on the plots indicate the 14°C, 8°C, and 6°C isotherms. Note that there are significant changes to the structure in the vertical. It is immediately apparent that the 14°C isotherm has moved northward, intersecting the surface at around 40°N in the A run while in the C run, the isotherm is 5°S at about 35°N. The Levitus field, which is being used as the subsurface observational field, also has this isotherm further to the north than it is in the C run. The subtropical front at around 40°N shows the isotherms closer together in the A run than in the C run. A strip of colder water has been introduced at around 43°N, which looks to be the cause of these compressed isotherms to the south. In the north, the 3.5 isotherm is higher in the water column in the A run at 54°N, similar to the observations. In addition, the 3-4°C isotherms in the north are more similar to the observations in the A run than in the C run. The assimilation process is attempting to adjust the subsurface values to those shown in the Levitus field. However, neither model run shows the lifting of the deep isotherms south of 37°N. (The observational salinity section from P13 is not available, therefore it is not shown.)

*b. Gulf Stream Region*

Starting again by showing two levels of plan views of five of the prognostic variables of the two model runs (Figures 56: level 2, 37.5 m and Figure 57: level 9, 435 m), it is easily seen that changes are occurring near the surface as well as at depth. The close examination of the path of the Gulf Stream shows that the assimilation run is attempting to correct, in temperature as well as in the velocity field, the path of the Gulf Stream (Figure 44). A meridional cross section at 70°W is shown in Figure 58a-c for the temperature fields from June of 1994 (a) C run, b) A run, and c) Levitus 94). The figure shows the northward shift of the 20°C isotherm in the A run.

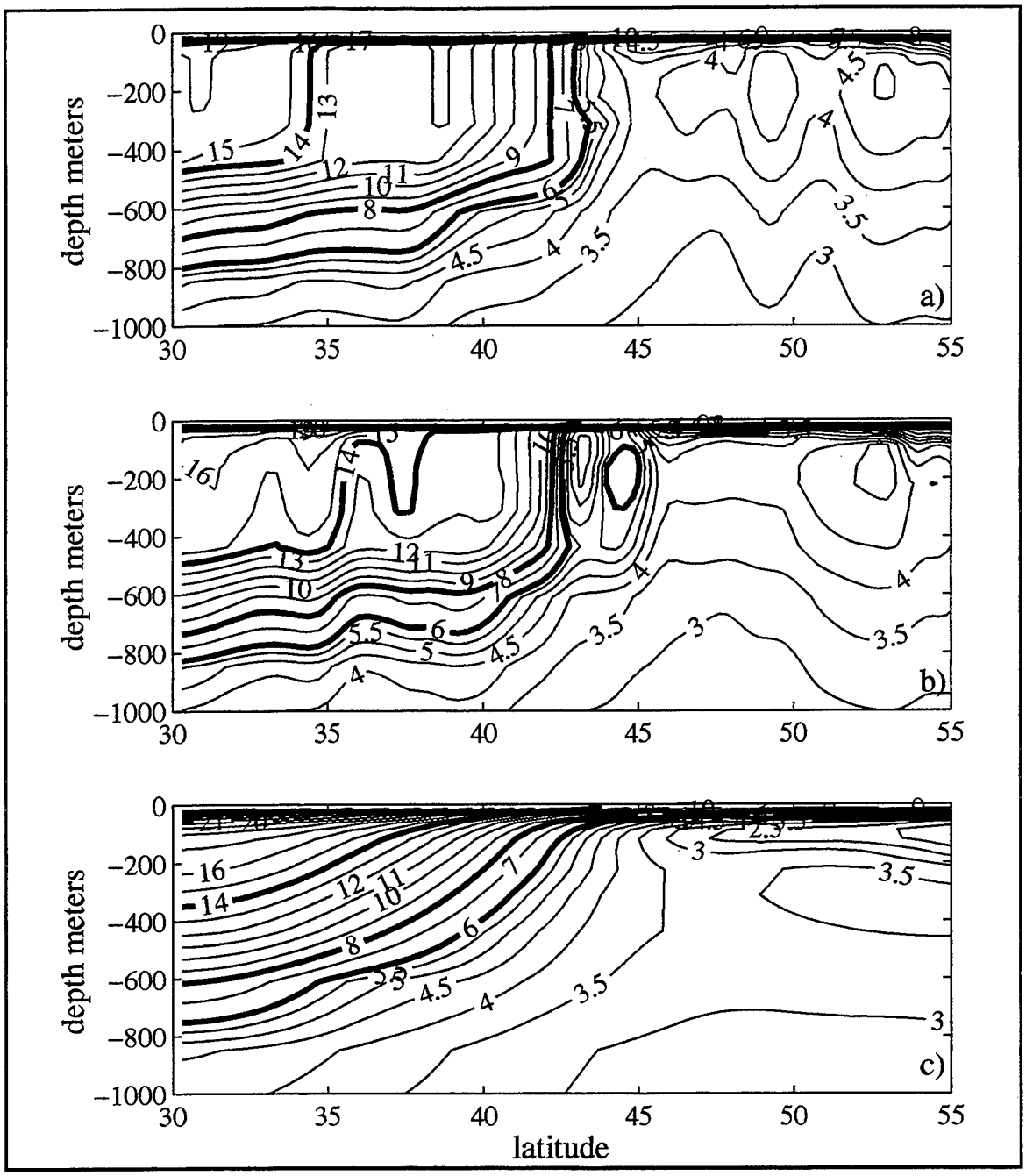


Figure 55. Meridional section along 165°E from a) C run, b) A run, and d) Levitus 94. Bold lines indicate the 14°C, 8°C, and 6°C isotherms.

Model sections from April of 1994 at 64°W are compared to the April 1985 Endeavor 129 hydrographic section in Figure 59. Although the years are different (model and observations), the comparison is still valid because it is comparing a single month, rather than a climatology (e.g. Levitus '94). For this plot, April of 1994 model temperatures are shown, with the A run as the bold line and the C run shown by the thin line. The in situ data were retrieved from the WOCE hydrographic archive site. The observational temperatures, interpolated to 222m (a) and 435m (b), are plotted as asterisks to show the difference in the temperatures at these two depths between the model runs and the observations. The two models are fairly similar in their representation of the temperature fields, especially at the 222m, and both are close to the observed values. Where there are differences, near 38°N and at 33°N, the A run is closer to the observed temperatures than is simulated in the C run. At a deeper depth of 432m, neither model run is simulating correctly the observed temperatures north of 35°N, however the A run appears to be adjusting the temperature values towards the observations. This is due to the use of a mean field from an earlier model version, and not the true mean of the ocean. For the salinities along this section (Figure 60), the assimilation is only slightly modifying the values of towards the observed field.

*c. Tropical Region*

A temperature section across 156°E has been extracted from the two runs of the model (Figure 61) for two months, July of 1993 (a,b) and six months later in January of 1994 (d,e). The corresponding *Levitus* 94 section is shown in the c and f panels of the figure. The sections for the C run are shown in Figure 61a and d, and the sections for the A run are in b and e. An examination of the meridional sections shows little change has occurred in the region of the western tropical Pacific.

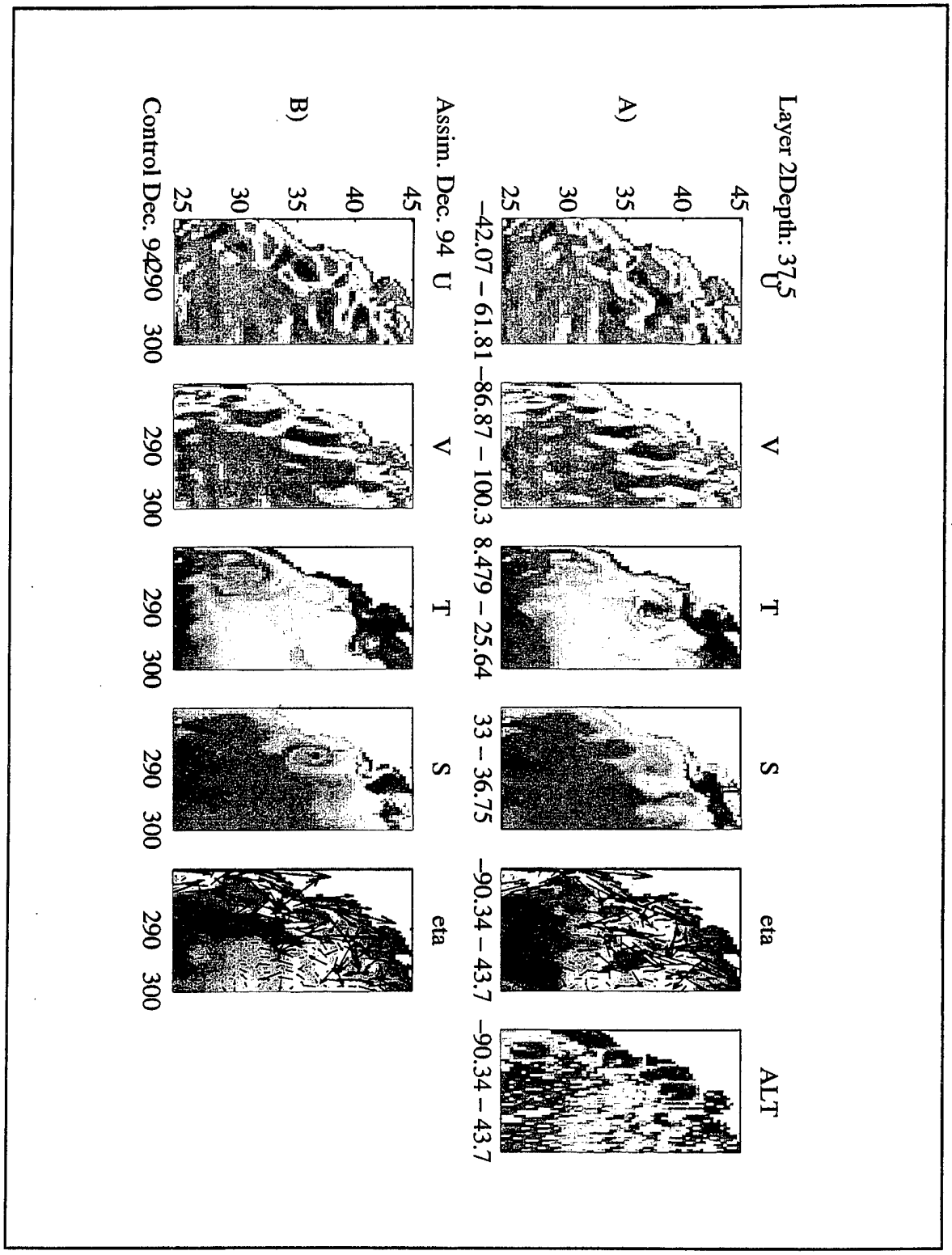


Figure 56. Same as Figure 52, but for the Gulf Stream region.

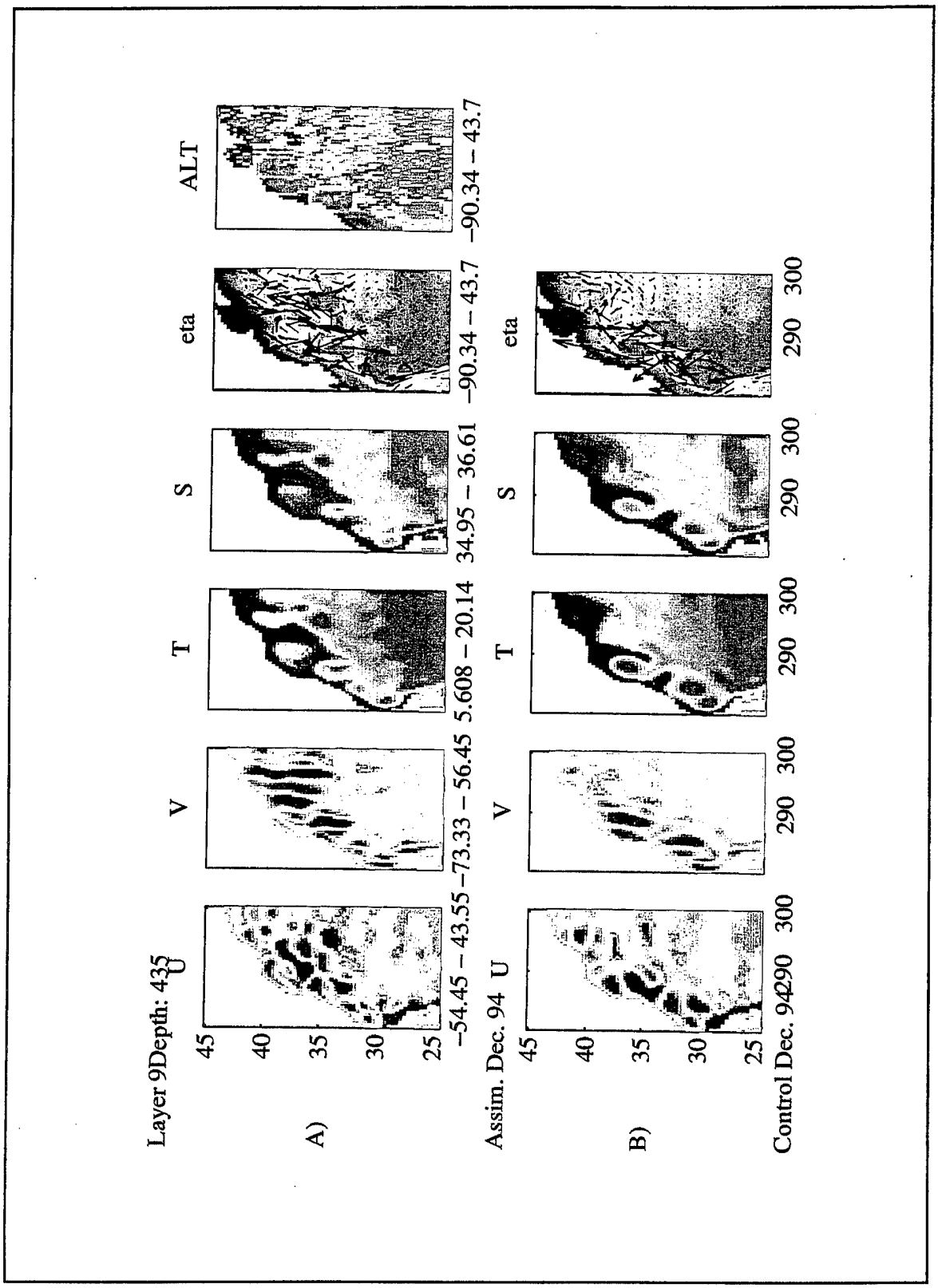


Figure 57. Same as Figure 56, but for layer 9 (435 meters).

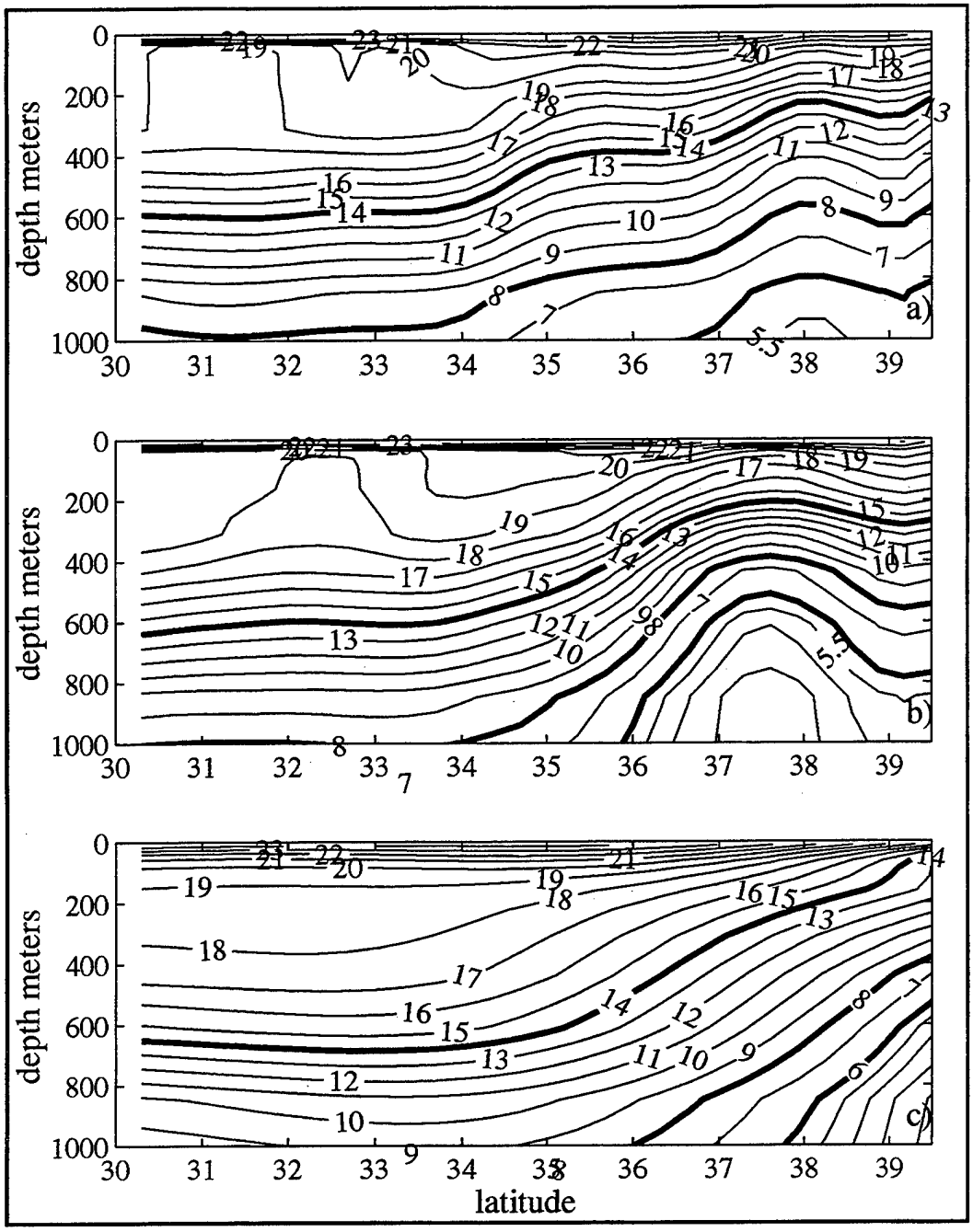


Figure 58. Meridional temperature section along 290°E in the North Atlantic for June of 1994. Bold lines indicate the 14°C, 8°C, and 6°C isotherms. a) C run temperatures, b) A run temperatures, and c) Levitus 94 climatology for June.

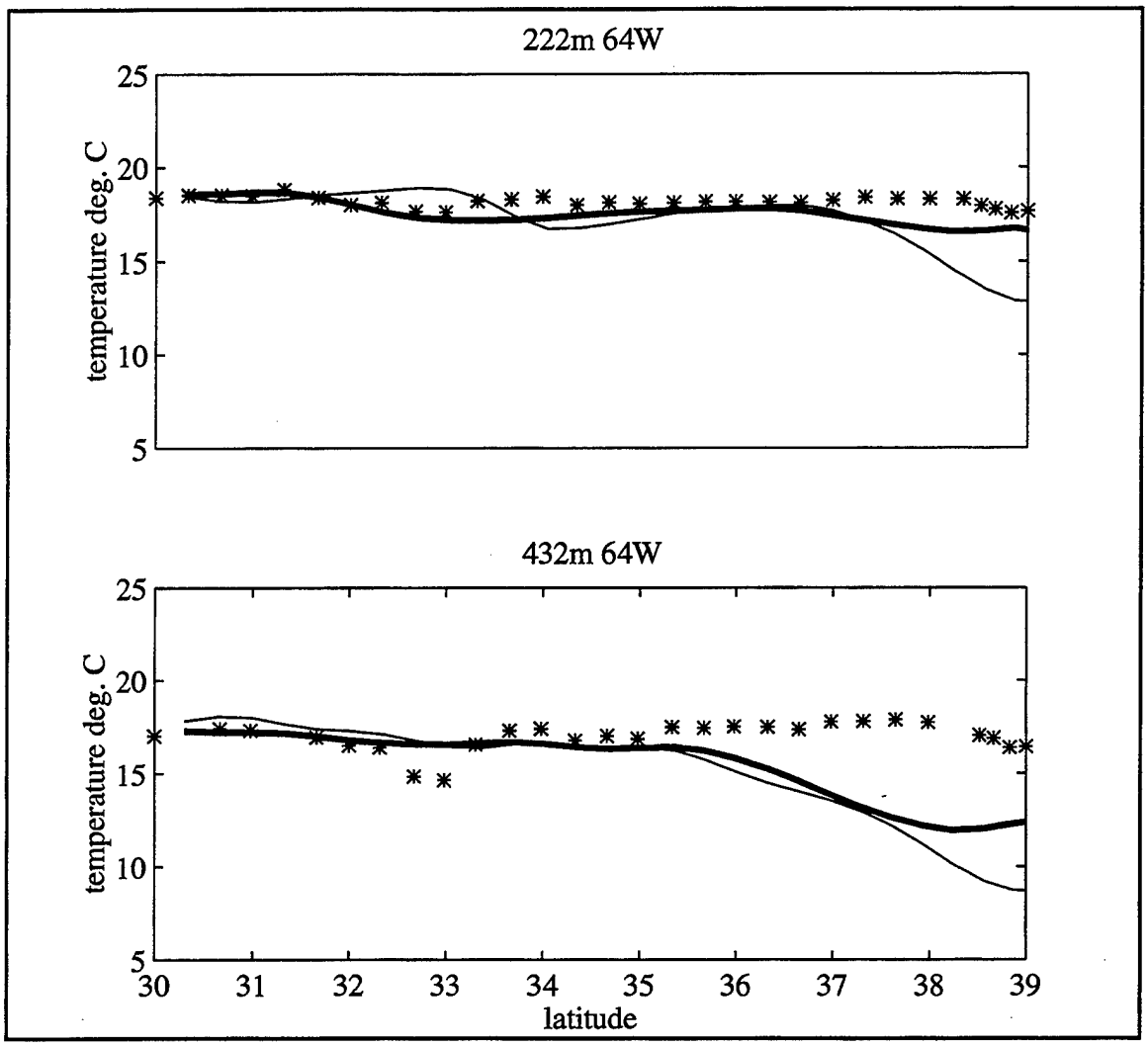


Figure 59. Temperatures along section shown in Figure 58 for April of 1994 at a) 222 meters and b) 432 meters. The bold line are the values from the A run, the thin line are from the C run and the astericks represent the observations from the hydrographic cruise Endeavor 129 (sampled in April of 1985).

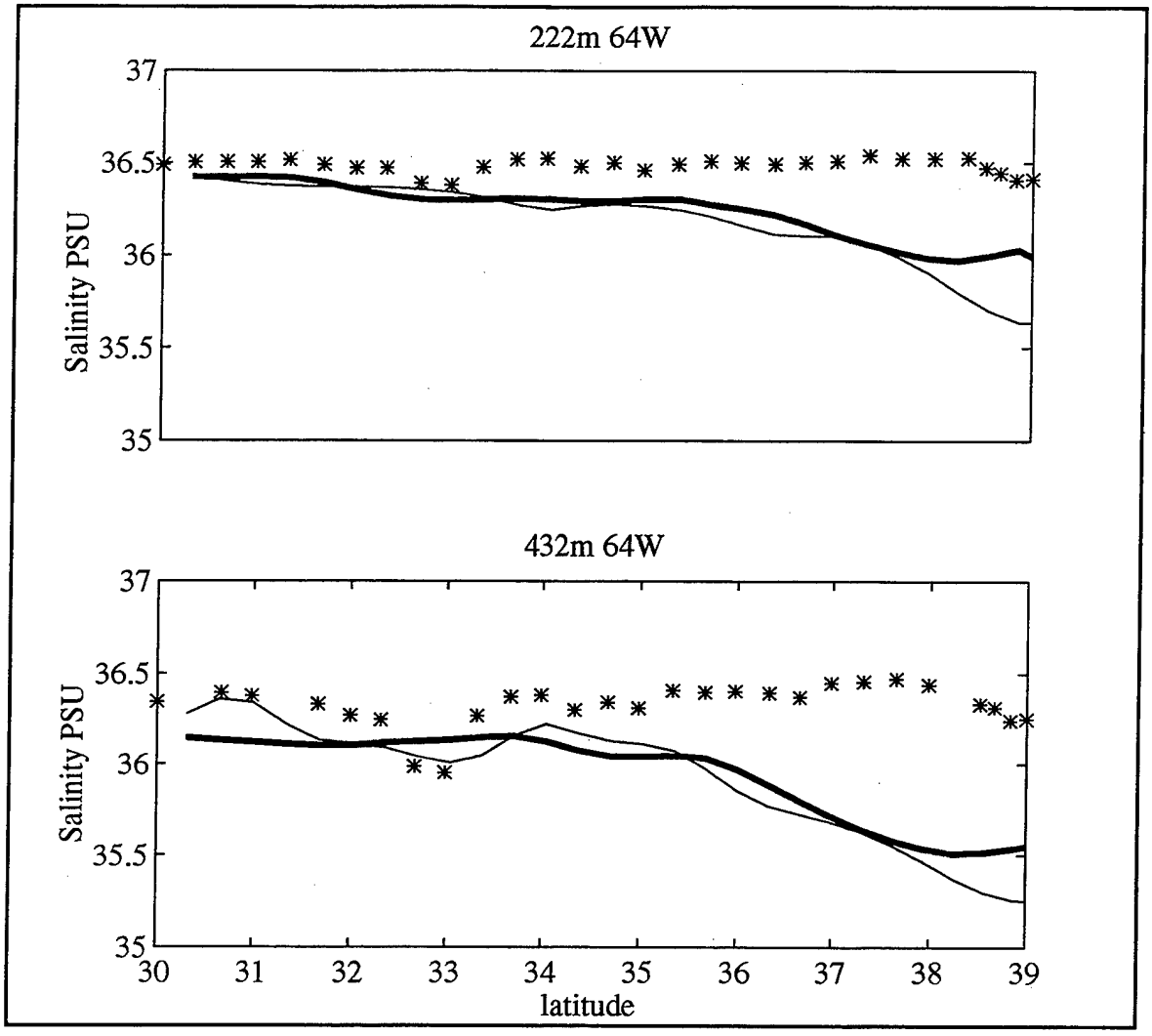


Figure 60. Same as Figure 59, but salinity values.

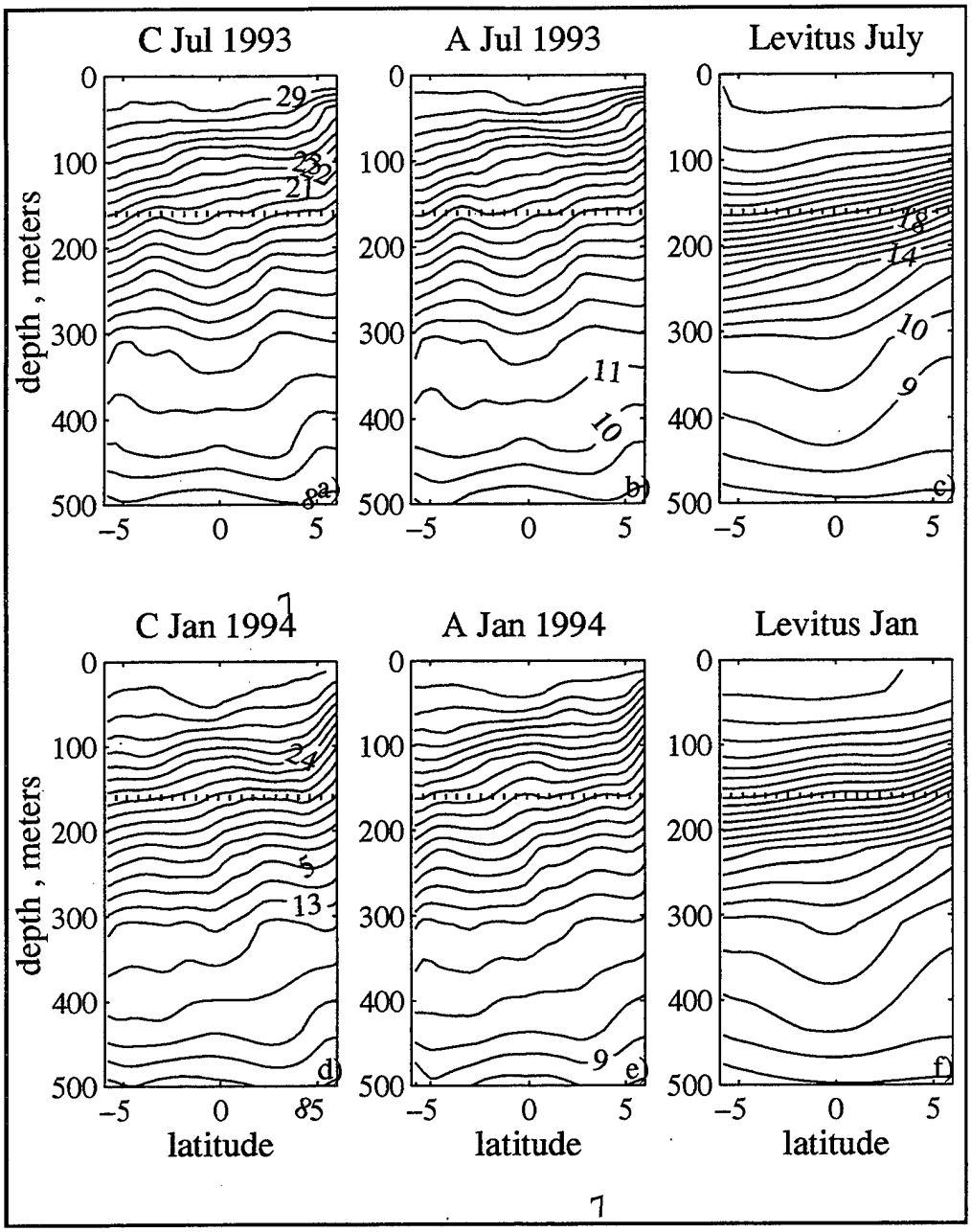


Figure 61. Meridional temperature section (156°E) in the tropical Pacific between +/- 8° for the months of July 1993 and January 1994. a) and d) are for the C run; b) and e) are the A run sections, and c) and f) are the Levitus 94 climatology.

A closer examination of temperatures across the level of 160 m are shown in Figure 62. The thin lines represent temperature values for July of 1993, while the bold lines are for January 1994. The A run temperatures (solid lines) are cooler as compared to either the Levitus data (dotted line) or the C run temperatures (dashed lines) for both months.

Observations taken from the TAO set of moorings at 156°E between 5°S and 5°N can be compared also to the model estimates to determine which run is simulating the observations better. Using the gridded maps of the TAO mooring data taken from the PMEL TOGA-TAO Web page (www.pmel.noaa.gov/toga-tao), approximate monthly mean temperature observations plus the associated anomaly are also plotted on this figure. The July 1993 mean temperature at the given latitudes and at 160 m are plotted as circles and January 1994 temperatures are plotted as asterisks. The model July 1993 temperatures are still too warm as compared to the observations (compare the thin lines to the circle values), but the A run has reduced the difference by approximately a degree. The A run at 5°N is accurately representing the ocean temperature, once again reducing the temperature from what is seen in the section from the C run. At 0°N, the A run has reduced the temperature, but not to the mean value seen in the observations. And in the south, the two runs differ by only a few tenths of a degree, with the C run closer to the observations than the A run. It is noted that the monthly mean model temperatures from both model runs are within the range of the temperatures seen in the observations over these two months. The Levitus climatology shows warmer values than the observed or modeled values. For the period 93/94, the observed values are cooler than the average values as seen in time/latitude plots of TAO data covering six years. Thus the model is making the adjustment to the temperature fields in the correct direction.

d) Southern Ocean

WOCE line A11 (*Saunders and King*, 1995), along 45°S between 60°W and 20°E in the Atlantic section, was sampled December, 1992 - February of 1993. It is in the earlier part of the assimilation experiment, but it can still provide some guide as to how realistic either of the model runs are. Zonal sections across 45°S are shown in Figure 63a,b for January of 1993 and in Figure 64a,b for January of 1994 for run C and run A,

respectively. The January 1993 plots, in the early part of the experiment, for the C (Figure 63a) run and for the A run (Figure 63b) are similar, with the major difference at 50°W, where the large plume like structure of warm water has increased in the A run. These can be compared to Figure 63c, the A11 observational temperatures sampled around January of

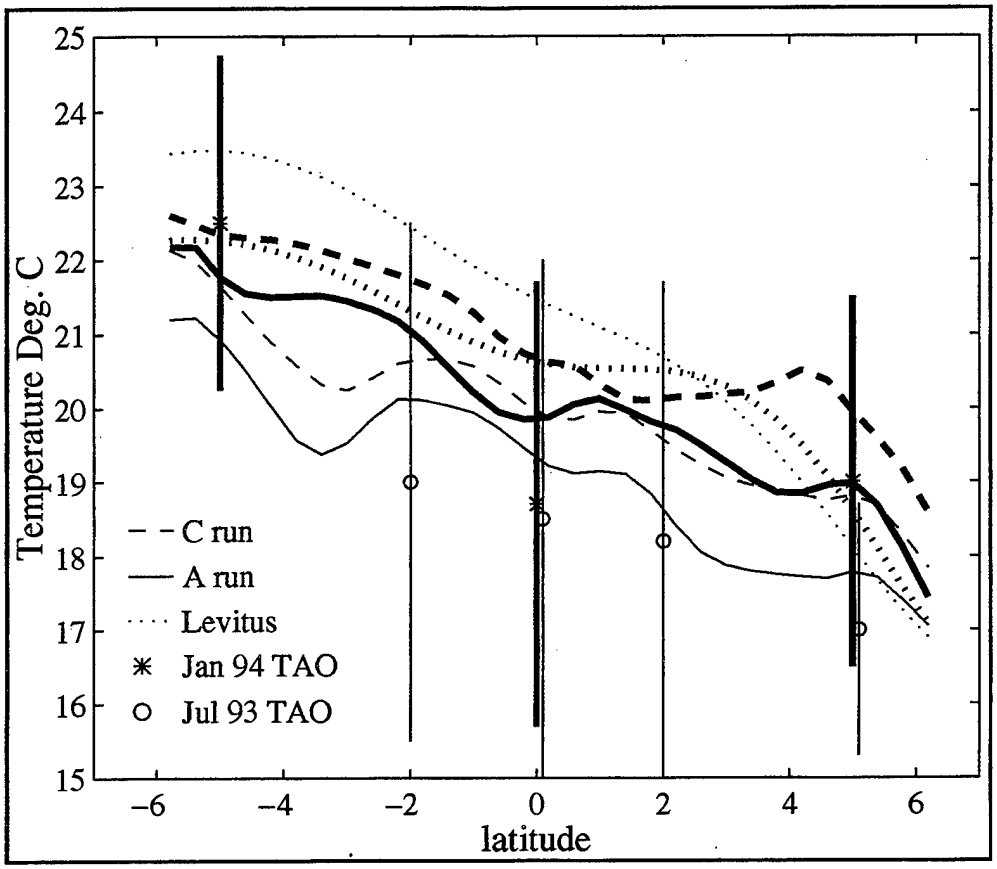


Figure 62. Tempertures at 160 meters for the section shown in Figure 61. The solid lines (bold = January, thin = July) are the A run temperatures, the dashed lines are from the C run and the dotted lines are the Levitus values. The astericks denote the January 1994 TAO observations and the circles, July 1993 TAO observations at the same depth and location with their associated variance.

1993. These plots are directly comparable. In the observations, the plume of warm water is located at 56°W rather than at 50°W as seen in the model. Another obvious difference is

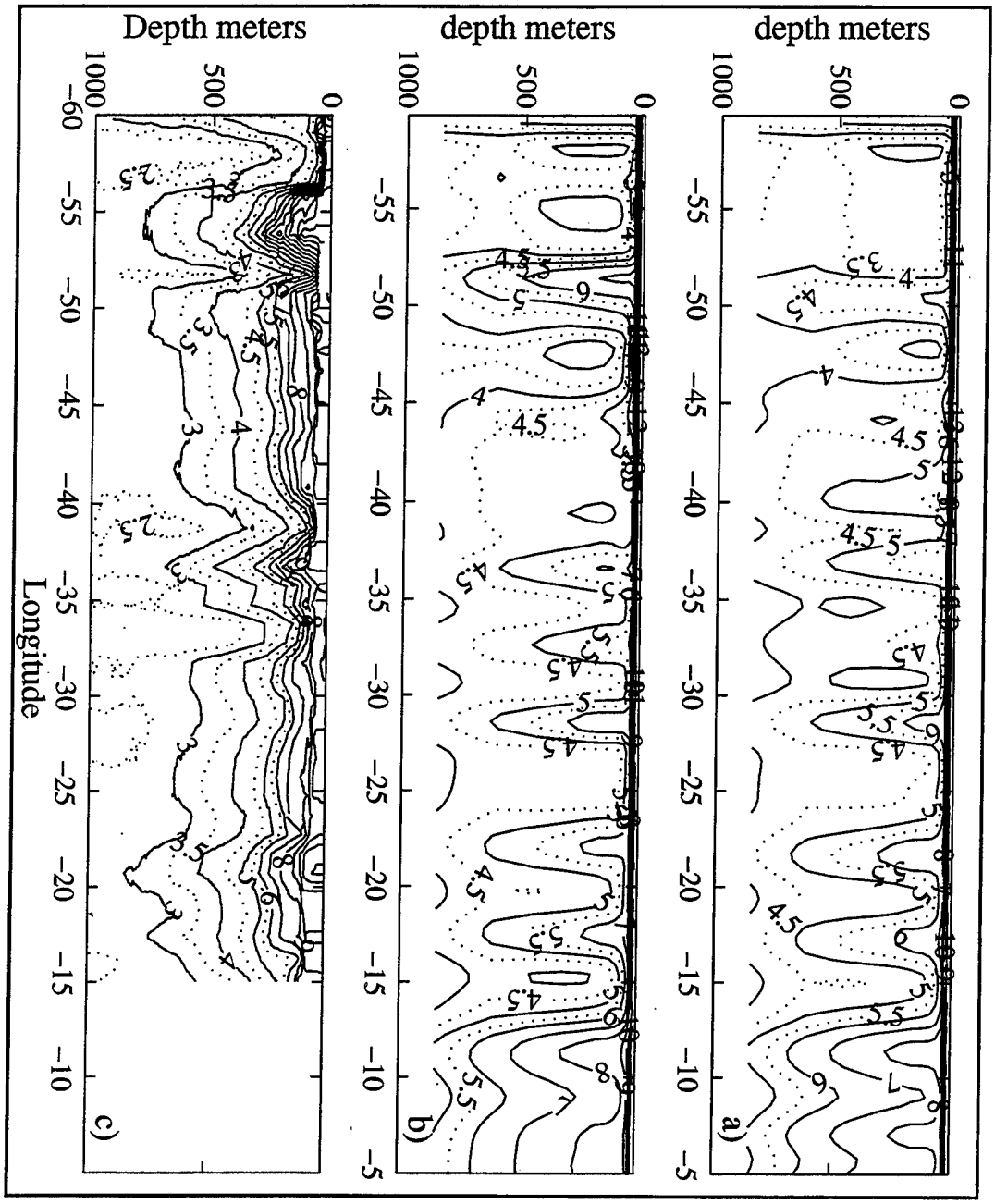


Figure 63. Zonal sections of temperatures along 45°S in the Atlantic Ocean (between 60°W and 0°E) for January of 1993 for a) the C run, b) the A run, and c) the A11 observed temperatures.

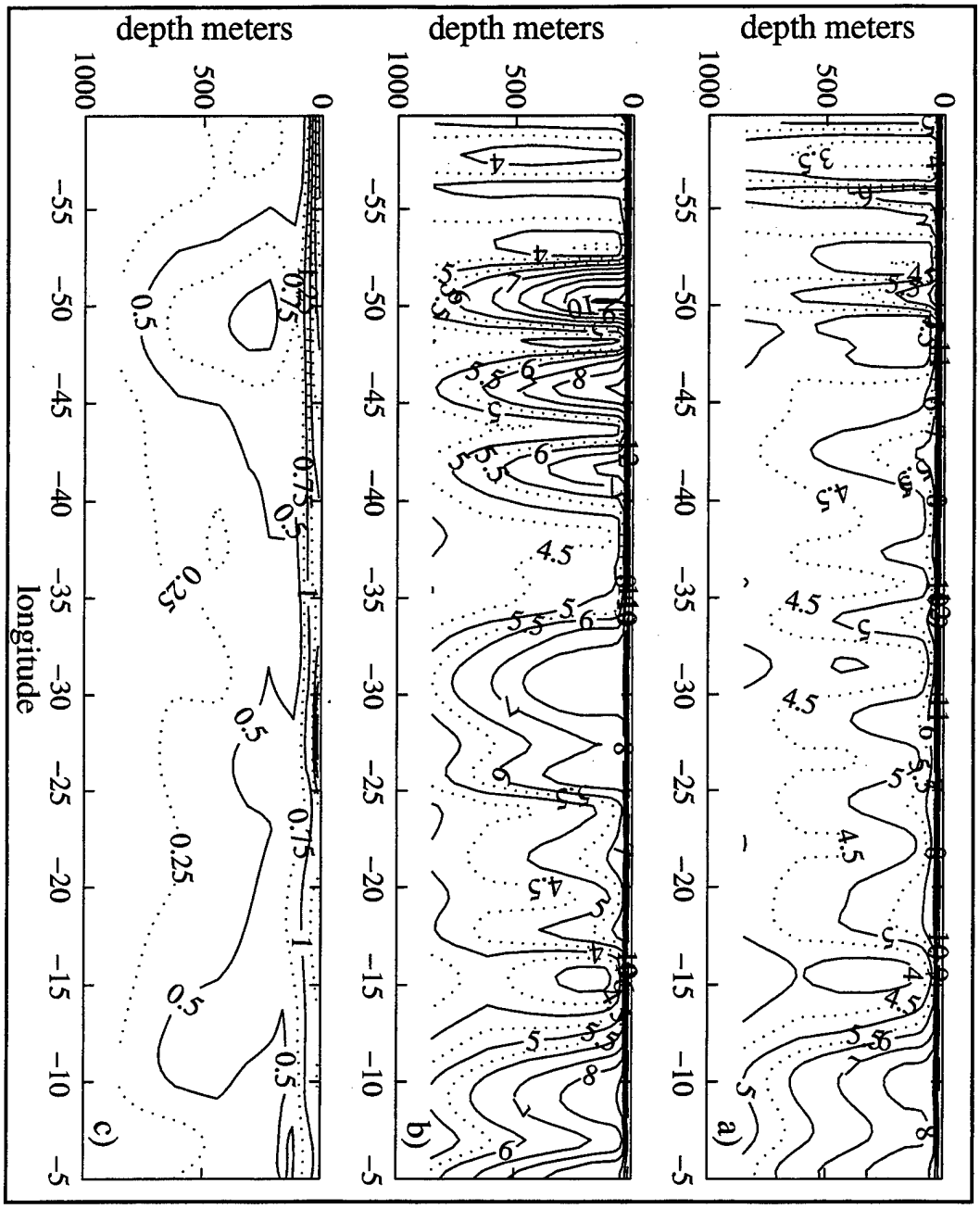


Figure 64. Zonal sections of temperatures along 45°S in the Atlantic Ocean (between 60°W and 0°E) for January of 1994 for a) the C run, b) the A run, and c) the variance map of the yearly Levitus climatology.

that the water at depth in the observations (Figure 56c) is cooler than either of the model runs. The observations also show fewer of the wave-like temperature structures visible in the model simulations. By January of 1994, the A run (Figure 64b) has developed many deep penetrating features, while the C run has remained approximately the same. Thus, this suggests that the wind field is quite similar between the two years because the C run is similar in both years, and the changes seen in the A run are purely due to the assimilation process.

In this region, the assimilation run is very unrealistic and the source of the model diverging away observations is the variance field seen in the monthly Levitus fields along this line (Figure 64c). It can be seen that between 50°W and 55°W, the variability of the Levitus data is relatively high. This, along with the corresponding functional, which shows a highly barotropic forcing function for this region down to a depth of 1000 meters or so, is responsible for the modifications of the model fields. Not much observational data has been collected in this region and the Levitus climatology may not be realistically representing the monthly temperature fields.

### 4. Heat Content and Transport

The heat content of the ocean is used as an indirect measure of how the ocean is transporting water, and thus heat around. Accurate or close representation of the heat content and transport in the ocean is necessary prior to coupling ocean models with atmospheric models to study climate change. Figure 65 shows the northward meridional heat transport in the model computed from the 2 year mean (1993/1994) for the C run (dashed line) and the A run (solid line). The global northward heat transport is shown in Figure 65a, with the basin integrated transports shown in b), for the Atlantic and c) for the Indo-Pacific region. The two runs have produced similar transport values. In the Atlantic, the two runs are virtually identical. Most of the difference in the values shown in the global

view is due to the differences seen in the Indo-Pacific basin. Here, run A has reduced the transports in both the northern and southern hemisphere.

There have been many studies which have attempted to estimate heat transport from the observational data. The heat transport values from a recent and comprehensive study by *Macdonald and Wunsch* (1996) are plotted on Figure 65, for the globe and both the basins as circles with an error bar. The model (both the A and C runs) is reproducing accurately the transports that are observed in the Atlantic. In the Indo-Pacific, Figure 65c, the A run heat transports are closer to the observed values in the northern hemisphere. In the southern hemisphere, the C run is closer, although the modeled values still deviate from the observations. *Macdonald and Wunsch* have also provided some estimates of heat flux across several lines in the Southern Pacific and Indian Oceans. These data (Table 5) show that it is the Indian Ocean (rather than the Pacific) in the model which is producing most of the difference between the observed transports and the modeled transports and between the 2 modeled transports at 32°S.

| Section | *Macdonald and Wunsch* | C run | A run |
|---|---|---|---|
| Pacific 28°S | -0.04 ±0.30 | 0.26 | 0.38 |
| Pacific 43°S | 0.26±0.28 | 0.33 | 0.37 |
| Indian 18°S | -1.45±0.30 | -0.37 | -0.31 |
| Indian 32°S | -1.30±0.28 | 0.87 | 1.13 |

Table 5. Heat flux in petawatts across specific zonal sections in the Indo-Pacific Oceans.

The amount of heat at a location is examined at various locations around the globe. Plots of the monthly cycle of the integrated heat content of the upper layers of the model (to 310m) with respect to the surface temperature are shown in Figures 66 (A run), 67 (C run), and 68 (Levitus 94). Monthly value of heat content are plotted separately for 1993 and 1994 Figures 66 and 67, with the bold line representing 1993. A realistic model should

show a hysteresis effect in the heat content. This means that the heat content of the ocean for a particular month should retain some of the heat of the prior month and should not be directly related to the changes seen in the surface temperatures. In other words, as the ocean cools during the winter months, some of the heat gained during the warmer months should still be retained in the water column. This is shown in the northern hemisphere by the months of September through February having higher heat content than in the months of August to March, even though the surface temperatures are similar. (The loop starts with December of the year before, denoted by the heavy dot.) The assimilation process (Figure 66) corrects the model's heat content to some extent, especially in 1994. In effect, the assimilation is forcing the model's temperatures to be more representative of the mixed layer seen in observations (somewhat represented by Figure 68, the Levitus data). If a mixed layer formulation is included in the model, this deficit of the model can be overcome without the need for assimilation (pers. comm. *Semtner*).

A closer look at one location, 35°N, 30°W (Figure 69) shows the differences in the monthly structure of the water column between the two runs of the model and between the two years of the model runs. In both years, beginning in February, the column is cooler in the A run than in the C run, with the 16°C isotherm surfacing in March of 1994. There is little difference in the surface waters (top 70m) during the second half of the year. In the winter months, the 16°C isotherm uplifted, showing a deeper "mixed" layer, especially in 1994.

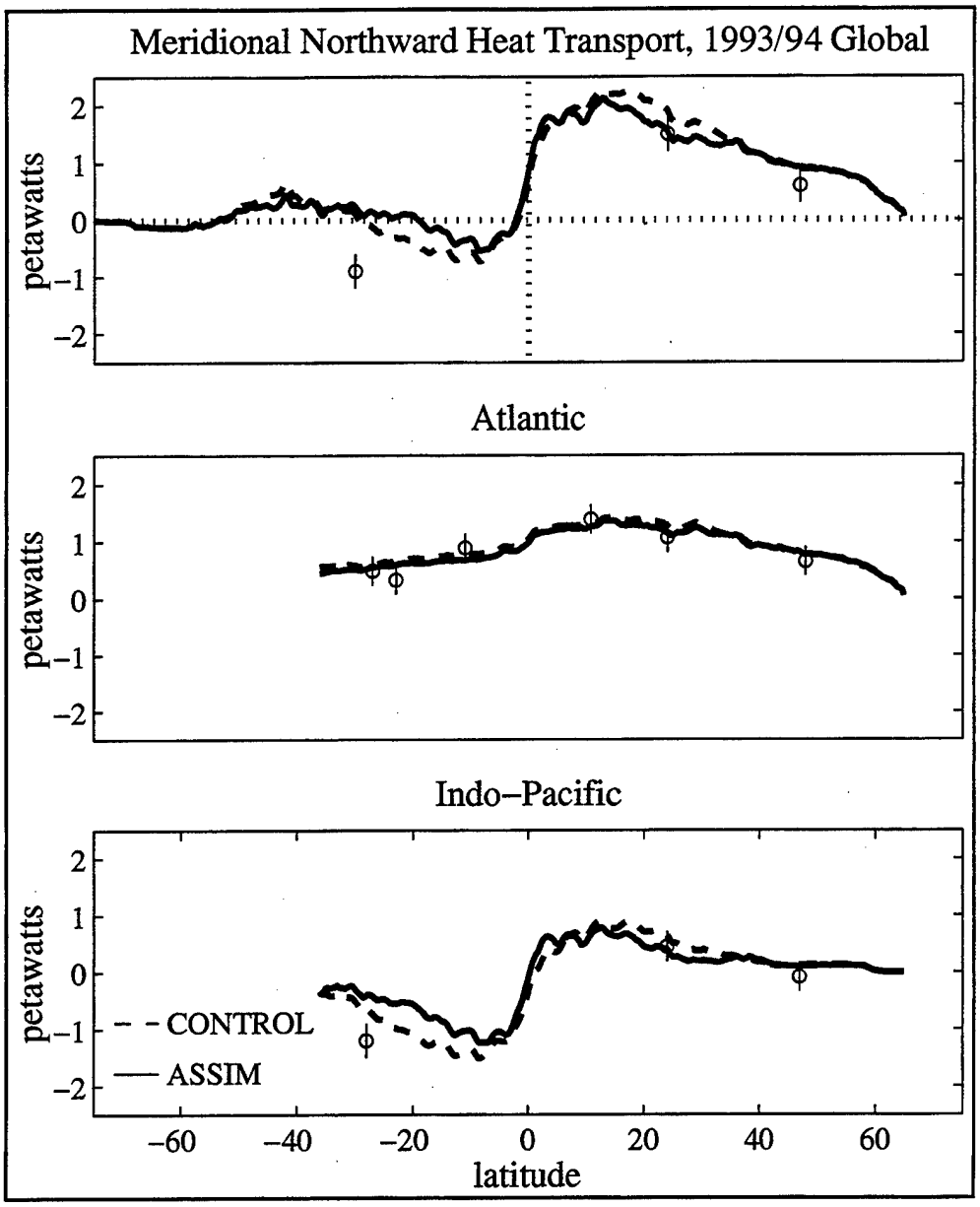


Figure 65. Meridional northward heat transport for the 2 year mean (93/94) for a) the globe, b) Atlantic, and c) Indo-Pacific. The bold line is the heat transport computed from the A run and the dashed line is the transport from the C run. The circles denote the *Macdonald and Wunsch* (1996) values computed from observations.

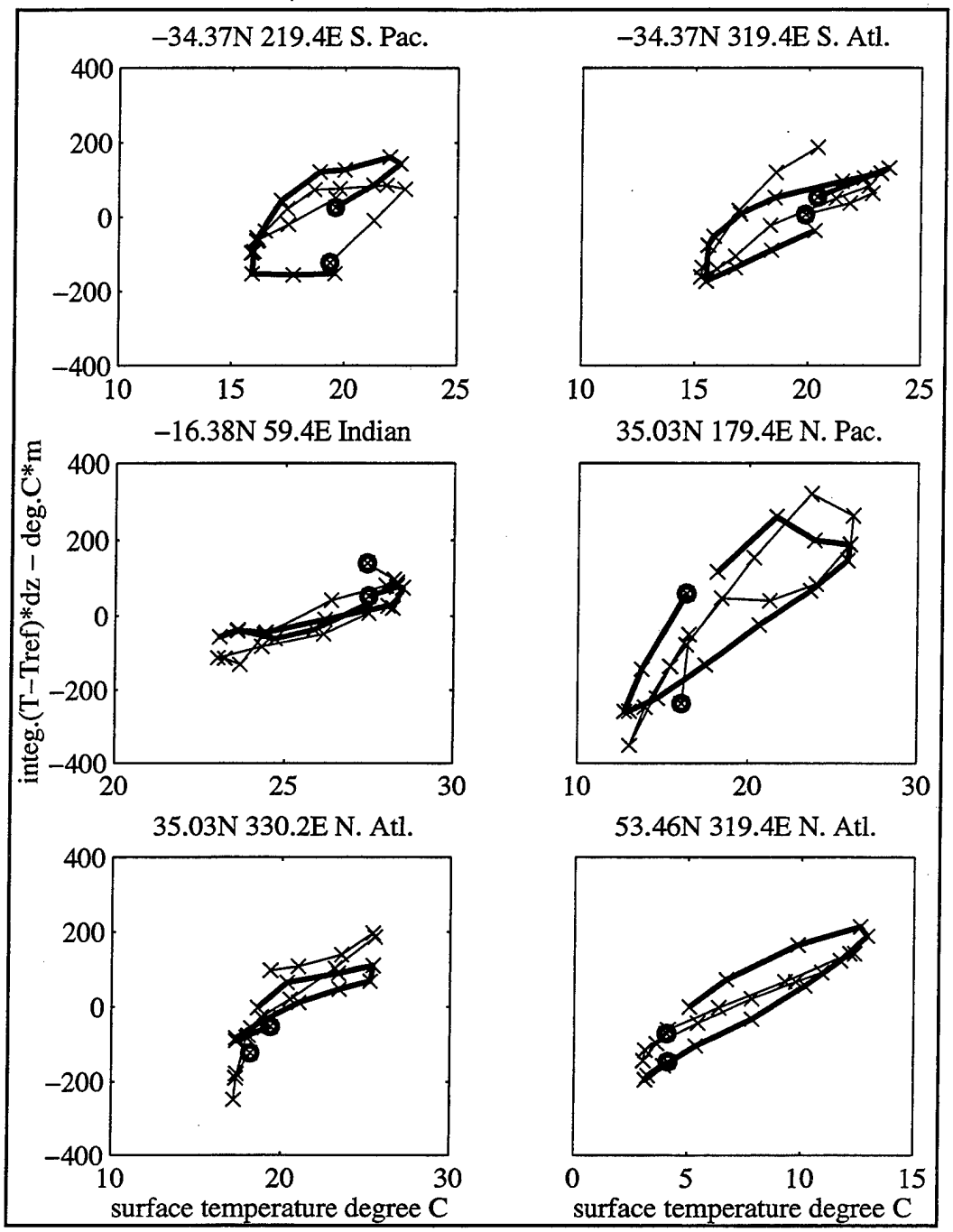


Figure 66. Hysteresis curves for heat content in run A at six locations; a) 34.37°S 219.4°E in the South Pacific, b) 34.37°S 319.4°E in the South Atlantic, c) 16.38°S 59.4° E in the Indian, d) 35.03°N 179.4°E in the North Pacific, e) 35.03°N 330.2°E in the North Atlantic, and f) 53.46°N 319.4°E in the North Atlantic. The bold curves are for 1994 and the thin lines are for 1993. The circles denote the starting location and x marks the months.

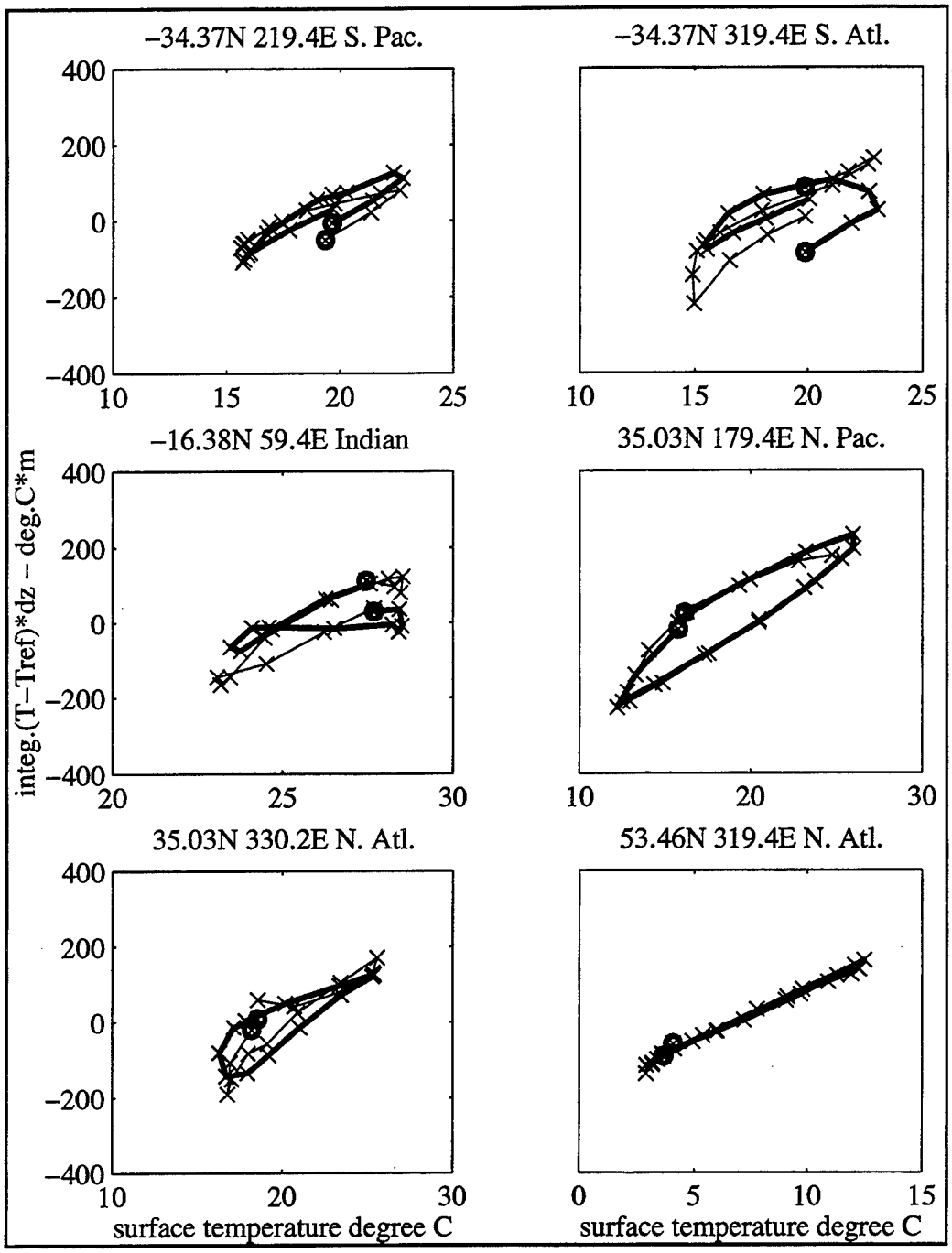


Figure 67. Same as Figure 66, but for the C run.

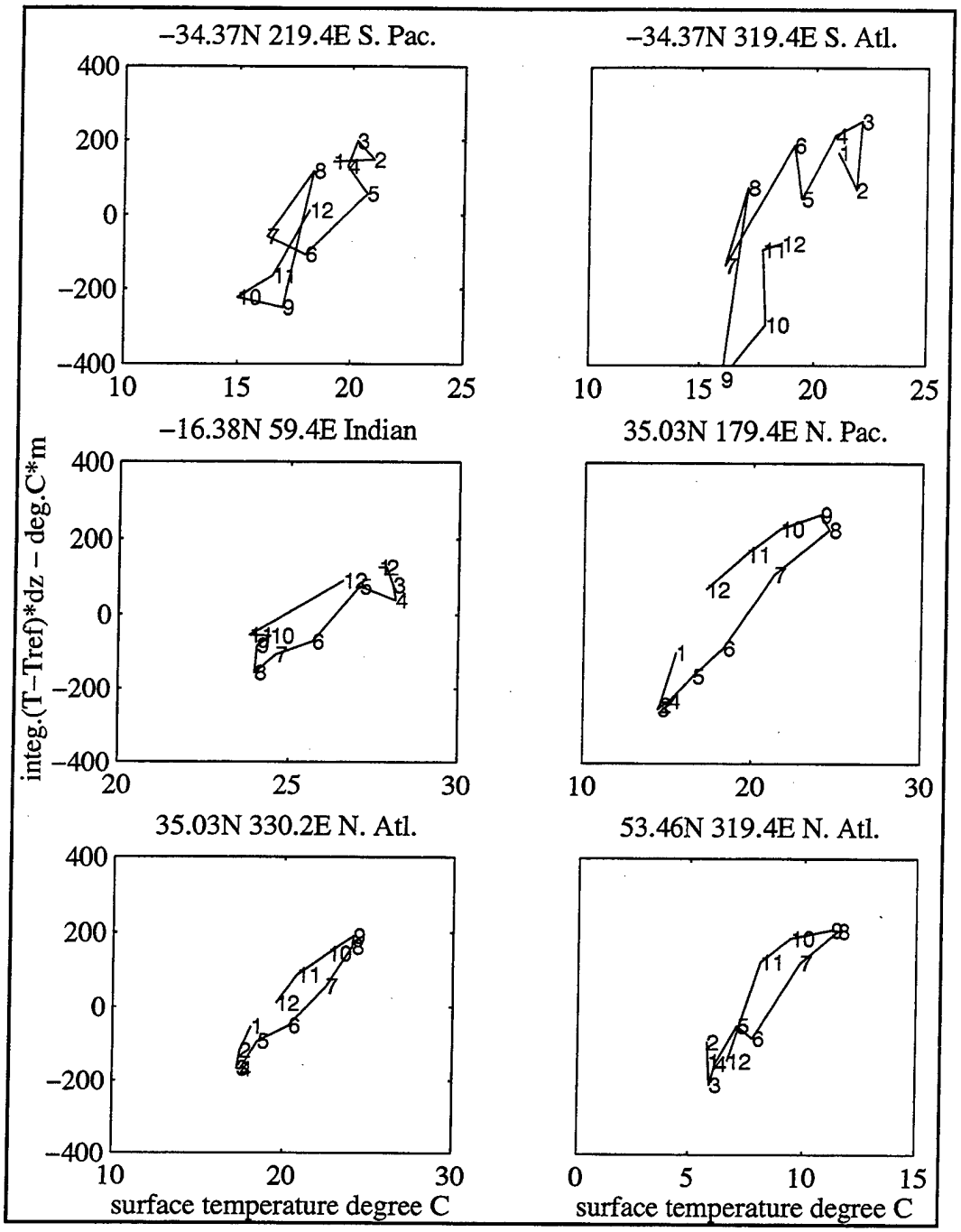


Figure 68. Same as Figure 66, but for the Levitus climatology.

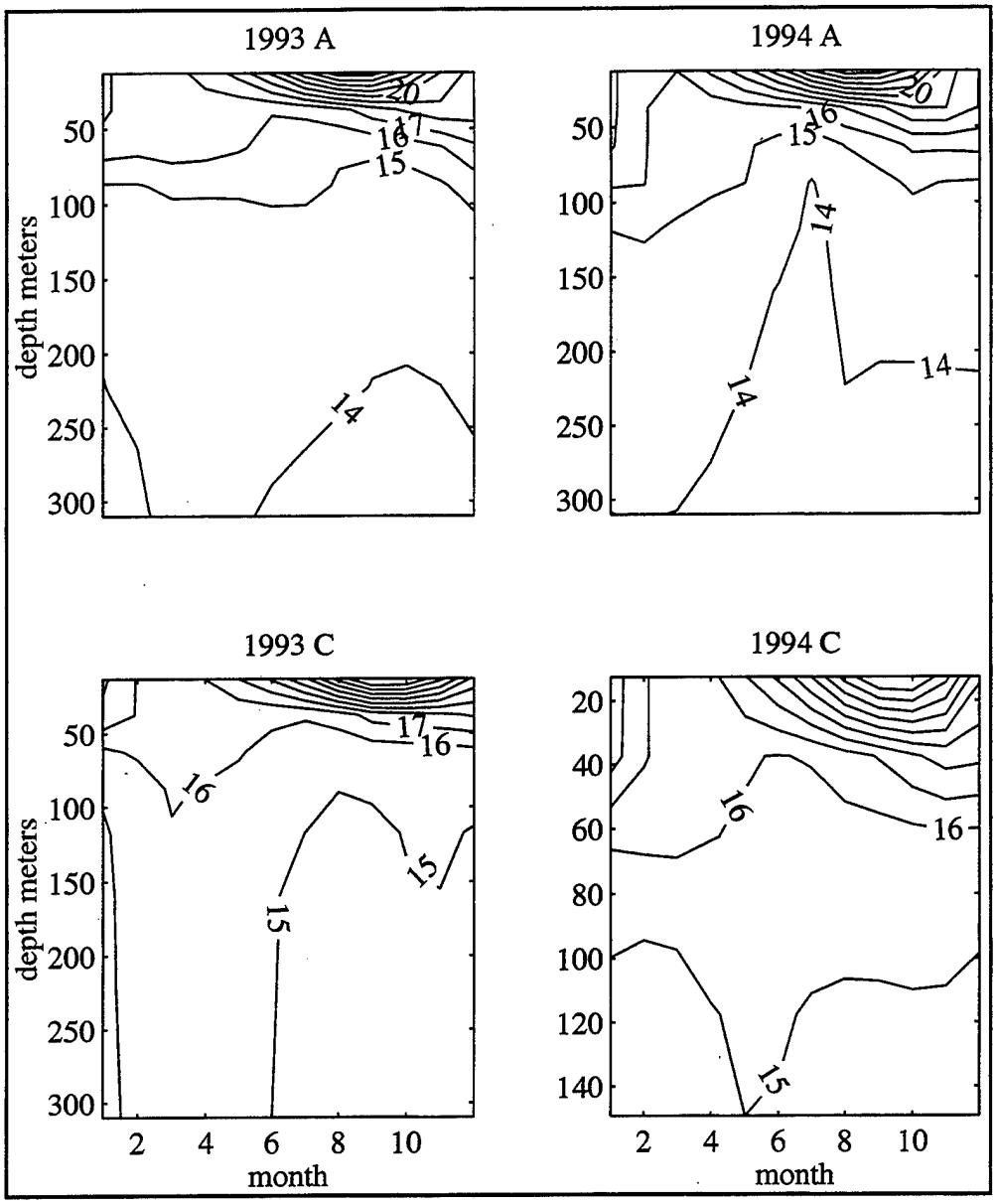


Figure 69. Time/depth plot of temperature at 35°N, 30°W for the a) 1993 A run, b) the 1994 A run, c) the 1993 C run, and d) the 1994 C run.

## 5. Thermohaline Circulation

The most easily detected changes resulting from the application of the assimilation process occur at or near the surface because the observational field that is related to the

surface quantity, SSH. Indirectly, what occurs at the surface will, in time, effect the deep circulation because of the changes made to the density of the water. This thermohaline circulation, relating to modifications to the temperature and salinity field, are seen in nature when, for example, there is change in the ice melt at high latitudes or changes in the evaporation-precipitation rates over an ocean. The assimilation experiment not only affects surface properties, but changes temperature and salinity at depth via the correlations of SSH with the vertical structure of temperature and salinity, in a more accelerated manner than occurs in nature. Thus, these changes at depth, should also change the thermohaline circulation of the model. The thermohaline structure will only be discussed in terms of the changes seen in the two model runs, since complete, global and detailed observational data is not available. Global WOCE data, covering about the same period of the model runs, should soon become available to make a complete comparison of the observational 1990s thermohaline circulation.

The meridional overturning streamfunction is one method to examine the differences in the model runs of the thermohaline circulation. Plots of meridional overturning show how water circulates between the north and south basins of an ocean. The streamlines can be used to trace the flow from where it enters at the surface down to the subsurface layers of the ocean, as is described by the ocean "conveyor belt " system. The equation for meridional overturning is:

$$\Psi(\lambda,\zeta) = \int \int_{z(\phi,\lambda,\zeta)}^{0} v(\phi,\lambda,z')\, a\, cos\, \lambda\, dz' d\phi \qquad 4.6,$$

where $\lambda$ and $\phi$ are latitude and longitude, respectively, and $a$ is equal to the radius of the earth. $\zeta$ is the depth of the surface being considered, either a density surface or the traditional level surface. The model meridional velocity is first integrated vertically to the specified surface (either level or density), then zonally integrated for the globe or a basin.

The Indo-Pacific, Atlantic, and global meridional overturning streamfunction defined on level surfaces is shown in Figure 70a-c, with the A run shown in the top panel

of each figure and the C run on the bottom for the mean of 1994. From the global meridional integrated sections, one can see the Antarctic cell (0-2000m, 65°S), the Deacon cell (between 60°S and 40°S and 500-3000m), the deep cell of northward following water, the shallow subtropical gyre circulations in both the north and the south and the mid-depth flow which represents the major transfer of the thermohaline transport of water from one basin to another.

There are several immediate differences seen between the model runs. In the Indo-Pacific region (Figure 70a), the major differences are in the flow of the intermediate waters at 20°S, defined by the shaded areas of the southern hemisphere. The assimilation run (A) shows strong northward flow (average of about 6 Sv), ventilating the interior of the Indian and/or the Pacific ocean to about 10°S, and then returning in the deeper layers. Most of the northward flux of water is in the Indian ocean as the suggested from the heat flux calculations (Table 5) shown in the previous section. This northward flow is nonexistent in the control run of the model. In the North Pacific, the mid-depth southward flow centered at 25°N in the C run is much reduced, or eliminated in the A run. The -2 Sv contour above 600 meters is much stronger in the A run than in the C run. In fact, it is similar to the streamlines calculated for the 0.5° resolution global ocean model run of the Semtern/Chervin model (*Semtner and Chervin*, 1992, Figure 9). The 0.5° model was constrained to Levitus data whereas the 1/4° resolution run was not (*i.e.*, the run C). The assimilation, in some fashion, also constrains the model to a Levitus data set, so it is not surprising that the streamlines of the A run resemble this earlier 0.5° model run.

The Atlantic region (Figure 70b) shows similar circulation patterns above 600m. In the deep ocean, too much forcing was applied at 35°N, where the flow looks somewhat unrealistic in the A run. The deep northward flow visible in the streamlines from the A run (denoted by the shaded region) is the Antarctic Bottom water. This water is not seen in the C run of the model (or is much smaller, below 2Sv.) Standard oceanography texts, such as *Pickard and Emery* (1986) show a similar deep flow. Figure 70c, showing the global

view of the overturning streamlines is included for completeness and to define where the streamlines for the deep flows in the southern hemisphere begin.

Following *Hirst, et al.* (1996) and *Döös and Webb* (1994), overturning flow can also be shown along surfaces of constant density. For this comparison, the $\sigma_3$ surface has been chosen because it is very similar to the representation of streamlines on neutral density surfaces (*Hirst, et al.*). Figures 71a-c show Indo-Pacific, Atlantic and global meridional overturning on $\sigma_3$ surfaces calculated from both the A (top panels) and C (bottom panels) runs of the model. Viewing streamlines on density surfaces shows the flow in a more realistic manner. The major recirculation cells again can be seen. For example, the Atlantic circulation associated with the transfer of water from the northern to southern hemisphere ("the conveyor belt") can be seen in Figure 71b, on the density surface of about 41. to 41.5. The panels for the Indo-Pacific region show similar features to the plots on the level surfaces. The A run has somewhat weaker circulation around the northern basin (shaded area) than the C run, and the deep flow is stronger in the A run than in the C run. The A run has removed what appears to be a narrow and deep penetrating feature (6Sv contour) located at 12°N. The deep northward flow of the Antarctic bottom water is visible, flowing northward to about 20°N, not quite as far north, as seen when plotted on level surfaces (Figure 70b).

Figure 71c, the global overturning streamfunction shows the intense equatorial features which are weaker in the A run, than in the C run. The Deacon cell, is denoted by a very small circulation cell, centered at about 50°S and on a density surface of 41 in Figure 71c.

### 6. Summary

This section of Chapter IV has shown, with both qualitative and quantitative comparisons made to observational data from altimeters, hydrographic sections, and tide-

gauges, the assimilation process is adjusting the model's prognostic variables towards observed values. These adjustments can be seen both in the surface fields and subsurface in the model's variables which have been directly nudged (SSH, temperature, salinity) and

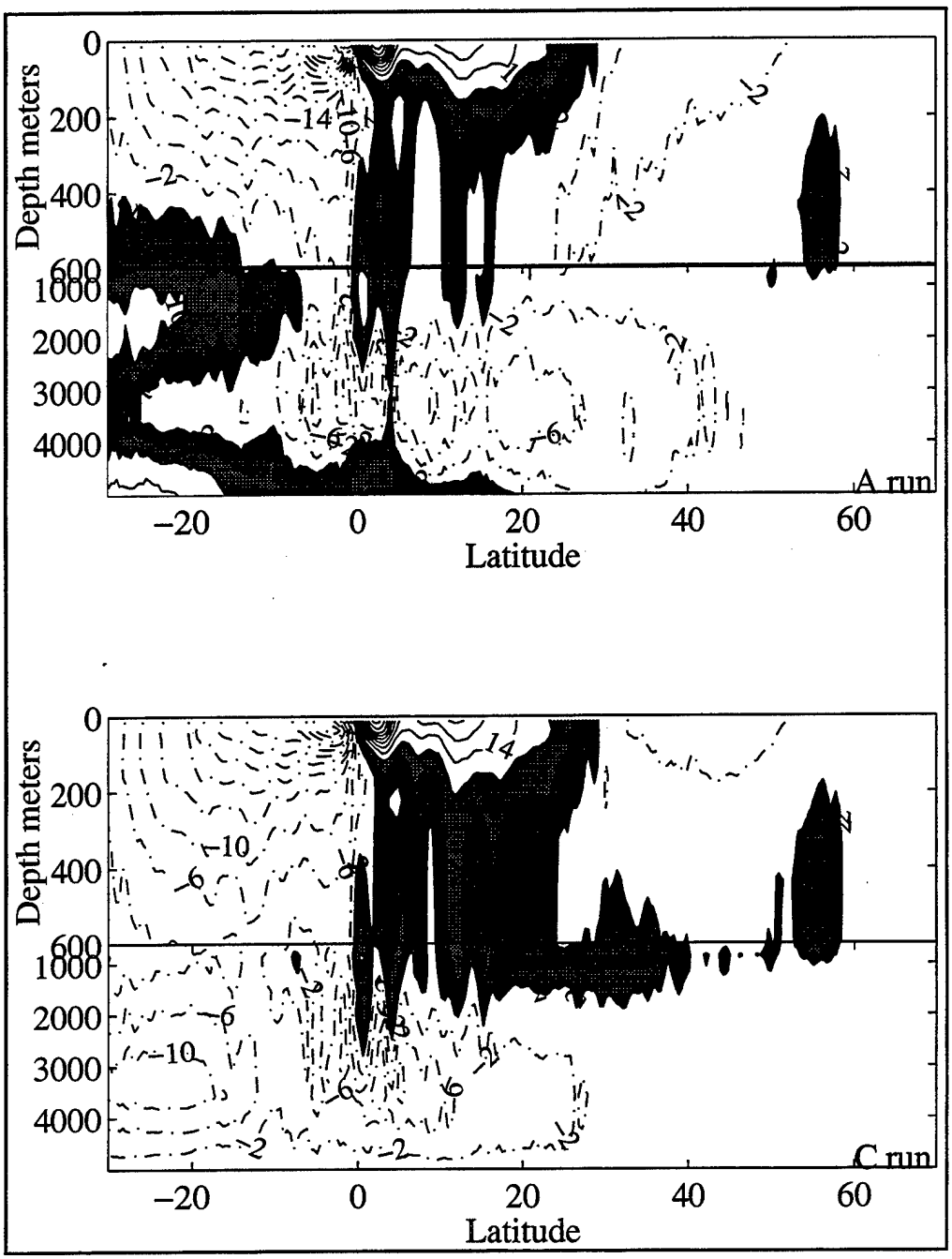


Figure 70a) Meridional overturning streamfunction defined on level surfaces for the Indo-Pacific region with the top panel showing the A run and the bottom panel, the C run. Contours are every 4 Sv. Shaded areas define regions referenced to in the text.

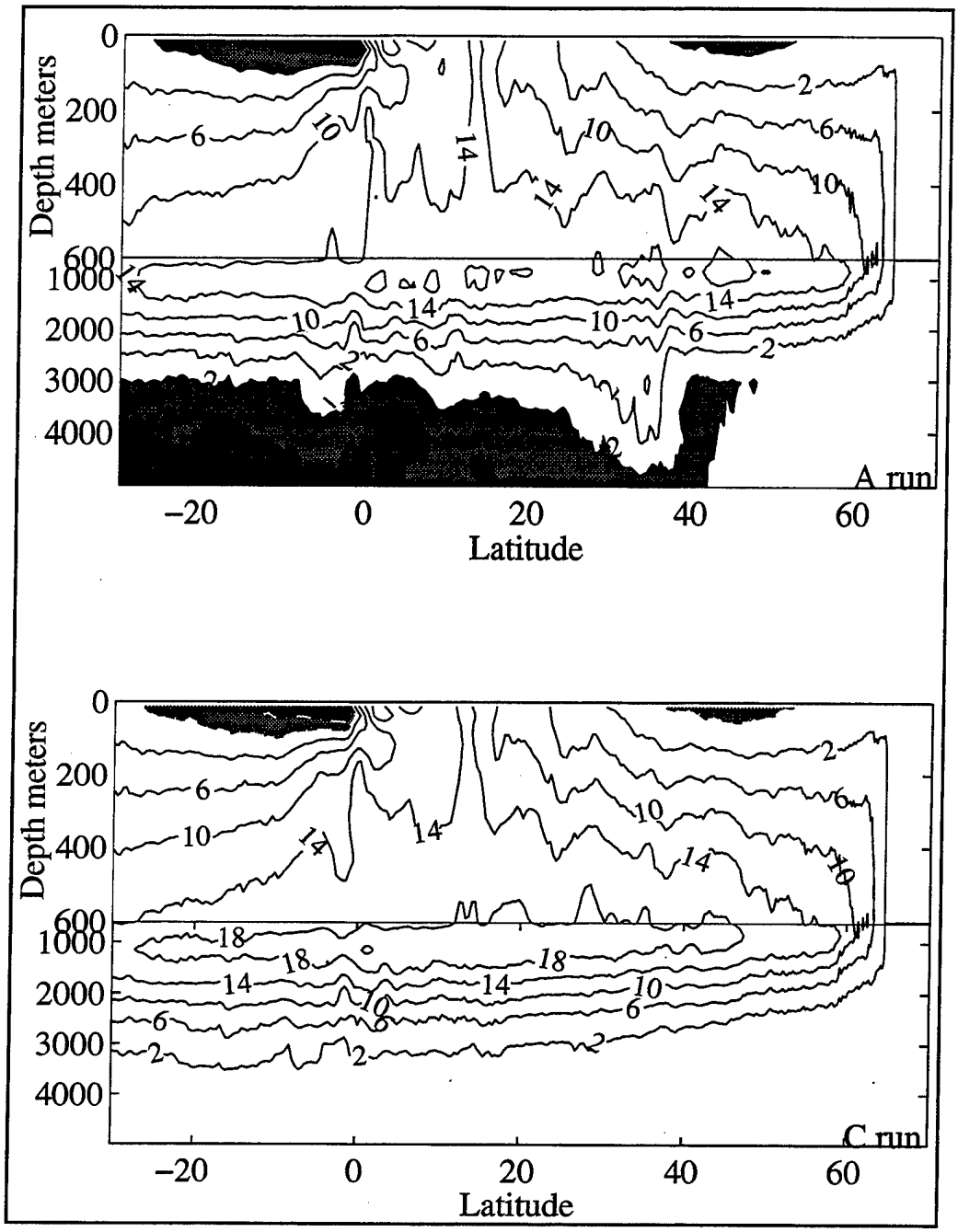


Figure 70b) Same as Figure 70a, but for the Atlantic.

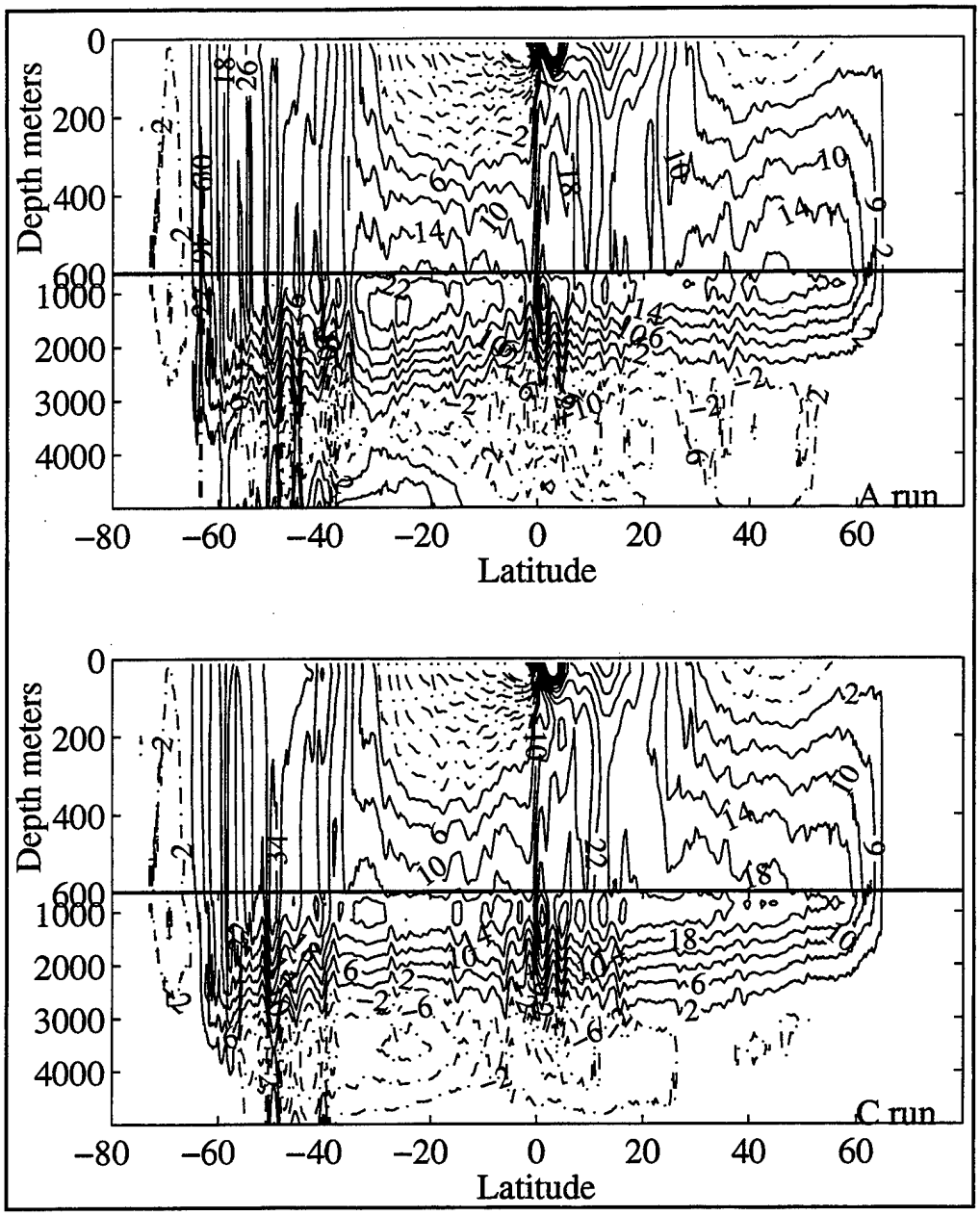


Figure 70c) Same as Figure 70c, but for the globe.

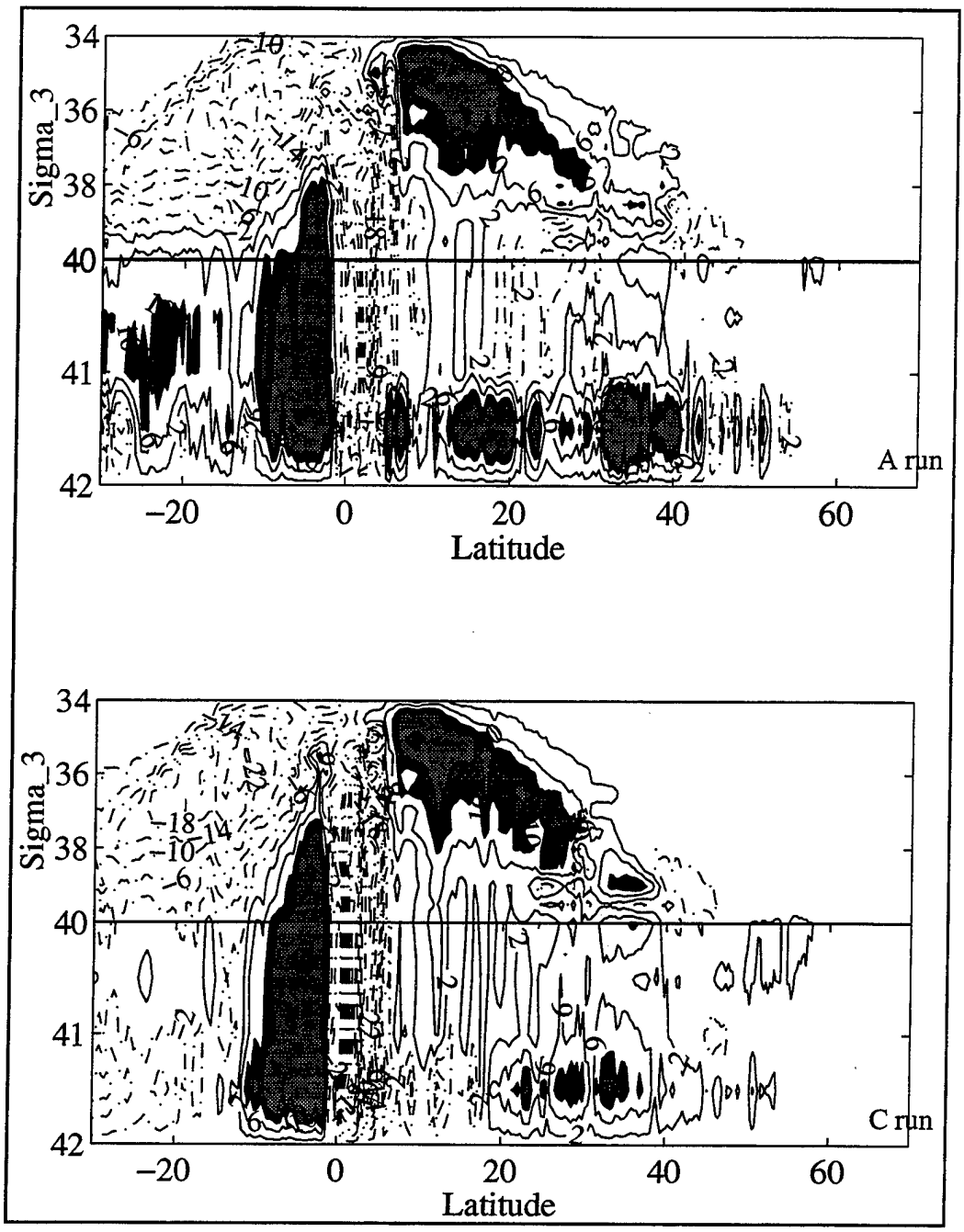


Figure 71a) Meridional overturning streamfunction defined on $\sigma_3$ surfaces for the Indo-Pacific region with the top panel showing the A run and the bottom panel, the C run. Contours are in SV 10e6 $kgm^{-3}$ and are shown by increment of 4 SV.

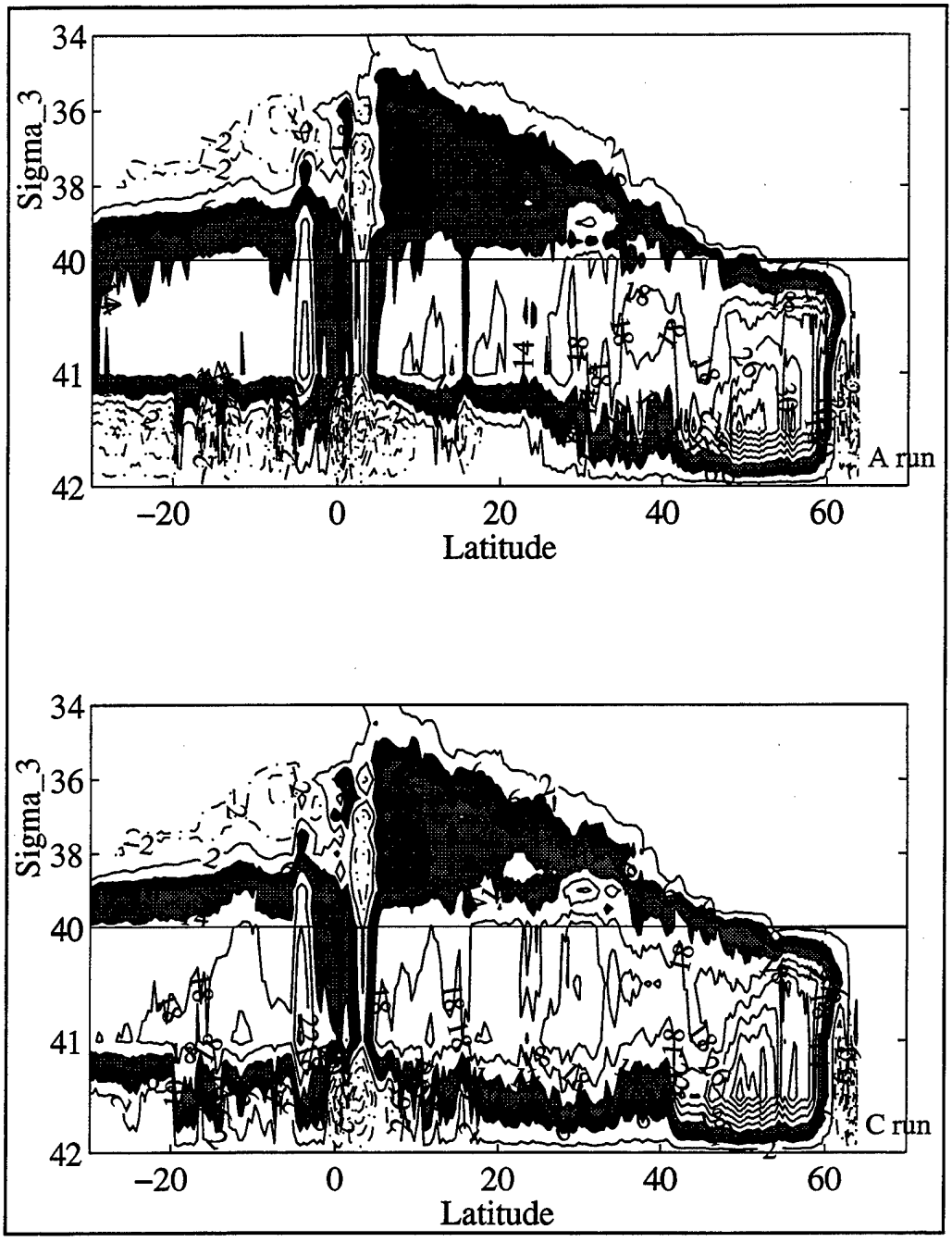


Figure 71b) Same as Figure 71a, but for the Atlantic.

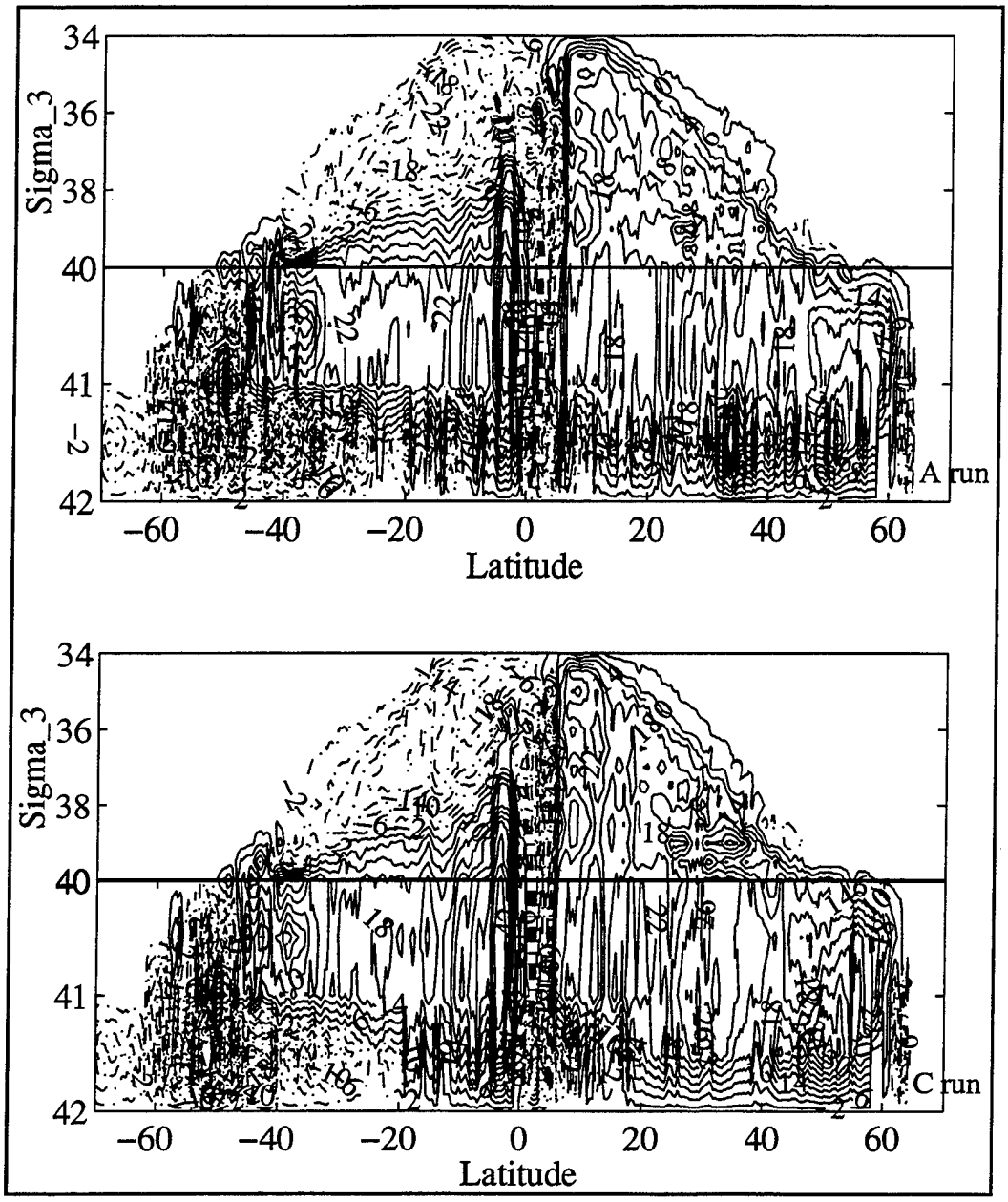


Figure 71c) Same as Figure 71a, but for the globe.

in the variables which are indirectly modified (velocity). Significant changes can also be seen in the diagnostic quantities such as meridional overturning and heat content. The assimilation process fails in those regions (mainly the Southern Ocean) where there is a lack of in situ data to correctly adjust the model's subsurface fields. These areas which under perform can be better simulated once the observational fields are improved.

## E. CONCLUSIONS

The assimilation process for the assimilation SSH and associated (via correlation functionals) temperatures and salinities has been described. The model's prognostic variables from the same period of time in the model run are statistically different between the assimilation run (A) and the control run (C) as shown with the use of the Student-t test and the F-test, and with the comparison of the mean and variance of SSH, temperature, and salinity. These differences are both at the surface and subsurface, showing that the assimilation process is making changes in both, though to a different degree. It has also been shown that the method is dynamically compatible with the numerics of the primitive equation ocean model. And finally, the synthesized ocean variables, in most of the regions with high variance, have been adjusted towards values seen in observations.

# V. IMPACT OF DIFFERENT SAMPLING PATTERNS IN OBSERVATIONS

Altimeter data from two different satellites have been used as observational SSH information for the second assimilation experiment. For 1993, both ERS-1 and T/P data were used, while in 1994, only T/P data was available. Each satellite has a different sampling period, ERS-1 at a 35 day repeat and T/P, with a 10 day repeat cycle. This provides an opportunity to quantify the advantage of having multiple satellites flying with different orbits over having just one satellite.

Statistics are used to quantify the difference in the two years of the assimilation run to establish which year was more successful at incorporating the observational SSH signal into the model. Statistics have been computed to determine 1) which year is closer in its representation of the assimilated SSH field and 2) which year has increased the variance of the SSH the most. The second question is asked because the model is known to be under representing the SSH variability when it is run without any assimilation.

For the first question (which is closer to the altimeter field it assimilated), the mean square difference (MSD) over all points is calculated between the monthly mean SSH of run A and the monthly mean of the altimeter data, as defined in equation 5.1.

$$\text{MSD-1} = \overline{[\langle M\rangle - \langle D\rangle]^2}_{i,j} \qquad 5.1,$$

where <M> is the monthly mean SSH of the model and <D> is the monthly mean SSH of the assimilated altimeter data at a location i,j. To compare the two years, 1993 and 1994, the MSD values calculated for each year are normalized by the variance of <D> over all i,j, to account for differences in the number of points at which observations were assimilated at for the two years. Equation 5.1, as used for this comparison is defined as:

$$\text{MSD-1} = \overline{[\langle M\rangle - \langle D\rangle]^2}_{i,j} / \text{Var}(\langle D\rangle) \qquad 5.2.$$

The two numbers from each year are compared, with the smaller number indicating which year is closer to the observations that were assimilated. Table 6 shows computed MSD values for the two years. For all the months, the values are smaller in 1993 than in 1994, suggesting that the increase in the number of observed locations (ERS-1 samples at a finer spatial resolution) is beneficial in the assimilation process.

| Month | MSD-1 93 | MSD-1 94 |
|---|---|---|
| JAN | 1.77 | 2.16 |
| FEB | 1.82 | 2.16 |
| MAR | 1.77 | 2.15 |
| APR | 1.82 | 2.16 |
| MAY | 1.80 | 2.17 |
| JUN | 1.83 | 2.20 |
| JUL | 1.82 | 2.22 |
| AUG | 1.84 | 2.23 |
| SEP | 1.86 | 2.25 |
| OCT | 1.84 | 2.24 |
| NOV | 1.86 | 2.23 |
| DEC | 1.99 | 2.18 |

Table 6: Monthly normalized mean square difference between run A SSH and Observed SSH.

Similarly, to examine whether or not the model's variance has increased, instead of computing the mean square difference between the assimilated run and the observations, the MSD is computed between monthly variances of run A and run C, so that equation 5.2 is rewritten as:

$$\text{MSD-2} = \overline{[\langle M\rangle - \langle C\rangle]^2}_{i,j} / \text{Var}(\langle C\rangle) \qquad 5.3,$$

where <M> is now the monthly variance at a grid point for run A and <C> is the same for

run C. The higher the value of MSD-2, the higher the difference in the variances between the two model runs, A and C. Table 7 shows the computed values. Eight of the twelve months have values higher in 1993 than in 1994, with two months (July and April) fairly similar and two months where the C run has the higher increase in its variance (January and May). It is not surprising that January of 1994 is higher than January of 1993, since January of 1993 is fairly early in the model run.

| Month | MSD 93 | MSD 94 |
|---|---|---|
| JAN | 0.43 | 0.49 |
| FEB | 0.94 | 0.58 |
| MAR | 0.63 | 0.45 |
| APR | 1.09 | 1.16 |
| MAY | 1.14 | 1.47 |
| JUN | 0.96 | 0.76 |
| JUL | 1.42 | 1.48 |
| AUG | 1.07 | 0.82 |
| SEP | 1.25 | 0.66 |
| OCT | 0.70 | 0.50 |
| NOV | 0.66 | 0.45 |
| DEC | 0.87 | 0.53 |

Table 7: Monthly normalized mean square difference between run A SSH and run C SSH.

To summarize, the above quantitative evaluation suggests that it is useful to use both ERS-1 data with its higher spatial sampling and T/P with its higher temporal sampling as the observational data set when ever possible. This has been determined by the lower mean square difference between the model SSH fields and the observations for 1993 (verse 1994). In addition, run A of the model also has a higher increase in variance in 1993, than in 1994, suggesting that it is the finer spatially sampled ERS-1 data, which includes mesoscale features, influencing this variance in the model.

# VI. POSSIBLE MODEL IMPROVEMENTS

As has been discussed in the previous chapters, when the ocean model is run without the assimilation of any observations, the model simulates the ocean adequately. The model is able to do this because its resolution is high enough to resolve narrow and fast currents, such as the western boundary currents (Gulf Stream and Kuroshio). The model has a free surface and well defined bathymetry which has not been smoothed and which influences the path of the currents. The model also uses monthly varying heat fluxes producing a seasonal signal in the model's SSH (*Stammer, et al.*, 1996). Most assimilation experiments previously have not used a control run which include these aspects, thus producing a control run which is much less accurate. For example, *Oschlies and Willibrand* [1996] use monthly mean wind stresses computed from climatological data sets for their assimilation experiment in the Atlantic ocean and *Carton, et al.* [1996] use a relatively low resolution PE model (0.5° x 2.5° grid in the tropics) and weekly 1000 mbar National Centers for Environmental Prediction (NCEP) wind fields rather than the higher temporal varying 3-day 10 m ECMWF winds, which are used in these experiments. Therefore, because this experiment is using more accurate forcing (compared to other assimilation experiments) and improved numerics (i.e. the inclusion of the free surface as a prognostic variable), the modifications made by the assimilation to adjust the model towards reality are relatively small. This chapter looks at where changes can be made in the model's numerical formulation, forcing fields, or initial conditions to better simulate the ocean circulation without the need for assimilation.

## A. IMPROVEMENT IN THE MODEL'S MIXED LAYER FORMULATION

The assimilation process adjusts the model's temperature field and in the process,

accounts for the temperature changes which would be seen if a numerical code to handle mixed layer dynamics were included in the model's formulation. This is the clearest of the assimilation effects on the model to understand. The bold line on Figure 72 shows the histerisis curve at various points from 1994 of run A, reproduced from Figure 66. The thin lines, on the same figure, represent the curve as calculated from an initial experiment which includes mixed layer dynamics in the model formulation (pers. comm., *Semtner*, 1997). The mixed layer formulation is the Krause-Turner (*Krause and Turne*r, 1967) type. The two model runs do not cover the same period. The A run is for 1994 and the mixed layer run covers a time period from Sept. of 1992 through August of 1993. There are similarities between the curves, especially at 35°S, 219°E in the South Pacific and 53.5°N, 319°E in the North Atlantic, where both differ from run C (see Figure 66).

The differences in the temporal change of the temperature fields over twelve months are shown in Figure 73 with panels showing the temperature with depth (to 300 m) for each of the six locations shown in Figure 72. As an example, in the North Atlantic at 53.5°N, 319°E (last row of panels on Figure 73), both the A run and the mixed layer run show increased temperatures at depth starting in about March over the temperatures seen in the C run. In the South Pacific (first row of panels on Figure 73), the deeper layers (below 100 m) cool between January and December for the A run and the mixed layer test, while the C run temperatures are fairly constant.

These figures, thus, suggest that assimilation can compensate for a model lacking in mixed layer dynamics by adjusting the temperatures in the upper layers to account for seasonal changes. There are inaccuracies in both model runs. Mixed layer run was an initial test of the numeric code and still needs improvements. At this point, it can not be said that mixed layer code will completely correct inaccuracies in the model's top layers and eliminate the use of assimilation to correct this deficit.

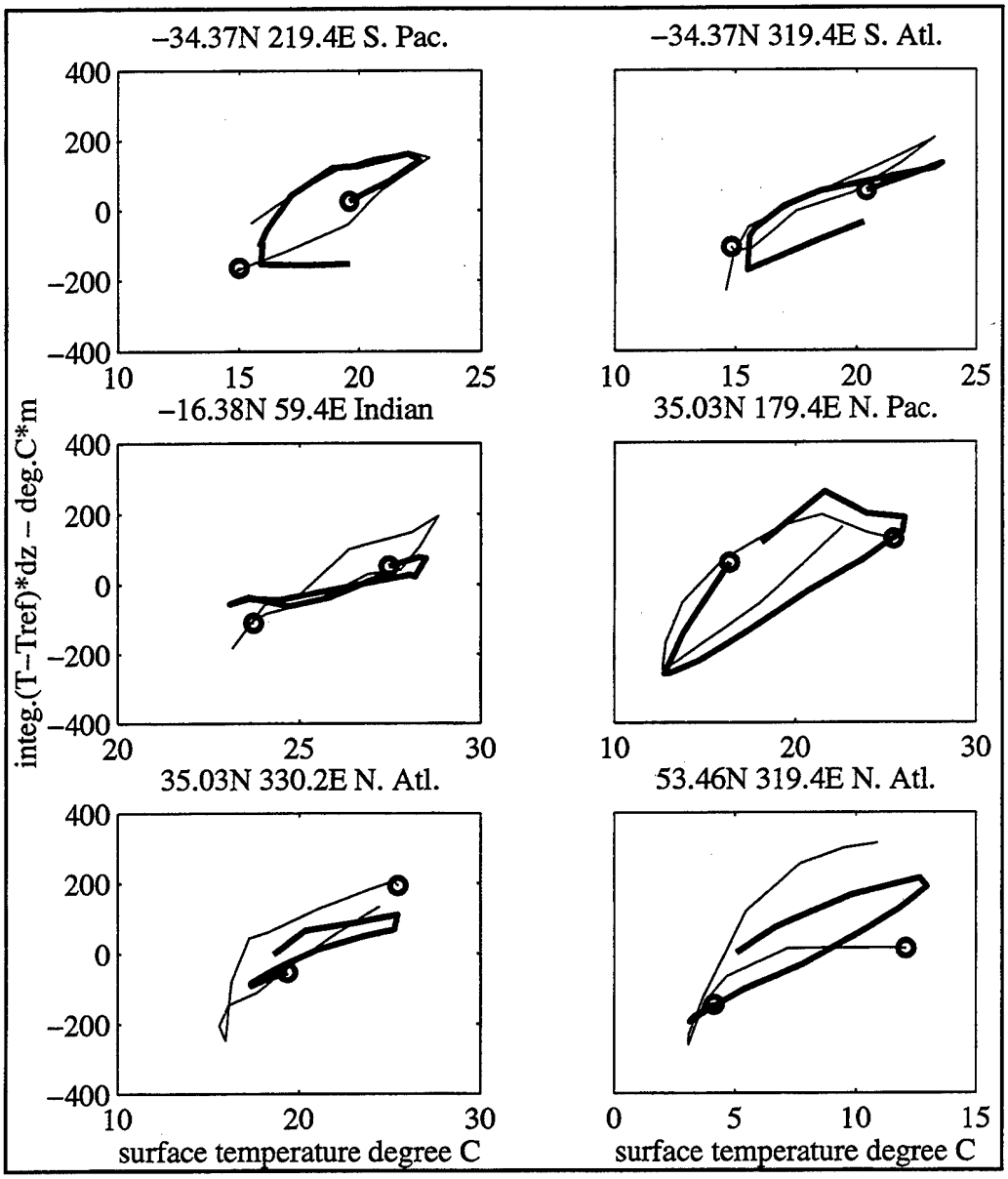


Figure 72. Heat Content for 1994 of the A run (bold line) and Mixed layer run,1992/3 (thin line) at six locations in various ocean basins.

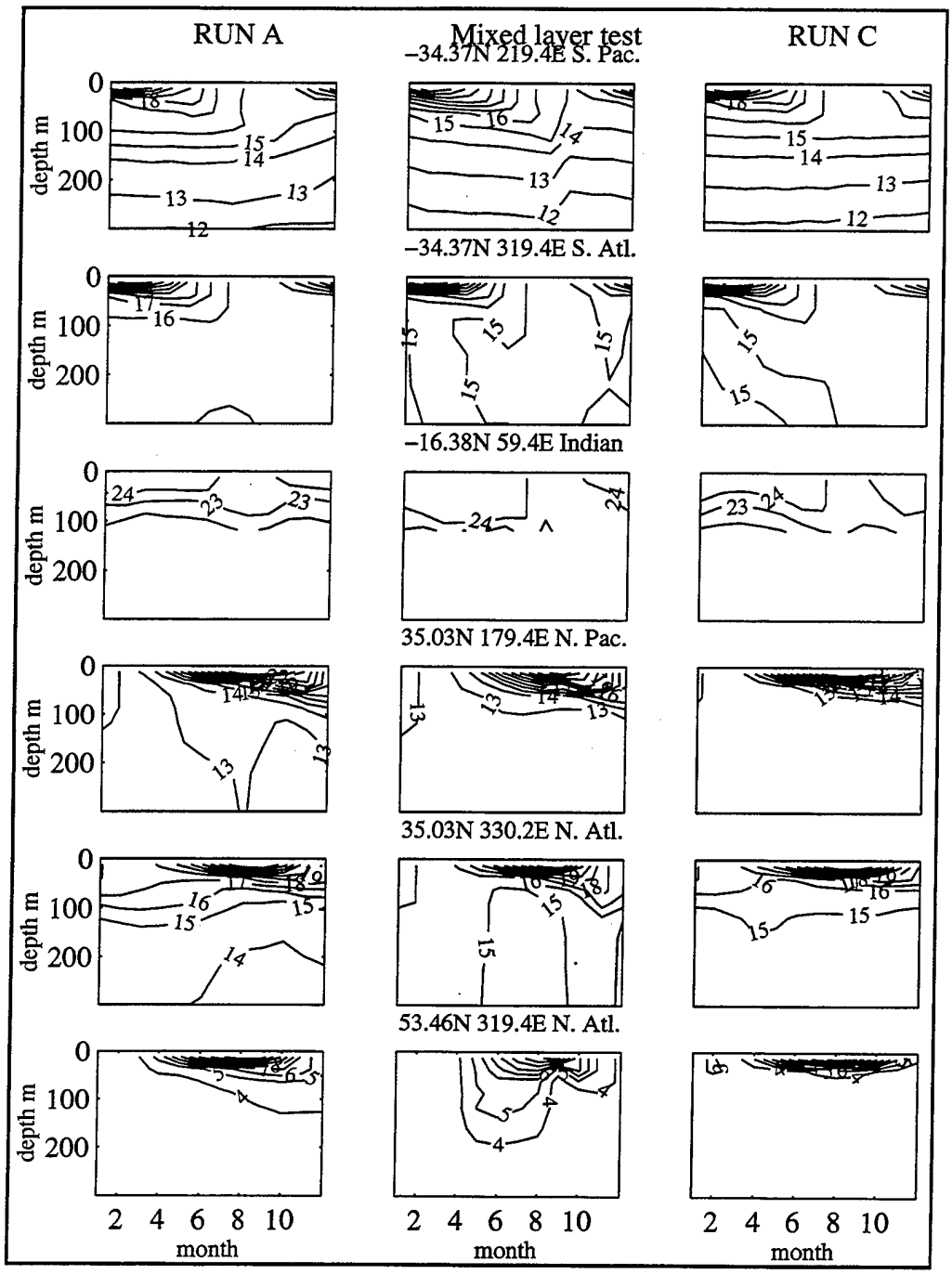


Figure 73. Temporal temperature change over 12 months at 6 locations for the A run, the C run, and mixed layer test. Contours are 1°C.

## B. IMPROVEMENT OF THE MODEL'S INITIAL CONDITIONS

Adjustments to the model's initial conditions can be made by examining the changes made to the mean over the two year period, 1993-1994. Figure 32a (Chapter IV) showed the difference in the mean field between the two model runs (A and C). The region to the east of Japan has a large change in its mean field at the surface (Figure 32a) and also in the temperature field at 160m (Figure 33a). If a meridional section of temperature and salinity is plotted along 165°E between 30° and 45°N, from the 2 year mean fields of the A run and C run, along with the Levitus 94 climatological data (Figure 74), run A qualitatively appears to be adjusting towards the Levitus data which has been used in the creation of the vertical functionals which relate SSH to temperature. The 14°C and 15°C isotherms in the A run are sloping upwards (from left to right ) similar that shown in the Levitus data, while the C run has a very sharp vertical front near 34°N. The RMS difference between the temperature fields are: A run and Levitus, 1.80°C (to 200 m); C run and Levitus, 1.96°C. For the salinity fields, the numbers are: between the A run and Levitus, 0.11‰; between C run and Levitus, 0.07‰. The average T/S diagram of the upper layers also shows and adjustment towards the Levitus data (Figure 75).

Similarly, a section can be looked at in the Indian Ocean, along 40°S between 30°E and 120°E (Figure 76). The western side shows large differences between run A (Figure 76b) and run C (Figure 76c), in the region of the Aghulas Current.

It was noted in Table 5, that across 32°S in the Indian Ocean, the heat flux is underestimated by both model runs, with a larger error seen in run A. An examination of the sections across 32°S (not shown) and 40°S, indicates that the difference between the two model runs is on the west side. The assimilation pushes the model towards the Levitus 94 mean (used as the observational field for the vertical functionals), which results in the weakening of the current southward and the heat flux balance increases northward. (Levitus shows little or no current, due to the low resolution of the climatology.) This is

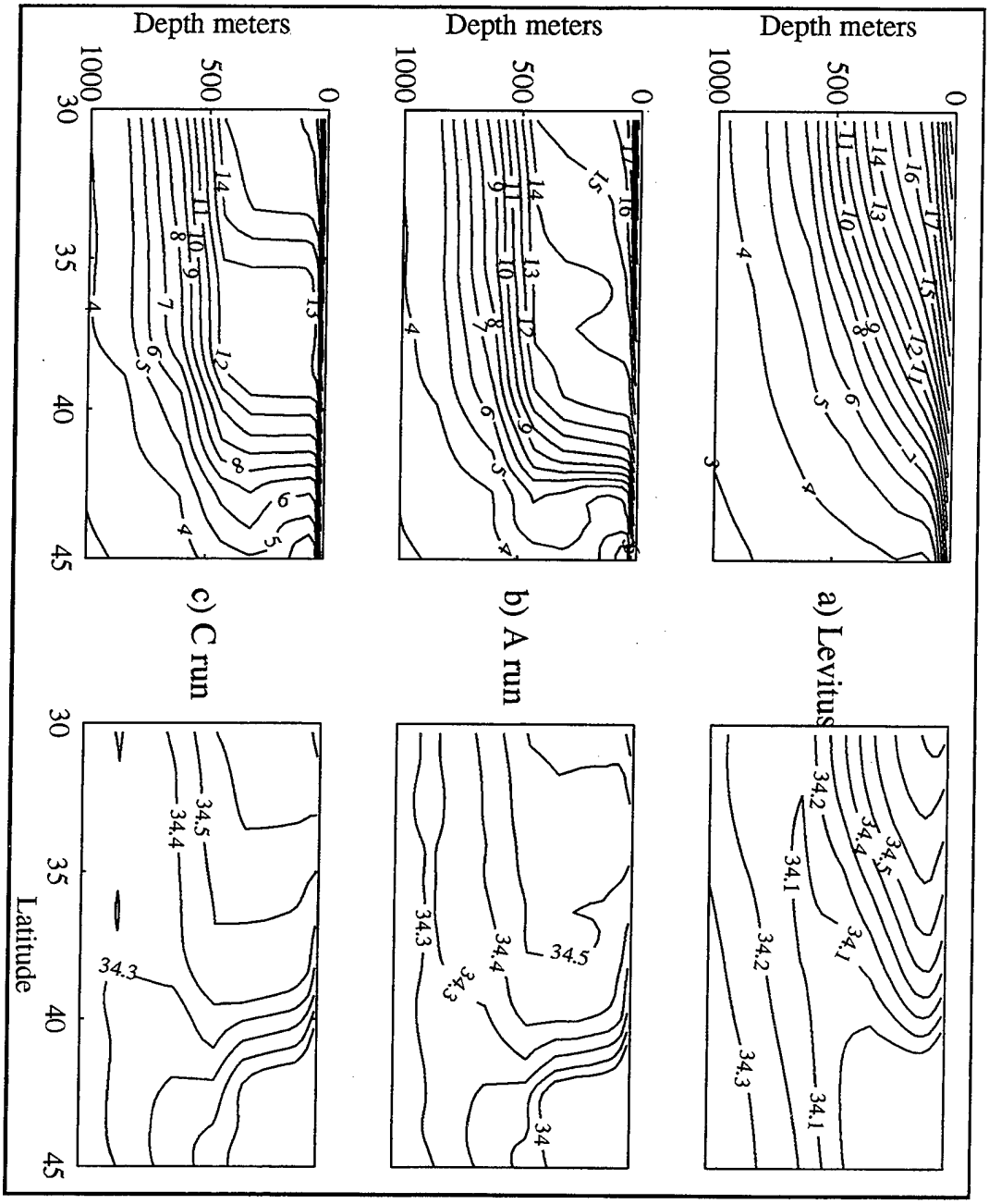


Figure 74. Meridional sections of temperature (left panels) and salinity (right panels) along 165°E in the North Pacific for a) Levitus 94 data, b) A run, and c) C run. Contours are 1°C for temperature and 0.1 S for salinity.

shown in Figure 77, which shows the T/S diagrams for the full zonal section (a), in the Aghulas current area (b) between 33.5°E and 37.5°E, and mid way along the section (c) between 65.5°E and 69.5°E. The RMS difference between the Levitus mean and the run A is 1.37°C for temperature and 0.16‰ for salinity and for run C, 1.41°C and 0.17‰, meaning that A is closer to Levitus than run C. The mean flow of either the model or that derived from the Levitus 94 data, is not correct, and thus limits the assimilation process in correcting for these errors in the model simulations. If given a different mean or initial condition, with associated confidence levels, which is more refined and accurate, the assimilation process can be used to adjust the model's prognostic variables towards this initial or mean state. The vertical structure which relates SSH to T and S does not need to be defined at high resolution over the globe, but should be at places which have known narrow currents.

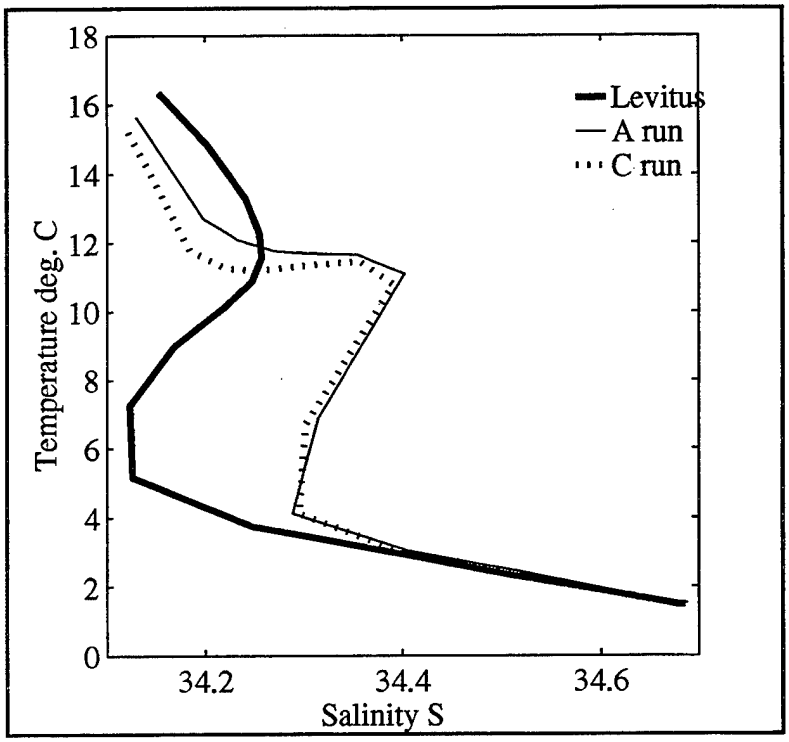


Figure 75. T/S diagram for meridional section shown in Figure 74. Bold line is for Levitus 94 data, thin line represents the A run values, and the dotted line represents the C run.

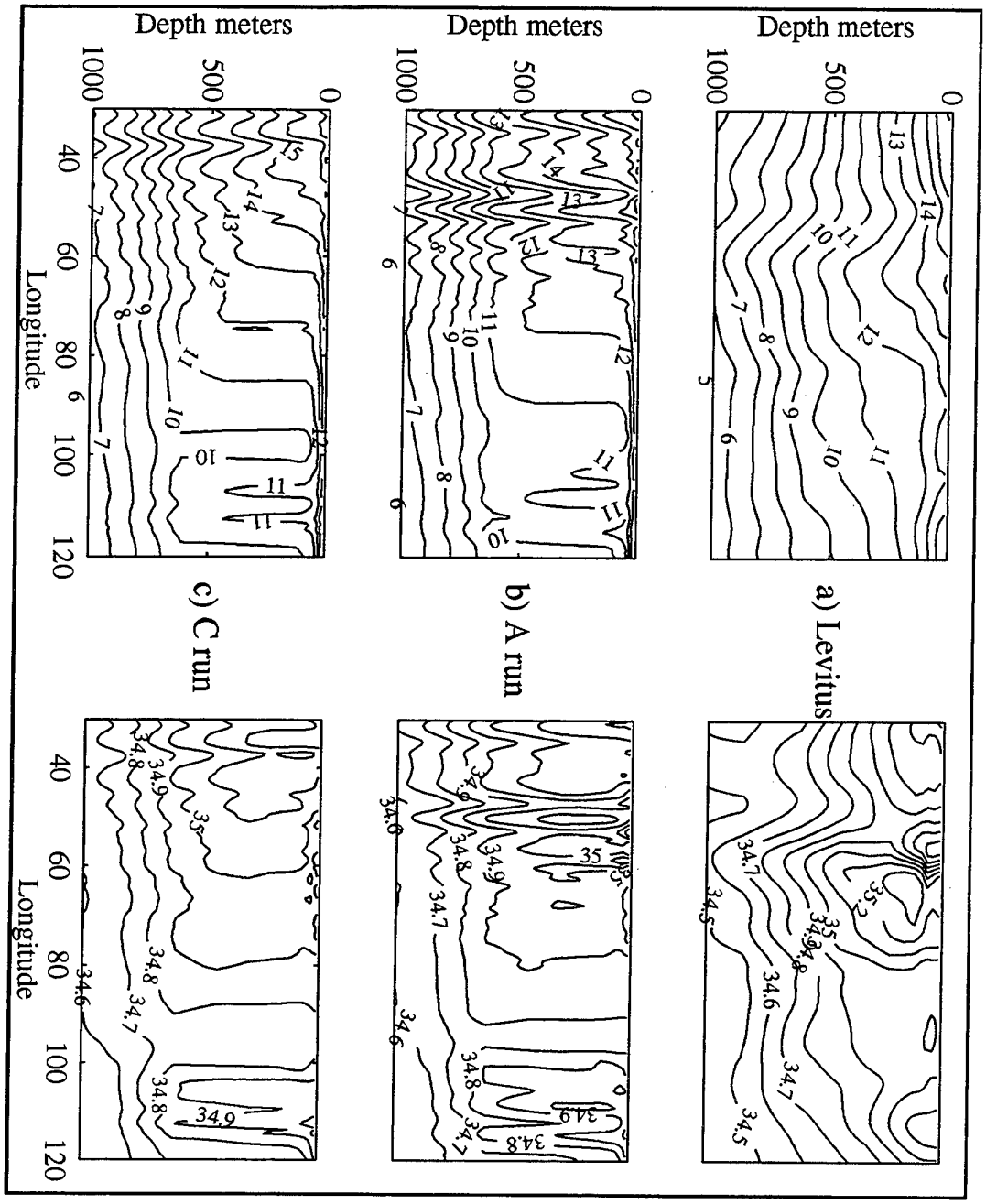


Figure 76. Same as Figure 74, except for 40°S in the Indian Ocean.

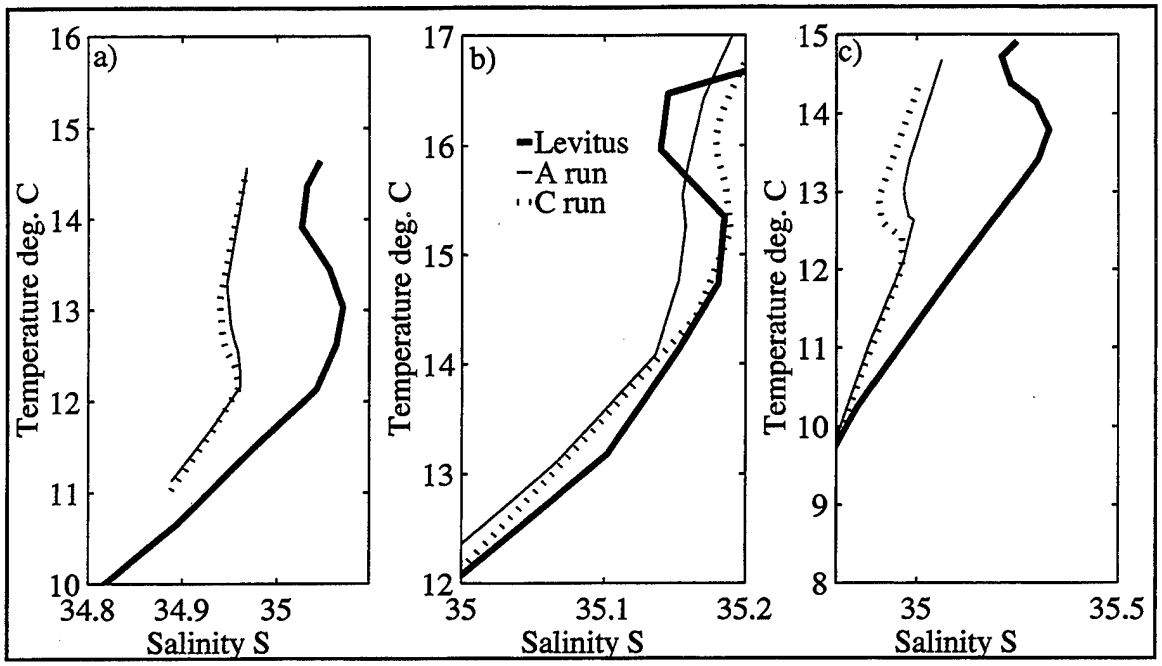


Figure 77. T/S diagram for zonal section shown in Figure 76. Bold line is for Levitus 94 data, thin line represents the A run values, and the dotted line represents the C run.

These examples are encouraging, given that the observational SSH field includes a mean a similar to the mean of the control run and uses a coarse monthly climatology to the surface SSH to subsurface temperature and salinity fields. More accurate adjustment should occur if the vertical relationships are computed using data at higher spatial resolution in areas where narrow currents occur. In addition, repeat WOCE hydrographic data can completely replace the empirical vertical T/S profiles with that of real data.

## C. IMPROVEMENT IN THE TEMPORAL VARIABILITY AT A LOCATION

The changes in the temporal variability of the ocean at a location has been previously examined when the time series of SSH from the model runs were compared to similar series obtained from tide-gauges. Another way to look at changes related mostly to

mesoscale processes is to look at a zonal section of SSH in time. Figure 78 shows such a section at 34°N in the Atlantic between 30°W and 0°, a region with a medium weighted nudging. The temporal mean SSH has been removed, along with an annual harmonic. Run A (top plot) shows stronger westward propagating waves in the eastern half of the domain than is visible in the plot for run C (lower plot). These westward propagating Rossby waves have been seen in altimeter data beginning with Geosat data (*Tokmakian and Challenor*, 1993), in addition to being observed in sea surface temperature maps (*Cipollini,* et al. 1997). Plotted in Figure 79, are maps of SSH for the region which can be used to compare to the observations gathered in July of 1993 (day 201) and September 1993 (day 250) by the French Semaphore experiment (*Hernandez and Le Traon*, 1995). A spatial mean over the area has been removed to more easily compare to the *Hernandez and Le Traon's* Figure 6. The A run (Figures 79a and c) show a depression in SSH centered at 25°W,35°N in July (day 201) which has moved to the west by day 250. The SSH structure is more closely resembling the hydrographic surface height than the SSH maps from ERS-1 and T/P shown by *Hernandez and Le Traon.* This is due to the having a mean SSH from a previous model run added to the SSH altimeter anomalies used in the assimilation process, rather than a true mean. It may also be due to a weak nudging coefficient.

This example shows that mesoscale features can be enhanced and introduced into the model. Other examples can be found in the flow of the Antarctic Circumpolar Current. Warm and cold core eddies of the Gulf Stream and the Aghulas are not as easily identifiable because the assimilation process needs to correct the mean path of the Gulf Stream (or Aghulas), in addition to correctly placing an eddy feature or removing an eddy.

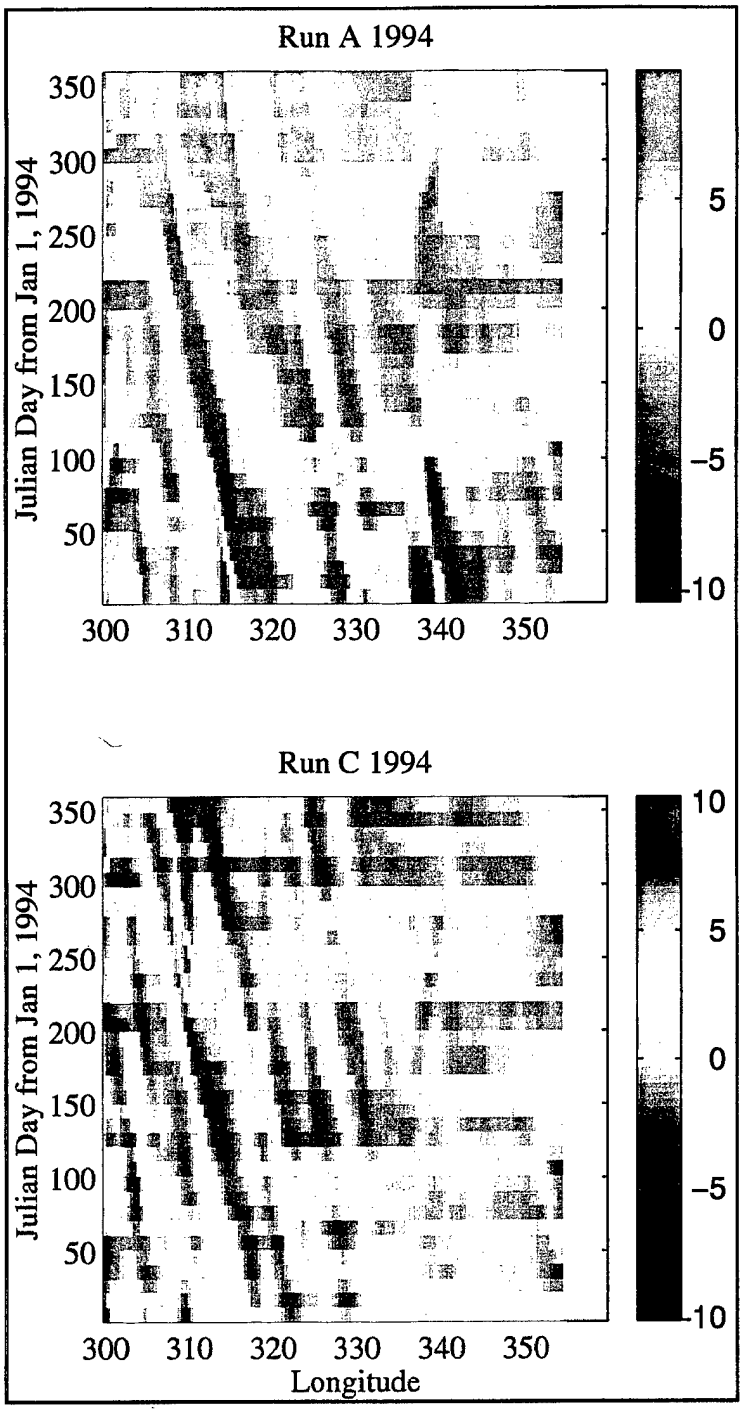


Figure 78. Time/longitude plot of SSH along 34°N in the North Atlantic in the region of the Azores Current, a) A run and b) C run.

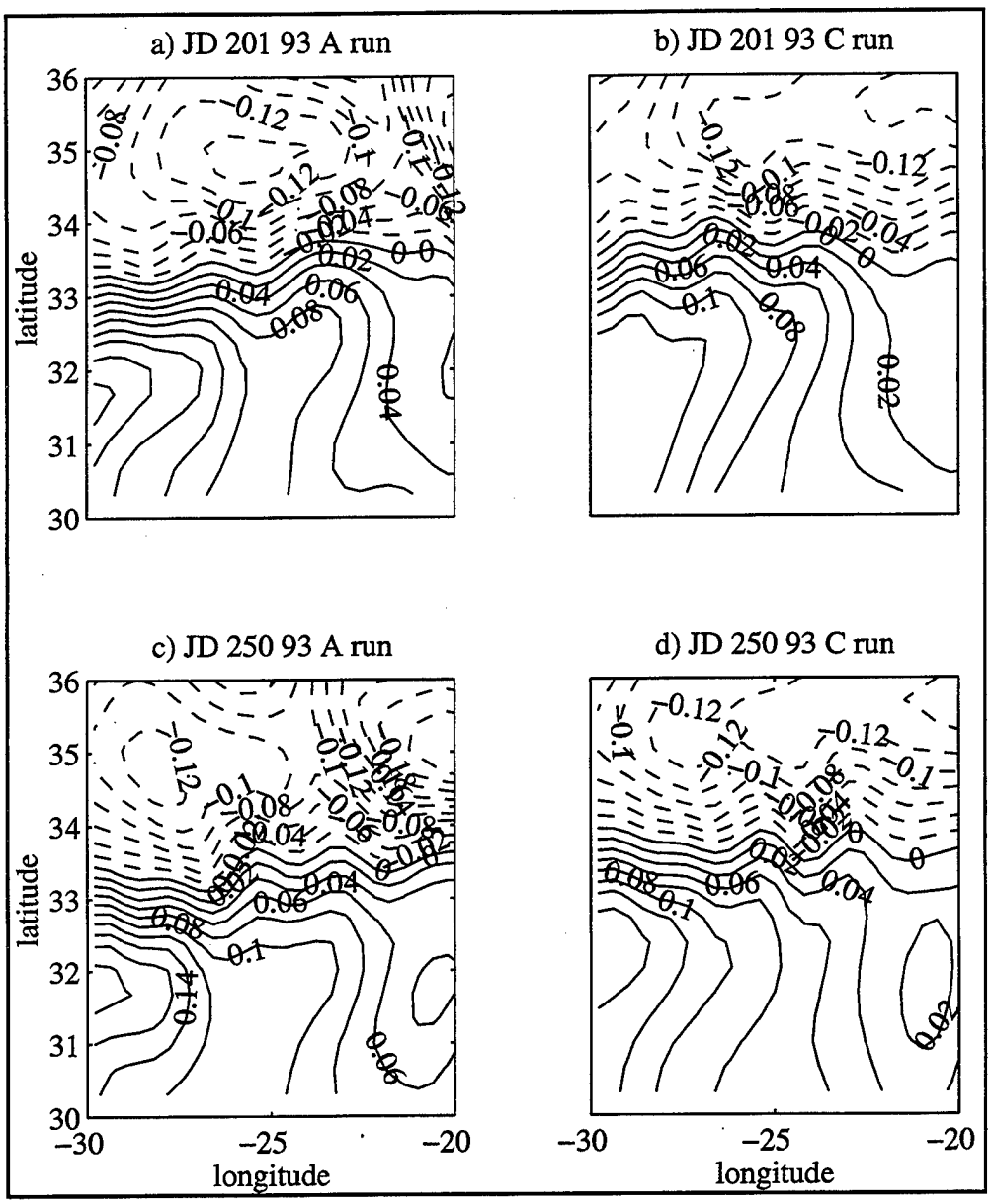


Figure 79. Plan maps of SSH for the North Atlantic in the region of the Azores current. a) Julian Day 201, 1993 for the A run, b) Julian Day 201, 1993 for the C run, c) Julian Day 250, 1993 for the A run, and d) Julian Day 250, 1993 for the C run.

## D. SUMMARY

The assimilation has changed the model, producing an ocean which includes some of the properties associated with a model which has included a mixed layer in its numerics.

Additionally, the assimilation has changed the model's mean state, which suggests that given a more accurate initial state, the model will reproduce observed and derived quantities, such as heat transport, more accurately. Each of these model "corrections" produced a model that is dynamically stable and compatible with the control run. This suggests that once a mixed layer is included in the numerics and an improved initial condition at high spatial resolution is incorporated, the assimilation process will not change these aspects of the model's output.

The shorter term variations in the ocean may not be as easily reproduced without having included in the forcing the event that caused the variability. For example, will a more accurate wind stress field in the region of the Azores Current reproduce the westward propagating Rossby waves or does the model need the assimilation to correctly "time" the events? It may never be possible to have a surface forcing field that is accurate enough to reproduce these events, thus if a model is being used to forecast the location of a front, or an eddy, assimilation is necessary. But if the model is used for climate purposes, if the events are statistically accounted for over a period of several years, than assimilation is probably not warranted.

In short, this experiment of using observational SSH anomaly measurements as the driver for the assimilation fields shows that a model can be modified to account for different initial conditions, or not having a mixed layer, and can introduce or enhance features that are not seen in the model run without assimilation.

# VII. CONCLUSIONS

The research presented in this thesis on the evaluation of two assimilation experiments has shown that it is feasible to assimilate a large quantity of observations into an eddy-resolving global ocean model.

First, it has been shown, using a twin experiment, that model diagnostic fields can be adjusted directly (SSH, temperature and salinity) and indirectly (velocity) using SSH measurements and empirically defined functions which relate SSH to subsurface temperature and salinity. After the assimilation of SSH using a simple nudging process, these prognostic fields of the twin run resemble the control fields rather than the initial fields.

The analysis of the second experiment (using SSH anomaly fields sampled with the ERS-1 and the TOPEX/POSEIDON altimeters) shows that assimilation using the nudging method is dynamically consistent with the control run of the model. This experiment has shown that the simulation has adjusted the model towards observed values of the global ocean. However, the subsurface values are a climatology and do not reflect the true ocean variability in time or space. Thus, the assimilation is not successful at recreating fine narrow structures, such as the Aghulas Current, accurately. The assimilation process has changed diagnostic quantities, and integrated quantities, indicating that assimilation can account for some processes, such as the seasonal mixed layer temperature variations, which may not be included the numerics of a model. Other analyses, for example the meridional overturning, show that assimilation modified the deep abyssal flow, as well as the near surface flow.

At the mesoscale, instabilities have been introduced where observations show that they exist, such as the Azores current. Nudging also has attempted to modify other mesoscale flow, such as incorrectly placed eddies and features in the region of the Gulf Stream. This is in addition to modifying the mean ocean circulation field.

This research has shown that a simple, straight forward method of assimilating observational data into a high-resolution global ocean model is dynamically consistent because the model's own dynamics correct for any dynamical inconsistencies in the observations. This is a reasonable method to use and can be further enhanced by replacing the Levitus 94 monthly climatology with regionally collected observations, especially those which have an associated variance. Such data are now, or soon to be, available in the form of the WOCE repeat hydrographic sections. Other WOCE data can be used to enhance the climatological field that has used data accumulated over many years. Subsurface data can also be assimilated in a direct manner, without relating it to the SSH as has been done for these experiments.

# LIST OF REFERENCES


Anthes, R. A., "Data assimilation and initialization of hurricane prediction models", *J. Atmos. Sci*, vol. 31, 701-719, 1974.

Barnier, B. , L. Siefridt and P. Marchesiello, "Thermal forcing for a global ocean circulation model from a three year climatology of ECMWF analyses", *J. Marine Sciences*, 363-380, 1994.

Bryan, K., "A numerical method for the study of the circulation of the World Ocean", *J. Comput. Physics*, vol. 4, 347-376, 1969.

Budgell, N. P., "Nonlinear data assimilation for shallow water equations in branched channels", *J. Geophys. Res.*, vol. 91, 10633-10644, 1986.

Carnes, M. R., J. L. Mitchell, P. W. DeWitt, "Synthetic temperature profiles derived from Geosat altimetry: Comparision with air-dropped expendable bathythermograph profiles", *J. Geophys. Res.*, vol. 95, 17979-17992, 1990.

Carton, J. A., B. S. Giese, X. Cao, and L. Miller, "Impact of altimeter, thermistor, and expendable bathythermograph data on retrospective analyses of the tropical Pacific Ocean", *J. Geophys. Res.*, vol. 101, 14147-14159, 1996.

Cipollini, P., D. Cromwell, M. S. Jones, G. D. Quartely, and P. G. Challenor, Concurrent TOPEX/POSEIDON altimeter and Along-Track Scanning Radimeter observations of Rossby wabve propagation near 34° N in the Northeast Atlantic, *Geophys. Res. Lett.*, in press, 1997.

Cooper M.and K. Haines, "Alimetric assimilation with water property conservation", *J. Geophys. Res.*, vol.101, 1059-1079, 1996.

Delcroix, T., J.-P. Boulanger, F. Masia, and C. Menkes, "Geosat-derived SL and surface current anomalies in the equatorial Pacific, during 1986-89 El Niño and La Niña", *J. Geophys. Res.*, vol. 99, 25093-25107, 1994.

Döös, K. and D. J. Webb, "The Deacon cell and other meridional cells in the Southern Ocean", *J. Phys. Oceanogr.*, vol. 24, 429-442, 1994.

Eanes, R.J., and S. F. Bettadpur, "The CSR 3.0 global ocean tide model", CSR-TM-05-06, Center for Space Research, Univ. of Texas at Austin, December, 1995.

Fu, L.-L., E. J. Christensen, C. A. Yamarone Jr., M. Lefebvre, Y. Menárd, M. Dorrer, and P. Escudier, "TOPEX/POSEIDON mission overview", *J. Geophys. Res.*, vol. 99, 24369-24381, 1994.

Fukumori, I., J. Benveniste, C. Wunsch, and D. B. Haidvogel, "Assimilation of sea surface topography into an ocean circulation model using a steady-state smoother", *J. Phys. Oceanogr.*, vol. 23, 1831-1855, 1993.

Fukumori, I., and P. Malanotte-Rizzoli, "An approximate Kalman filter for ocean data assimilation; An example with an idealized Gulf Stream model", *J. Geophys. Res.*, vol. 100, 6777-6793, 1995.

Ghil, Michael and Paola Malanotte-Rizzoli, "Data assimilation in meteorology and oceanography", *Advances in Geophysics*, vol. 33, 141-266, 1991.

Gille, S. T., "Non-conservation of potential vorticity in the Southern Ocean", in press, *J. Phys. Oceanogr.*, 1997.

Haines, K., "A direct method for assimilating sea surface height data into ocean models with adjustments to the deep circulation", *J. Phys. Oceanogr.*, vol. 21, 843-868, 1991.

Hayes, S. P., L. J. Mangum, J. Picaut, A. Sumi, and K. Takeuchi, "TOGA-TAO: A moored array for real-time measurements in the tropical Pacific Ocean., *Bull. Amer. Meteor. Soc.*, vol. 72, 339-327, 1991.

Hernandez, F., and P.-Y. Le Traon, "Mapping mesoscale variability of the Azores Current using TOPEX/POSEIDON and ERS-1 altimetry, together with hydrographic and Lagrangian measurements", *J. Geophys. Res.*, vol. 100, 24995-25006, 1995.

Hirst, A. C., D. R. Jackett, and T.J. McDougall, "The meridional overturning cells of a world ocean model in neutral density coordinates", *J. Phys. Oceanogr.*, vol. 23, 775-791, 1996.

Holland, W. R., and P. Malanotte-Rizzoli, "Assimilation of altimeter data into an ocean circulation model: space versus time resolution studies", *J. Phys. Oceanogr.*, vol. 19, 1507-1534, 1989.

Hurlburt, H. E., "Dynamic transfer of simulated altimeter data into subsurface information by a numerical ocean model", *J. Geophys. Res.*, vol. 91, 23272-24000, 1986.

Killworth, P. E., D.J. Webb, D. Staniforth, and S. M.. Patterson, "The development of a free- surface Bryan-Cox-Semtner ocean model", *J. Phys. Oceanogr.*, vol. 21, 1333-1348, 1991.

Krause, E. B., and Turner, "A one-dimensional model of the seasonal thermocline. Part II", *Tellus*, vol. 19, 98-105, 1967.

Le Traon, P. Y., P. Gaspar, H. Makhmara, "Using Topex/Poseidon data to enhance ERS-1 data", *J. Atmos. Tech.*, vol. 12, 161- 170,1995.

Levitus, S., "Climatological Atlas of the World Ocean", *NOAA Professional Paper 13*, U.S. Government Printing Office, Washington, D.C., 173 pp., 1982.

Levitus, S. and T.P. Boyer, "World Ocean Atlas 1994, Volume 4: Temperature", NOAA Atlas NESDIS 4, *U.S. Dept. of Commerce*, Washington,D.C., 117 pp., 1994.

Levitus, S, R. Burgett, and T. Boyer, "World Ocean Atlas 1994, Volume 3: Salinity", NOAA Atlas NESDIS 3, *U.S. Dept. of Commerce*, Washington,D.C., 99pp., 1994.

Macdonald, A., and C. Wunsch, "Oceanic estimates of global ocean heat transport", International WOCE newsletter, #24, 5-6, 1996.

McClean, J. L., A. J. Semtner, V. Zlotnicki, "Comparisons of mesoscale variability in the Semtner/Chervin quarter-degree model, the Los Alamos POP sixth-degree

model, and Topex/Poseidon data, submitted to *J. Geophys. Res.*, 1997.

Mellor, George L. and Tal Ezer, "A Gulf Stream model and an altimetry assimilation scheme", *J. Geophys. Res.*, vol. 96, 8779-8795., 1991.

Mesinger, F., and A. Arakawa, "Numerical methods used in atmospheric models", Vol. 1, WMO, GARP Publ. Serv., 17, 64pp., 1976.

Montgomery, R. B., "A suggested method for representing gradient flow in isentropic surfaces", *Bull. AMS*, June-July, 210-212, 1937.

New, A., Y. Jia, R. Marsh, M. Huddleston, and S. Bernard, "An isopycnic model study of the North Atlantic Ocean. Part I: Model experiment." , *J. Phys. Oceanogr.*, vol. 25, 2667-2699, 1995.

Oscilles, A., and J. Willebrand, "Assimilation of Geosat altimeter data into an eddy-resolving primitive equation of the North Atlantic Ocean", *J. Geophys. Res.*, vol. 101, 14175-14190, 1996.

Pickard, G. L, and W. J. Emery, "Descriptive Physical Oceanography 4th Edition", Pergamon Press, New York, NY, pp. 247, 1986.

Rapp, R. H., C. Zhang, and Y. Yuchan, "Analysis of dynamic ocean topography using TOPEX data and orthonormal functions", *J. Geophys. Res.*, vol. 101, 22583-22598, 1996.

Saunders, P. M. and B. A. King, "Bottom currents derived from a shipborne ADCP on WOCE Cruise A11 in the South Atlantic", *J. Phys. Oceanogr.*, vol. 25, 329-347, 1995.

Semtner, A. J., "A general circulation model for the world ocean", UCLA Dept. of Metero., Tech. Rep. No. 8, 99pp., 1974.

Semtner, A. J., and R. M. Chervin, "Simulation of the global ocean circulation with resolved eddies", *J. Geophys. Res.*, vol. 93, 15502-15522, 1988.

Semtner, A. J., and R. M. Chervin, "Ocean general circulation from a global eddy-resolving model", *J. Geophys. Res.*, vol. 97, 5493-5550, 1992.

Semtner, A. J., "Modeling ocean circulation", *Science*, vol. 269, 1379-1385, 1995.

Sirkes, Z., E. Tziperman, and W. C. Thacker, "Combining data and a global primitive equation ocean general circulation model using the adjoint method", in *Modern Approaches to Data Assimilation in Ocean Modeling*, pp. 119-145, Ed. P. Malanotte-Rizzoli, Elsevier Science, 1996.

Snedecor, G. W., and W. G. Cochran, Statistical Methods, Iowa State Univ. Press, Ames, Iowa, 503 p., 1989.

Stammer, D., and. C.W. Böning, Mesoscale variability in the Atlantic Ocean from GEOSAT altimetry and WOCE high resolution modeling, , *J. Phys. Oceanogr.*, vol. 22, 1732-752, 1992.

Stammer, D., R. Tokmakian, A. J. Semtner, and C. Wunsch, "How well does a 1/4°

global ocean model simulate large-scale observations?", *J. Geophys. Res.*, vol. 101, 25779-25811, 1996.

Taft, B., "Subtropic gyre of the western Pacific", International WOCE newsletter, #19, 6-7, 1995.

Tokmakian R. and P. G. Challenor, "Observations in the Canary Basin and the Azores frontal region using Geosat data", *J. Geophys. Res.*, vol. 98, 4761-4773, 1993.

Tokmakian, R., "Comparisons of time series from two global models with tide-gauge data", *Geophys. Res. Lett.*, vol. 23, 3759-3762, 1996.

Tziperman, E., and. W. C. Thacker, "An optimal control/adjoint equation approach to studying the oceanic general circulation, *J. Phys. Oceanogr.*, vol. 19, 1471-1485, 1989.

Zhang, H.-M., and N. G. Hogg, "Circulation and water mass balance in the Brazil Basin", *J. of Marine Res.*, vol. 50, 385-420, 1992.

# APPENDIX

The mean SSH field (<SSH_observed>) which is added to the altimeter SSH anomalies effects part of the change in the resulting yearly mean SSH field. In the assimilation run (run A), a mean different from the control run's mean SSH field is used to show what may occur if a mean computed from observations (assumed to be different from the control run's mean) where to be used. To understand the effect of this mean SSH field on the simulation, a short (approximately 1 year) test (referred to as the E run) was conducted using the 2 year SSH mean (93/94) from the C run instead of the 3-year mean (87-89) from the POCM_4A run (see Figure 28). Figure 80 shows the difference between the two mean fields of Figure 28. Some of the differences are due to the different forcing used, with the POCM_4A run using the ECMWF 1000mb wind stress fields, known to be overestimated, while the POCM_4B run (the control run) used the more accurate 10 m wind fields.

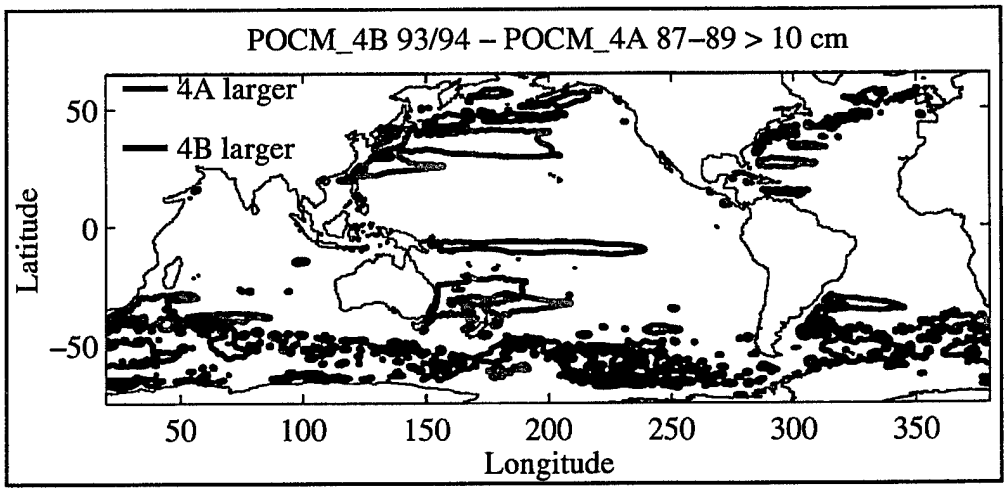


Figure 80. Difference in the mean SSH field for 3 years (87-89) of the POCM_4A run and the POCM_4B run (93/94). Red indicates POCM_4A is larger (-10cm) and blue indicates where POCM_4B is larger (10cm). (These are not absolute differences, e.g.. if 4A = -200 cm and 4B = -190 cm, then 4B - 4A = 10cm. The color scheme is being used to show just that there are differences.)

The next two figures show the effect each of the <SSH_observed> fields has on the simulation. Figure 81a and b show the differences in the simulated 1993 SSH mean field as compared to the control run (run C) for the E run (<SSH_observed> = POCM_4B, 93-94) and for the A run (<SSH_observed> = POCM_4A, 87-89). When the <SSH_observed> is the mean of the control run, the differences between the control run and the assimilation are reduced, especially in the area of the Kuroshio Extension (Figure 81a). The mean SSH of the assimilation runs were still modified, though, independent of which mean SSH field was added to the altimeter SSH anomalies as shown in Figure 81c. Here, the difference between the assimilation runs shows only small differences outside of the Kuroshio area (such as in the Gulf Stream region) and no difference between the two assimilation runs in the Indian Ocean. Both assimilation runs show changes in the mean SSH field occurring in the Indian Ocean even though there is little if no difference in the <SSH_observed> field (see Figure 80).

In the plot of the mean 1993 temperature field at 160m (level 6 of the model), the <SSH_observed> has mostly contributed to the change seen in the Kuroshio region of the A run (Figure 82c). As with the SSH fields, the mean temperature field at depth is modified independent of which <SSH_observed> was used, such as in the Southern Ocean between 20° and 70°E, 45°S (Figures 82a,b).

In summary, both the <SSH_observed> and the SSH anomalies combined with the associated vertical adjustments, modify the mean fields of temperature and SSH when assimilating observations in the global model. In some cases, such as in the Kuroshio, the difference in the mean fields can be directly related to the <SSH_observed> used. Also, the simulated mean SSH does not always change, when there is a change in the mean temperature field does, as is seen in the temperature field of the tropical ocean in Figure 33a verse what is shown in the mean SSH field (Figure 32a).

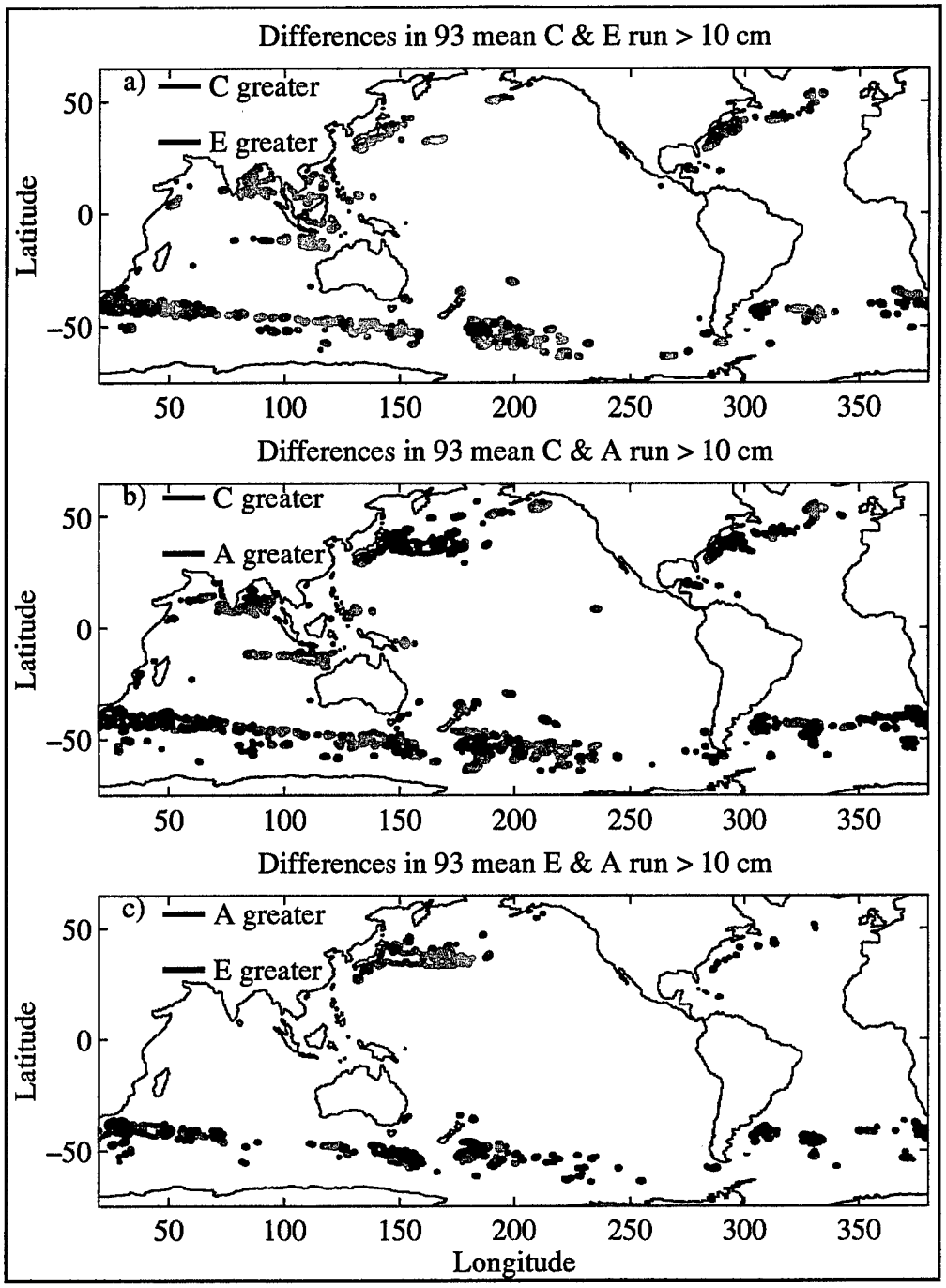


Figure 81. Differences between pairs of simulated mean SSH fields, a) between the C run and the E run, b) between the C run and the A run, c) between the two assimilation runs, A and E. Red indicates -10cm or smaller (*i.e.* , more negative) and blue indicates 10 cm or larger.

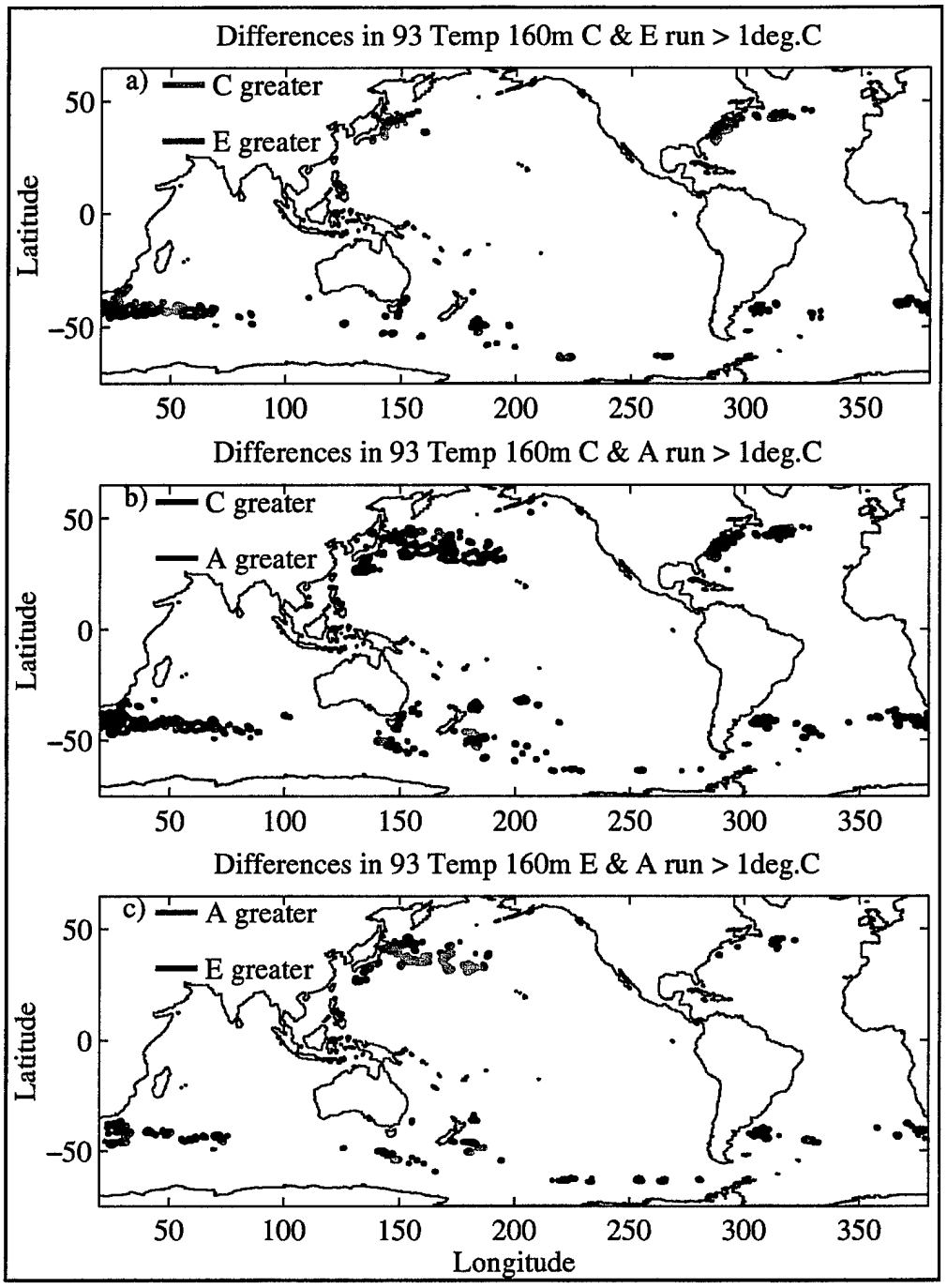


Figure 82. Differences between pairs of simulated mean temperature fields at 160m, a) between the C run and the E run, b) between the C run and the A run, c) between the two assimilation runs, A and E. Red indicates -1°C and smaller (*i.e.* , more negative) and blue indicates 1°C and larger.

# INITIAL DISTRIBUTION LIST

1. Defense Technical Information Center.....2
   8725 John J. Kingman Road, Ste 0944
   Ft. Belvoir, VA 22060-6218

2. Dudley Knox Library.....2
   Naval Postgraduate School
   411 Dyer Rd
   Monterey, CA 93943-5101

3. Professor Robert H. Bourke.....1
   Chairman, Department of Oceanography, Code OC/Bf
   Naval Postgraduate School
   Monterey, CA 93943-5000

4. Professor Albert J. Semtner.....1
   Department of Oceanography, Code OC/Se
   Naval Postgraduate School
   Monterey, CA 93943-5000

5. LCDR Emil Petruncio, USN.....1
   CNMOC
   1020 Balch Blvd.
   Stennis Space Center, MS 39529-5005

6. Robin Tokmakian.....4
   Department of Oceanography, Code OC/tk
   Naval Postgraduate School
   Monterey, CA 93943-5000

7. Oceanographer of the Navy.....1
   Naval Observatory
   34th and MAssachusetts Avenue NW
   Washington, CD 20390

8. Commander.....1
Naval Meteorology and Oceanography Command
Stennis Space Center, MS 39522-5001

9. Commanding Officer.....1
Naval Oceanographic Office
Stennis Space Center, MS 39522-5001

10. Commanding Officer.....1
Fleet Numerical Meteorology and Oceanography Center
Attn. Mike Clancy
7 Grace Hooper Ave Stop 1
Monterey, CA 93943-5501